6-2005

Load Interaction Effects on Fatigue Crack Growth

Stoyan Ivanov Stoychev
Western Michigan University

LOAD INTERACTION EFFECTS ON FATIGUE CRACK GROWTH

by

Stoyan Ivanov Stoychev

A Dissertation
Submitted to the
Faculty of the Graduate College
In partial fulfillment of the
requirements for the
Degree of Doctor of Philosophy
Department of Mechanical and Aeronautical Engineering

Western Michigan University
Kalamazoo, Michigan
June 2005

LOAD INTERACTION EFFECTS ON FATIGUE CRACK GROWTH

Stoyan Ivanov Stoychev, Ph.D

Western Michigan University, 2005

The fatigue crack propagation rate can be either increased or decreased by the previous load history (overload, block loading, different load ratio, etc). Currently, these load sequence effects can be explained either by using crack closure or internal stress concepts. They are studied in Part I and II of the dissertation accordingly.

In Part I the last 35 years of research in the crack closure area were carefully reviewed. A new Quadrature (Q) method for crack closure estimation, based on integration rather than differentiation of the load-displacement data, was developed and compared to the 'best' methods from the literature. The new method was able to reduce the scatter in the opening load estimations to a negligible level, but does not collapse the results for different load ratios (0.1 and 0.9). In Part II a general relationship between fatigue crack growth rate (da/dN) and the two-parameter (ΔK_{tip} and ${}_{tip}K_{max}$) crack driving force was derived using fundamental fatigue (ε-N curve) properties. Based on this analysis, a new way of representing the da/dN data by means of the crack propagation (CP) table was proposed. In order to make the CP table sensitive to the load history effects, it was scaled using the applied and internal stresses and the corresponding stress intensity factors, characteristic for the crack tip. Two methods for calculating the internal stress intensity factors were developed, adopting the weight function and the new clamping force concepts accordingly.

Finally, the CP table at the crack tip was successfully used together with the two-parameter crack driving force equation to predict da/dN for different load ratios,

block loading and a single overload. Calculation of the crack closure was not needed in order to predict the experimental data accurately.

ProQuest Information and Learning Company
300 North Zeeb Road
P.O. Box 1346
Ann Arbor, MI 48106-1346

ACKNOWLEDGEMENTS

I would like to thank Dr. Daniel Kujawski for guiding me through the study that is contained in this dissertation and also for the time he took to discuss all the important and challenging issues with me.

I would also like to thank Kevin Braat and the members of my thesis committee - Dr. Judah Ari-Gur, Dr. Philip Guichelaar, and Dr. Giora Kimmel, for taking the time to review my work.

Finally, I would like to thank my wife and my family for their patience and moral support.

This investigation was supported by the Office of Naval Research grant No. N000 1.4-01-1-0952 monitored by Dr. A. K. Vasudevan.

Stoyan Ivanov Stoychev

TABLE OF CONTENTS

Table of Contents-Continued

Table of Contents-Continued

LIST OF TABLES

LIST OF FIGURES

List of Figures-Continued

List of Figures-Continued

List of Figures-Continued

NOMENCLATURE

a	crack length
b	fatigue strength exponent
c	fatigue ductility exponent
C	fatigue crack growth constant
CC	crack closure
CMOD	crack mouth opening displacement
CTOD	crack tip opening displacement
da/dN	crack growth rate
E	modulus of elasticity
FCG	fatigue crack growth
K	stress intensity factor
K_{res}	residual stress intensity factor
K_{int}	internal stress intensity factor
ΔK_{th}	threshold stress intensity range
ΔK^*	two parameter driving force
m	Paris' equation exponent
m(x,a)	weight function
N	number of cycles
N_f	number of cycles to failure
n'	cyclic strain hardening exponent
P	applied load
P_{op}	crack opening load
P_{cl}	crack closing load
P_w	wedge force

R	load ratio (P_{min}/P_{max} or K_{min}/K_{max})
S_{max}	maximum applied nominal (remote) stress
S_{min}	minimum applied nominal (remote) stress
SWT	Smith-Watson-Topper fatigue damage parameter
x	distance from the crack tip
ε	strain ahead of the crack tip
ε_0	yield strain
ε_a	strain amplitude ahead of the crack tip
ρ^*	crack tip process zone
σ	stress ahead of the crack tip
σ'_f	fatigue strength coefficient
σ_{max}	maximum stress ahead of the crack tip
σ_{res}	residual stress distribution ahead of the crack tip
σ_{int}	internal stress distribution ahead of the crack tip
σ_0	yield stress

Introduction

It is a well known fact that the majority of mechanical failures in practice are caused by fatigue – a phenomenon where the nominal stresses in the component may never exceed the yield strength of the material and still, a crack will nucleate and propagate, causing failure. It is of critical importance then, to answer these questions:

1. Will the component fail?
2. How long before it fails?

The quest for a solution of these questions started in 1829 (Albert - Effects of Repeated Loads). Almost 200 years later, it is still difficult to predict the fracture process and the resulting fatigue life. The existing methods for crack growth prediction are largely empirical and often result in unacceptable errors. The most fundamental problem that is faced currently by the researchers is how to predict correctly the effects of the load history on the fatigue crack growth rate (load interaction effects). Generally, in the literature there are only three ways to do that and they are shown schematically in Figure 1.

Traditionally, the fatigue crack growth rate, da/dN, is described by one parameter – the stress intensity factor range, ΔK. Other influences like the load ratio, R, or the overload effects are handled by utilizing the crack closure (CC) concept. The CC concept was introduced by Elber in 1971 [1-3] as a phenomena where premature contact between opposing crack faces can occur even in tension, due to the plastic deformation left at the crack wake from previous cycles. It is assumed than that any loads below the load where CC occurs (P_{op}) are not damaging. This effectively adds a second factor in the crack driving force calculation – opening stress intensity factor (K_{op}), which corresponds to P_{op}. This method is the most widely

accepted of the three (Figure 1) and as such will be studied extensively in Part I of the dissertation.

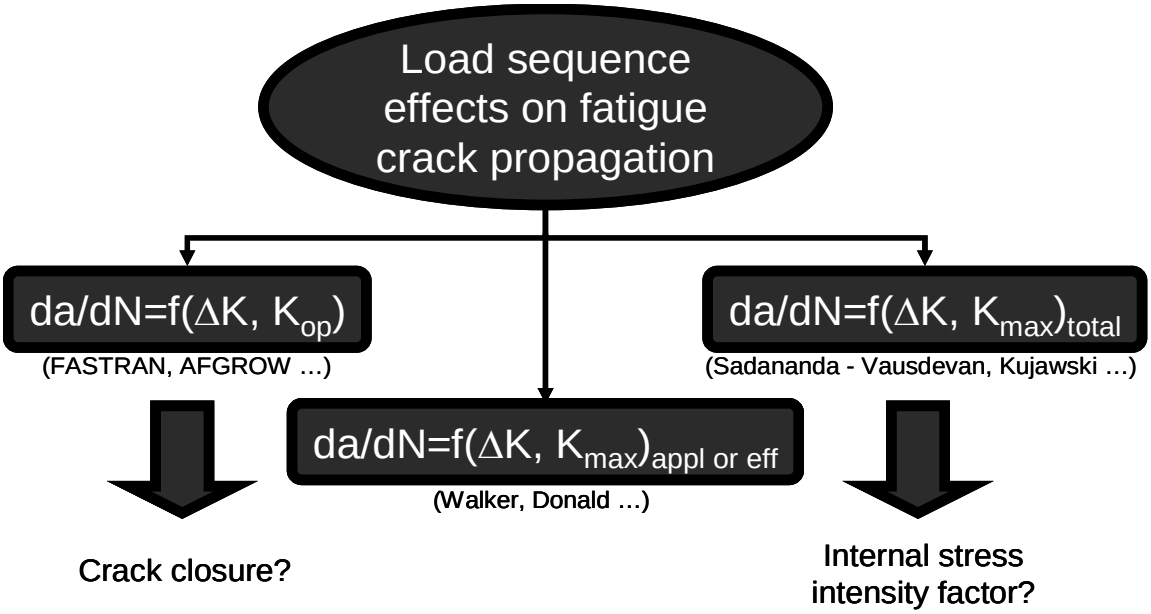

Figure 1 Current state of fracture related research

As an alternative, the unified approach for fatigue crack growth description has been proposed by Vasudevan, Sadananda and co-workers [4] using two fundamental fracture mechanics parameters, ΔK and K_{max} (Figure 1). Distinctive feature of this method is that it does not use the applied values of the stress intensity factor. Instead the total values (at the crack tip) are calculated using the internal stresses ahead of the crack tip. These stresses and the corresponding stress intensity factor (K_{int}) are dependent on the load history and allow the effects of such loading to be modeled with the unified approach to fatigue without invoking the questionable CC concept. Due to problems with the internal stress intensity factor estimation, however, unified approach to fatigue still remains mainly a philosophy rather than a prediction tool. Therefore, two new methods for K_{int} estimation are developed and the unified approach to fatigue is explored in Part II.

Part I - Crack Closure

Review on opening load determination methods

Crack closure has been the most widely accepted mechanism for crack growth modeling since 1971. It is not surprising that it is very well publicized. Therefore, Part I will begin with a review of the literature on crack closure/opening load and the corresponding crack tip shielding determination methods. Commonly used 'subjective' (visual) and 'non-subjective' approaches have been included. Procedures, associated with determinations of an effective crack driving force for both Elber type and that of partial (or incremental) crack closure models have been covered. Comparisons among different methods of analyses based on compliance and fatigue crack growth rate measurements are discussed together with their implications and difficulties on fatigue crack growth correlations.

For the last 25 years a number of review articles [5-15, 118] on the fatigue crack closure/opening topic have been published, as shown in Table 1.1. These reviews discussed important and challenging issues associated with theoretical, numerical, and experimental attempts aimed in determining crack closure/opening loads. The most extensive is the review by Banerjee [6], which covers all methods for opening/closure load determination up to 1983. Later Phillips [11, 12] discussed results of two ASTM Round Robins associated with experimental scatter of the most relevant (until 1993) methods. A number of concerns surfaced during those Round Robins, starting an additional 'wave' of studies associated with new methods and suggested improvements to the existing methods. The most recent reviews [13-15, 118] were concentrated on specific type of methods such as curve fitting, finite element, smoothing of raw data, etc. Until now, there is no systematic review of the

existing methods (developed before and after the ASTM Round Robins) Part I is intended to fill the gap.

Table 1 Review papers on crack closure

Author(s)	Year	Reference
Macha, Corbly and. Jones	1979	[5]
Banerjee	1983	[6]
Allison	1988	[7]
Allison, Ku and Pompetzki	1988	[8]
Ray, Alten and Grandt	1988	[9]
Schijve	1988	[10]
Phillips - (ASTM Round Robin #1)	1989	[11]
Phillips - (ASTM Round Robin #2)	1993	[12]
Huang, Lang, Wu and Doker	1998	[13]
Newman	1999	[14]
Donald and Phillips	1999	[118]
Xu, Gregson and Sinclair	2000	[15]

In general, experimental techniques used for crack closure (CC) or crack opening (CO) determination fall into two categories, i.e., direct and indirect methods. The term ‘direct’ refers to techniques associated with direct observations of the distance between the crack faces at the surface but not to the apparent crack tip shielding. Up to now, there is no direct experimental method, for metallic materials, that is capable of measuring the actual development of through-thickness crack closure. A common assumption is that when the crack starts to close at the surface, the crack tip is fully shielded from further damage (Figure 2). The direct techniques include the following: optical and scanning electron microscopy observations [15-27, 55], photography [28,29], optical and laser interferometry [5, 9, 30-46, 57], replica [8, 15, 17-24, 27, 55], surface strain [9, 13, 15, 28, 48-62, 77-81, 92, 101], X-Ray tomography [63-70], and caustics [71-76].

Elber was the first researcher who determined the opening load, P_{op}, indirectly from the experimentally measured compliance curve [1-3]. He also introduced the

effective stress intensity factor (SIF) range, ΔK_{eff}, defined as:

$$\Delta K_{eff} = K_{max} - K_{op} \qquad (1.1a)$$

It corresponds to a fully open crack, where K_{max} is the SIF calculated for the maximum load, P_{max}, and K_{op} is the SIF value calculated for the crack opening load, P_{op} (**Figure 2**). The effective SIF range, ΔK_{eff} was related to the applied SIF range, $\Delta K = K_{max} - K_{min}$, via the following relationship:

$$U = \frac{\Delta K_{eff}}{\Delta K} \qquad (1.1b)$$

In Eq. 1.1b, U is the stress intensity ratio.

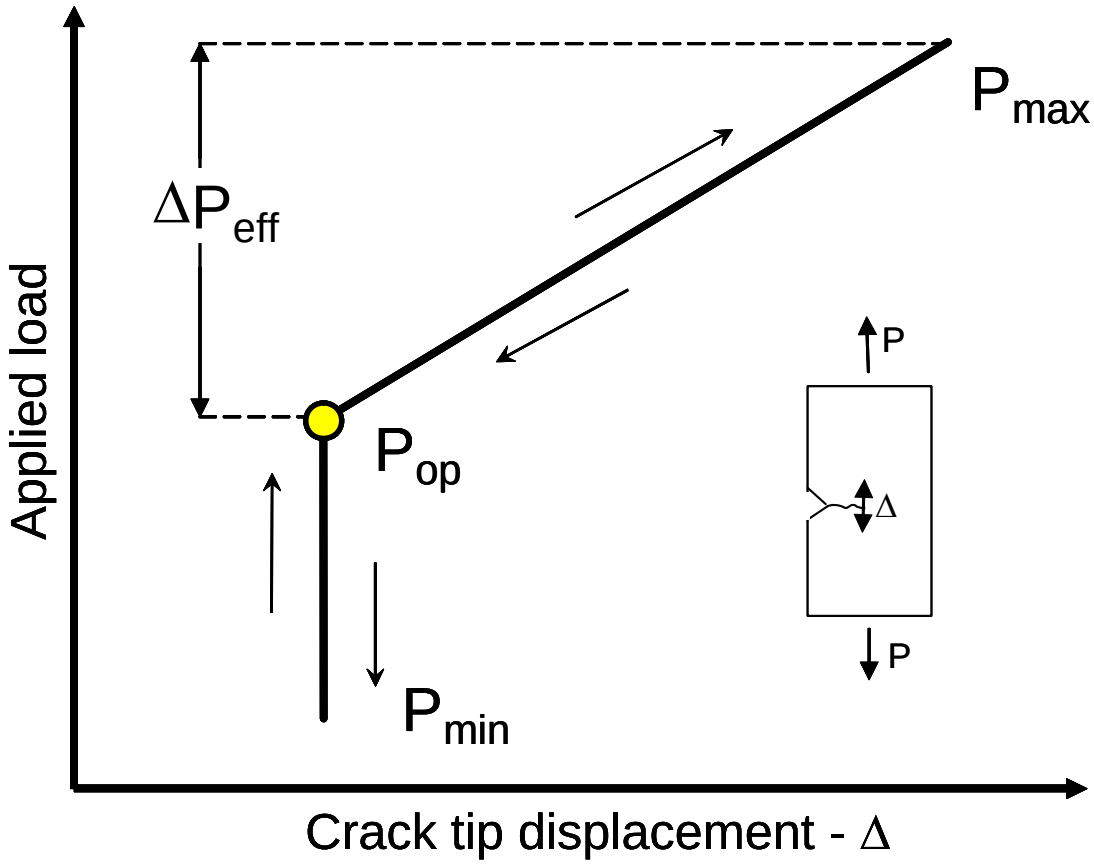

Figure 2 Ideal crack closure as defined by Elber

According to Elber, U is dependent solely on the load ratio, $R=P_{min}/P_{max}$. The

most common indirect techniques which utilize the compliance curve are: back face strain (BFS) [8, 9, 13, 15, 28, 49, 52, 53, 54, 77-81], crack mouth opening displacement (CMOD) [5, 8, 9, 15, 28, 48, 49, 53, 55, 77-92], near crack tip gage (NCTG) [5, 15, 48, 49, 57, 2, 78, 79, 81, 90, 92-96, 101] and 'push rod' gage [23, 77] measurements. In addition, other methods such as acoustic emission (AE) [5, 80, 102, 103], eddy current [97,98], potential drop (PD) [13,99-101], ultrasonic isoscanning [102], and dynamic compliance [88] are also used.

Usually, the CMOD, BFS, and 'push rod' methods give similar results [23, 49, 77, 80], whereas the NCTG [23, 49, 77] and AE measurements result in somewhat higher values of P_{op} [80]. These differences are usually explained using the plane stress versus plane strain arguments. At the specimen surface, the plane stress condition prevails, whereas, in the interior or bulk of the specimen, plane strain dominates. Under plane stress condition, the crack tip plastic zone is larger than that for plane strain and therefore, plasticity induced crack closure would be more pronounced near the surface. In general, both AE and NCTG measurements capture the near surface crack closure and that is why they indicated higher P_{op} results than BFS and CMOD measurements.

The use of AE or PD methods involves different set of problems [6, 7]. The reason for this is that the asperities may cause acoustical and/or electrical short circuits and both methods would register unrealistically high values of P_{op} [6, 100]. Thus, acoustically or electrically closed/open crack is not equivalent to mechanically closed/open crack, especially at the threshold region where the crack opening is relatively small.

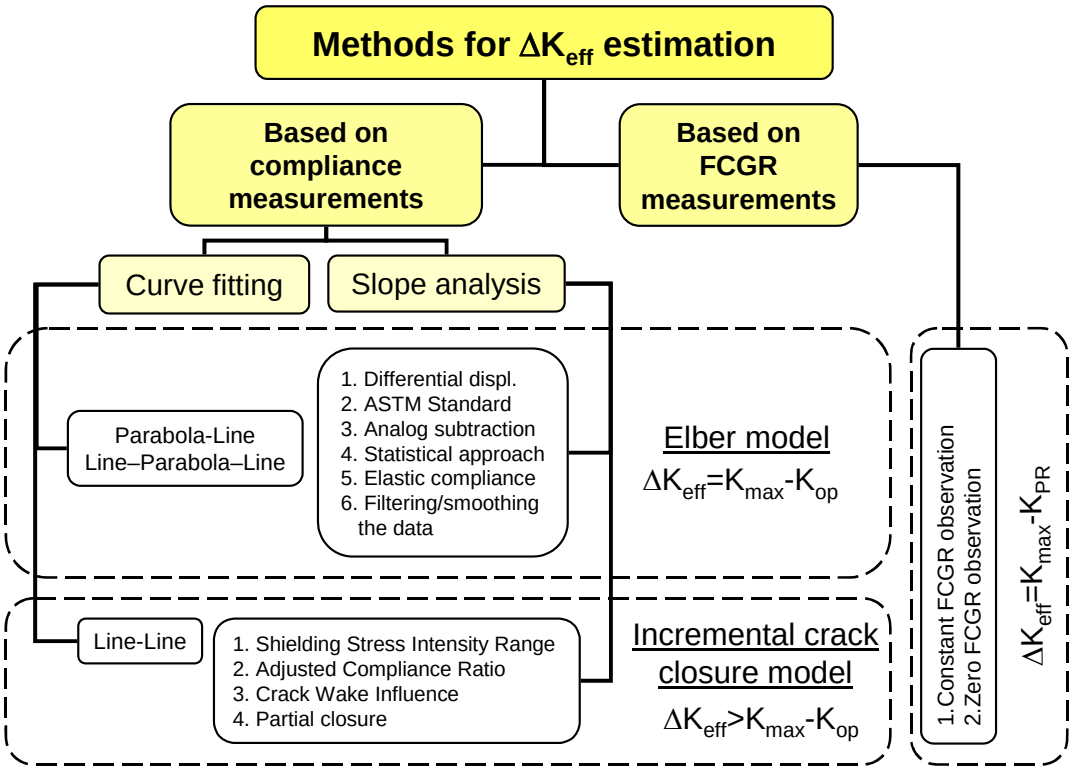

Figure 3 Procedures used for K_{op} or ΔK_{eff} determination

Most of the crack closure studies are based on analysis of specimen compliance and fatigue crack growth rate (FCGR) measurements. For this reason, the present review is focused on compliance-based and FCGR techniques and procedures for crack closure investigations. Figure 3 shows a classification of the reviewing techniques and procedures for ΔK_{eff} determination depending on the performed measurements and assumed models for crack closure. It indicates that there is a distinct separation and some overlapping among different approaches. It can be seen that both curve fitting and slope analysis methods may belong either to the 'Elber' or the incremental crack closure models. On the other hand, FCGR techniques form a separate group which utilizes SIF for crack propagation (K_{PR}), instead of K_{op}.

Compliance based crack opening load determination methods

Methods associated with the Elber crack closure model

A practical application of the Elber crack closure model given by Eq. (1a) requires P_{op} (or K_{op}) to be determined in order to calculate ΔK_{eff}. In other words, the Elber crack closure model assumes that the crack fully opens along the entire crack front at a discrete load, P_{op}, whereas it is closed and fully shielded below P_{op} from any damage related to the applied load. The following section discusses different methods commonly used to determine this P_{op} value.

Visual method

Until 1988, the determination of P_{op} from compliance data had been performed customarily by means of visual judgment regarding the observed non-linearity in the load-displacement curve. At that time, most of the experimental measurement techniques were already developed, however the calculated K_{op} and corresponding ΔK_{eff} did not correlate with experimental data. In some cases the crack closure measurements even increased the scatter in correlation of fatigue crack growth data for the same material investigated [56, 104].

Phillips [11] reported the results from the first ASTM Round Robin exercise on opening load measurements and determination methods. These investigations were conducted in 1989 and involved 11 laboratories. A wide variety of measurement techniques were used to acquire the load-displacement/strain data. The goal was to determine the scatter and repeatability in P_{op} determination by analyzing specimen compliance behavior using several different analysis methods illustrated in Figure 4 and Figure 5.

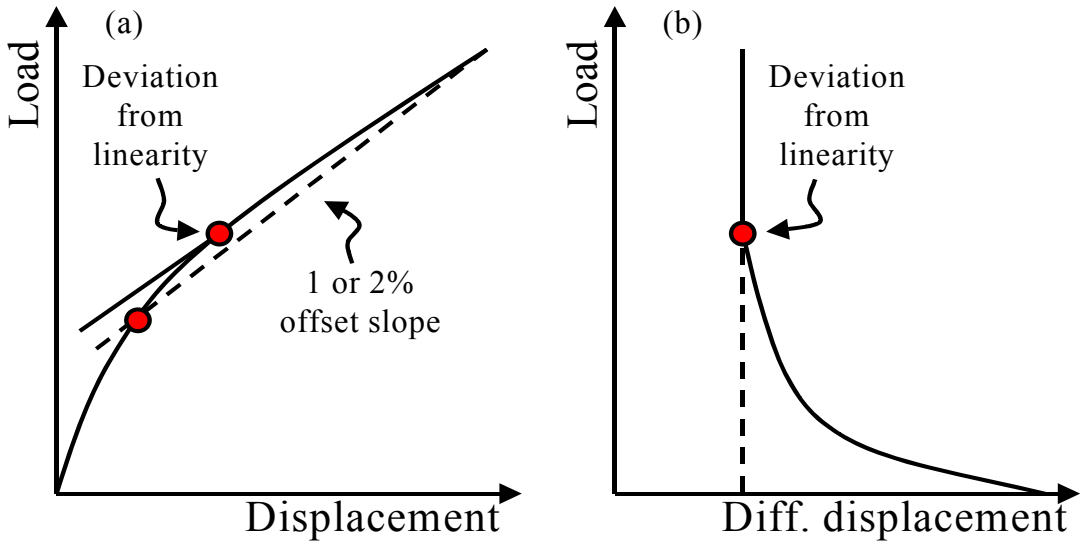

Figure 4 Schematic diagrams of (a) load vs. displacement and (b) load vs. differential displacement

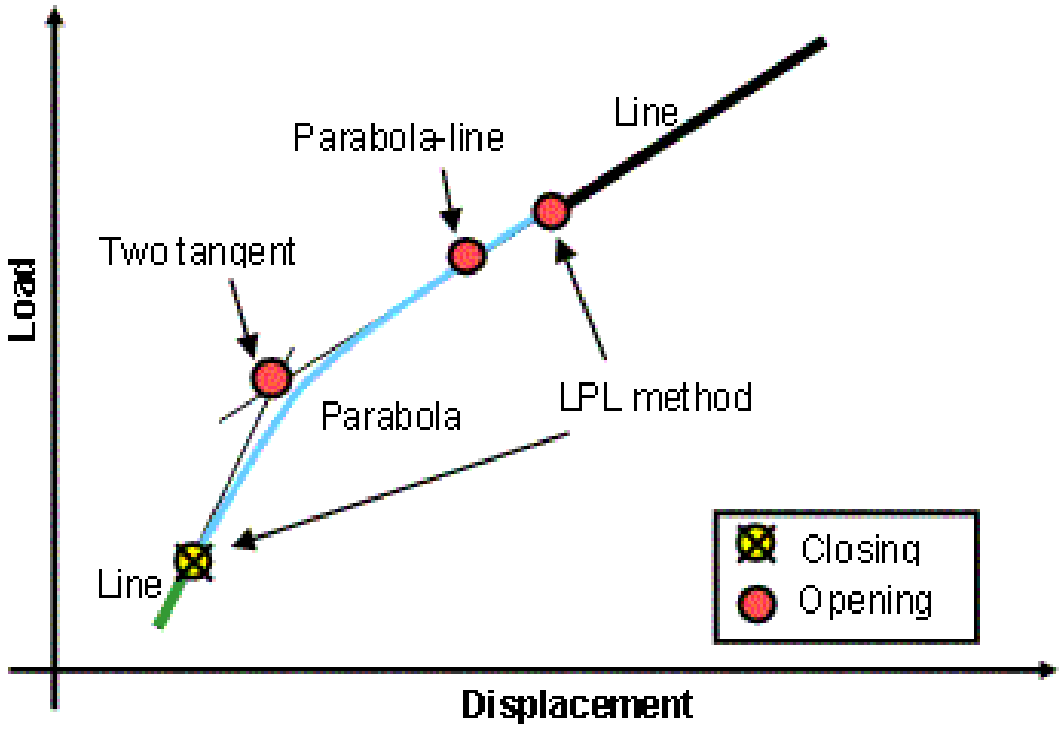

Figure 5 Curve fitting methods

The following methods for P_{op} determination were investigated:

1. P_{op} is the load at which the upper portion of the loading curve deviates from linearity (Figure 4a).
2. Nonvisual 1% offset slope method (Figure 4a).
3. As method 1, but using the differential displacement curve (Figure 4b).
4. The intersection point between two tangent lines, fitted to the upper and lower linear parts of the load–displacement curve (Figure 5).

Methods 1 and 3 contain a high level of subjectivity, since the researcher has to pick the P_{op} point 'by eye'. Also, method 4 has some subjectivity depending on the segments size used for the tangent lines fit. As a result these three methods showed a largest dispersion in P_{op} values. It was believed, that the results would have been improved if a computer program were used instead of the subjective visual analysis. Only method 2 was the 'non-subjective' (nonvisual) approach, which involved computer programming in P_{op} determination. Therefore, it was not surprising that method 2 turned out to be the most consistent in terms of scatter and repeatability. Due to a large overall dispersion of the results reported in the first Round Robin, the following general conclusion was stated: *"The accuracy of the opening-load measurements reported in the Round Robin cannot be determined at present because an accepted method of establishing the "true" opening load does not exist."* Another unexpected observation reported was that *"none of the measurement types or analysis methods showed a systematic change in the opening loads after overload, even though the crack growth showed a large drop in rate or even arrest in some cases. These results suggest that either the opening-load detection methods were not sufficiently sensitive to detect the changes in closure behavior or that closure mechanisms were not responsible for the drop in growth rate."* It was concluded that

in order to achieve more consistent results, a standardized procedure that does not depend on the individual researcher's skill or judgment would be required.

Consequently, ASTM standard E647-99 [104] was implemented and a number of alternative procedures were developed [12, 91, 92, 95, 96, 108, 109, 111, 112, 114, 118, 125].

Compliance offset method

First, Donald [106] suggested that P_{op} could be identified as the point where the slope of the load-displacement curve deviates by some small amount, e.g., 2% offset from the 'linear upper' part of the compliance curve (Figure 4a). In general, the offset procedure underestimates P_{op} because when some percentage of slopes offset is used, that means that the crack is already partially closed. Later, Roberson and Kirk [86] proposed a variation of this procedure, based on Dunnett's [107] statistical analysis. The advantage of this method was that it eliminated some subjectivity associated with the chosen percentage of the slope offset variation. On the other hand, it also caused some disadvantages since the results were varied with the size of the segments used in statistical analysis.

The offset method was examined in the second ASTM Round Robin on P_{op} determination [12] in which 14 laboratories participated. All participating laboratories have used the same test conditions to evaluate: (1) procedures for establishing the acceptability of the raw load-displacement/strain data, and (2) non-subjective methods of analyzing the compliance data to determine P_{op}. The objective of the second Round Robin was to establish a basis for proposing a recommended procedure for P_{op} determination from compliance data. The second Round Robin results demonstrated that the scatter in the P_{op} determination were reduced by 50% or more

when some of the compliance data were excluded from the analysis population based on an accept/reject criterion for raw data quality. The main conclusion was that *"The use of 2% offset criterion in the compliance offset opening load analysis method produced relatively low scatter in opening load values and mean values of opening load that seemed reasonable in terms of collapsing low-R and high-R crack growth results onto a single ΔK_{eff} rate curve."* As a result, the 2% offset method was then adopted into the ASTM standard E647 recommendation [104].

Subsequently, Blandford, Daniewicz and Skinner [108] examined the influence of the length of the opened crack portion of the load-displacement data and the size of the segment in the ASTM standard procedure for P_{op} determination. They argued that this part of the compliance curve should vary with the load ratio considered. One problem associated with their suggestion is that this 'linear' part might vary also with the crack length. However, the question of how to define the 'linear segment' non-subjectively remains open.

Curve fitting methods

In the past, a number of different curve fitting methods have been utilized to analyze load-displacement data. First, Carman, Turner and Hilberry [96] fitted the nonlinear portion of the data with a quadratic polynomial and defined P_{op} as the point where the tangent line becomes parallel to the upper 'linear' portion of the curve. This approach worked well for NCTG method. However, no results for the CMOD method were reported, presumably because the change in the slope is not well pronounced.

Later, Yisheng and Schijve [95, 109] used a similar approach in which they fitted a straight line and quadratic polynomial to the load-displacement data. The

transition point between the straight line and the quadratic polynomial defined P_{op} (Figure 5). This point was determined using nonlinear regression analysis. The advantage of this method was that the results were almost independent of the location of the crack opening displacement gage from the crack tip. Newman [14] confirmed this observation, using computer simulations based on the modified Dugdale strip yield model.

Similarly as Yisheng and Schijve, Xu, Gregson and Sinclair [15] utilized a straight line to the 'upper' part and a quadratic polynomial to the 'lower' portion of the load-displacement data. Each curve was fitted by least squares fit method. They used two numerical methods for determination of P_{op}. In the fist method, P_{op} was defined as the point where the absolute distance between the two curves is minimal. In the second one, P_{op} was defined as the point where the slope difference between the two fitted lines was minimized. For the same test data, the authors also utilized the ASTM standard E647 recommendation [104]. They concluded that the former method gave much more consistent results regardless of the location of the displacement gage.

Slope analysis of the compliance curve methods

A number of researchers have utilized a slope analysis of the compliance curve for P_{op} determination. First, Kim and Song [94] and later Oh et al. [93] determined P_{op} using the differential displacement data (Figure 4b). Load and displacement signals were subtracted using an analog subtraction circuit directly on the load frame (before the discretization). This makes their method very fast and therefore suitable for analysis of variable/random amplitude testing. They defined the slope of the linear portion of the fully open crack as the slope with the highest

probability to occur. The main drawback of this method is that the size of the segments used to calculate the slope has to be chosen arbitrarily (~10% in that study). Also a custom made analog circuit is needed.

On the other hand, Seetharam and Dash [89] used a fourth degree polynomial to fit the entire load-displacement curve. They assumed that the rate of load change with respect to CMOD would decrease only during the crack opening process and stay constant anywhere else. Such an assumption allowed them to determine both P_{cl} and P_{op} values associated with fully closed and fully open crack, respectively. The results were compared with those from the tangent lines method, which were always in the interval between P_{cl} and P_{op}. Subsequently, they examined what hypothetical values of P_{op} are needed in order to collapse the low R data onto the 'closure free' R = 0.7 data. They concluded that none of the methods performed satisfactory in the all investigated cases.

On the contrary, Chen and Nisitani [52] defined P_{op} as the inflection point on the unloading curve. This method proved to be good for steel but could not correlate the fatigue crack growth rate (FCGR) for different R near the threshold. It can be noted that Joyce and Sutton [110] have used this approach earlier for automated J-integral testing.

Recently, Scorupa, et al., [111] argued that even for fully open fatigue crack the compliance would change either due to crack propagation or plastic deformation ahead of the crack tip. Therefore, the only constant slope would correspond to 'true' elastic compliance, which should be the same for both loading and unloading load-displacement curves. This suggestion was supported by experimental observation reported by Chen and Nisitani [52] and Toyosada and Niwa [112]. Chen and Nisitani defined the elastic compliance during unloading as the slope of the uppermost 5% of

the unloading (load-displacement) curve. Then the opening load was determined as the uppermost point on the loading (load-displacement) curve with the same slope. This approach gave satisfactory results for most of the cases studied; however it was shown in [111] that in some cases P_{op} could be significantly underestimated. On the other hand, Toyosada and Niwa defined the elastic compliance in the interval where loading and unloading curves have equal slope. Such definition is the only one that is independent from any arbitrary rigid rotation of the compliance curve. In order to observe the nonlinear behavior in the regions commonly considered to be linear, the differential displacement analysis is needed. This in turn would also increase the noise and, therefore, a reliable smoothing method of the raw data becomes necessary.

Smoothing of the raw data

Several researchers have developed methods for smoothing the raw data by filtering or fitting splines to the data. This is not one of the methods for determination of P_{op} by itself, but can be used to modify anyone of them. Improvement of the noise response is expected in most of the cases. Curve fitting methods; however use least squares minimization procedure, which inherently averages the noise in the load-displacement signal, therefore the effect of the smoothing procedure will be small.

Scorupa, et al., [111] investigated three numerical methods for smoothing the raw data using moving averages, Butterworth filters, and cubic splines. A large variety of random Gaussian errors based on different variation coefficients and frequencies were superimposed on a noise-free load displacement data with a known P_{op}. The comparison was made, based on scatter and bias in the P_{op} results from different methods. The cubic splines method gave the best results. This method consists of dividing the raw data on equal segments and fitting a cubic spline to each

of them. At a joining point each two spline segments must have equal coordinates and first derivatives.

Another method was developed by Dougherty [113] in which he fitted quadratic polynomials to both load and displacement signals separately and then used the fitted data to plot the compliance curve. Although there is no systematic study on how this method will compare with any of the other numerical procedures it can be inferred that this is the best method in terms of speed and simplicity.

On the other hand, Daniewicz [114] constructed a far more sophisticated low pass filter to smooth the experimental load-displacement data. He represented the data with Taylor series and estimated the error term, using dynamic programming methods. This makes the method 'adjustable' to a different amount of noise in the data. It can be speculated that it should give results independent of the measurement method and the gage location. However, this statement awaits further experimental verification, especially for different R values or overload situations.

In conclusion, any 'traditional' analog filter could be replaced by an equivalent or better, computerized numerical procedure. It is suggested that the raw data should be stored also for any necessary further references.

Methods associated with the incremental crack closure model

In general, the crack does not open along the entire crack front at a 'distinct' load, P_{op}, but rather it opens incrementally over some range of the applied load. Similarly, the crack does not close instantly below P_{op}, but it also closes incrementally as shown in Figure 6.

In Figure 6 a rigid wedge having the shape of the crack at load P_{op} is inserted to simulate ideal CC throughout the whole crack length (dashed line). The same crack

containing only segment of the rigid wedge (hatched region) will close incrementally.

This well recognized incremental crack opening/closure phenomena would perhaps also induce incremental crack-tip shielding effect. Therefore, during the last several years a number of approaches have been proposed in order to modify the conventional ΔK_{eff} calculations. These approaches account for an additional damage associated with the load below P_{op}.

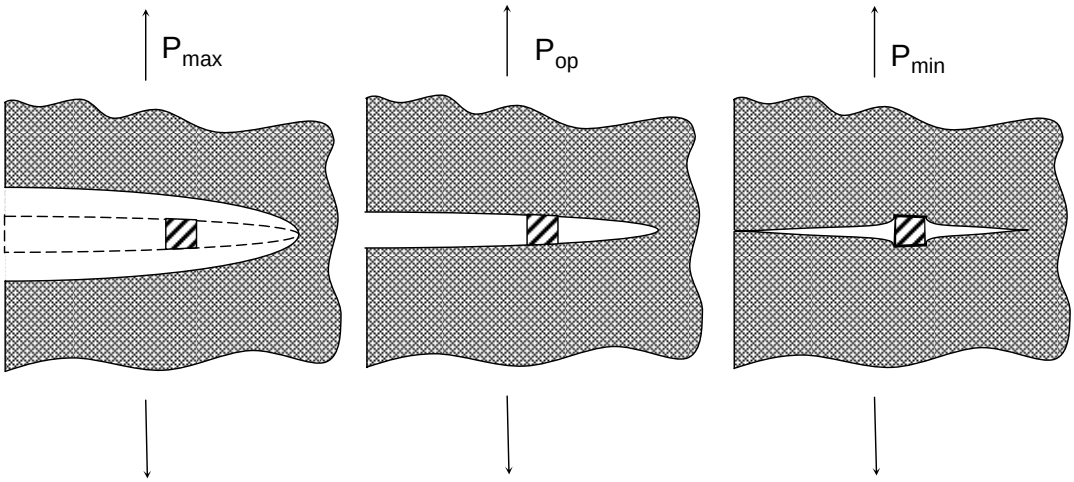

Figure 6 Partial crack closure

Shielding stress intensity range approach

Weiss, Chen and Stickler [115], observed that an additional damage below P_{op} has to be included in order to collapse crack growth data for negative R into closure free data. Based on elastic consideration of compliance variations a new approach was proposed. Accordingly, a modified effective SIF range, ΔK_{effM}, was defined as:

$$\Delta K_{effM} = \Delta K - \Delta K_{sh} \qquad (1.2)$$

ΔK_{sh} is the shielded range of the SIF range defined as the difference between the K_{sh}

and K_{min} as it is illustrated in Figure 7.

The authors showed that the ΔK_{effM} values were invariant of the testing conditions and crack length. This approach clearly indicates that the shielding effect induced by crack closure determined from compliance measurements is relatively small. It can be noted that this observation is in agreement with earlier suggestions of Sadananda, Vasudevan and Louat [116] who argued that Eq. (1.1a) excessively overestimates the shielding effects of plasticity induced crack closure.

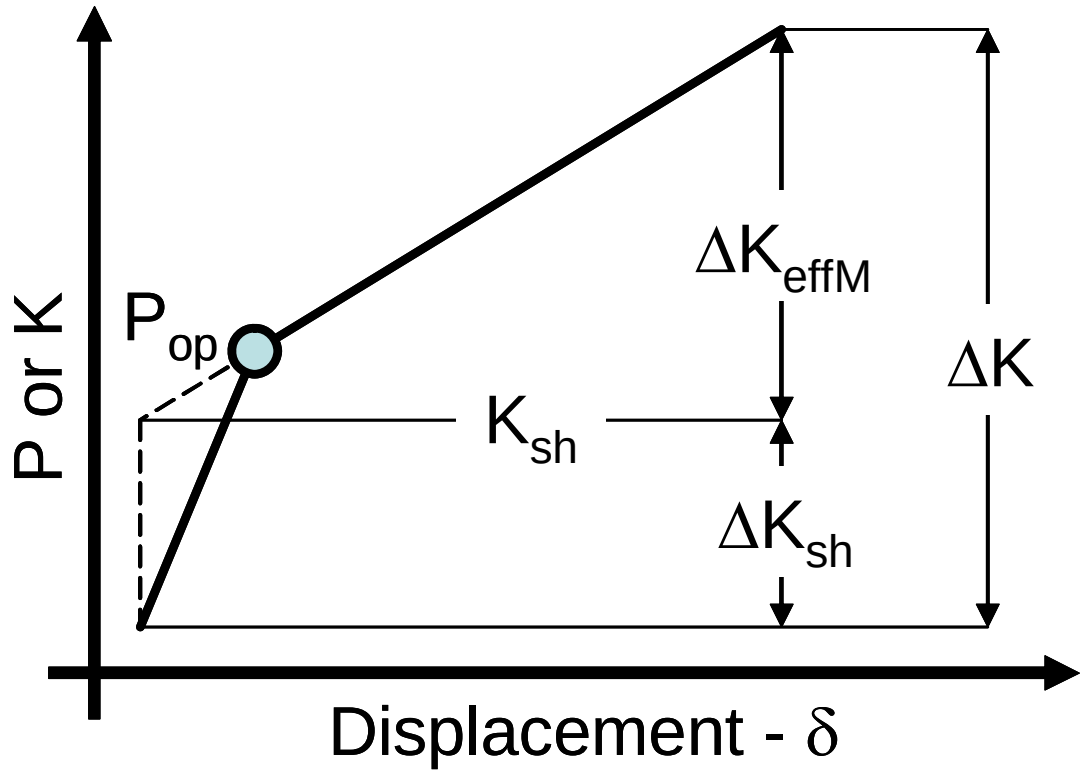

Figure 7 Shielding stress intensity range method

Crack wake influence model

In 1997, Donald [92] found that the effects of R on the da/dN data near threshold could not be explained using the conventional ΔK_{eff} approach, so-called

Donald's effect. Soon after this observation, together with Connelly, Paris and Tada, he proposed a new empirical approach for ΔK_{eff} estimation using the Crack Wake Influence (CWI) model [81].

Basically, it is a mathematical model of the influence of a contact force somewhere at the crack wake, on the stress intensity factor at the crack tip. Subsequently, the effective SIF, K_{eff}, can be calculated as:

$$K_{eff} = K - K_{cwi} \tag{1.3}$$

In Eq. 1.3, K_{cwi} is the SIF due to the contact force in the crack wake and K is the SIF due to remote stress.

The CWI model provides a theoretical basis for two other approaches known as an adjusted compliance ratio and a partial crack closure model.

Adjusted compliance ratio method

Figure 8 illustrates the adjusted compliance ratio (ACR) method [90]. The ACR value is determined by subtracting the compliance prior to the initiation of a crack, C_i, from the secant compliance, C_s, and the compliance above the opening load, C_o, as follows:

$$ACR = \frac{C_s - C_i}{C_o - C_i} \tag{1.4}$$

This ratio appears to be independent of the measurement location and can be used to directly calculate the effective cyclic stress intensity.

$$\Delta K_{eff} = ACR \cdot \Delta K \tag{1.5}$$

The *ACR* represents the shielding effect at the crack tip due to the closure action in the crack wake. It can be noted that without direct measurement of the P_{op} the *ACR* accounts for the shielding effect due to crack closure.

Later it was recognized that the ACR method is a reasonable approximation only if the force distribution on the crack wake surfaces is fairly uniform. However, due to crack profile considerations (especially at stress ratios progressively greater than R=0) the force distribution should be greater near the crack tip.

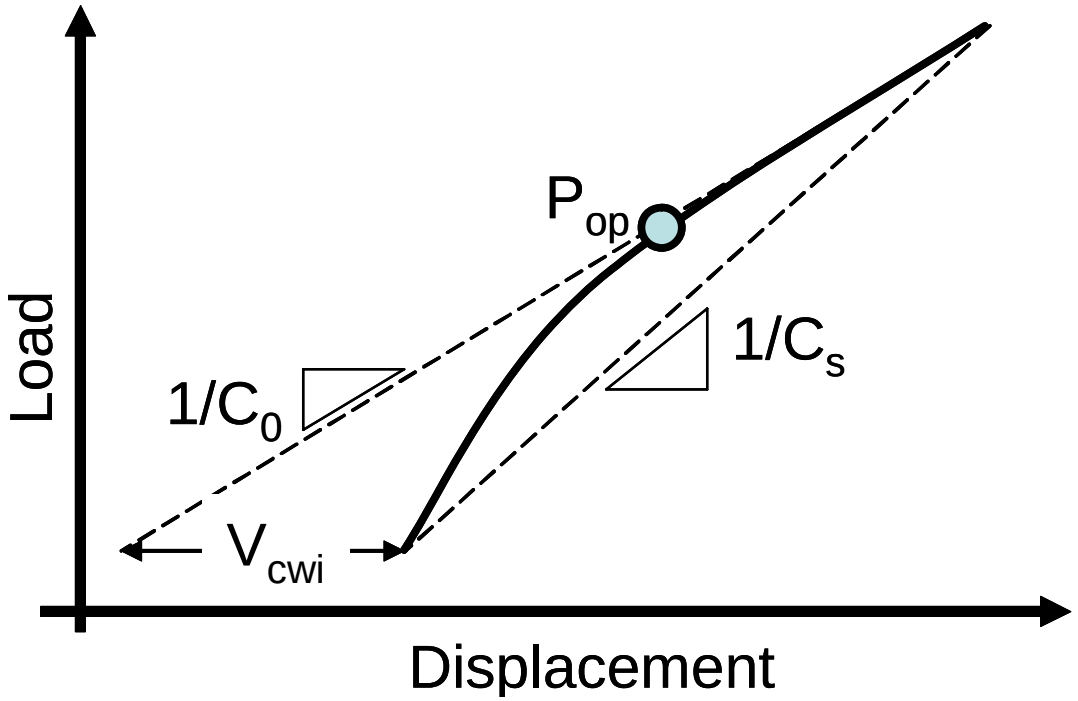

Figure 8 Adjusted compliance ratio method

Furthermore, the role of plasticity-induced closure is enhanced as K is increased due to the transition from plane strain to plane stress behavior. This will also modify the force distribution. Therefore, the following modification of the ACR method has been proposed [91]:

$$ACR_M = \frac{C_s - C_n}{C_0 - C_n} \qquad (1.6)$$

In this Eq. 1.6, C_n is the average value of two slopes, first between 2% and 12% of ΔP_{appl} and the second between 9% and 19%. It was found that the ACR_M is

independent of the gage location, specimen geometry, and the applied SIF, and weakly dependent on the crack length [91].

The above-mentioned observations and conclusions, concerning the ACR method are supported by a recent investigation, conducted by Donald and Phillips [118]. They analyzed the load-displacement data from the second ASTM Round Robin program on opening load measurement, using both ASTM and ACR methods.

From comparison of Eq. 1.6 with Eq. 1.1b it is seen that the ACR is equivalent to Elber's stress intensity ratio, U.

McClung [140] in his extensive investigations of the influence of K_{max} on U stated that there are three distinct regions for U variations, namely:

1. Near the threshold U decreases with increasing K_{max},
2. In the Paris region U is independent of K_{max}, and
3. At high ΔK values, U decreases with increasing K_{max}.

McClung's observations should be also applicable to ACR, since U and ACR are equivalent. Recently, Donald et al. [90] showed that the fatigue crack growth rate is not determined solely by ΔK_{eff}, but also depends on K_{max}.

Partial crack closure model

Partial crack closure model accounts directly for the crack-tip damage below the opening load [91] due to interference behind the crack tip (crack wake). The crack wake interference is modeled as a thin rigid wedge of uniform thickness inserted with a small gap from the crack tip. The SIF associated with the inserted wedge, K_w, can be calculated [117] as:

$$K_w = \frac{Et}{\sqrt{2\pi d}} \qquad (1.7)$$

In Eq. 1.7, E is the modulus of elasticity, t is 1/2 of the wedge thickness, and d is the

distance between the wedge and the crack tip. On the other hand, when only an external load is applied the corresponding SIF, *K*, is expressed as:

$$K = \frac{Eh}{2}\sqrt{\frac{\pi}{2d}} \tag{1.8}$$

In Eq. 1.8, *h* is 1/2 crack opening displacement at distance *d* from the crack tip. Combining Eqs. 1.7 and 1.8 and noting, that K = K_{op} when *h* = *t* the following relation is obtained:

$$K_w = \frac{2}{\pi}K_{op} \tag{1.9}$$

Equation 1.9 indicates that the actual damage is extended below K_{op} down to $(2/\pi)$ K_{op}. Therefore, ΔK_{eff} can be estimated as:

$$\Delta K_{eff} = K_{\max} - \frac{2}{\pi}K_{op} \quad \text{if} \quad \frac{2}{\pi}K_{op} \geq K_{\min} \tag{1.10a}$$

$$\Delta K_{eff} = K_{\max} - K_{\min} \quad \text{if} \quad \frac{2}{\pi}K_{op} < K_{\min}\,. \tag{1.10b}$$

Equation 1.10 dramatically improved the correlation of data at the near threshold region; however in the Paris region the conventional Elber model given by Eq. 1.1a demonstrated better correlation than the partial crack closure approach.

Recently, Kujawski [119] proposed a modification of Eq. 1.10a as follows:

$$\Delta K_{eff} = K_{\max} - K_{op}\left[1 + \left(\frac{2}{\pi} - 1\right)g\right] \tag{1.11}$$

by introducing a transition function g given as

$$g = \exp - \left(\frac{K_{\max}}{K_{\max\ th}} - 1\right) \tag{1.12}$$

In this equation $K_{max\ th}$ is the maximum SIF at threshold for a given R. The g function transforms gradually Eq. 1.10a into Eq. 1.1a as K_{max} increases from the threshold to its higher values in the Paris region. In other words, g = 1 when $K_{max} = K_{max\ th}$, and g

= 0 when $K_{max} >> K_{max\ th}$. This function was found to be very effective and consistent in the correlation of R effects for both long and short fatigue crack growth [120].

Zero crack propagation load method for K_{pr} determination

In order to investigate the SIF corresponding to crack propagation, K_{PR}, the following experimental procedure could be utilized as it is illustrated in Figure 9. A specimen is cycled with ΔK value, which is somewhat larger than the expected ΔK_{th}. If for such loading the FCG does not occur, then K_{max} is increased by a small increment δ keeping the ΔK constant. This procedure is repeated until the crack starts to propagate continuously. Then, the K_{PR} is calculated as a value between $K_{max} - \Delta K_{th}$ and $K_{max} - \Delta K_{th} - \delta$. This method was initially proposed by Pellas, Buaudin and Roberts [121] and also used by Marci [122-124], Doker and Bachmann [125].

Huang, Lang, Wu and Doker [13] used the NCTG, CMOD, and potential drop measurement to obtain the compliance data. The tangent lines method was used to calculate P_{op}. The results were compared with P_{PR} determined using the zero crack propagation load (ZCPL) method. The tangent lines method gave significantly lower results than ZCPL regardless of the compliance measurement used. The ZCPL results are considered to be correct, since they were able to collapse FCG data for different load ratios. It seems that the ZCPL method could be suitable for fundamental studies of load history effects and related phenomena. A drawback of this method is that a precise value of ΔK_{th} for the different R has to be known in advance. Also it requires more time to acquire the P_{PR} value than any other method.

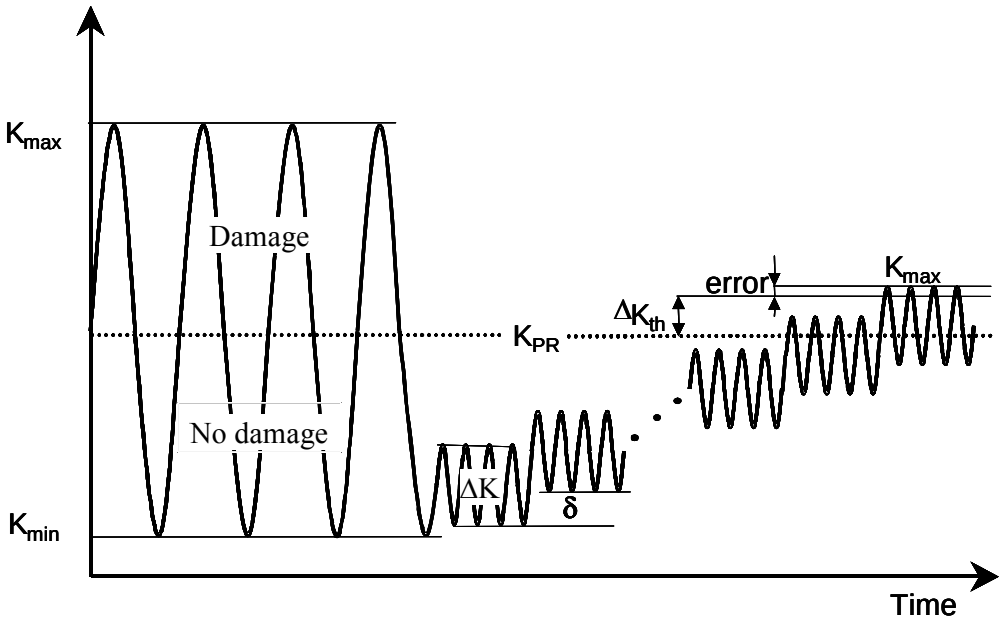

Figure 9 Schematic illustration of the zero crack propagation load method

Recently, Lang [126-127] adopted the ZCPL method to study the load interaction effects. The predictions showed fairly good correlation with the experimental results.

A similar approach was used earlier by DeKoning [129]. Instead of using blocks with constant ΔK, he used blocks with constant K_{min}. He then increased the maximum load until crack propagation occurred. Another variation of this method was proposed by Pelloux [130]. He kept the maximum load constant while decreasing K_{min}. The opening load was defined as the point where the striation spacing stops to grow.

Later Sunder and Dash [131] did not use block loading at all. Instead they kept K_{max} constant and varied K_{min} (either decreasing or increasing). They found that the striation spacing increased proportionally to ΔK only until K_{op} was reached. The absence of load blocks makes this method very fast, compared with the other methods in this group, but also limits the applicability only to materials and load conditions

that will produce striations.

Problems with the existing methods for P_{op} determination

Using numerical analysis Newman [14] demonstrated that the P_{op} determined from the load-displacement data is independent of measurement location behind the crack tip. That means that P_{op} determined from CMOD and NCTG measurements should be the same. In practice, experimental data usually indicate that the NCTG yields higher P_{op} than CMOD. Observed differences appear to be caused by noise and nonlinearity in the measurement systems used. This calls for improvement of the measurement or analysis methods of the raw data.

Another comparative study with FEA was conducted by Tsukuda et al. [50]. For a medium carbon structural steel he compared the readings among surface strain (SS), NCTG, and FEA calculations at the same location. Experimental crack closure was registered only for R below 0.5, whereas for R>0.5 the crack was open during the whole loading cycle. In contrary, from the finite elements simulation, this boundary was at R = 0.7, perhaps due to increased sensitivity of FEA.

In contrast, Booth and Maddox [104] found out that there is better correlation between the crack growth rates for different load ratios (between 0.67 and -4) if the crack closure is ignored all together. Assuming $\Delta K_{eff} = K_{appl}$, in their analysis the negative part of the applied load was neglected . The study was conducted on three different C-Mn structural steels.

Similarly, Vecchio, Crompton and Hertzberg [56] investigated Astroloy nickel based alloy with two different grain sizes. They found excellent agreement of the crack growth data as a function of applied SIF (ΔK_{appl}). This calls for equal ΔK_{eff} independent of R, however the experiments indicated significant differences among

P_{op} levels for different R investigated.

In other studies, Allison and You [84] compared the ASTM standard and tangent lines methods for P_{op} evaluation for reinforced 2124 Al alloy. They found out that ASTM with 1% compliance offset overestimates, with 5% offset underestimates, and tangent lines method underestimates the value of P_{op} even more. The best correlation between the FCGR data for different R was achieved using 2% offset in the Paris region and 1.5% offset in threshold. For the same material, without reinforcement, the best results were obtained with 15% offset in the Paris region. No good correlation in the threshold was found, even with the tangent lines method. The only conclusion is that the P_{op} is both material and stress intensity dependent.

On the other hand, Vecchio, Crompton and Hertzberg [56] investigated artificial crack closure simulated by inserting a needle tip into the crack mouth at various positions behind the crack tip. In another test Hertzberg, Newton and Jaccard [85] used shims instead of needle tip inserted into the crack wake In all these cases P_{op} was recorded, but the crack growth rate failed to decrease to the level, suggested by the measured P_{op}. The experimental results were confirmed also using FEA. Finally, they concluded, "*either the crack closure is not the only mechanism influencing the crack driving force, or the crack closure measurements were not correct.*"

It can be noted that Schijve [142, 143] was the first researcher who indicated that crack closure is responsible only for half of the effects on the crack growth behavior due to prestraining caused by large scale yielding. Later, Garz and Jones [53] showed that the nonlinearity in the unloading curve is different for compact tension and rotating bending specimens. Also, P_{op} was much lower than needed for a good correlation of the results for different R.

Conclusions of the review

From the review of studies on opening load determination methods it is seen that the emphasis is on collapsing the FCGR data for different R into a single curve using ΔK_{eff} dominates as a judging criterion. For most materials, the FCGR rate data for different load ratios cannot be collapsed to a single curve through the whole stress intensity range (from the threshold to the Paris region and above). Also, the experiments with artificially induced crack closure do not show the expected FCGR behavior.

Although literature is available for the Elber and incremental crack opening/closure models, the former has drawn the attention of a greater number of researchers. The Elber P_{op} load model assumes that the crack tip is fully shielded from any load below P_{op}. Numerous references, which in the last 30 years signaled some kind of difficulties with this traditional crack closure model, were ignored. Only recently more attention has been devoted on the incremental crack closure models, which recognize that the crack opening/closing phenomenon as well as the shielding effect is also incremental. These approaches account for additional damage associated with the load range below P_{op}. It is still not clear if these methods can solve all the problems mentioned in this review.

Overall, it seems that no consensus can be stated on how to measure and analyze crack closure, despite reviewing 35 years of research in this area.

In order to achieve more fundamental data, automated test procedures and analysis methods should be developed. This would minimize the existing margin of subjectivity in the analysis of the raw load-displacement data. Further improvement can be achieved through improving the noise sensitivity of the opening load determination procedures or more accurate modeling of the nonlinear regions of the

load displacement curve. All these suggestions are adressed in the next sections and two new methods for P_{op} estimation are developed.

New methods for opening load determination

Two methods were developed as a part of this dissertation in order to address the concerns raised in the previous section.

First, the Line–Parabola–Line (LPL) method was developed because it offers a more accurate representation of the load – displacement curve. Naturally, it requires much more computational resources than any other method which limits its usefulness in the practice.

Second – the quadrature (Q) method was designed to include the partial crack closure model into consideration. It is also very fast and numerically stable, which reduces the scatter in the opening load estimations.

Line-parabola-line method

LPL method (Kujawski and Stoychev [145]) was developed recently as a variation of the curve fitting procedures described in the literature review. This method is described graphically in Figure 5. First the parabola is fitted between the two chosen transition points, using least squares procedure:

$$P(\Delta) = p_1\Delta^2 + p_2\Delta + p_3 \qquad (1.13)$$

This part of the load displacement curve represents the partially opened crack. The lower and upper portions of the load-displacement curve, corresponding to fully closed and fully opened crack, respectively are represented by straight lines. The coefficients, needed to define the upper line were calculated, assuming that it intersects the parabola at the transition point and also has the same slope as the

parabola at that point. Thus the resulting load displacement curve is both continuous and smooth at the transition point:

$$\begin{Vmatrix} L(\Delta) = P(\Delta) \\ L'(\Delta) = P'(\Delta) \end{Vmatrix} \Leftrightarrow \begin{Vmatrix} l_1\Delta + l_2 = p_1\Delta^2 + p_2\Delta + p_3 \\ l_1 = 2p_1\Delta + p_2 \end{Vmatrix} \qquad (1.14)$$

This system of equations can be solved easily for l_1 and l_2:

$$\begin{aligned} l_1 &= 2p_1\Delta + p_2 \\ l_2 &= P(\Delta) - l_1\Delta \end{aligned} \qquad (1.15)$$

The same procedure is followed to find the coefficients of the lower linear fit.

Next, both transition points, between the parabola and the straight lines were varied and the correlation factors for all possible positions were calculated using the following formula:

$$C = \frac{1}{\sum (\text{Fitted} - \text{Experimental})^2} \qquad (1.16)$$

In Eq. 1.16, 'Fitted' and 'Experimental' refer to the values of the load.

A matrix with the correlation factors was then generated, where rows correspond to the first and columns to the second transition point, respectively. The matrix element with the largest value of the correlating factor represents the "best fit". The transition points, corresponding to the "best fit" constitute the boundary for the partially opened crack. Beyond these points, the crack is either fully opened or fully closed. As a result, the LPL procedure is the only method that identifies two boundary points, these points correspond to crack opening and crack closing load, respectively.

LPL method can be implemented also using slightly different algorithm. The lines can be fitted first and the coefficients of the parabola determined using the same boundary conditions (Eq. 1.14). Both algorithms were proven to be equivalent in terms of results and computation time, using MatLab.

Another variation of the LPL method (LPL2) can be obtained by simply fitting both lines and the parabola between them using least squares procedure. This improves the correlation between the model and the experimental data but also causes the resulting curve to be discontinuous.

Lately, Tada and Paris [144] provided an analytical solution for the load-displacement curve in the case of partial crack closure due to a rigid wedge with arbitrary dimensions and position. Their analytical analysis shows that:

1. The load-displacement curve is linear for fully closed or fully opened crack.
2. For partially opened or closed crack they indicated that a second order polynomial could be a good approximation.
3. The transition between the linear and nonlinear parts in the load-displacement curve should be smooth with equal coordinates and slopes.

Thus, the Tada and Paris analysis provides the theoretical basis of the LPL method.

Quadrature (Q) method

The ASTM standard E647 recommendation procedure for P_{op} determination from compliance measurements is based on numerical differentiation algorithm, making the noise in the experimental data major source of problems, especially in the threshold region. With this in mind, a new method for P_{op} determination was developed (Kujawski and Stoychev [132]), based on integration rather than differentiation of the compliance data. This gives the name of the method – 'Q' (from quadrature – numerical integration). The scatter in the opening load estimations is

reduced simply because the numerical integration algorithms (like trapezoidal rule for example) are stable and easy to implement. Here the derivation of the Q method is discussed together with its relation to the ASTM procedure, and both methods are used to analyze experimental data of 2324-T39 and 7475-T7351 Al. alloys, tested at 0.1 and 0.9 load ratios. On average, the crack opening load values from the Q method are smaller by a factor of $2/\pi$ in comparison to those obtained from ASTM procedure.

Derivation

Load-displacement curves for ideal and partial crack closure are shown schematically on Figure 10a and b, respectively. If there is no CC, the area A_{ABC} can be calculated using compliance C_0 when the crack is open.

$$A_{ABC} = \frac{C_0(\Delta P)^2}{2} \qquad (1.17)$$

The 'real' area A_Q under the load-displacement curve represents the effect of crack closure. The difference between these two areas, A_{cl}, is called 'closure area' and can be calculated as:

$$A_{cl} = A_{ABC} - A_Q \qquad (1.18)$$

In the case of ideal CC, A_{cl} forms a right triangle ADE (Figure 10a). For PCC the associated 'closure area' (Figure 10b) can be represented by the equivalent right triangle AD'E' which corresponds to an ideal CC behavior. The 'closure areas' can be calculated from

$$A_{cl} = \frac{C_0(P_{op} - P_{\min})^2}{2} \qquad (1.19)$$

Substituting Eqs. 1.17 and 1.18 into Eq. 1.19 and solving for P_{op} we get:

$$P_{op} = P_{\min} + \sqrt{(\Delta P)^2 - (2/C_0)A_Q} \qquad (1.20)$$

Two limits for P_{op} can be derived from Eq. 1.19, for $A_{cl} = 0$, $P_{op} = P_{min}$ and for $A_{cl} = A_{ABC}$, $P_{op} = P_{max}$, which corresponds to no-closure and full-closure situations, respectively.

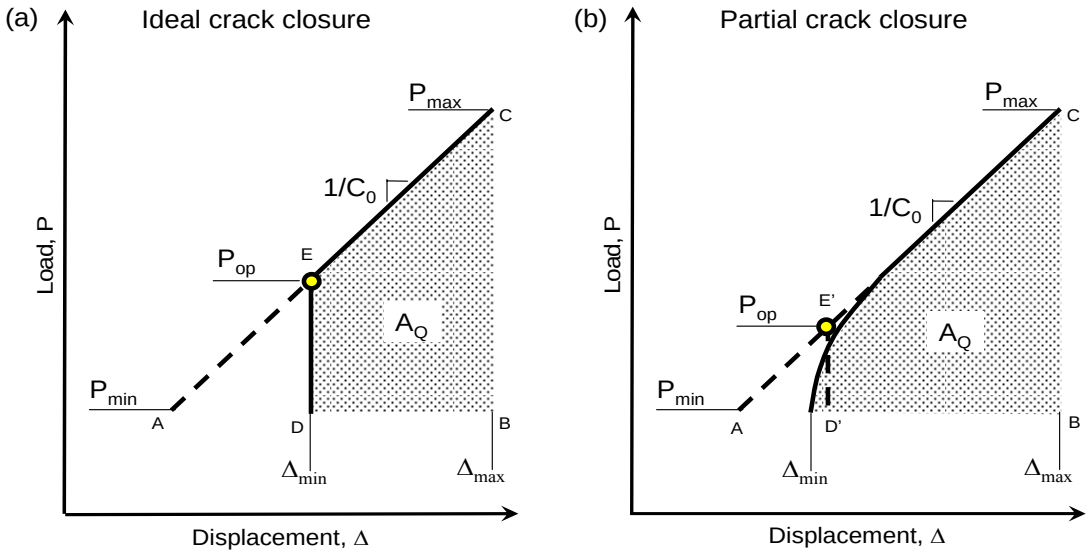

Figure 10 Illustration of the Q method for (a) ideal crack closure and (b) partial crack closure

Theoretical comparison with ASTM standard method

Figure 11 shows four cases of crack closure. The crack is shown in all cases at maximum load, P_{max}. In case (a) a rigid wedge having the shape of the crack at load P_w is inserted to simulate ideal CC throughout the whole crack length. Horizontal dashed lines in Figure 11 correspond to P_w. The other cases (b, c, and d) show the same crack containing different segments of the rigid wedge (hatched region). For all cases the crack faces would contact the inserted wedge during unloading when $P = P_w$. The graphs on the left show P versus crack mouth opening displacement (CMOD) curves. Also on these graphs the values of P_{op} are indicated as determined using Q and ASTM methods. The graphs on the right show P versus CTOD curves together

with the 'real' P_{op} values (at the crack tip). All four possible cases of crack closure are analyzed in detail below.

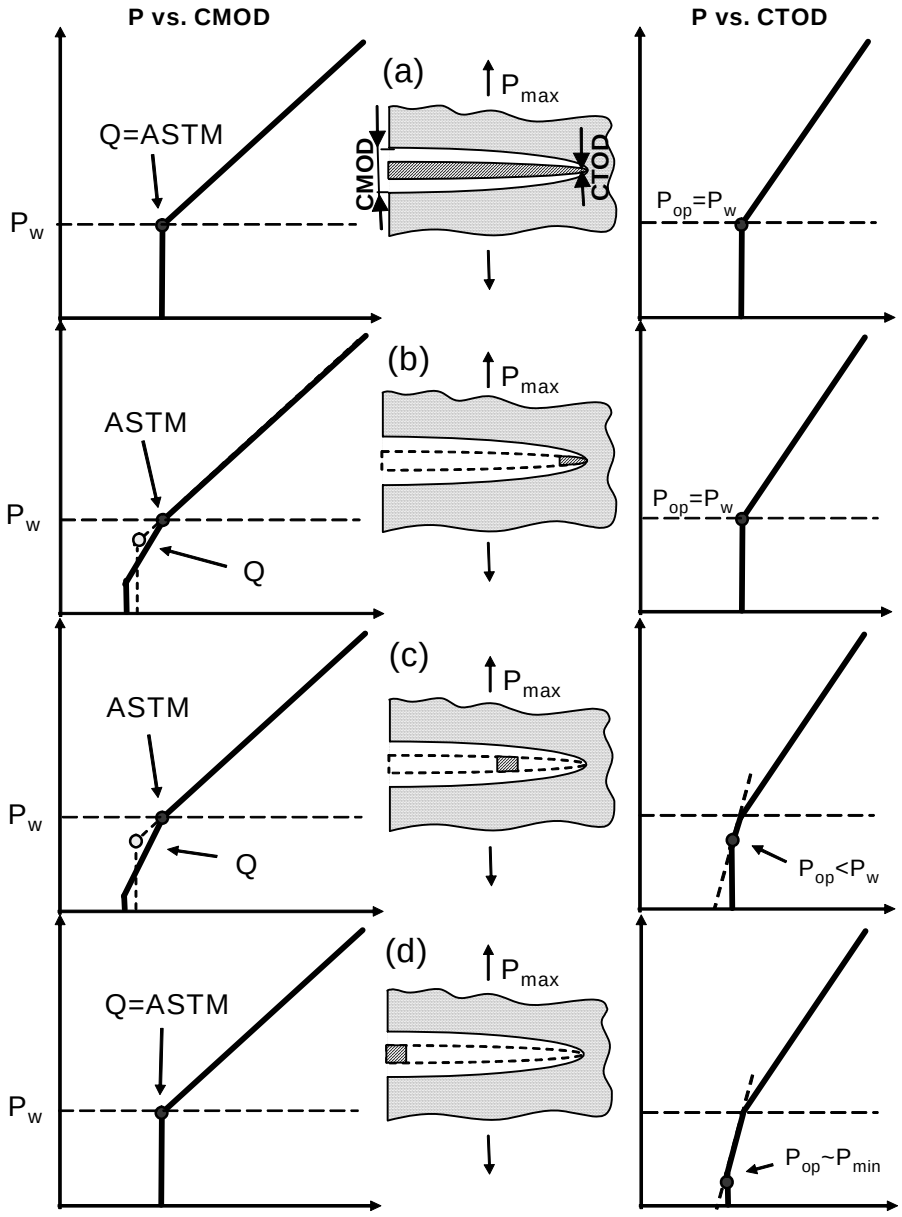

Figure 11 Theoretical comparisons between Q and ASTM methods

In the case of ideal crack closure (Figure 11a), the crack closes along the

whole length at the same time (full shielding effect, or 'Elber' crack closure). In this case there is no difference between the CMOD and CTOD curves. Theoretically, both Q and ASTM methods should give the exact values for opening load, $P_{op} = P_w$. However, the real CMOD data contains noise and ASTM method requires at least 1%, 2%, or 4% compliance offset to occur in order to register P_{op}. This affects the accuracy of the ASTM method because P_{op} will be always somewhat lower than the real value of P_w. On the other hand, the Q method does not require any arbitrary offset and is expected to give the exact result in terms of accuracy. Regarding the precision, Q method is also advantageous since the numerical integration of the whole curve is more stable than the differentiation which is performed using small segments.

If crack starts to close from the tip (Figure 11b), the tip will be shielded immediately at $P_{op} = P_w$. However, the crack mouth displacement will continue to decrease with a slower rate and eventually stop before reaching P_{min}. Due to the noise in the raw data the ASTM method will detect the first 1%, 2%, or 4% compliance offset, i.e. $P_{op} \approx P_w$. The Q method will give $P_{op} < P_w$, corresponding to A_{cl} that is transformed to a right triangle (Figure 10b). There are two factors that minimize the error. First, metals have significant stiffness which makes the shape of the 'closure area' almost a right triangle (especially in the threshold region). Second, the crack can actually close at the mouth as well, before the load is reduced to P_{min}.

In general, crack closure can occur at some arbitrary position along the crack (Figure 11c). In this case the ASTM method will register the load of the first contact between the crack faces as $P_{op} = P_w$. Both crack mouth and crack tip will continue to experience deformation below P_w. The actual opening load at the crack tip will be bounded by P_{min} and P_w. The Q method will adjust the P_{op} value by transforming the

'closure area' at the crack mouth to a right triangle (Figure 10b). This will result in the P_{op} value somewhere between P_{min} and P_w. In general, the Q method is sensitive to partial crack closure (PCC) whereas the ASTM procedure is not. It is expected that the Q method will give P_{op} close to the opening load at the crack tip.

Finally, crack can start to close from the mouth (Figure 11d). This is a limiting case and is not likely to be observed in the practice. Both Q and ASTM methods (and any other compliance based method) will register erroneous $P_{op} = P_w$. It will correspond to the point where the crack mouth touches the wedge. The crack tip however will continue to deform, causing more damage at the crack tip. Thus, both methods will give the same error in this hypothetical case.

The proposed Q method (and any other compliance based method) is phenomenological because it is impossible to relate mathematically the crack 'closure area' at the crack mouth to any of the fatigue mechanics parameters at the tip (K, G or J) without knowing the area and the position of the contact of crack faces.

Parametric study on the variability of the opening load determination

In the previous sections, the most commonly used methods for determinations of P_{op} were reviewed. Based on this review, the methods shown in Figure 12 were selected as most promising candidates for further evaluation. In addition, a variations of PL and LPL methods are also included in the evaluation, in particular PL2 and LPL2 variations, which are not shown on the block diagram for clarity. Each of the methods for P_{op} determination shown in Figure 12 has its own set of parameters that can be 'adjusted'. These parameters were varied independently (one by one) within the recommended intervals in order to assess the scatter in the crack opening load. Comparisons among different methods of analyses will be discussed together with the

implications on fatigue crack growth correlations at the end of the section.

The methods in Figure 12 are divided in two groups – partial and full crack closure methods. The full crack closure methods register the first onset of nonlinearity in the load-displacement curve during unloading as P_{op}. An assumption is made that the deformations at the crack tip (and therefore the fatigue damage) stop as soon as the crack faces touch anywhere behind the crack tip. Partial crack closure methods on the other hand, recognize the possibility that this contact does not necessary occur immediately along the whole crack wake (ideal crack closure as defined by Elber). Therefore instead of finding the load at which the crack starts to close, they are aimed at the load where crack tip is effectively shielded from further deformation by the contact or contacts in the crack wake. This causes P_{op} determined with partial crack closure methods to be smaller than the full crack closure estimates by approximately a factor of $2/\pi$ (calculated theoretically by Donald and Paris [91]).

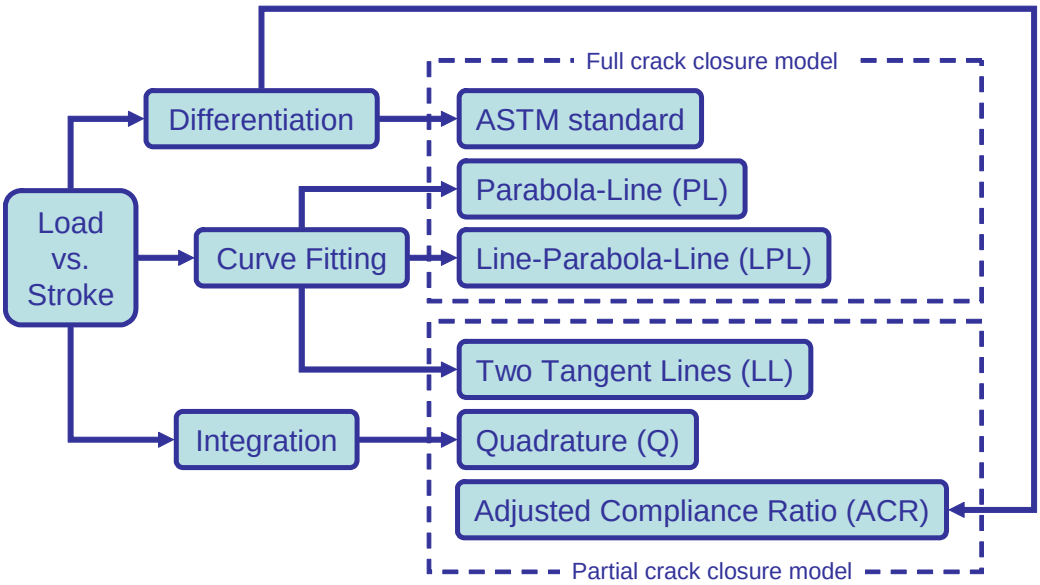

Figure 12 Classification of the investigated methods for P_{op} determination

Specimen and testing procedure

The load-displacement data were obtained from 2324-T39 and 7475-T7351 aluminum alloys. The specimen geometry is shown in Figure 13.

Specimens with the thickness of 2.54 and 5.08 mm were used to generate the data. Each specimen was precracked using compression-compression loading in order to minimize any load history effects [146]. Then, a constant load range scheme was applied in tension at a load ratio R = 0.1. The tension tests were started with a ΔK value somewhat smaller than the expected threshold level. If no crack propagation was observed for 10^6 cycles, then the ΔK value was increased by 0.1 $MPam^{0.5}$. Once progressive crack growth rate was achieved, the specimen was cycled at that constant ΔP value until failure. Figure 14 graphically illustrates the above testing procedure.

During the test, digital pictures of the crack tip area were taken using a Charge Coupled Device (CCD) camera with a resolution of 10^6 pixels. This allowed for 5μm resolution in the crack length measurement.

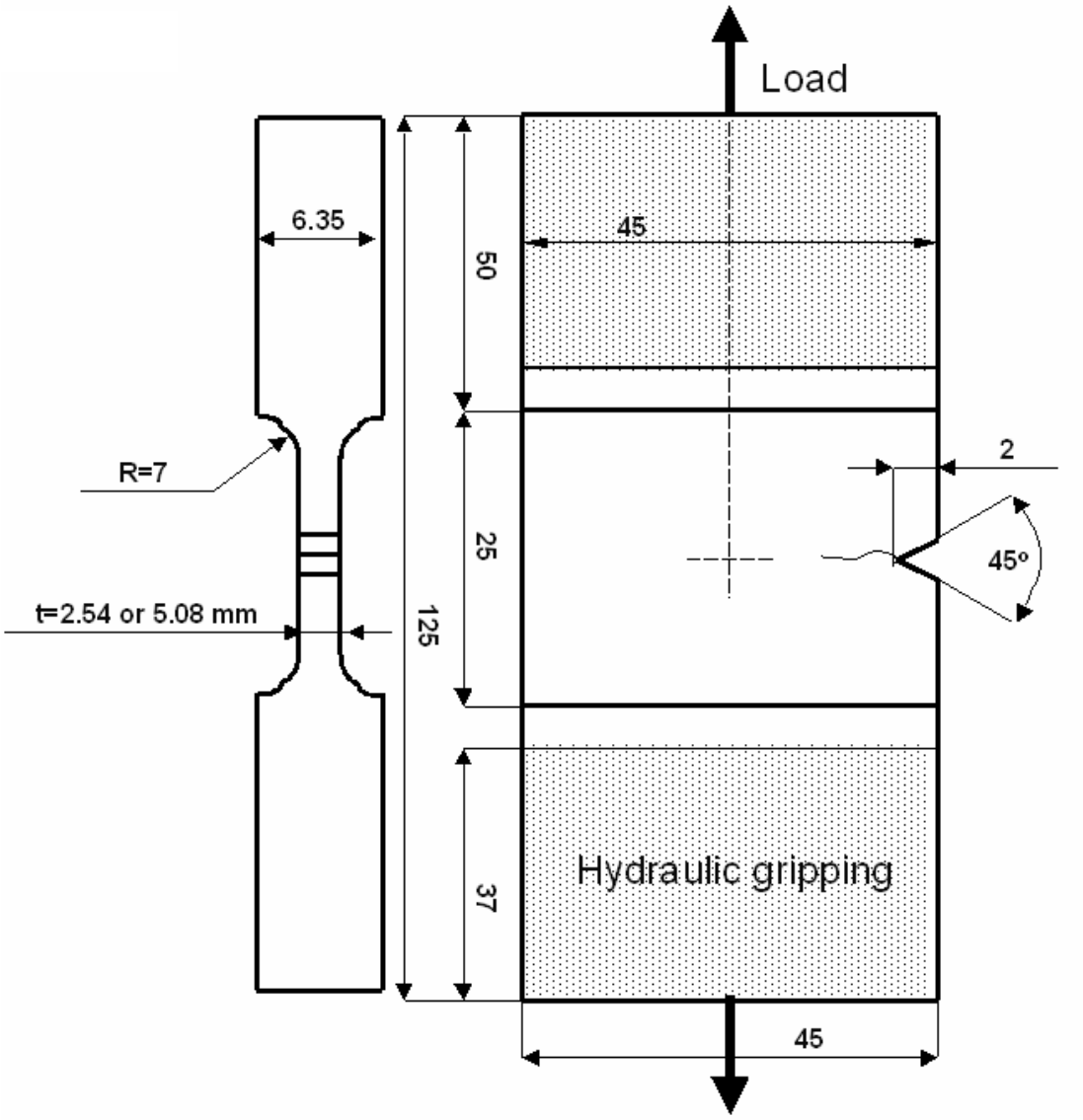

Figure 13 Specimen dimensions

In addition, the crack mouth opening displacement (CMOD) was measured using a 'clip on' gage. Each compliance curve consists of 600 load-displacement pairs, spaced at equal load intervals. This procedure was used for both the loading and unloading compliance curves. Approximately 55 measurements were taken from each specimen at equal crack length intervals.

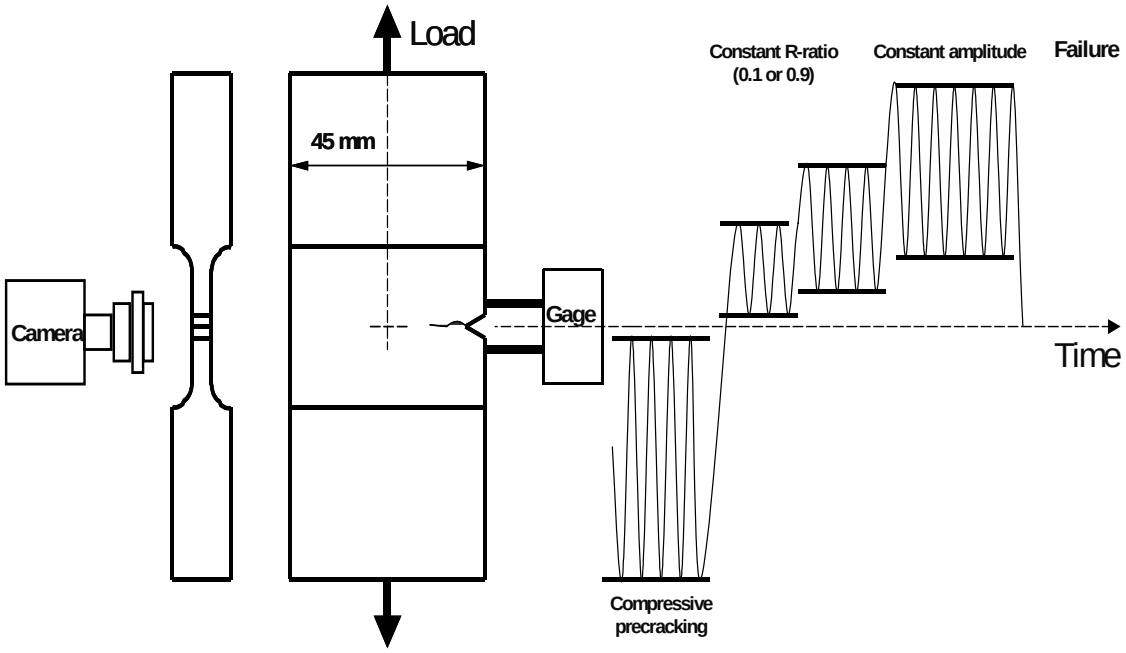

Figure 14 Schematic of the testing procedure

Description of the numerical procedures and investigated parameters

According to ASTM E647 standard [104] the opening load is defined as the load at the point where the 'compliance offset' is equal to 1, 2 or 4% (depending on the noise in the raw data). Compliance offset is calculated using the following formula:

$$ComplinceOffset = \frac{OpenCrackCompliance - Compliance}{OpenCrackCompliance}100 \qquad (1.21)$$

Open crack compliance is calculated by fitting a straight line to the 'upper' 25% of the unloading data, starting from $(0.9 \div 0.99)P_{max}$. If P_{op} is bigger than half of the maximum load the fitting range should be decreased until the open crack compliance remains constant.

Another requirement of the standard is that compliance have to be calculated using the loading data. Hence, load displacement data are first divided into equal

segments, starting from $(0.95 \div 0.99)P_{max}$. Each segment covers half of the neighboring segments and spans over ~$0.1\Delta P$ (approximately 20 segments total). The compliance for each segment is calculated using a linear least squares fit.

There are five parameters that can be adjusted in the described procedure. These parameters are:

1. Number of the experimental points. At least one data pair is needed per $0.2\Delta P$ increase of the load. No upper limit is specified. (>50 points).
2. Starting point for the opened crack linear fit (~$0.95P_{max}$).
3. Range for the opened crack linear fit (~$0.25\Delta P$).
4. Segment size (~$0.1\Delta P$).
5. Maximum compliance offset (1, 2, or 4%).

The recommended values from the standard are given in the parentheses. Figure 15 graphically depicts the ASTM procedure and corresponding parameters, which were studied using a one by one scheme.

The curve fitting methods selected for this numerical study are graphically illustrated in Figure 5. In the LL method, two straight lines are fitted to the 'upper' and 'lower' portions of the load-displacement curve. Similar method was discussed in the second ASTM Round Robin [12]. To make this method computer friendly, the following procedure was adopted.

First, a starting transition point for the two straight lines was chosen. Next, these lines were fitted to the data (above and below the transition point). Correlation factor was calculated as the reciprocal value of the sum of the distances (absolute value) between every experimental, and the corresponding fitted value of the load. Then the transition point was varied until the correlation factor for all possible

experimental points was obtained. The opening load is defined as the point where maximum correlation factor is achieved. The same procedure was used to calculate the correlation factor for all curve-fitting methods. This procedure is a modification of Allison et al. [8] and Sunder [83] approaches.

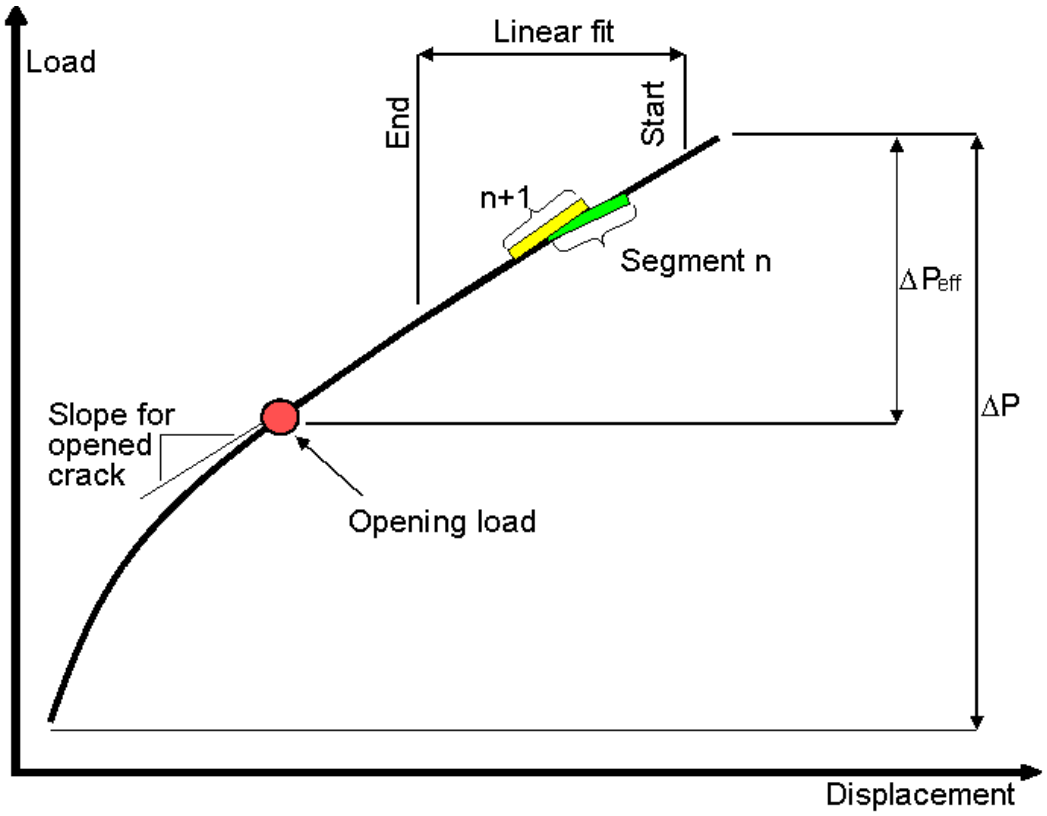

Figure 15 ASTM standard recommended procedure for opening load determination

PL, LPL (and their variations PL2 and LPL2) and Q methods were explained already in detail in 'New methods for opening load determination' section.

ACR method was described already in 'Adjusted Compliance Ratio' section.

Results and discussion

In this investigation 200, 400, and 600 equally spaced experimental points

were used to determine P_{op}. For all methods the results were practically the same regardless of the number of experimental points used (the variability of the results was also the same). Therefore, only 200 points were used for the rest of the numerical study in order to save computation time.

ASTM standard method

First parameter to be investigated was the point where the linear extrapolation for the opened crack compliance starts. The ASTM standard suggests choosing this point 'just below the maximum load', but not less than $0.9P_{max}$. Three values of this parameter, i.e. 0.9, 0.95, and 0.99 P_{max} were investigated. The results indicated that there was not a systematic dependence on this parameter in terms of P_{op} and the scatter.

Next, the range of the load displacement data used for determination of the open crack compliance was varied. According to the ASTM standard, this range should be 'approximately 25% percent of the cyclic force range'. For the purpose of this parametric study a $\pm 5\%$ variation of this value was is considered allowable. Similarly as in the starting point case, no systematic dependence on this parameter was observed. Blandford et al. [108] investigated bigger deviations of this parameter (25, 50, 75 and 100%). The use of the bigger range of the load-displacement data for determination of the opened crack compliance was justified at relatively high load ratios (0.3), since P_{op} is small. They concluded that the variation of this parameter could improve the existing ASTM standard if it is adjusted according to P_{op} (or load ratio).

The investigated segment size variation (9, 10, 11%) did not have any systematic influence on the results (Figure 16). This small variation was chosen because it is assumed to be permitted in the ASTM standard ('approximately' 10%).

More thorough investigation of this parameter was performed by Blandford et al. [108]. He investigated how smaller segment sizes will affect the accuracy of the ASTM method. When 2% segment size was used the calculated compliance showed a significant scatter. This scatter was reduced, using the software low-pass filter, developed by Daniewicz [114]. It seems however that this filter provided similar smoothing of the raw data as the original ASTM method with 10% segment size.

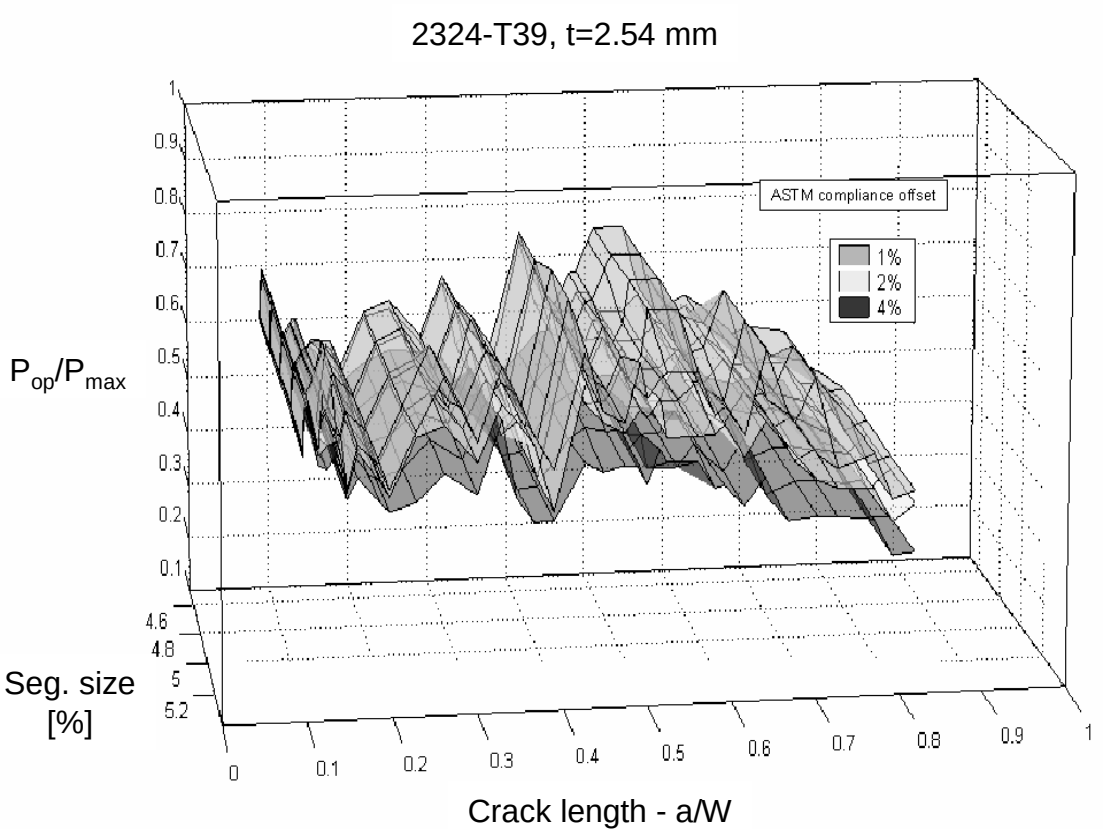

Figure 16 Variation of segment size and maximum compliance offset in ASTM method

Figure 16 shows also the scatter in the opening load estimates due to variation of the maximum compliance offset. It can be seen that the noise in P_{op} determination is dominated by the chosen maximum compliance offset. Choosing larger values for the compliance offset can decrease the scatter, but also leads to artificially low

closure loads. Allison et al. [8] showed this effect using 1, 5 and 15% compliance offset. The investigation showed that the calculated P_{op} is strongly dependent on this parameter with variations as high as 25-35%.

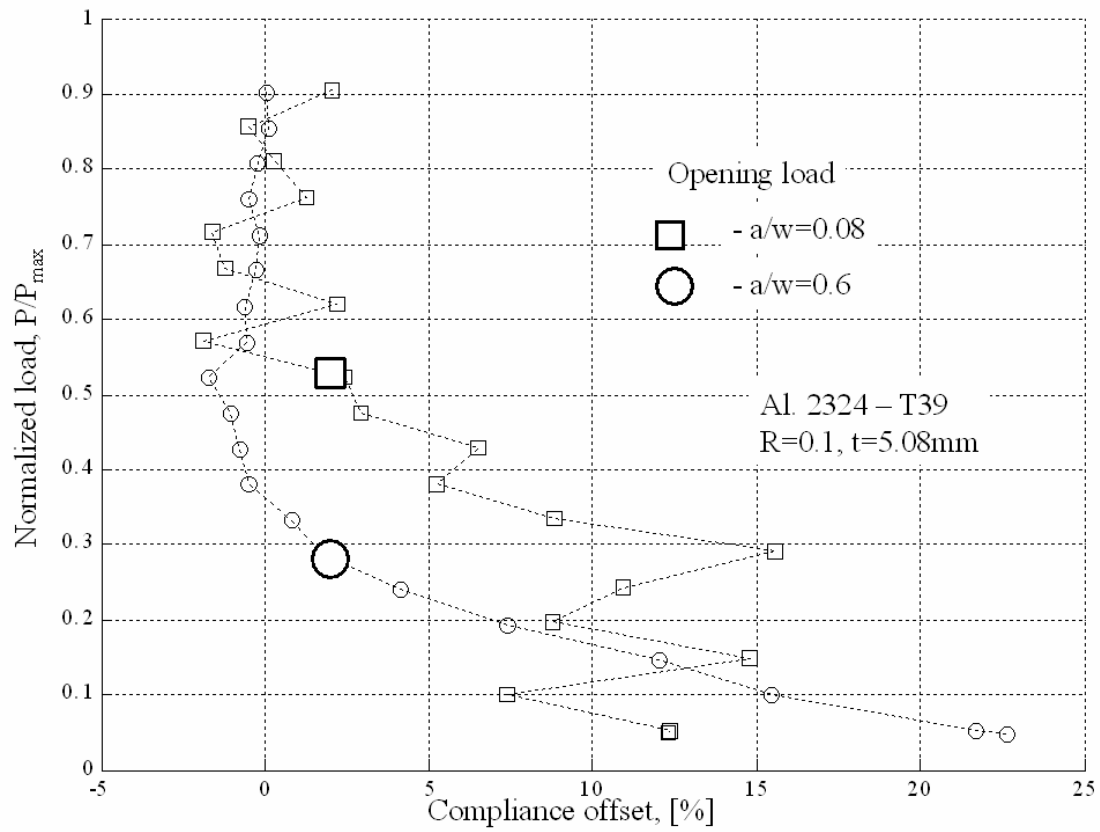

Figure 17 'Crack length' effect on the relative noise in the experimental data

If the optimal value of the maximum compliance offset is chosen for a given crack length, this does not necessarily mean that it would work equally well for another crack length. That is because the opened crack compliance changes due to crack propagation (the CMOD is increasing with the increase of the crack length). This means that the relative level of the noise in the experimental data would be bigger for a smaller crack than for the longer crack. Therefore crack length will influence the amount of noise in compliance offset plot as shown in Figure 17. It can

be seen that the maximum compliance offset of 2% or larger is needed for the crack length of a/W = 0.08 (or a = 4 mm), otherwise multiple crossings will be recorded. On the other hand, for a/W = 0.6, one can use compliance offset of 1%, which would increase the sensitivity of the analysis.

In contrast to the ASTM procedure, the curve fitting methods are relatively more resistant to the noise and therefore, they are supposedly not sensitive to the 'crack length' effect.

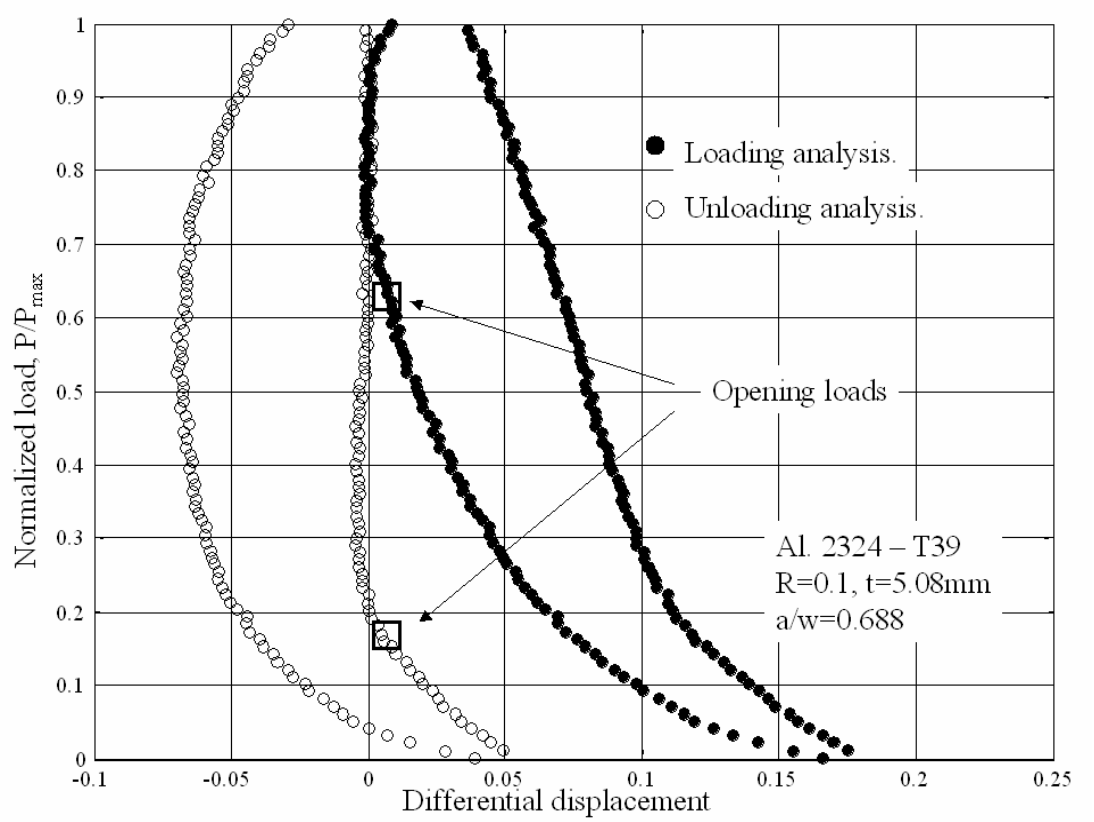

Figure 18 Variation of P_{op}, caused by using loading or unloading part of the same load cycle

Another source of error in P_{op} determination comes from the fact that the upper part of the load-displacement curve, which represents the stiffness of the specimen with fully opened crack, is approximated by a straight line. All the

investigated methods use this approximation. In the practice this is not true especially for the loading curve (Figure 18).

The latest version of the ASTM standard E647-00 [104] specifies that the unloading curve should be used for calculation of the opened crack compliance. However, the previous versions of the standard did not specify which one to use. That is why there is a lot of data in the literature where the loading curve was used. In such cases there is a strong possibility that the opening load was significantly overestimated.

In general, load-displacement loading curves have four distinct regions, which are:

1. A lower linear region where the crack is fully closed.
2. A lower nonlinear region where the crack opens (or closes). The load-bearing cross-section of the specimen changes and so does the compliance. A second-order polynomial is a good approximation of this region.
3. An upper linear region, where the crack is fully opened, but does not propagate.
4. An upper nonlinear region where the crack propagates and the crack tip plastic zone moves forward.

Thus, the nonlinearity in the upper part of the loading curve is caused by two mechanisms; the crack propagation and an expansion of the forward plastic deformation of the material around the crack tip. On the other hand, rather limited nonlinearity in the unloading curve would be present since the reversed plastic zone around the crack tip is much smaller than the forward plastic zone. However, some researchers prefer to use the loading curve because it will give bigger difference

between the compliance of fully closed versus opened cracks.

The nonlinearity in the upper portion of the load-displacement curve would cause difference in the opened crack compliances, determined from loading and unloading curves. This will result in significant differences in the compliance plot even for he same cycle, as shown in Figure 19.

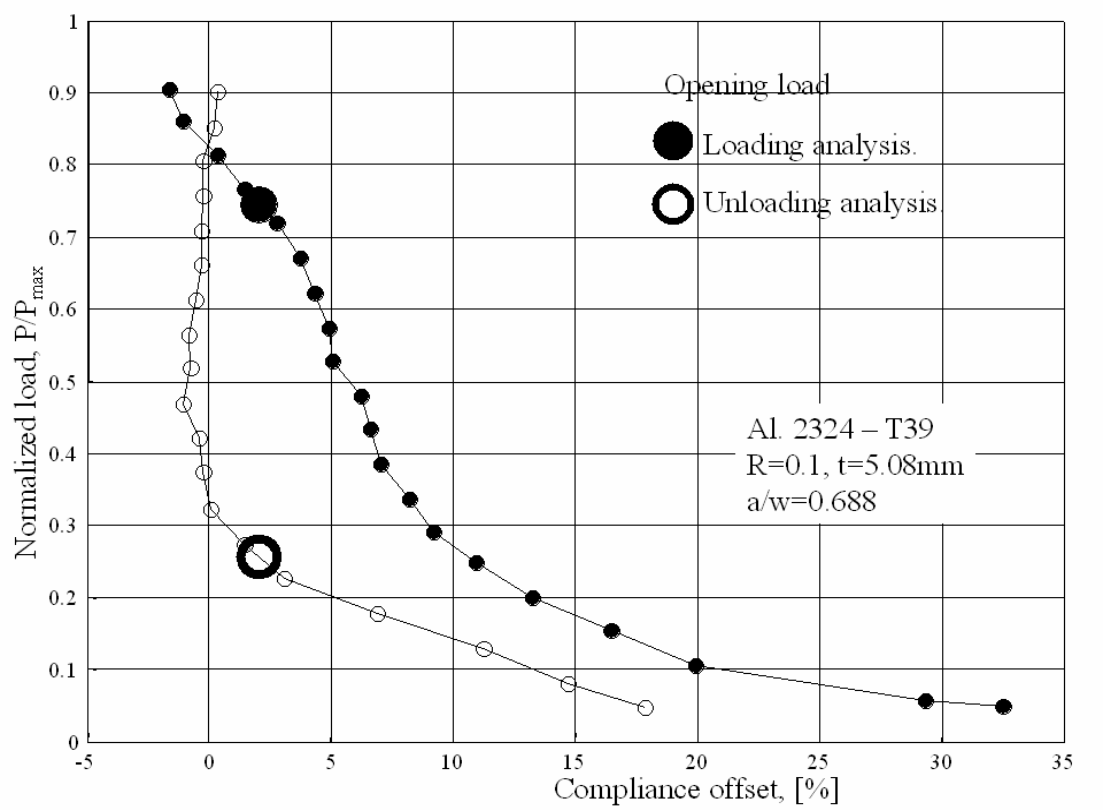

Figure 19 Differences in the compliance plot for loading and unloading part of the load cycle

Figure 20 shows the normalized opening load versus normalized crack length for both loading and unloading curves. The scatter is bigger for the case of loading curve analysis. It can be seen also that P_{op}/P_{max} values are decreasing when the unloading curve is used and they show an opposite trend when the loading curves are utilized. This trend was not observed for the thin specimen.

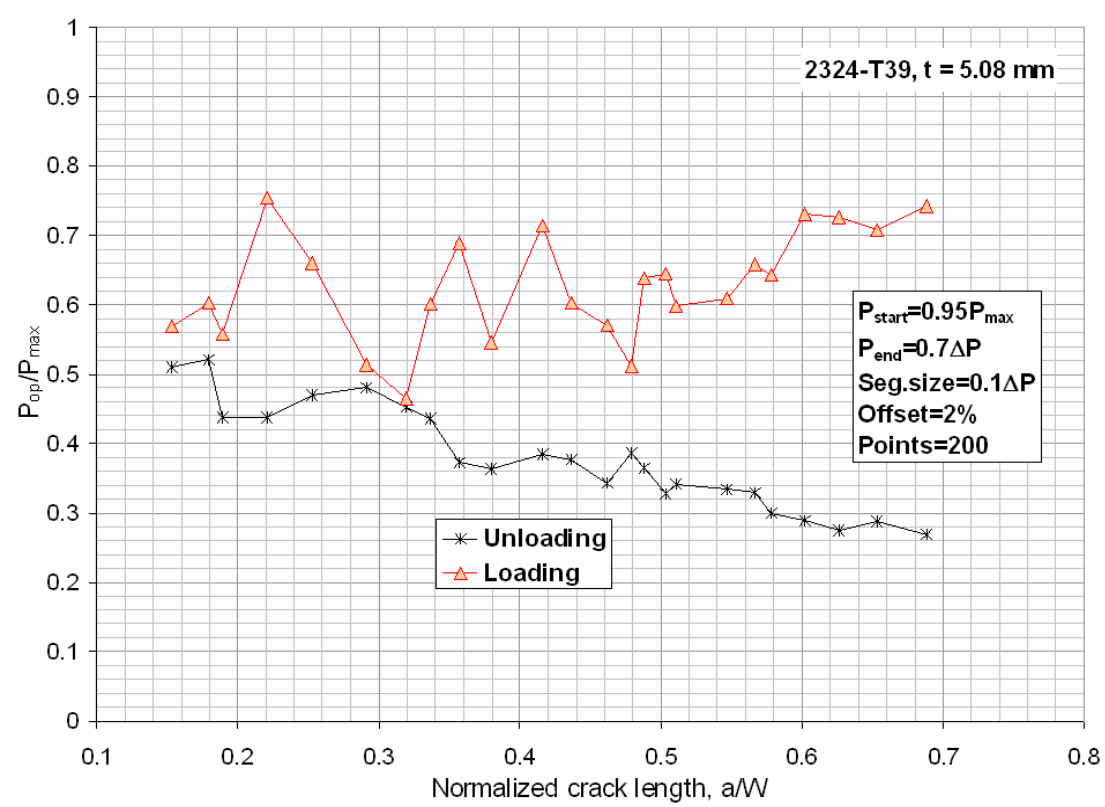

Figure 20 Effect of using loading or unloading part of the load cycle in the opening load determination

Finally, ASTM method for P_{op} determination was evaluated in terms of the overall scatter in the results for both aluminum alloys and thicknesses (Figure 21). It can be seen that P_{op} is continuously decreasing with the crack length. This poses significant problem for prediction of the fatigue crack growth, because according to plasticity induced crack closure concept, P_{op} should remain constant.

The correlation coefficient was calculated at every experimental point as a ratio of the difference between minimum and maximum calculated P_{op} and the applied load range:

$$\text{Corr.coeff} = 1 - \frac{P_{op}^{max} - P_{op}^{min}}{\Delta P} \qquad 1.22$$

It can be seen that all experiments show poor correlation for small crack lengths.

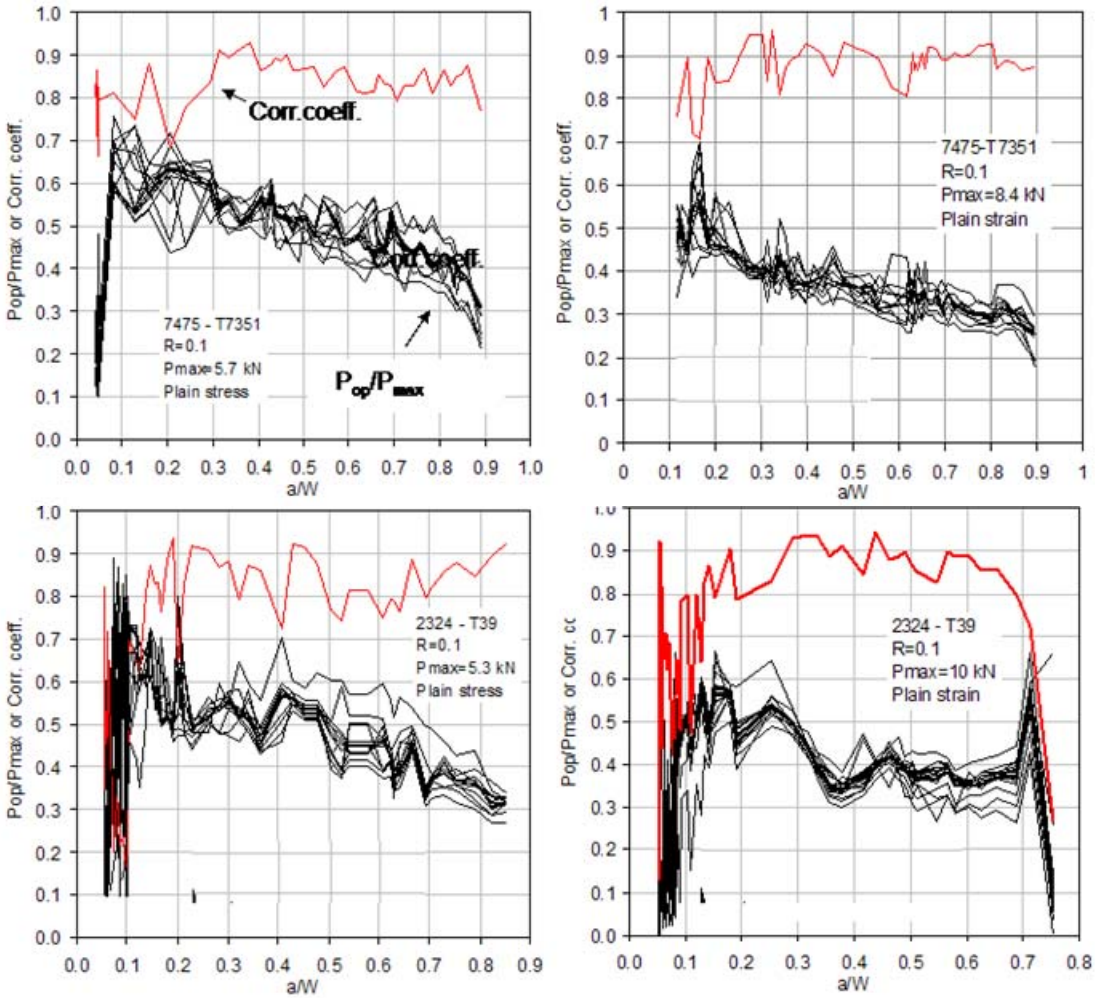

Figure 21 Overall correlation of P_{op} for all experiments using ASTM standard method

Curve fitting methods

Utilization of the loading curve may also cause numerical problems for some curve fitting methods. These problems would arise because the upper segment of the load-displacement curve (corresponding to fully opened crack) is fitted with a straight line. For the loading curve this is not valid due to its inherent non-linearity. Therefore, when the PL or LPL method is used, occasionally, the parabola would span over the entire load interval, translating the opening point to P_{max} (Figure 22). In contrast, the two tangent lines method does not have this problem because two

straight lines are used to fit the experimental data.

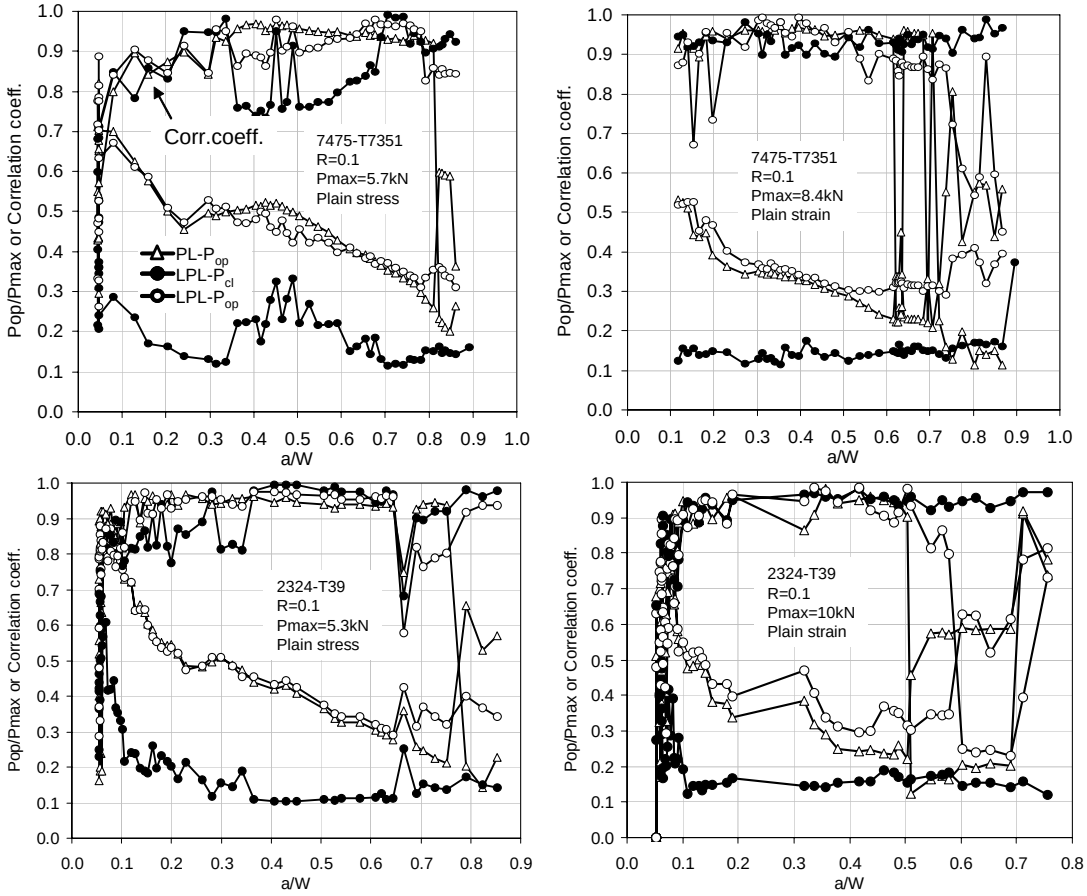

Figure 22 Overall correlation of P_{op} for all experiments using the PL and LPL methods

It can be seen that PL and LPL methods agree very well. Also, compared with ASTM standard method, the scatter in the P_{op} results at small crack length is much smaller. Unfortunately at long crack lengths both PL and LPL become unstable, because the nonlinearity in the upper portion of the load-displacement curve increases.

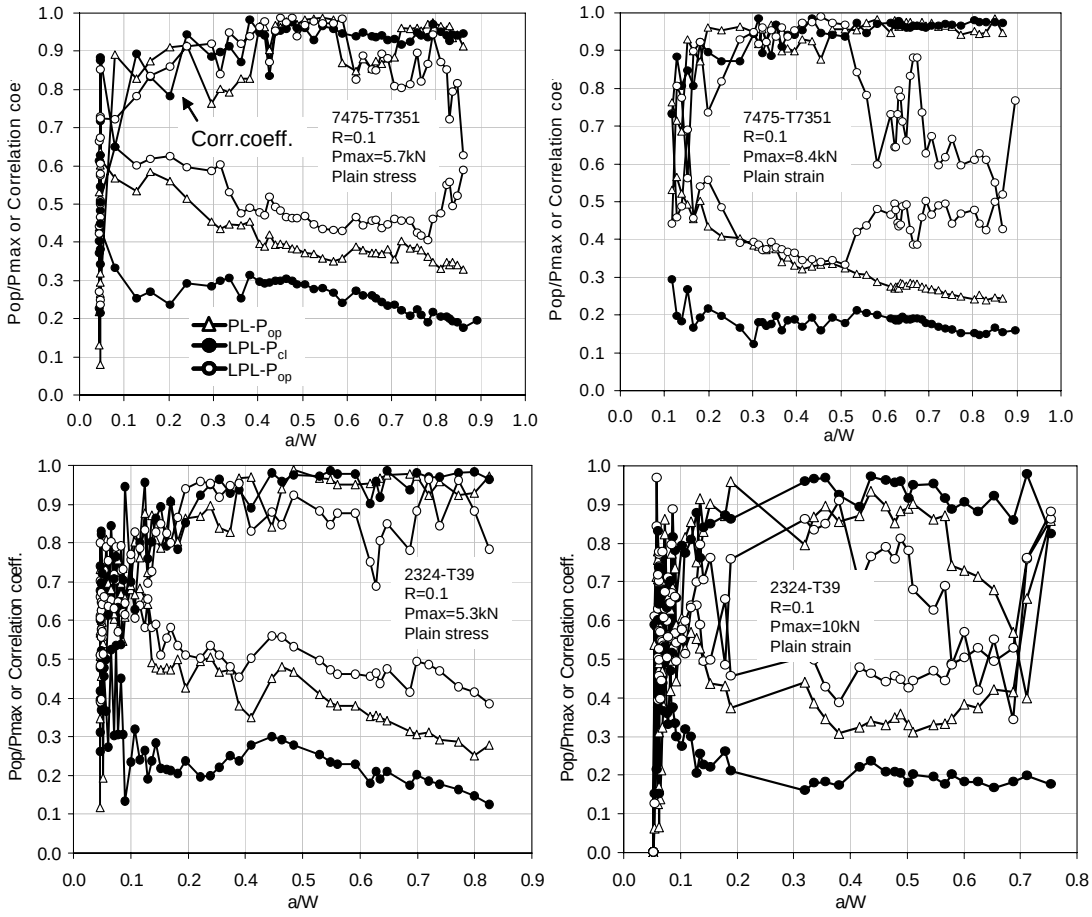

Figure 23 Overall correlation of P_{op} for all experiments using the modified PL and LPL methods

Another drawback of these methods is their speed. Due to the heavy calculation load on the processor it typically takes 3 to 4 hours to analyze the load displacement curves from a single experiment using LPL method (ASTM it takes only 30 seconds). Therefore the curve fitting methods are not suitable for real time calculations of P_{op}. PL2 and LPL2 are even more computationally intensive and sensitive to nonlinearities in the load-displacement curve (Figure 23).

Partial crack closure methods

Five calculations were done with each method – using loading or unloading

curve and varying the number of experimental load-displacement points (200, 400 and 600).

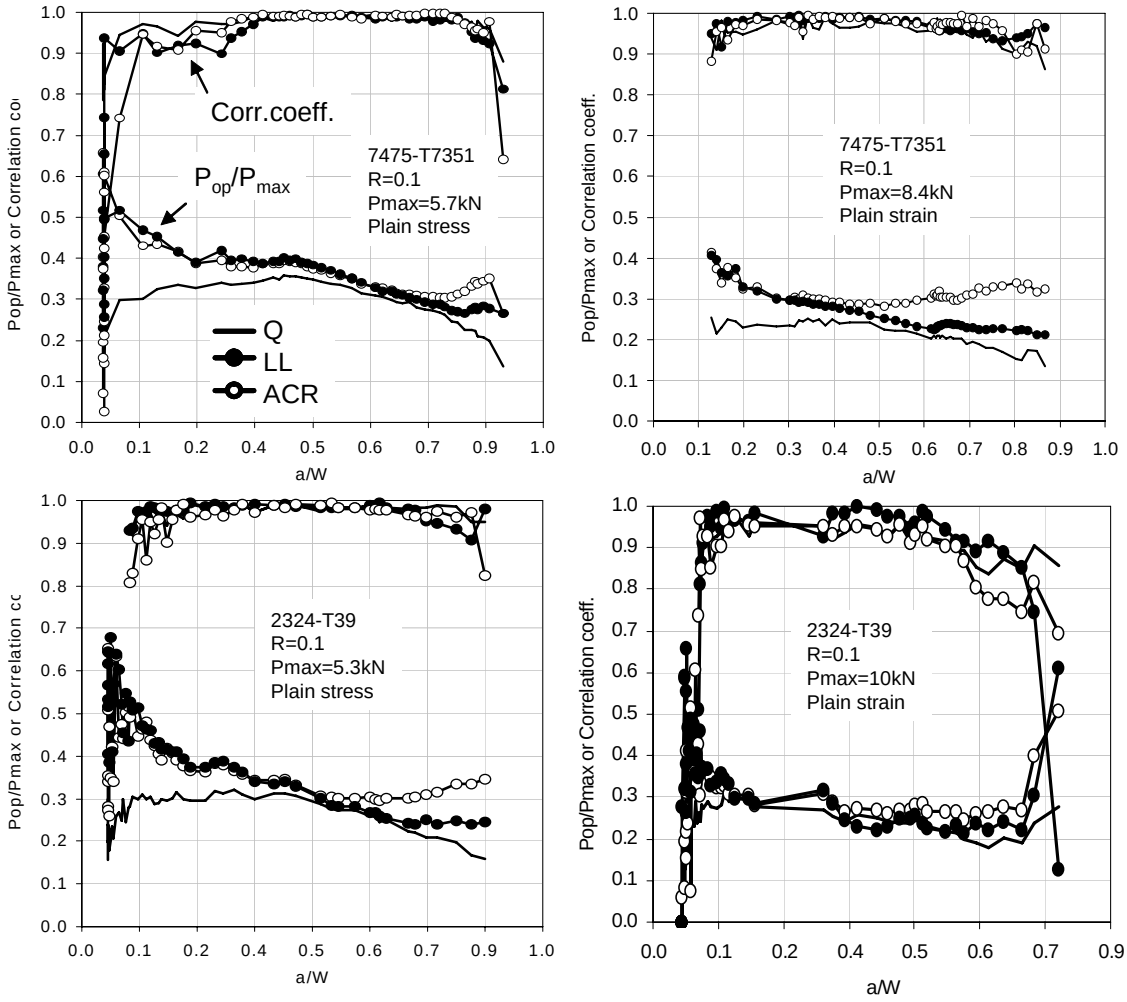

Figure 24 Overall correlation of P_{op} for all experiments using partial crack closure methods

All three methods in this category showed consistent results (Figure 24) with very small amount of scatter. LL method uses actually a curve fitting algorithm but gives results, similar to partial crack closure methods. This could be expected, because the intersection (or transition) point of the two straight lines corresponds to the load level, which is somewhere between a fully opened and a fully closed crack.

Comparison of all methods

The results for all methods are summarized graphically in Figure 25. For clarity only the mean of all simulations with every method are plotted.

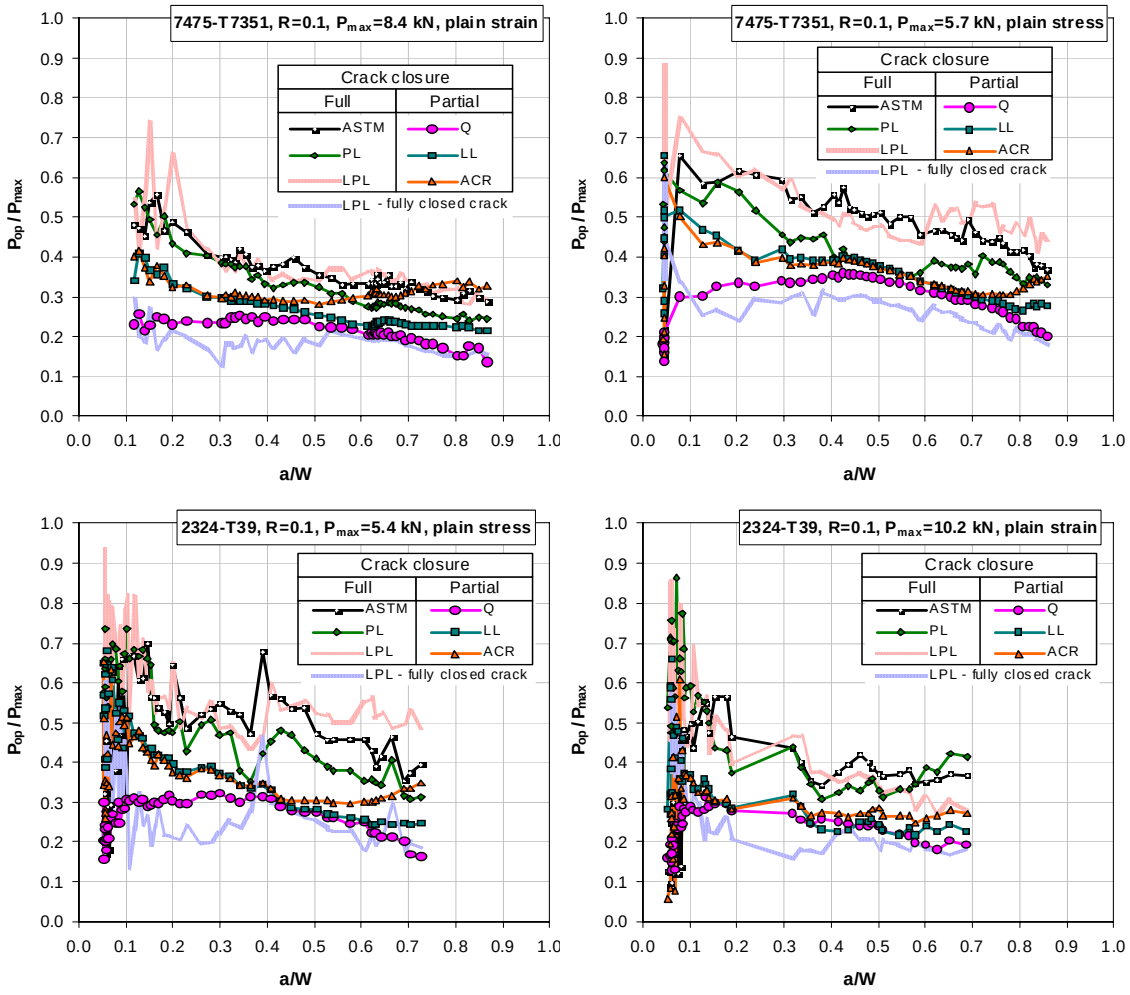

Figure 25 Mean values of P_{op} for all methods

The partial crack closure methods (Figure 12) expectedly show lower levels of P_{op}. It should be noted, however, that they cannot be compared directly with the others. A factor of approximately $2/\pi$ should be applied to the methods that utilize Elber crack closure concept in order to facilitate a fair comparison (Figure 26). Of course, the opposite is also true - partial crack closure results can be converted to full

closure by multiplying with $\pi/2$.

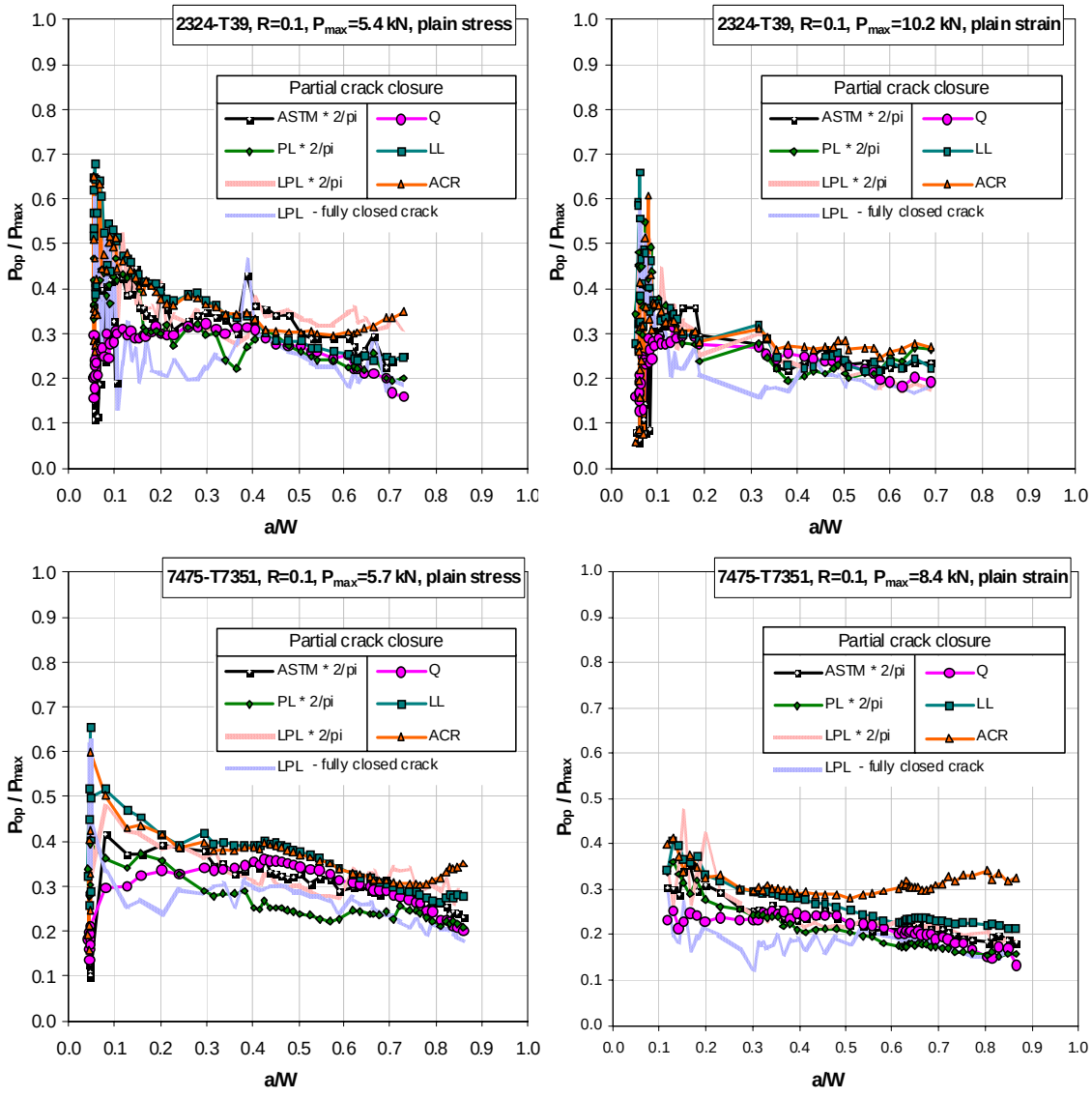

Figure 26 Mean values of P_{op} for partial crack closure model

Upon close examination of Figure 26, it can be concluded that there are two distinct trends. First – P_{op} develops gradually from P_{min} to some value that remains constant almost to the end of the specimen (Q method). This trend is in agreement with compression-compression pre-cracking and subsequent tensile crack growth. It is widely accepted that compression-compression pre-cracking generates a closure-

free crack which will develop closure under tensile growth from the threshold to the Paris region. The second trend observed in the experiments shows sharp increase of P_{op} and then decrease to the steady state value (all methods except Q). This spike cannot be explained by Elber theory.

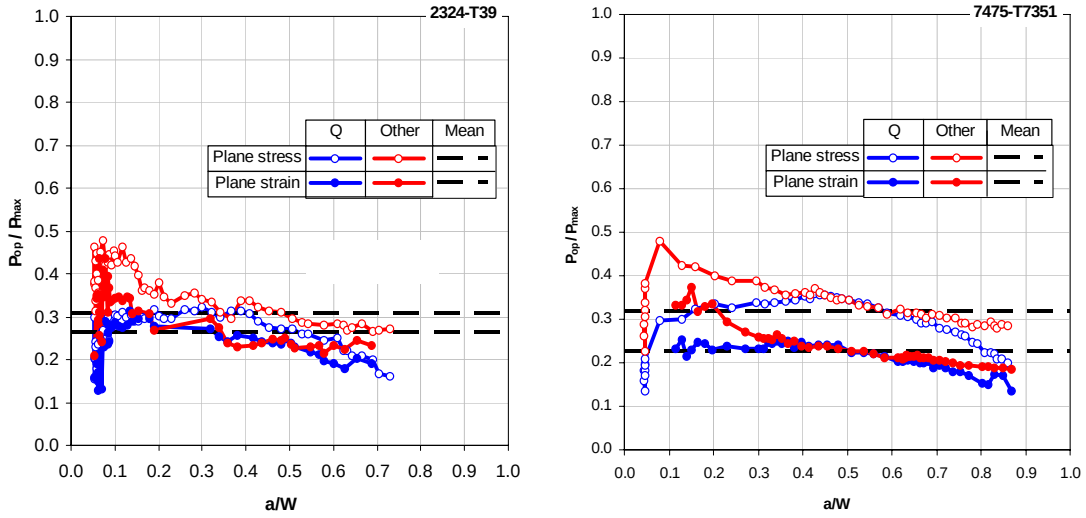

Figure 27 Partial crack closure levels for plain stress and plain strain

Figure 27 shows both trends in P_{op} in a more clear fashion. For the particular test the difference between Q and the other methods corresponds to the threshold of the fatigue crack growth. In this region the crack closure is believed to be caused by asperities. This means that the crack face contact appears at some distance behind the crack tip, causing all methods to register unrealistically high P_{op} in this partial crack closure situation. In contrast, the Q method shows a gradual increase in opening load.

Figure 27 also compares plane stress and plain strain levels of crack closure for both alloys that were studied. It is not a surprise that crack closure is less pronounced for the plain strain specimens of both materials

Finally, both the full and the partial crack closure levels (the dashed lines in Figure 27) are plotted in Figure 28. For comparison, previous results from Elber,

Schijve and Lang for similar aluminum alloys are added. It should be noted that Lang results are derived directly from the observed crack growth rates (see 'Zero Crack Propagation Load method for K_{pr} determination'). Therefore, results that do not agree with this curve cannot be expected to correlate the crack growth rates under different load ratios. It can be seen that only the results for plain stress (for both materials) agree well with the literature data. Therefore, crack closure alone cannot explain the experimental results, except for plane stress (full closure model).

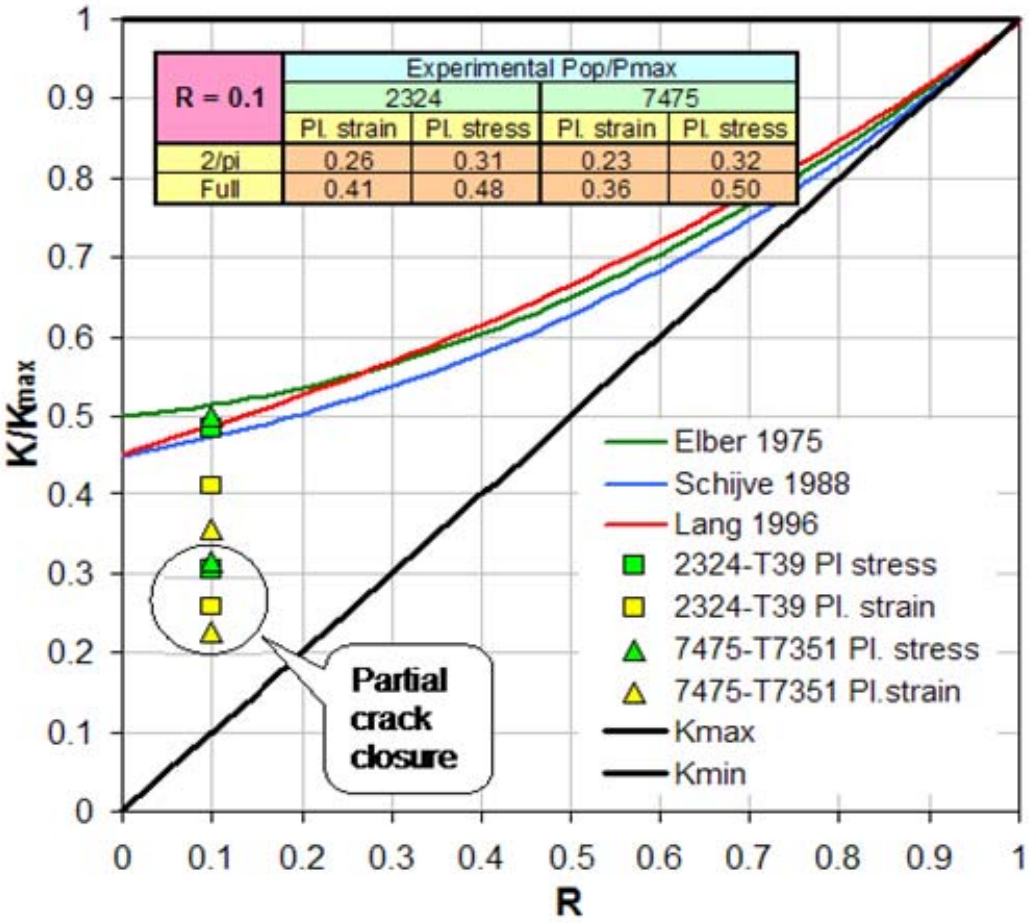

Figure 28 Comparison between the results for the literature and the experiments

Partial crack closure results are shown on Figure 28 for the sole purpose of comparison. If they are to be used for fatigue crack growth predictions, the influence

of K_{max} cannot be neglected and the use of two parameter (ΔK and K_{max}) crack driving force model should be considered.

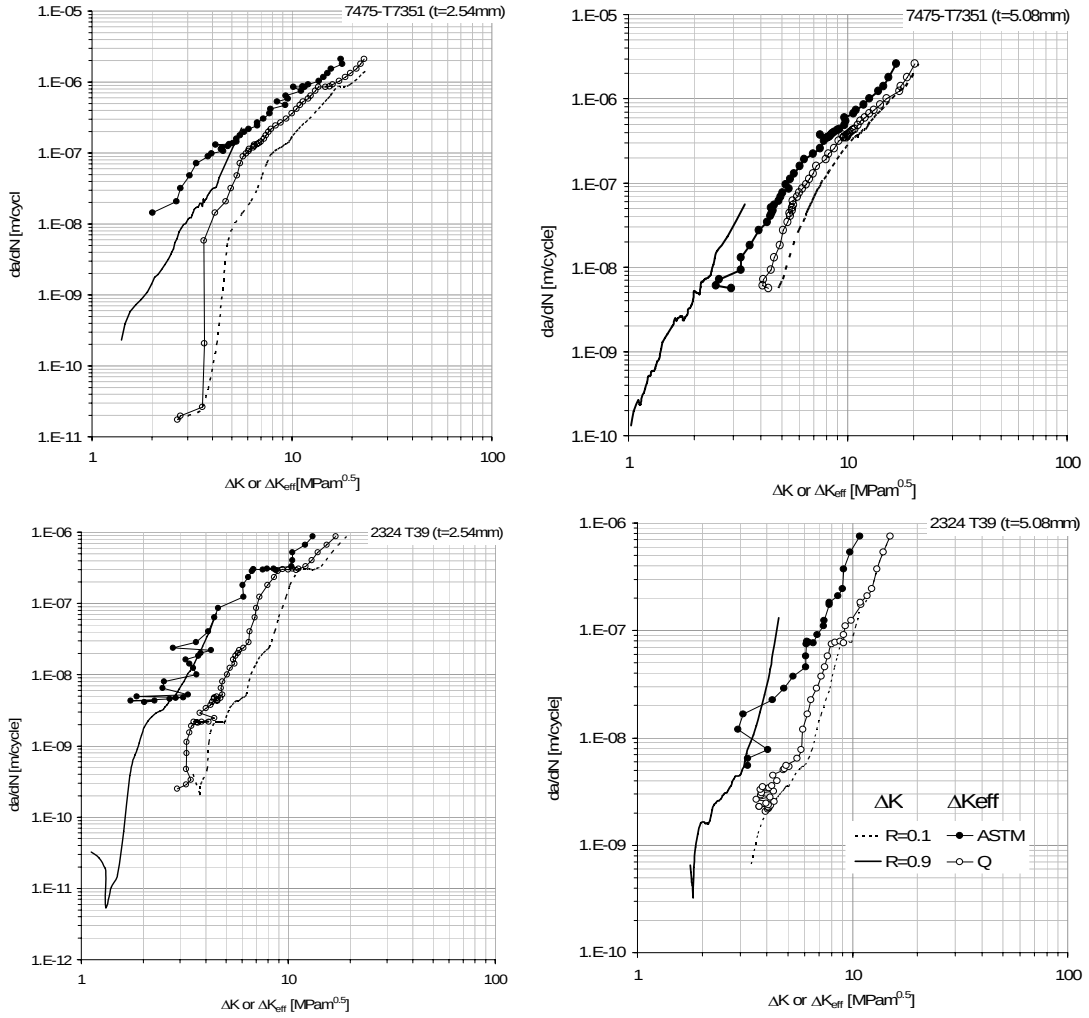

Figure 29 Crack growth rate in terms of ΔK or ΔKeff

Another comparison was made based on the correlation between da/dN vs. ΔK_{eff} data for R = 0.1 and the closure free data obtained at R = 0.9 using both the ASTM and Q methods (Figure 29). An examination of this figure indicates that both methods fail to collapse the R = 0.1 data on that of R = 0.9. This can be possibly attributed to K_{max} effects as proposed by Vasudevan et al. [116].

The performance of different methods for P_{op} determination can be judged also by the scatter in the estimations due to variation of the parameters that are allowed to be 'adjusted' (Figure 30). It can be seen, that all methods show improvement in the correlation under plain stress conditions, regardless of the material. It can be speculated that the reason for this is the increased nonlinearity in the load-displacement curve in the plain stress cases, which makes the changes in the slope easier to detect.

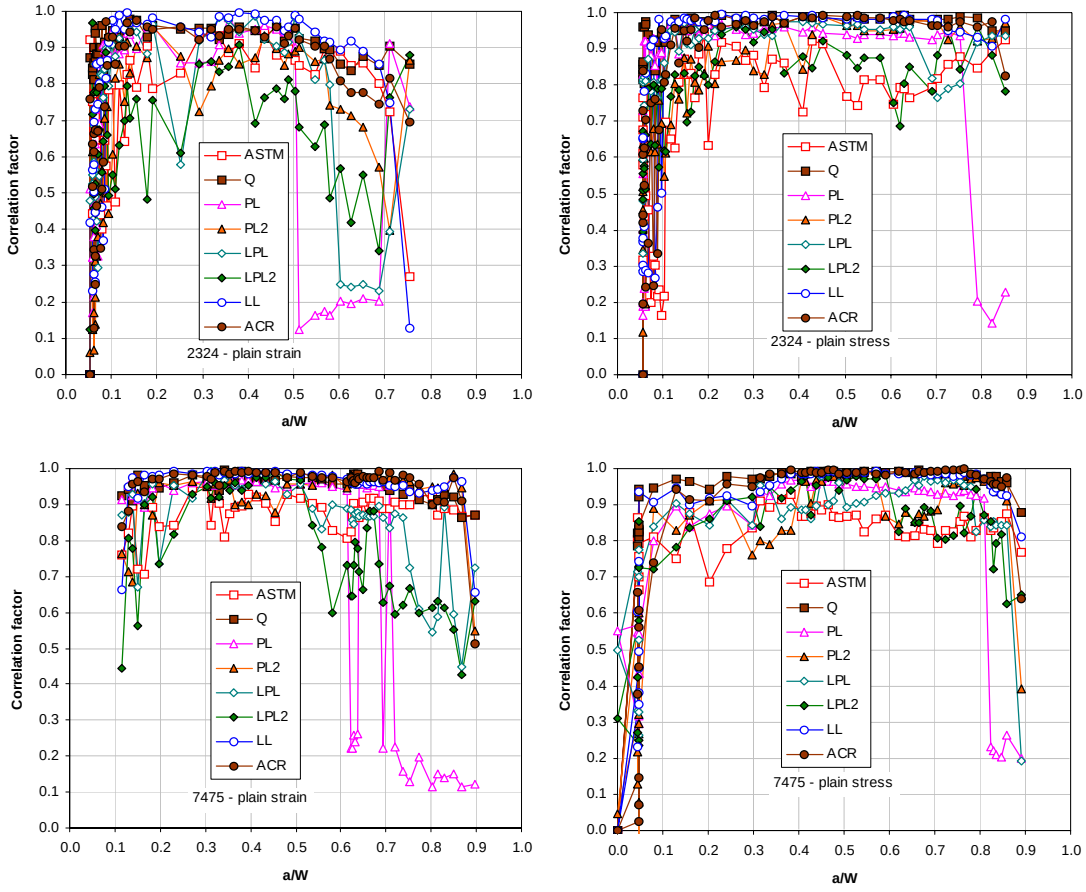

Figure 30 Variations of the correlation coefficient for all methods and specimens

In order to simplify the comparison, the mean value of the correlation coefficient for different specimens was calculated and plotted in Figure 31.

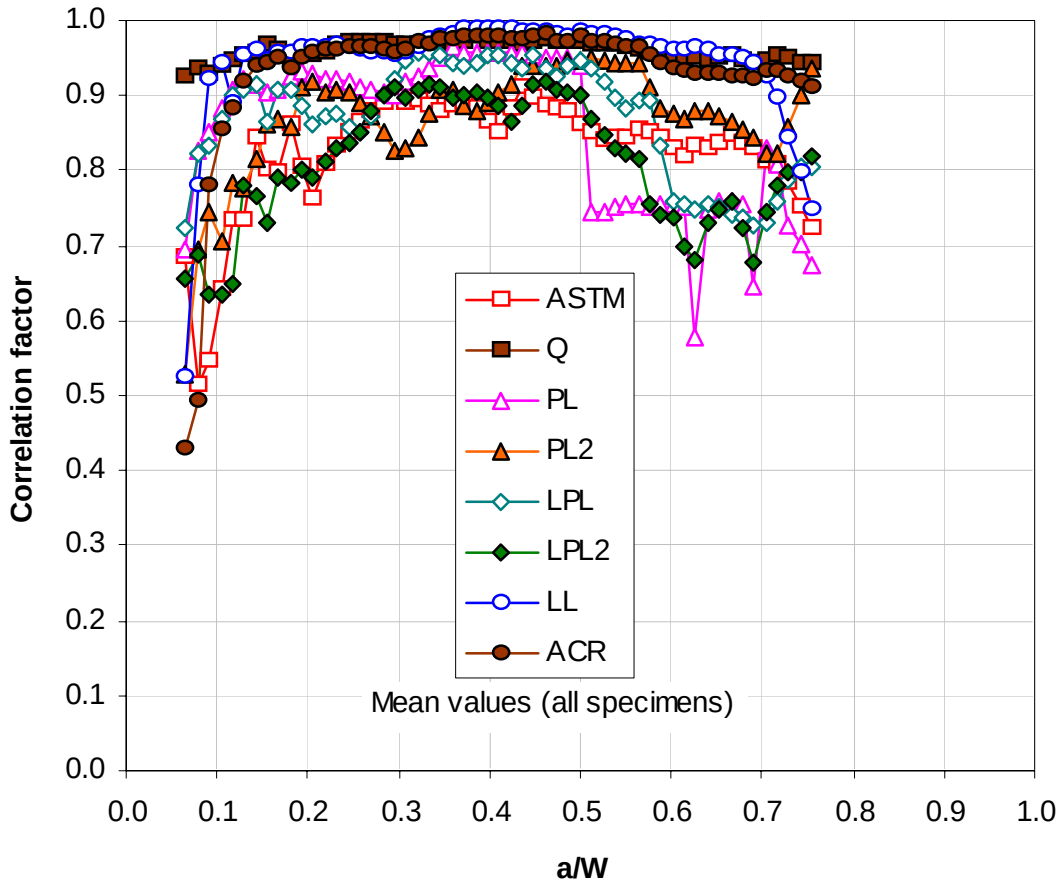

Figure 31 Comparison of all methods in terms of correlation coefficient for all specimens

Almost all methods for P_{op} determination show reduced scatter compared to the ASTM procedure, especially when a crack is relatively short, i.e. when $a/W < 0.2$. Unfortunately, this advantage is lost for the curve fitting methods (except LL) when $a/W>0.5$. Partial crack closure methods show the best correlation, Q method being the best among them. ACR and LL methods, however, still have problems for small crack lengths. The correlation coefficient for LL method drops for a long crack as well, leaving the Q method as the only one with consistently low scatter of the P_{op} estimates through the whole range of specimens and crack lengths that were tested (Figure 32).

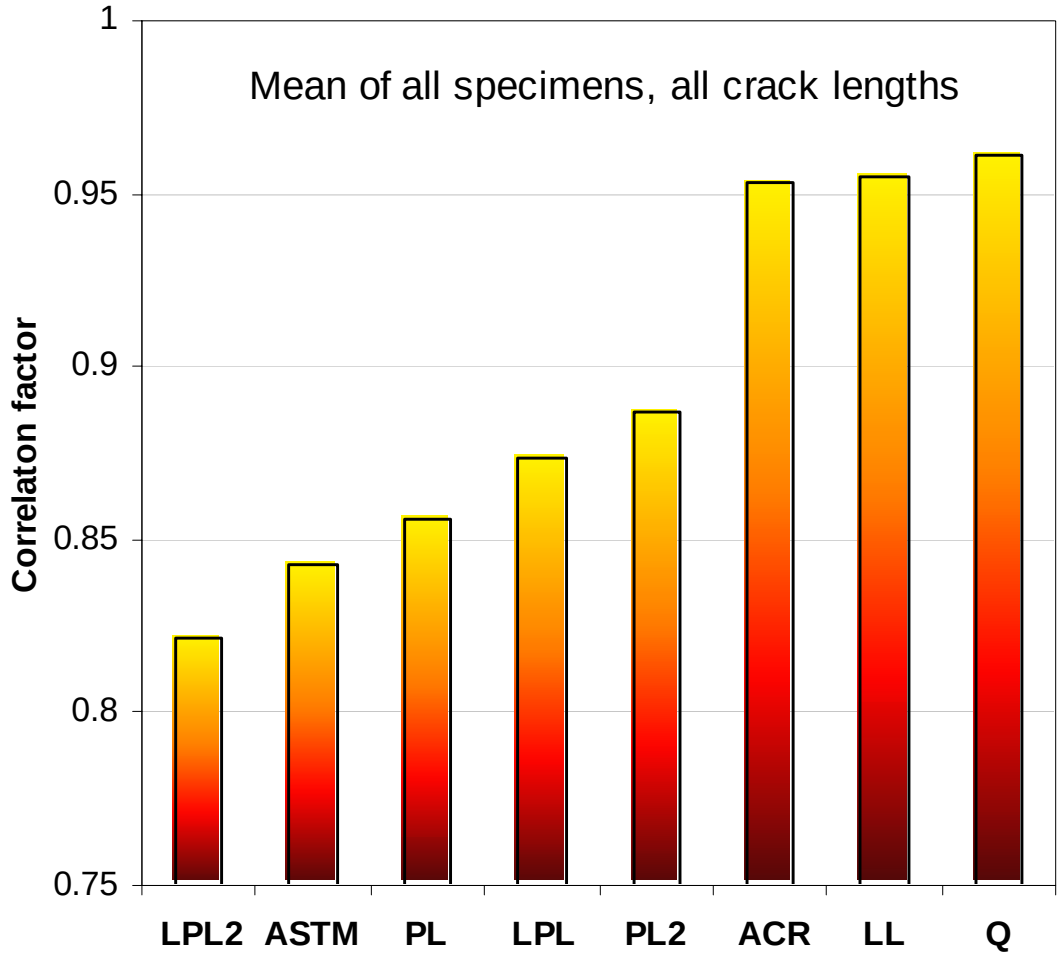

Figure 32 Comparison of all methods in terms of correlation coefficient for all specimens and crack lengths

Conclusions of Part I

1. There are a lot of experimental and numerical techniques for determination of the crack opening/closure load. They share one common characteristic - the generated results are very different. For example, the scatter of the opening (or closure) loads inferred from compliance measurements for even the same specimen under the same loading conditions could vary significantly between different methods or laboratories. This can be partly related to the inherent

subjectivity of some of the methods used for determination of the opening load. On the other hand, the change in compliance slope from nonlinear to linear behavior can not be simply related to the crack tip shielding because the amount of load transfer through the contacting crack faces and its location is generally unknown. Consequently, neither the standard method, ASTM E-647 recommendation, nor the two Round Robins on CC measurements [11, 12] were able to unite the entire fatigue community around the crack closure concept.

2. The noise in the raw load-displacement data decreases with increasing crack length. Thus, for long cracks a smaller compliance offset could be used in the ASTM standard method.
3. The use of the loading/unloading curve in the ASTM standard procedure caused P_{op} to increase/decrease correspondingly with respect to the crack length (Figure 20). This problem was observed under plane strain conditions, for the thick (t=5.08mm) specimen only. This indicates that the crack extension is not the cause since the crack growth rate was independent of the thickness. However it can be related to the plastic zone sizes in the thin and thick specimens. This problem is fixed in the latest version of the ASTM standard by specifying that only the loading part of the load-displacement curve should be used for opening load determination. There are plenty of results in the literature, however, where the old version of the standard was used and the reported crack closure levels can be overestimated by as much as 50%.
4. The non-linearity in the loading curve data, induced by crack extension or plastic zone expansion, could lead to artificially high values of P_{op} when the curve fitting methods are used (except LL). Using an unloading curve instead of the loading curve eliminates this problem.

5. In general, unloading should be utilized to find the open crack compliance, regardless of the method that is used.
6. The results from PL, LPL, PL2, LPL2 and ASTM standard show essentially the same amount of crack closure.
7. The curve fitting methods, however, use a non-subjective correlation-based criterion that defines the load-displacement interval for the linear fit corresponding to fully open crack. This eliminates the various 'adjustment' coefficients that are present in ASTM standard and reduces significantly the uncertainty in the opening load estimations (once loading or unloading curve is chosen for the analysis).
8. The curve fitting methods require a lot of calculations and still cannot be used on a cycle by cycle basis in real time applications with the current level of technology.
9. LL method surprisingly showed results, identical to the partial crack closure methods. In the literature, however it is often used as a replacement of ASTM standard procedure to estimate the 'full' closure.
10. Q method proved to be most stable numerically. It allows P_{op} to be determined where multiple crossings on the compliance offset plot will invalidate ASTM results (typically at $a/W<0.1$). It does not involve any fitting parameters and is also the fastest and easiest to implement method for P_{op} determination due to the simple numerical integration algorithm that is used.
11. Only the curve fitting methods (LL, Q and ACR) showed results almost independent of the crack length, where all other methods registered unrealistically high P_{op}, probably caused by asperities contact or noise in the data, near the crack growth threshold ($a/W<0.2$).

Finally, the variability in the crack closure estimations is too big to be used for a reliable fatigue crack growth predictions. This problem was eliminated with the new Q method for opening load determination, but the estimated crack closure levels were not sufficient to correlate the experimental data for different load ratios (Figure 29). This indicates that there is additional fatigue damage that is not accounted in ΔK_{eff}. Therefore the next part of the thesis constitutes an attempt to take into consideration K_{max} parameter as suggested in the unified approach to fatigue proposed by Vasudevan, Sadananda and co-workers [3].

Part II – Two parameter crack driving force model

Introduction

The last 35 years of research in the crack closure area were carefully reviewed in Part I of the dissertation and the best methods for opening load determination were identified. Consequently, two new methods (Q and LPL) were carefully designed to avoid previous modeling problems. Despite these efforts, experimental results even for the simplest case of loading (constant load ratio) were poorly correlated by the crack closure concept. The noise in the data and the crack length had significant influence on the opening load estimations. These problems were solved with the newly developed Q method, but the effect of the changing load ratio was significantly underestimated. This indicates that additional fatigue crack damage parameter is needed - K_{max}. Kujawski [160, 161] has recently introduced a two-parameter crack driving force parameter – ΔK^*, which can account for this additional influence. However, a robust method for predicting the fatigue crack growth rates that incorporates this parameter is still missing. Therefore, this part of the dissertation is devoted to the development of such a method.

First a general relationship between fatigue crack growth rate, da/dN, and a two-parameter ΔK and K_{max} driving force is derived using fundamental fatigue (ε-N curve) properties. A power-law relationship between ΔK and K_{max} is obtained by relating the crack growth rate to the fatigue life of the 'process zone'. The analysis of the experimental data indicates that there are two distinct regions on the crack growth plot, ΔK and K_{max} dominated, corresponding to high and low load ratios, respectively.

Next, based on the findings from the analytical modeling, a new way of

representing the da/dN data in terms of ΔK and K_{max} by means of the crack propagation (CP) table is proposed. It is a convenient way to represent and analyze the fatigue crack growth data, using simple data reduction schemes.

Finally, the application of the CP table for predicting the crack growth rate for different load ratios, block loading and a simple overload is explained and discussed.

Analytical derivation of the two-parameter crack driving force

Several investigators have attempted to correlate the fatigue crack propagation rate with the usual cyclic stress-strain and fatigue properties of smooth uniaxial specimens [167 - 173]. In such approaches, fatigue resistance of the material in the 'process zone' ahead of the crack tip is assumed to be governed by the local state of stress and strain in the direction perpendicular to the crack growth. The 'process zone' is assumed to be the minimum region that is described in macroscopic terms and to which a fatigue failure criterion can be applied. Thus, a fatigue crack growth rate can be formulated by coupling the cyclic stress-strain distribution at the 'process zone' with a suitable failure criterion. In the following, an analytical verification of the two-parameter crack driving force based on the above-mentioned concepts is presented.

The fatigue crack growth (FCG) rate, da/dN, can be calculated as:

$$da / dN = \rho^* / N_f \qquad (2.1)$$

In Eq. 2.1, N_f is a number of cycles required to fail the 'process zone' element ρ^* (Figure 33).

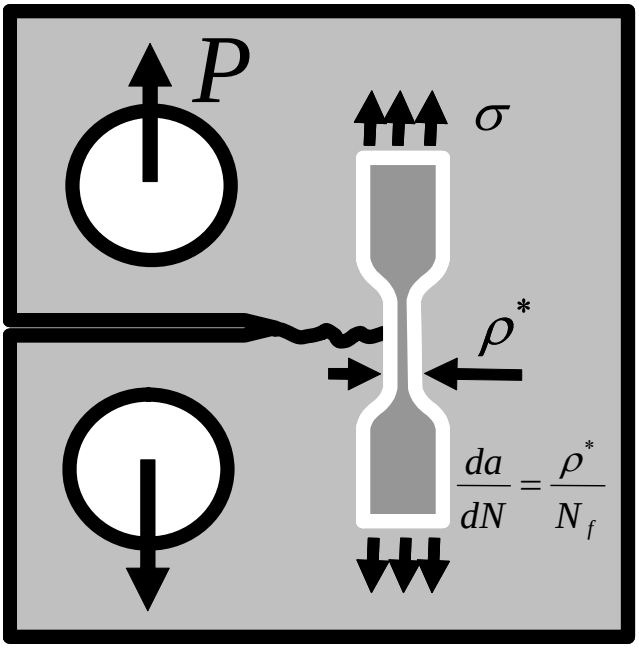

Figure 33 Connection between fatigue and fracture

This analogy allows the fatigue life diagram (ε-N curve) to be utilized to the 'process zone' and to calculate FCG rate. In order to account for the load ratio effects, the widely accepted Smith-Watson-Topper (SWT) parameter [172] will be adopted as a fatigue failure criterion:

$$\sigma_{\max}\varepsilon_a = \frac{\sigma_f'^2}{E}(2N_f)^{2b} + \sigma_f'\varepsilon_f'(2N_f)^{b+c} \qquad (2.2)$$

In Eq.2.2, σ_{max} and ε_a are the local values (at the crack tip) of the maximum stress and the strain amplitude accordingly. σ_f', ε_f', b and c are material constants, which can be found in any reference book.

Using Eq. (2.1), Eq. (2.2) ca be written in the following form:

$$\sigma_{\max}\varepsilon_a = \frac{\sigma_f'^2}{E}\left(2\frac{\rho^*}{\rho^*}N_f\right)^{2b} + \sigma_f'\varepsilon_f'\left(2\frac{\rho^*}{\rho^*}N_f\right)^{b+c}$$

$$\sigma_{\max}\varepsilon_a = \frac{\sigma_f'^2}{E}\left(2\frac{\rho^*}{da/dN}\right)^{2b} + \sigma_f'\varepsilon_f'\left(2\frac{\rho^*}{da/dN}\right)^{b+c} = \text{Constant} \qquad (2.3)$$

Equation 2.3 indicates that in order to maintain a constant crack growth rate, the SWT parameter, $\sigma_{max}\varepsilon_a$, has to be kept constant.

The stress and strain at the crack tip 'process zone' can be estimated by adopting for Mode I, the Rice solution of a crack loaded in the antiplane shear [174 - 175], Eq. (2.4).

Rice	Modified Rice
$\tau = \tau_0\left(\frac{K^2}{(1+n)\pi\tau_0^2(x+\rho^*)}\right)^{\frac{n}{1+n}}$	$\sigma = \sigma_0\left(\frac{K^2}{(1+n)\pi\sigma_0^2(x+\rho^*)}\right)^{\frac{n}{1+n}}$
$\gamma = \gamma_0\left(\frac{K^2}{(1+n)\pi\gamma_0^2(x+\rho^*)}\right)^{\frac{1}{1+n}}$	$\varepsilon = \varepsilon_0\left(\frac{K^2}{(1+n)\pi\sigma_0^2(x+\rho^*)}\right)^{\frac{1}{1+n}}$
Valid for: $\tau = \tau_0\left(\frac{\gamma}{\gamma_0}\right)^{n'} \geq \tau_0$	Valid for: $\sigma = \sigma_0\left(\frac{\varepsilon}{\varepsilon_0}\right)^{n'} \geq \sigma_0$

(2.4)

Equation (2.4) allows calculation of stress and strain only in the plastic region. In the elastic region, the following equations are used:

$$\sigma_{max} = \frac{K_{max}}{\sqrt{2\pi(x+\rho^*)}}$$

$$\varepsilon_a = \frac{\Delta\varepsilon}{2} = \frac{\Delta\sigma}{2E} = \frac{\Delta K}{2E\sqrt{2\pi(x+\rho^*)}} \qquad (2.5)$$

In Eqs. 2.4 and 2.5, x = 0 corresponds to the crack tip, and σ_0 and $\varepsilon_0 = \sigma_0/E$ are the yield stress and strain, respectively and n' is the strain hardening exponent. In SWT equation, both σ_{max} and ε_a are independent variables and as such they have to be calculated separately, using either plastic or elastic solution. This defines four possible combinations as shown below:

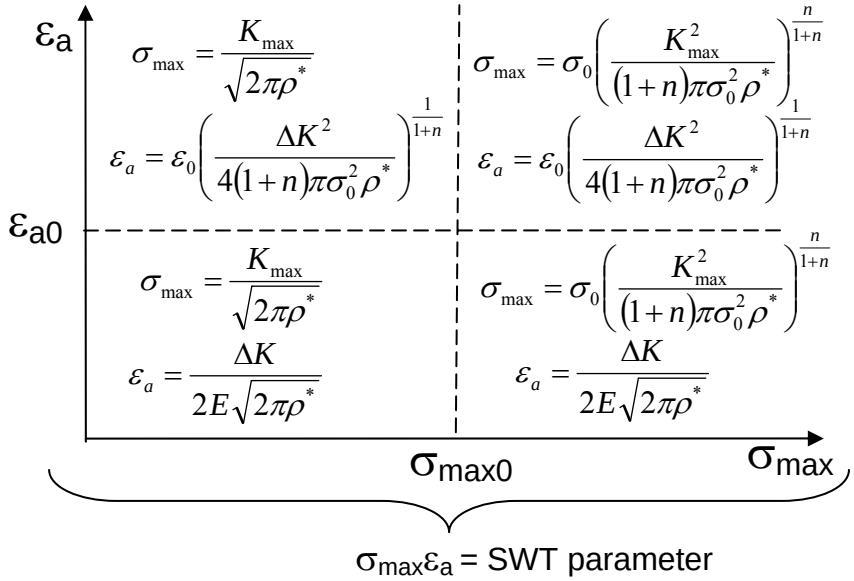

$$\begin{cases} \sigma_{\max} = \dfrac{K_{\max}}{\sqrt{2\pi\rho^*}} \\ \varepsilon_a = \varepsilon_0 \left(\dfrac{\Delta K^2}{4(1+n)\pi\sigma_0^2\rho^*} \right)^{\frac{1}{1+n}} \end{cases} \quad \begin{cases} \sigma_{\max} = \sigma_0 \left(\dfrac{K_{\max}^2}{(1+n)\pi\sigma_0^2\rho^*} \right)^{\frac{n}{1+n}} \\ \varepsilon_a = \varepsilon_0 \left(\dfrac{\Delta K^2}{4(1+n)\pi\sigma_0^2\rho^*} \right)^{\frac{1}{1+n}} \end{cases}$$

$$\begin{cases} \sigma_{\max} = \dfrac{K_{\max}}{\sqrt{2\pi\rho^*}} \\ \varepsilon_a = \dfrac{\Delta K}{2E\sqrt{2\pi\rho^*}} \end{cases} \quad \begin{cases} \sigma_{\max} = \sigma_0 \left(\dfrac{K_{\max}^2}{(1+n)\pi\sigma_0^2\rho^*} \right)^{\frac{n}{1+n}} \\ \varepsilon_a = \dfrac{\Delta K}{2E\sqrt{2\pi\rho^*}} \end{cases} \tag{2.6}$$

The solutions from such a system of equations can be represented in the following form:

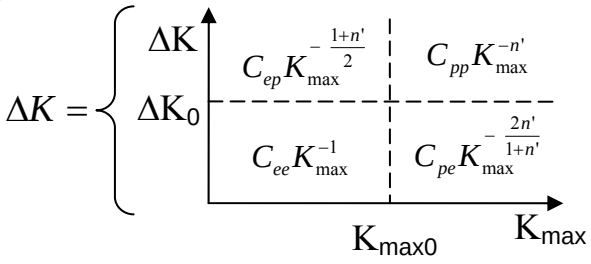

$$\Delta K = \begin{cases} \Delta K & C_{ep} K_{\max}^{-\frac{1+n'}{2}} \quad C_{pp} K_{\max}^{-n'} \\ \Delta K_0 & C_{ee} K_{\max}^{-1} \quad C_{pe} K_{\max}^{-\frac{2n'}{1+n'}} \end{cases}$$

where:

$$C_{pp} = 2\left((1+n')\pi E\rho^* SWT\right)^{\frac{1+n'}{2}}$$

$$C_{ee} = 4E\pi\rho^* SWT$$

$$C_{ep} = \left(SWT \frac{\sqrt{2\pi\rho^*}\left(4(1+n')\pi\sigma_0^2\rho^*\right)^{\frac{1}{1+n'}}}{\varepsilon_0} \right)^{\frac{1+n'}{2}} \tag{2.7}$$

$$C_{pe} = 2\ SWT \frac{\sqrt{2\pi\rho^*}\left((1+n')\pi\sigma_0^2\rho^*\right)^{\frac{n'}{1+n'}}}{\varepsilon_0}$$

$$SWT = \sigma_f' \varepsilon_f' \left(\frac{2\rho^*}{da/dN} \right)^{b+c} + \frac{\sigma_f'^2}{E} \left(\frac{2\rho^*}{da/dN} \right)^{2b}$$

It can be seen, that four solutions given by Eq. (2.7) are a power law relations between ΔK and K_{max} and therefore they are straight lines on a log-log plot. Aluminum alloy 7075-T6 was selected to illustrate the above relationships between ΔK vs. K_{max} (Figure 34). This figure was generated, using the cyclic and fatigue properties of 7075-T6 Al alloy [173], which are listed in Table 2.

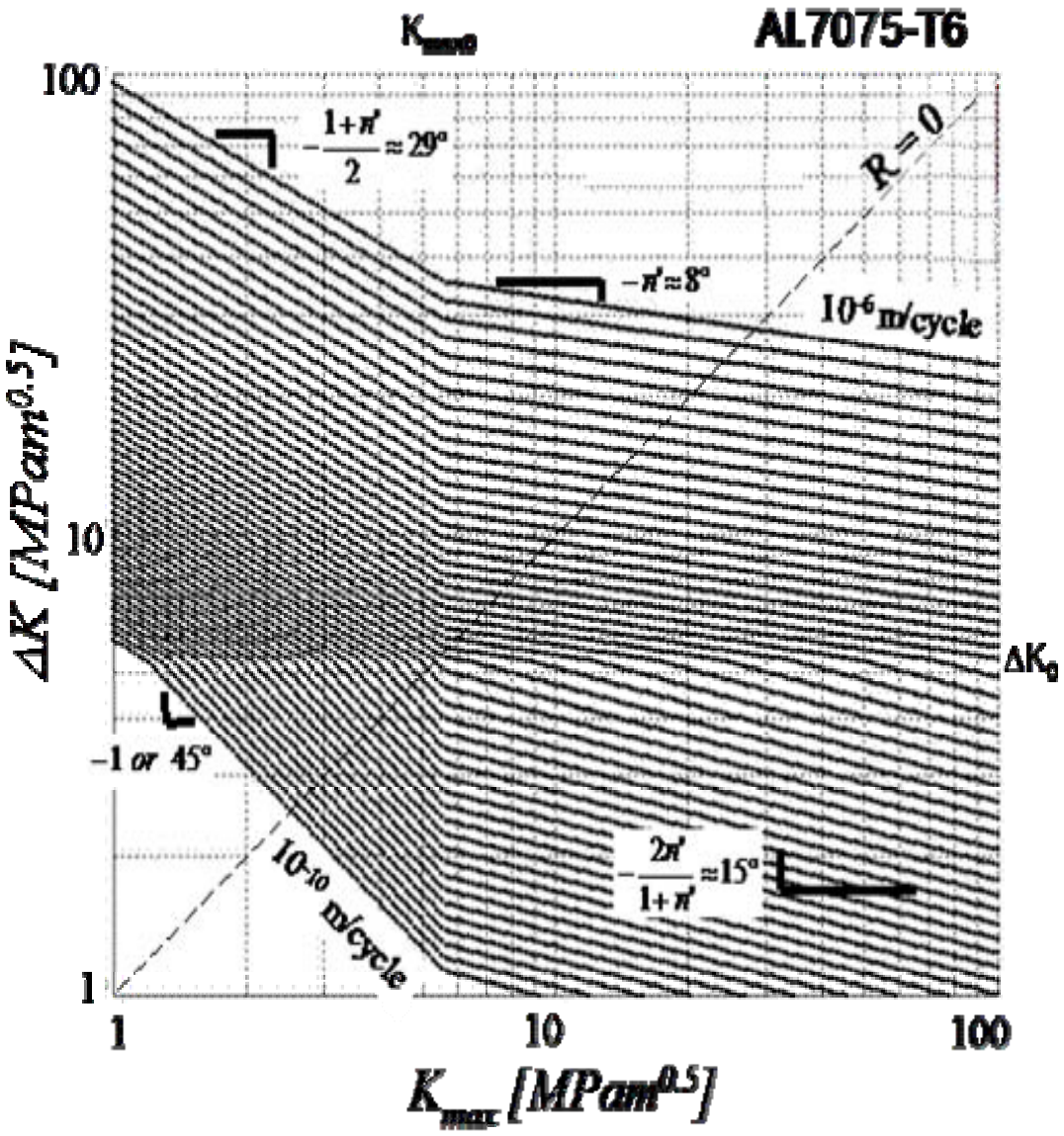

Figure 34 Analytical plot of ΔK vs. K_{max} for various da/dN

E [GPa]	H' [MPa]	b	n'	c	ε'_f	σ'_f [MPa]
72.4	1280	-0.176	0.107	-0.839	0.8	1917

Table 2 Properties of 7475-T7351 Al alloy [173]

The calculations for negative load ratios are hypothetical (since a potential contact between crack faces is neglected in the model). The SWT parameter does not exhibit the fatigue limit. As a result, no attempt was made to calculate any threshold values either for K_{max} or ΔK since only the general trends will be used later for modeling.

An examination of Figure 34 allows for the following conclusions to be drawn:

1. Two curves with constant da/dN never intersect on a K_{max} vs. ΔK plot.
2. For intermediate and high da/dN there are two slopes: $-(1+n')/2$ and $-n'$.
3. The difference between these slopes is too small to be noticed experimentally.
4. For very low da/dN there are two slopes: $-2n'/(1+n')$ and -1.
5. Similar results have been reported in [25] where the generalized Neuber rule was used for the stress and strain calculation at the 'process zone'.

The well known Morrow or Goodman equations can be adopted instead of the SWT parameter in order to account for the mean stress effect. Also, the stress/strain distribution at the crack tip can be calculated using Finite Element Analysis (FEA) instead of Rice and elastic solutions. However, none of these methods will give a closed form analytical solution of the problem and neither of them will be more general than those presented above. For completeness and as a summary of this section, Figure 35 illustrates other possible approaches.

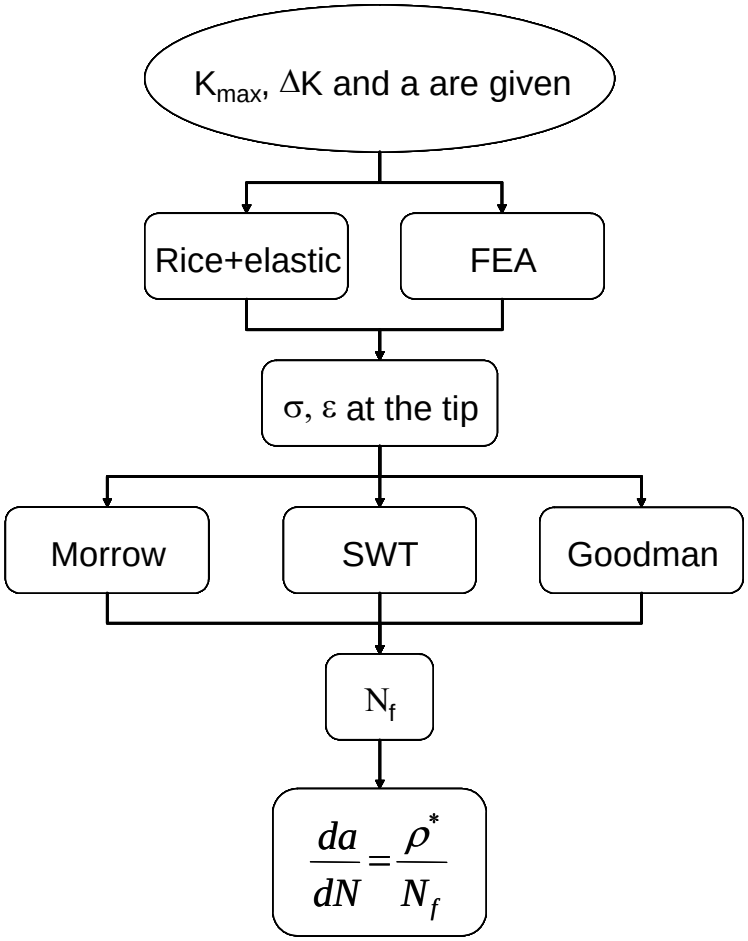

Figure 35 Possible algorithms for derivation of the two-parameter FCG rate equation crack propagation table

Based on the analytical verification of the two-parameter crack driving force the following conclusions can be drawn:

The two-parameter crack driving force in terms of ΔK and K_{max} represents a fundamental fatigue crack growth behavior.

- Logarithmic plot of ΔK vs. K_{max} indicates the power-law relationship.
- There are two crack propagation regions - ΔK and K_{max} dominated, corresponding to high and low load ratios, respectively.
- The transition between ΔK and K_{max} dominated regions occurs at load

ratios ranging from 0 to 0.5.

- The slope of the constant da/dN line plotted on log(ΔK) vs. log(K_{max}) graph is shown to be related to the strain hardening exponent n'.
- Theoretically, there are four different slopes depending on the particular combinations of ΔK and K_{max}.

Because of the limitations above, the theoretical model in this paper is just a step in the development of the CP table presented in the next section and should not be used alone for prediction of the fatigue life in real applications.

Crack propagation table

Figure 34 indicates that ΔK is the dominant fatigue crack driving force parameter since the slope on the ΔK vs. K_{max} plot for a constant da/dN never exceeds -1. However, K_{max} has also significant contribution to the fatigue crack driving force and cannot be omitted, even in the high load ratio region where R > 0.5. In this region there is a general agreement that the crack closure is negligible but the K_{max} effect still exists.

In order to confirm these observations and also to compare the predicted crack propagation rates with the experimental data, the concept of crack propagation (CP) table was developed as illustrated in Figure 36. FCG rates are determined at 25 equally spaced (on a log scale) locations between the threshold and fracture toughness values for both ΔK and K_{max} parameters. Every element of this table containes da/dN for a particular combination of ΔK and K_{max}. This allows plotting of the table as a three dimensional surface (Figure 39) with da/dN being the height (z). The CP table can be constructed with any number of da/dN elements. In this study, the 25 FCG rates used in the AFGROW software package, were adopted as ‘standard’ values.

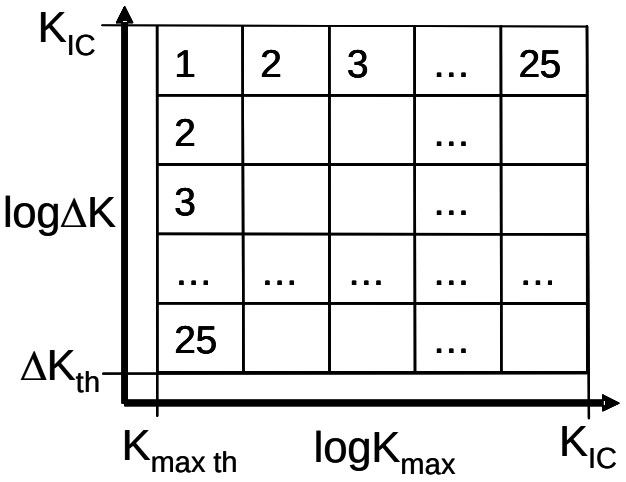

$$K_{\max_i} = \Delta K_i = \Delta K_{th}\left(\frac{K_{IC}}{\Delta K_{th}}\right)^{\frac{i-1}{24}}$$

, where i = 1, 2, 3 … 25

Figure 36 Crack propagation table basics

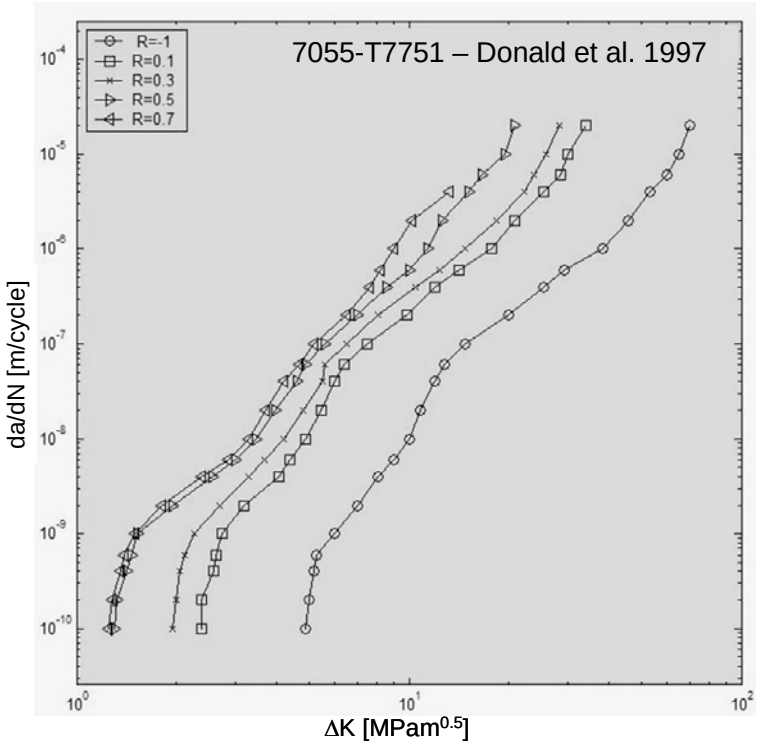

Standard' da/dN values:

2.54E-04
1.02E-02
2.54E-05
2.03E-05
1.52E-05
1.02E-05
5.08E-06
2.54E-06
1.02E-06
5.08E-07
2.54E-07
1.02E-07
5.08E-08
2.54E-08
1.52E-08
1.02E-08
7.62E-09
5.08E-09
2.54E-09
1.52E-09
1.02E-09
5.08E-10
2.54E-10
5.08E-11
2.54E-11

Figure 37 Experimental data [176] and 'standard' da/dN values

Most of the experimental data in the literature are for constant ampitude loading tests conducted at different load ratios, R. In order to use such a data to construct the CP table, they first have to be digitized for a constant da/dN. Figure 37

shows da/dN vs. ΔK data for 7055-T7751 Al alloy. In the present study a MatLab procedure was developed for this purpose (see Appendix C). It generates ΔK for every combination of da/dN and R using linear interpolation between the experimental points.

The following relationship was used to calculate the corresponding K_{max} values:

$$K_{\max} = \frac{\Delta K}{1 - R} \qquad (2.8)$$

In such a way, all the coordinates needed for the CP table are readily determined (ΔK, K_{max} and da/dN). These values, however, are experimental and generally do not match the 'standard' values which are needed for the generation of the CP table (Figure 37).

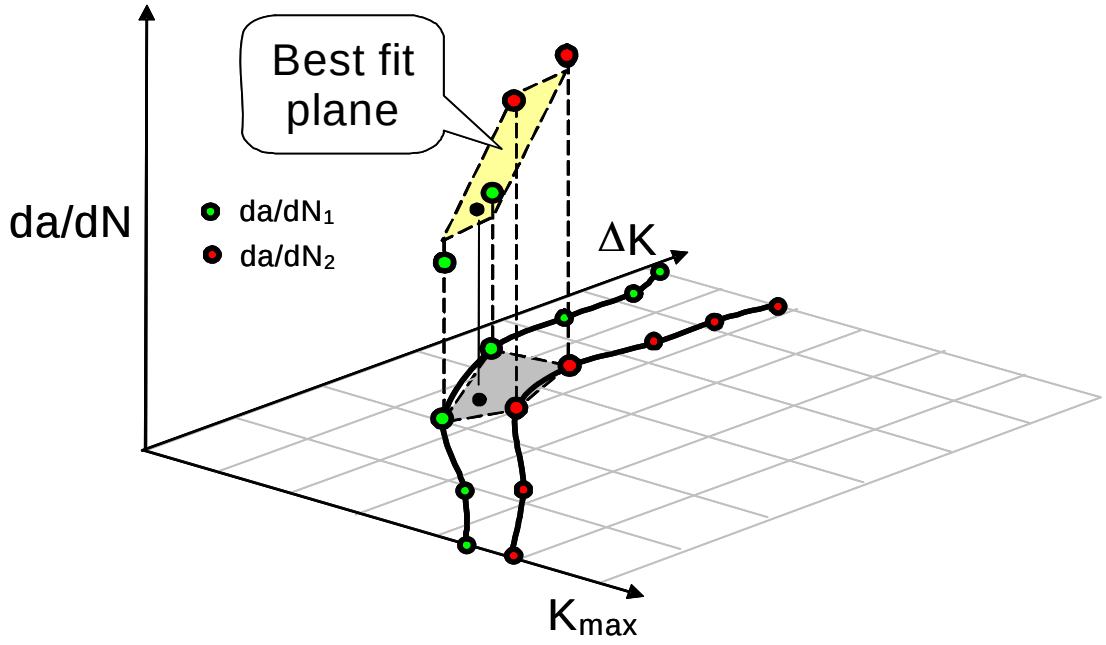

Figure 38 Procedure for interpolation between the experimental data for different fatigue crack growth rates

Figure 38 shows how linear interpolation between the experimental points can

be used to obtain the da/dN values for the CP table. First, the closest four experimental points are identified. Then a least squares procedure is used to fit a plane between these four points, da/dN = f(ΔK, K_{max}). This equation is used to find da/dN in the point of interest. As an alternative, a MatLab command can be used (griddata). It is based on Delaunay triangulation of the data that uses Qhull [177].

Figure 39 shows a CP table, constructed using the procedure, outlined above. The experimental data is largely insufficient and for most of the ΔK-K_{max} combinations, da/dN is still unknown.

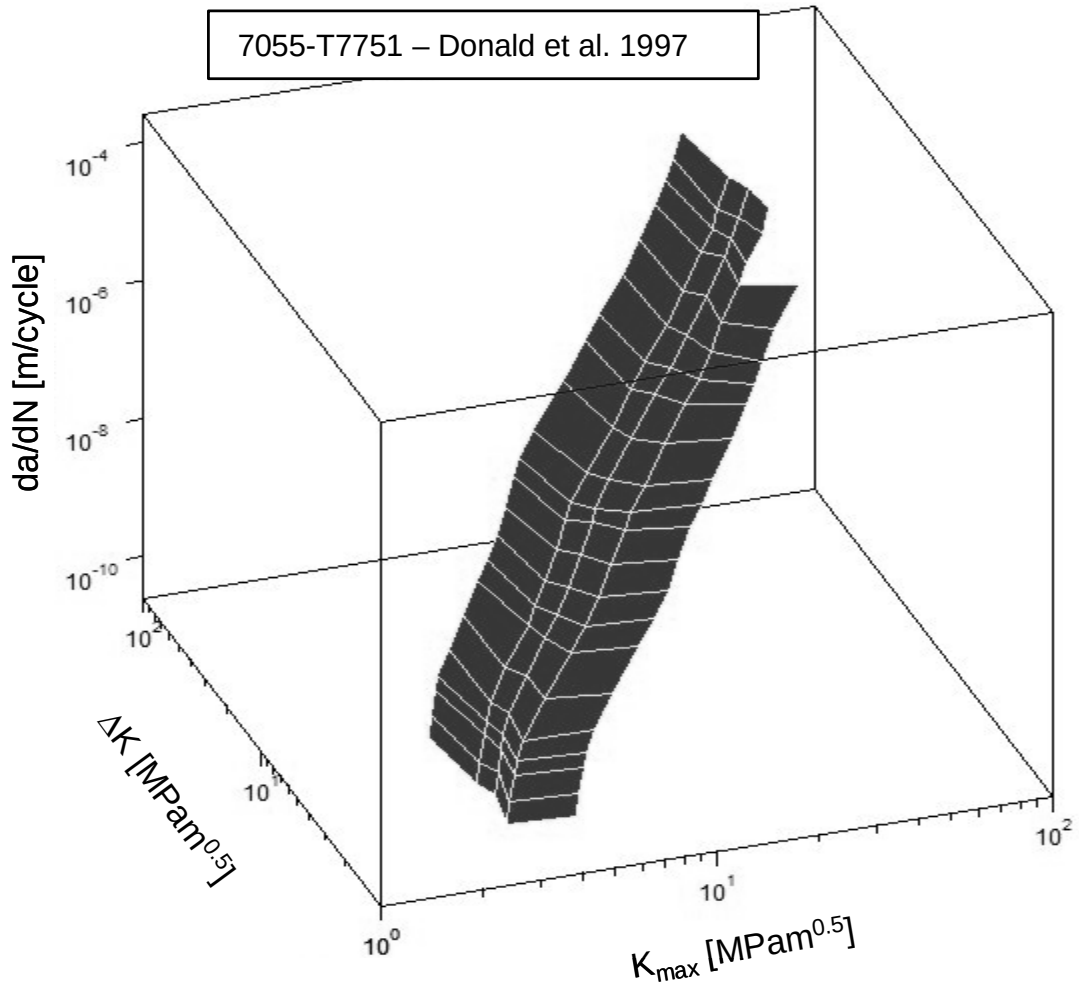

Figure 39 Experimental crack propagation table

This problem can be solved either by adding more data from other sources for the same or similar materials, or by extrapolation. In order to find the extrapolation rules, a log-log plot of ΔK vs. K_{max} was constructed (Figure 40). The experimental data clearly shows double linear dependence between ΔK and K_{max} for any particular da/dN.

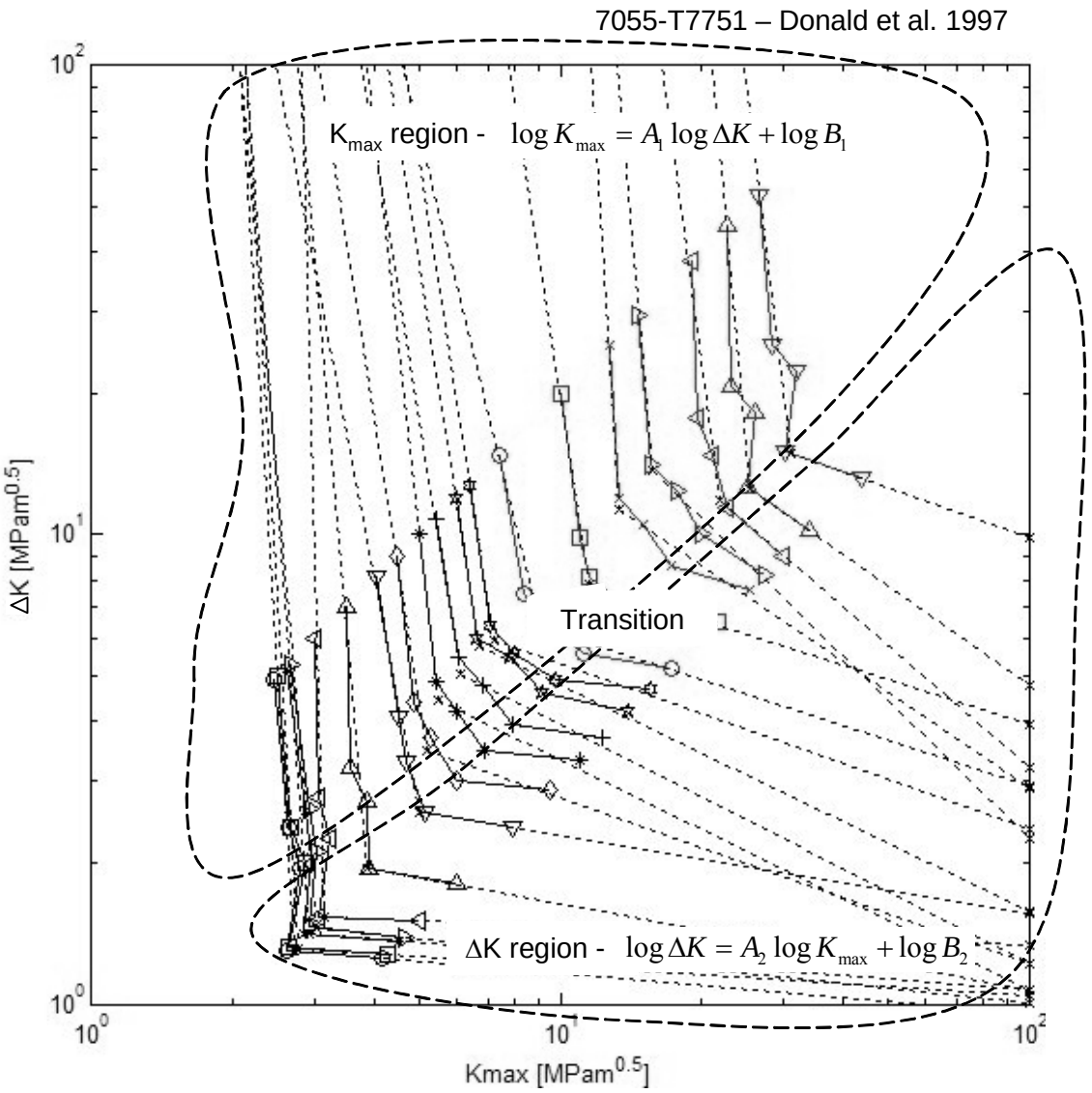

Figure 40 Extrapolation of the experimental data in the crack propagation table

The slope, however, is changing. It is almost vertical for low load ratios, R. This means that the crack growth rate in this region is controlled mainly by K_{max}. At high R values the slope is almost horizontal, thus this region is called a ΔK controlled region. These observations show that fatigue crack growth data has to be extrapolated using separate least squares fits above and below the transition point (dashed lines in Figure 40). In order to avoid numerical problems with the least squares procedure in the ΔK dominated region, K_{max} should be the independent variable. In the K_{max} dominated region, ΔK should be the independent variable.

The existence of two distinct regions depicted in Figure 40 confirms the two-parameter nature of the fatigue crack driving force as postulated by Vasudevan and Sadananda [1 - 159] and Kujawski [160 - 161]. The slope in the ΔK controlled region was correctly predicted to be almost horizontal in the previous section, which confirms the validity of the theoretical analysis. This analysis, however cannot explain the existence of a K_{max} dominated region. It can be speculated that the transition occurs due to crack face contact, especially for $R<0$. When the crack faces are in contact, the stress concentration at the tip no longer exists, but the stress at the crack tip continues to decrease with decreasing load. Applied stresses are a lot lower than the local stresses, hence the change of slope on the ΔK vs. K_{max} plot.

In order to perform the fitting of the equations in Figure 40, the transition point has to be determined first. It can be seen that it varies approximately from R = 0 to 0.5. In the ASTM standard E647 it is suggested that for $R<0$, $\Delta K=K_{max}$. This assumption effectively defines the transition point is at R=0, which may cause significant error, especially in the threshold region.

In the present study, a numerical procedure was used to find the transition point for every da/dN with the minimum error allowed by the experimental data. First

a pair of straight lines is fitted to the particular da/dN curve, using any of the experimental points on the curve as a transition.

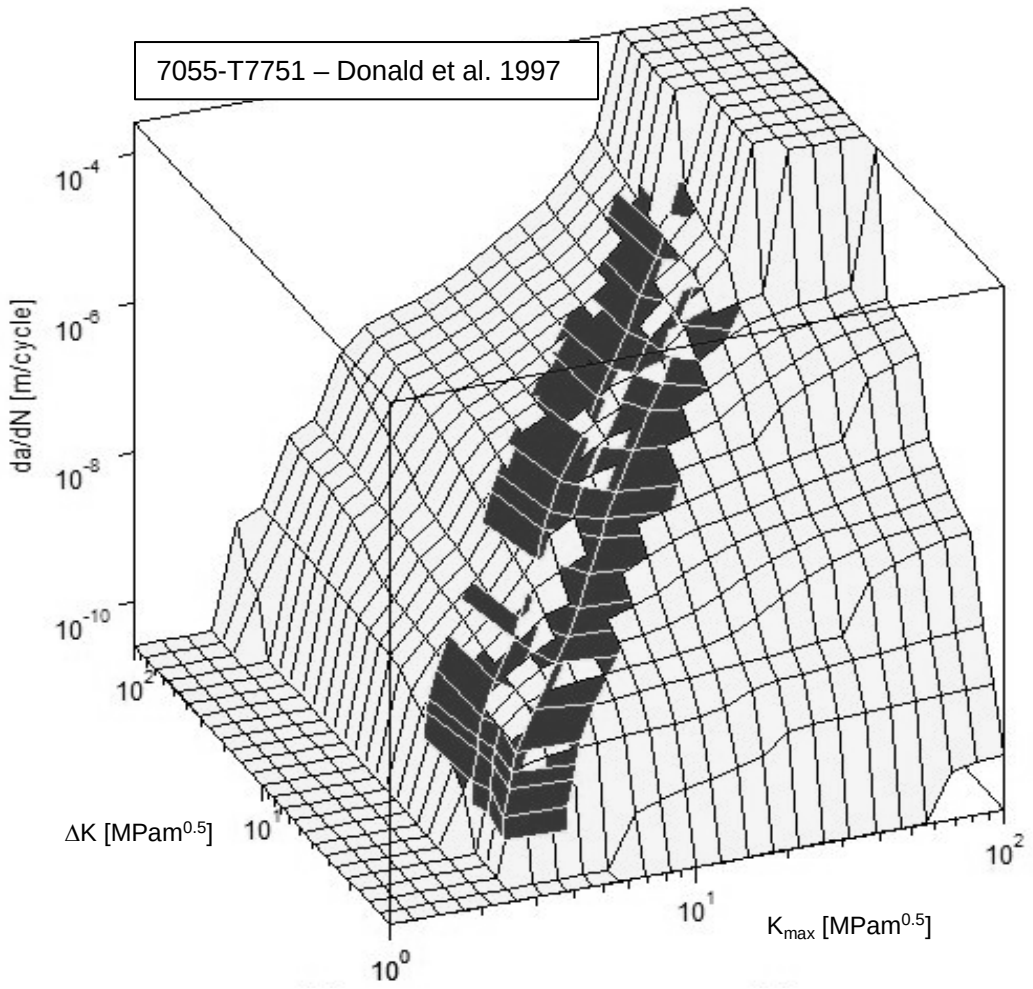

Figure 41 Comparison between experimental data and the results from the extrapolation procedure

Then an error coefficient is calculated for every pair of lines as a sum of the squared distances between the lines and the experimental points. The pair with the least error coefficient defines the actual transition point. The dashed lines in Figure 40 were fitted using this procedure. After that, the interpolation procedure, illustrated in Figure 38, was utilized to complete the CP table for this material as shown in Figure

41. It can be seen that the fitted surface matches the experimental results closely.

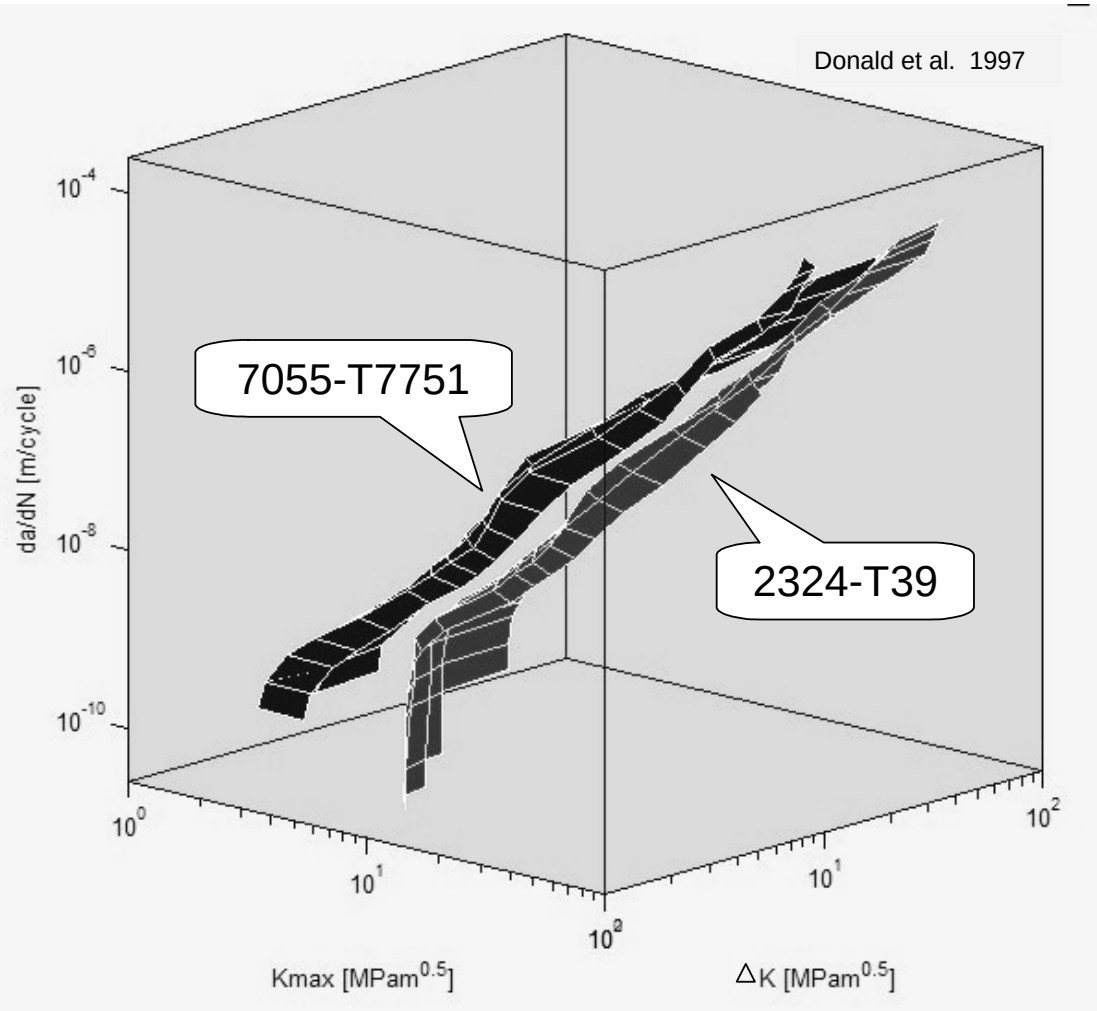

Figure 42 Comparison of the fatigue crack growth in different materials, using the crack propagation table concept

Extrapolation was performed only for constant da/dN where experimental data are available. For the $\Delta K - K_{max}$ combinations requiring da/dN out of that range, crack growth rate was assumed to be equal to the maximum value – corresponding to sudden fracture, or to the minimum value – corresponding to threshold conditions accordingly. This assumption was made just to complete the CP table, even for the cases where experimental data is not sufficient. This can cause the predicted fatigue

life to be unrealistically high if raw data does not start from the threshold (~$1x10^{-11}$ m/cycle).

The CP table is a convenient way to represent and discuss the fatigue crack growth data, using simple data reduction schemes. It can be represented as 2D or 3D images as it is illustrated by Figure 40 and Figure 41, respectively. The CP table also offers a convenient way to compare crack propagation in different materials, environments, etc. as it is depicted in Figure 42 for two aluminum alloys.

The trends, observed in the experimental data on CP table were explained by analytical derivations based on analogy between process zone and smooth fatigue specimen. This assumption however, is not valid if there is interaction between the crack faces. This defines two distinct regions in the CP table – ΔK and K_{max} dependent. The transition between them is easy to explain when the applied load becomes negative (at negative R), but in general the experiments show a different trend - transition at R=0 to 0.5 (Figure 40). This phenomenon can be explained with premature crack face contact due to asperities, oxidation or plastically deformed material behind the crack tip. This approach, known as 'crack closure' was developed in 1971 [147] and has been improved ever since. This is a well-known concept with many strengths and weaknesses (studied in part I). In the next section, a different approach is developed, using the stresses ahead of the crack tip (internal stresses).

Local crack propagation table (at the crack tip)

The CP table described in previous section is composed from the applied values of ΔK and K_{max}, which do not experience any dependence on the previous load history and therefore cannot be used to predict the load interaction effects. The strains at the crack tip 'process zone' have to be bigger than the elastic limit of the material if

there is any crack propagation at all. These strains will not recover upon unloading and will induce internal stresses (Figure 43). These internal stresses retain information of the previous load history. Therefore, if the CP table is constructed using the total ΔK and K_{max} values at the crack tip instead of the applied ones it can be used for prediction of the load history effects. However, the internal stress intensity factor (K_{int}) and the internal stresses that cause it have to be calculated first.

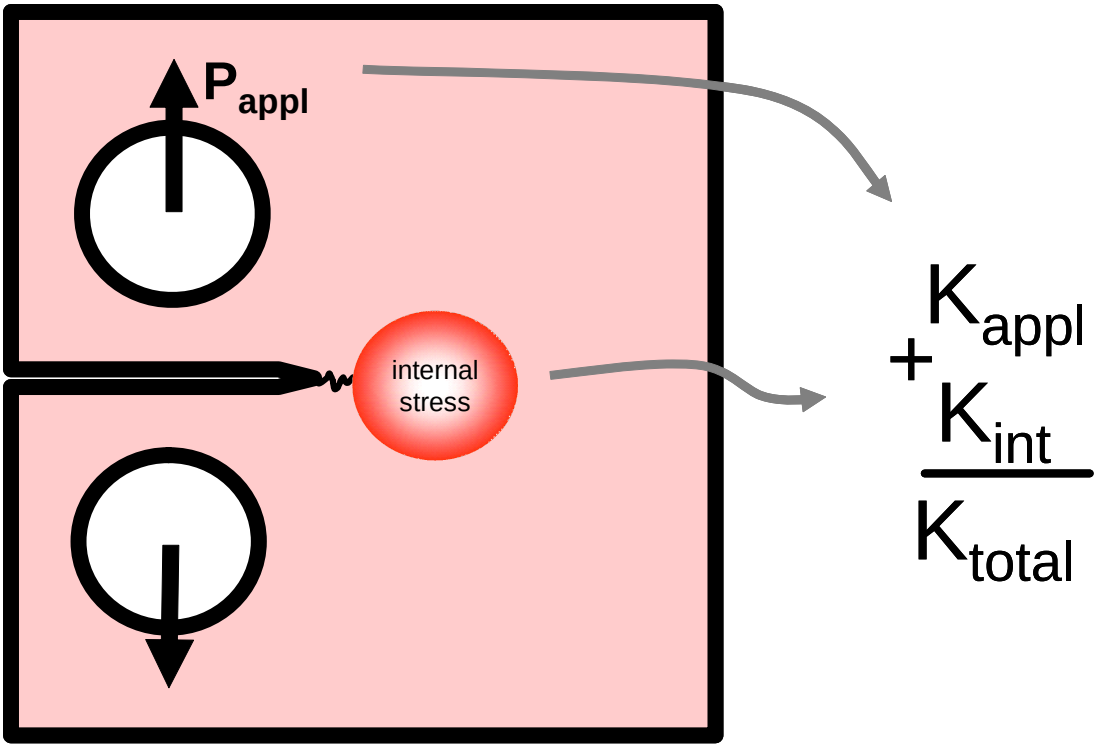

Figure 43 Calculation of the total stress intensity factor at the crack tip (either K_{min} or K_{max})

Calculation of the internal stresses

The stress distribution ahead of the crack tip is calculated using the same material model that was utilized to derive the two parameter crack driving force (Eq. 2.4 and 2.5). In this section the model will be explained in more detail and a simple

loading case will be simulated as an example. The results will be analyzed and compared using a finite element simulation.

For a known K_{max}, the maximum stress profile is calculated using Rice equation in the plastic zone and the linear-elastic solution elsewhere:

$$\sigma_{max} = \sigma_0 \left(\frac{K_{max}}{(1+n')\pi\sigma_0^2 (x+\rho^*)} \right)^{\frac{n'}{1+n'}} \quad \text{(Rice)}$$

$$\sigma_{max} = \frac{K_{max}}{\sqrt{2\pi(x+\rho^*)}} \quad \text{(elastic)} \qquad (2.9)$$

In Eq. 2.9, ρ* is the 'process zone' size. Stress and strain are assumed to be constant in the process zone. The effect of this parameter on the fatigue crack growth prediction will be discussed later in the dissertation. The elastic solution is 'offset' in the direction of crack propagation by the amount needed to coincide with the yield point from Rice equation (approximately half of the plastic zone size, $x_0/2=(K_{max}/\sigma_0)^2/(2\pi)$, as suggested by Irwin).

Figure 44 illustrates how the procedure, outlined above is used to calculate the maximum stress distribution ahead of the crack tip. The stress range, $\Delta\sigma$ is calculated using the same procedure for a given ΔK. The minimum (internal) stress profile is calculated by subtracting $\Delta\sigma$ from σmax. Residual stress profile is calculated by when $\Delta K = Kmax$ (unloading to zero).

The stresses, calculated with the procedure presented above were validated using a plane stress 2D finite element simulation (R = 0). The mesh was generated with triangular plane stress elements. The results are shown in Figure 45. It can be seen that the correlation is good around the cyclic and monotonic plastic zone boundaries. Close to the crack tip, however the stresses were underestimated by the

analytical model. This indicates a possibility for further refinement of the crack growth predictions by using finite element calculations of the internal stresses. In this study the analytical formulas were used since they are much faster (FEA requires selection of material model, mesh size, boundary conditions etc).

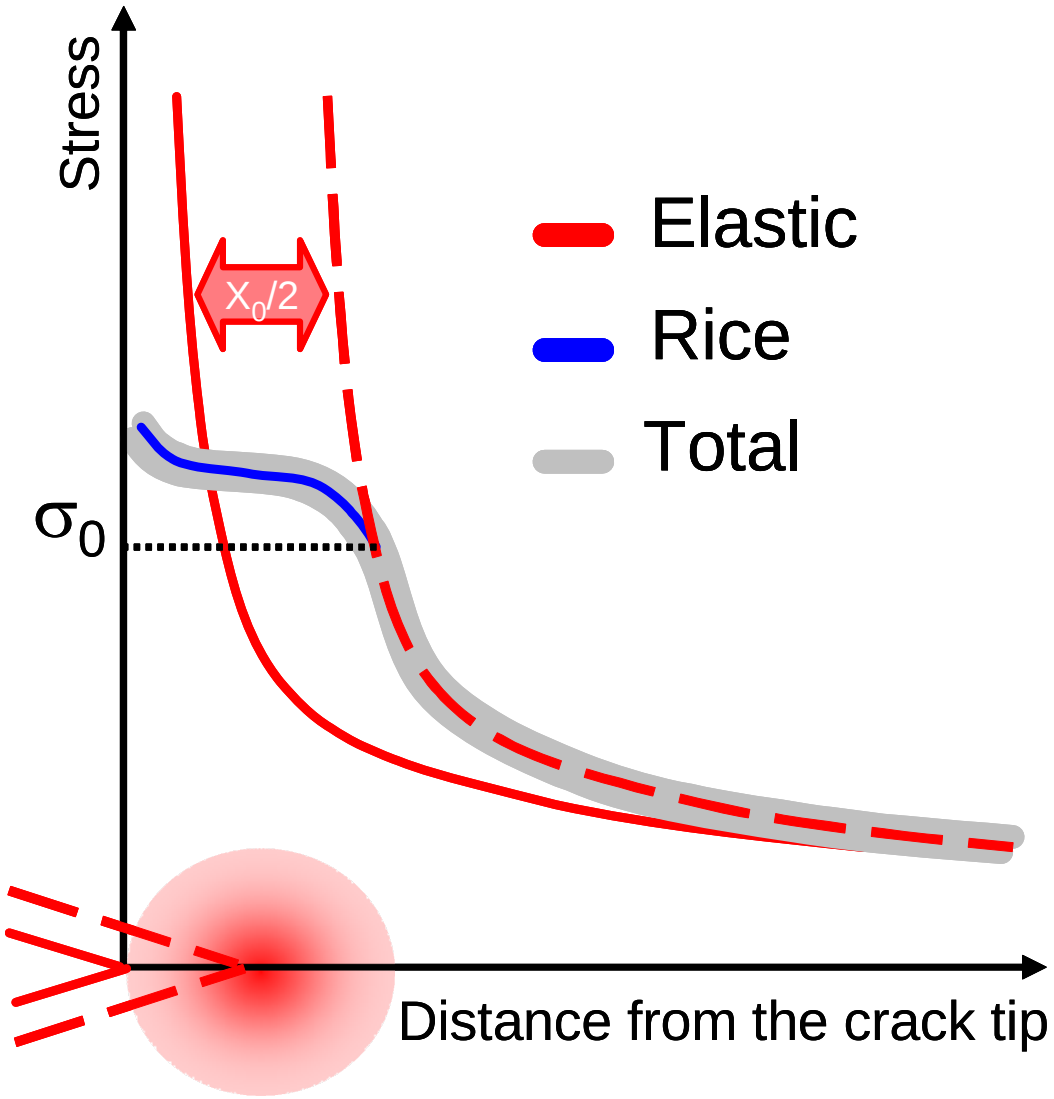

Figure 44 Stress distributions ahead of the crack tip

The procedure, outlined above is valid only for positive load ratios. When the minimum applied stress (S_{min}) is reduced to zero, the crack faces would touch and the

crossection area, bearing stress in the crack plane, will increase. Therefore, if the specimen is subjected to compressive loads the stress concentration at the crack tip will be eliminated and the local elastic stresses will change the same amount as the applied ones.

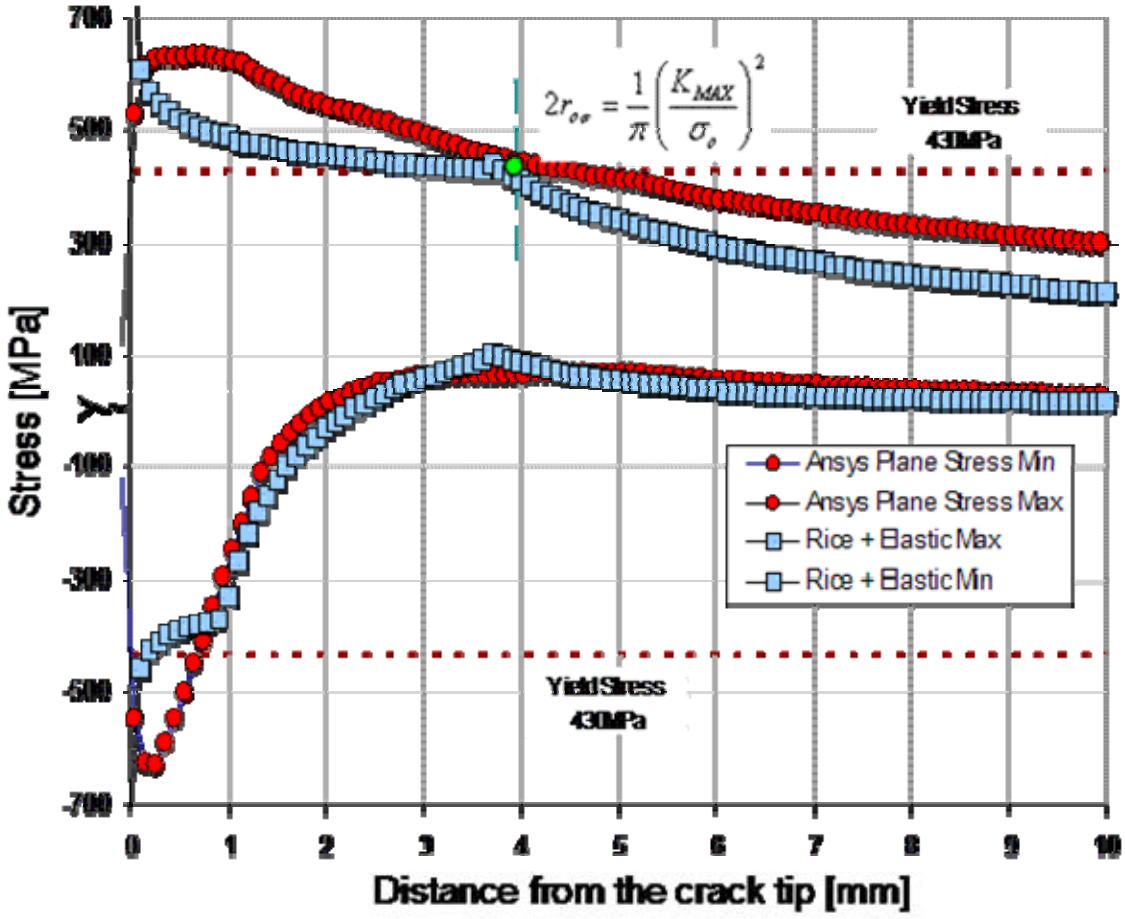

Figure 45 Comparison between the analytical and finite element calculations of the internal stresses (Al 2324-T39)

Figure 46 was constructed to illustrate this concept. Ten minimum stresses were simulated in steps or 10 MPa starting from 0, keeping the maximum load constant. First the residual stress profile σ_{res} was calculated for R=0. Then σ_{res} was offset down by the applied S_{min} to get the local σ_{min}. These stresses can be added only

in the elastic region. Rice equation was used in the plastic region ($\sigma_{min} < \sigma_{max}-2S_y$) by simply fitting a power law equation with exponent equal to the strain-hardening exponent (n') through the new yield point.

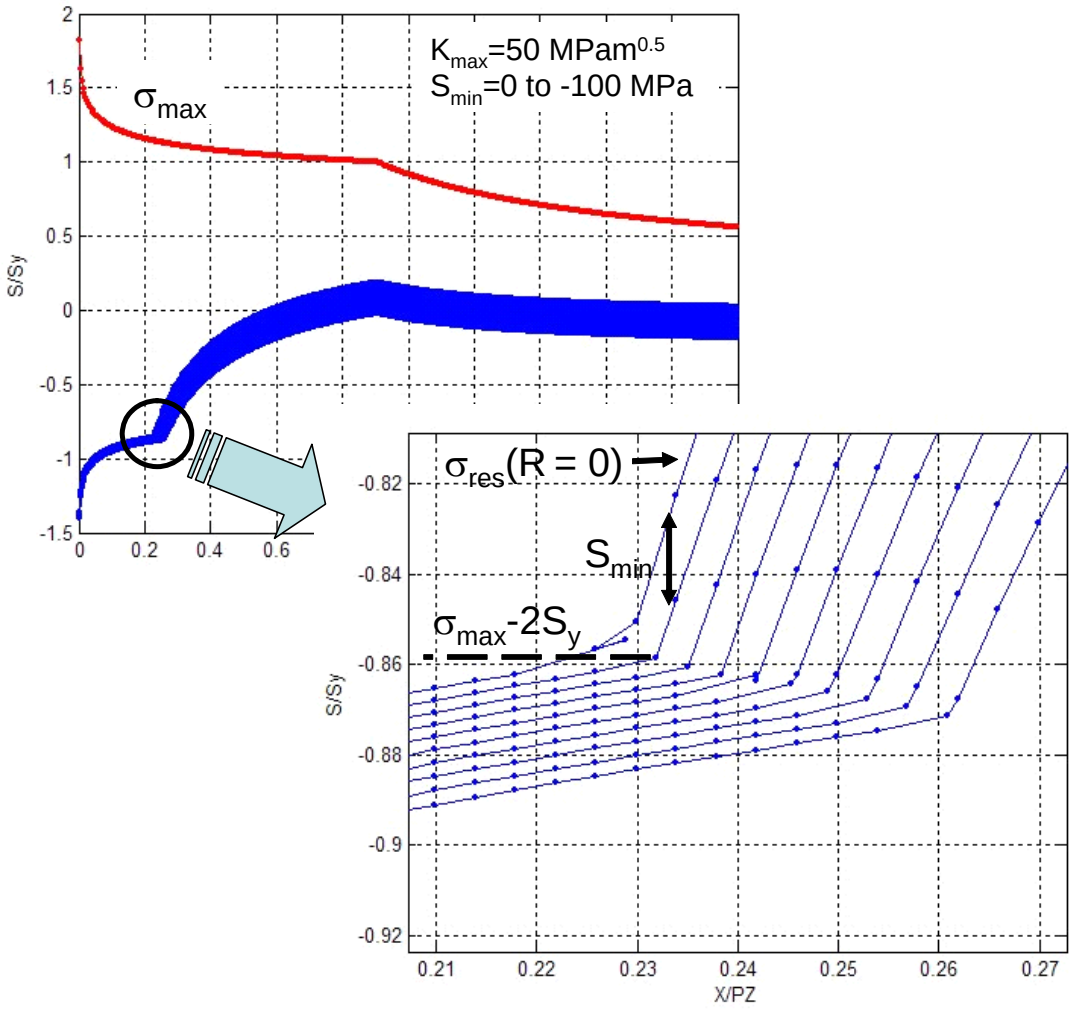

Figure 46 Calculation scheme for the minimum stress profile ahead of the crack tip for negative load ratio (Al 2324-T39).

Calculation of the internal stress intensity factors

The stresses calculated in the previous section can be used to calculate the internal stress intensity factor. The easiest and most widely accepted method is the

weight function. This concept is customarily used to evaluate the stress intensity factor due to residual stresses. Here this approach will be adopted to analyze minimum stress profiles as well, which requires some phenomenological assumptions to be made. Therefore, another approach called clamping force method was developed. It has sound physical basis and generates results similar to that of the weight function. Both methods will be explained and compared in the next sections.

Weight function method

Weight function uses a simple integration scheme to calculate the effect of the internal stresses at the crack tip on the stress intensity factor:

$$K = \int_0^a \sigma(x) m(x, a) dx \qquad (2.10)$$

In Eq. 2.10, 'a' is the current crack length, 'σ(x)' is the internal stress profile as a function of the distance from the crack tip, x, and 'm(x, a)' is the weight function. The weight function is geometry dependent – solutions for a particular case can be found elsewhere in the literature. In general, the weight function solution will integrate the stresses in the crack wake, giving more weight to the ones closer to the crack tip.

Residual stresses can be introduced by welding, inclusions, phase transformations etc. These stresses are actually the internal stresses when the applied load is zero. In case of a cracked member cyclic loading would cause internal stresses even if none of the factors mentioned above is present. They are caused simply by the crack tip yielding from the applied loading. If both K_{max} and ΔK remain constant, the whole stress field around the crack tip moves with the crack. Only internal stresses in the crack wake can be used to calculate K_{int} with the weight function. To find what

part of the stress profile should be used for the calculation of K_{int} a simulation was done using the load history shown in Figure 47. For this load history, the maximum stress profile remains the same, only the minimum stress distribution changes with the load ratio. For every load step the crack was propagated through the whole length of the minimum stress profile from the previous step and the evolution of the residual stress intensity factor was calculated (Figure 48).

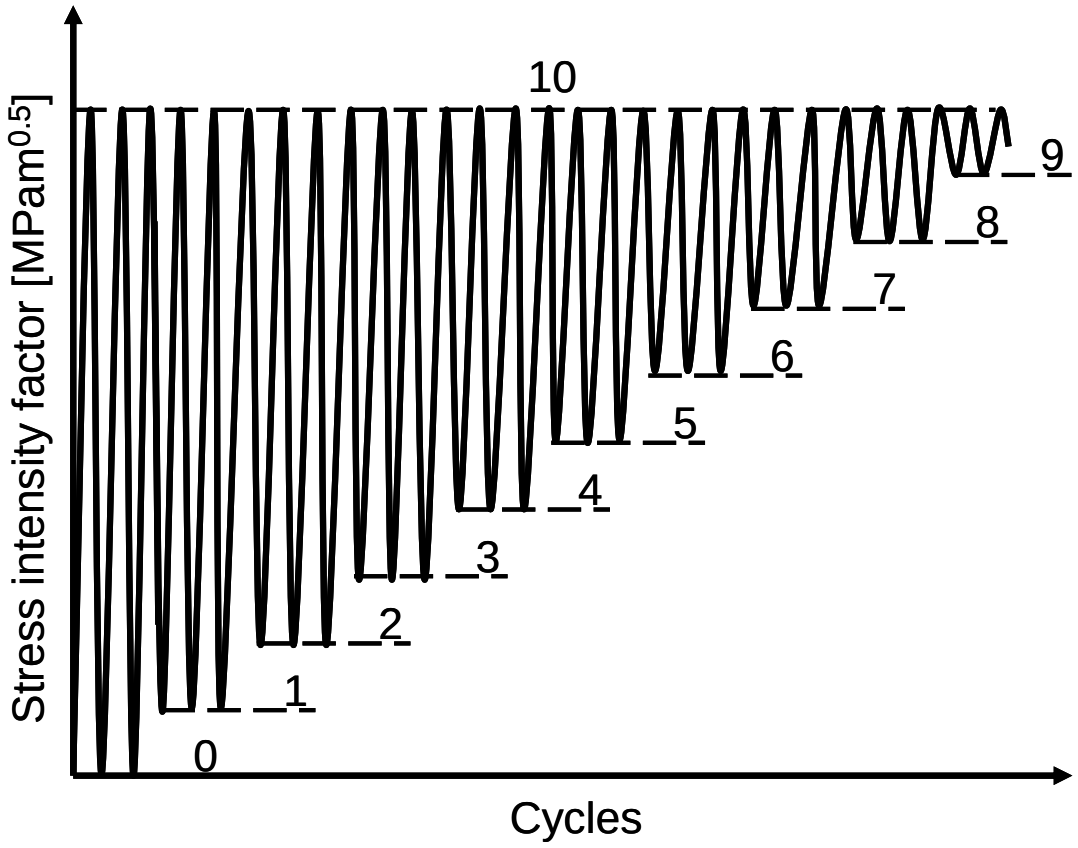

Figure 47 Load history for the numerical simulations

From the results of this numerical simulation it was determined that the residual stress intensity factor reaches minimum at the end of the cyclic plastic zone. These values will be shown later to give the best predictions of the experimental data. This means that the crack has to be advanced to the extent of the cyclic plastic zone

just for the calculation of K_{int}. An analogy can be made with the Dugdale model or Irwin plastic zone correction, where the crack tip is moved by (approximately) the same amount.

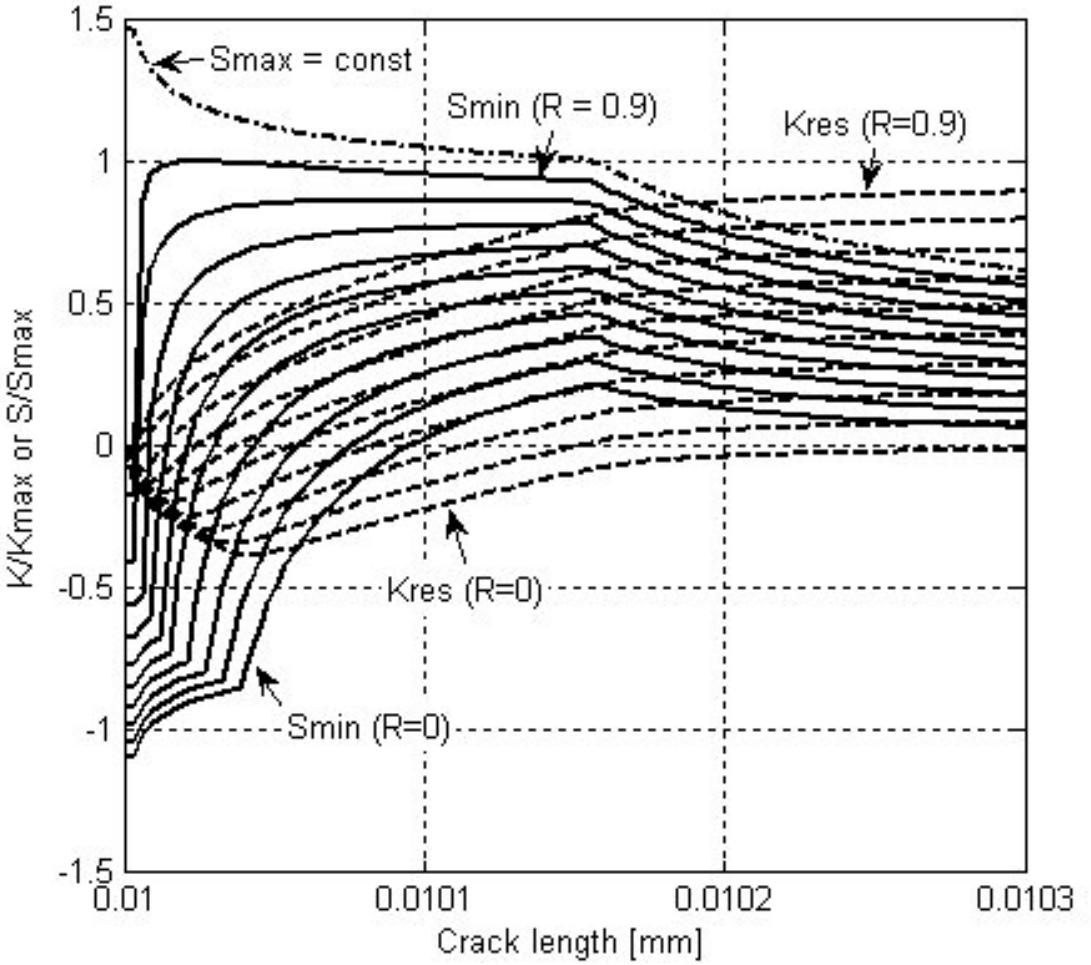

Figure 48 Stress profiles and internal stress intensity factor profiles for different load ratios

Figure 49 shows the final results for the internal stress intensity factor calculated using the weight function method. The number of the load ratios is increased in order to obtain more accurate shape of the curve.

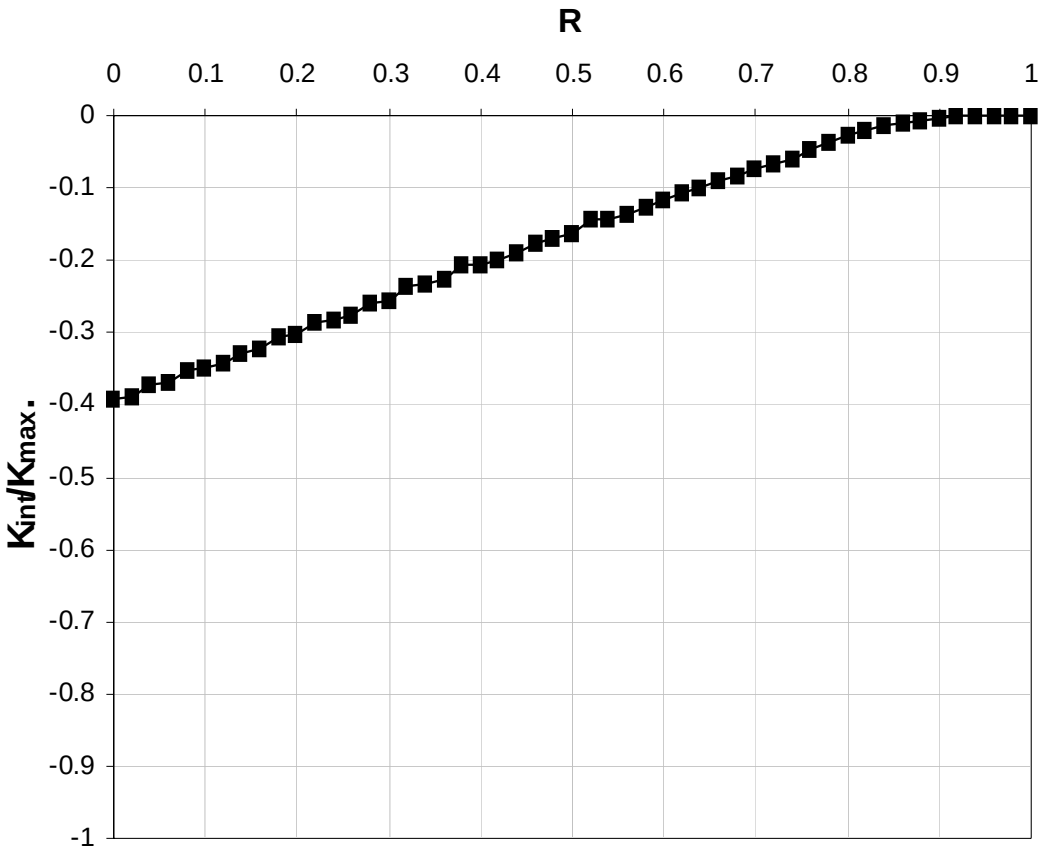

Figure 49 Results from the numerical simulation of the weight function method for different load ratios

Clamping force method

The weight function method for calculation of the internal stress intensity factor has two disadvantages. First, the crack has to be artificially propagated just for the calculation of the weight function integral. Second, this integral has to be calculated for every point on the stress profile. This limits the applicability of the weight function approach to simple load histories. Therefore, the method of clamping force was developed in an attempt to overcome these problems.

To illustrate how the clamping force method works, a simulation was done for R = 0 (Figure 50). Internal stresses were calculated using a simplified material model

– elastic perfectly plastic. This was done in order to make the method effective and easy to apply.

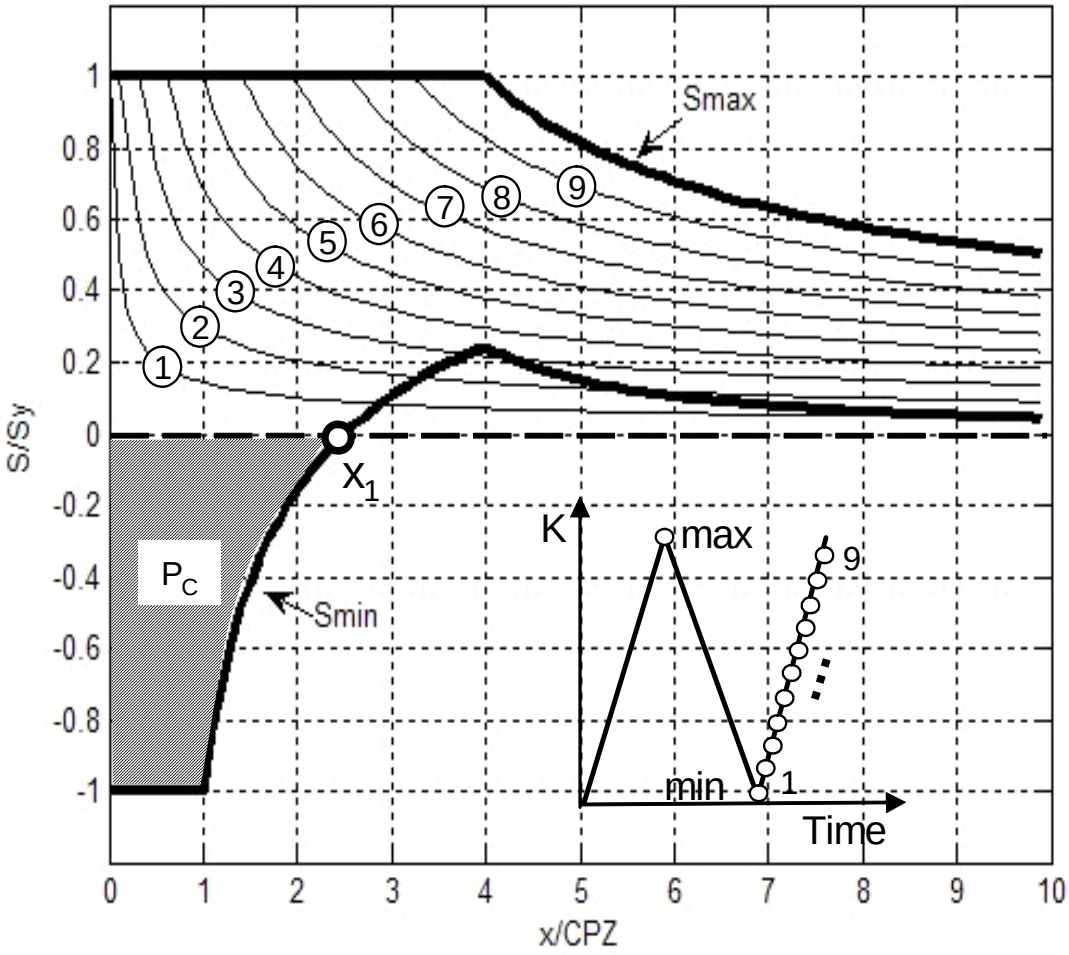

Figure 50 Incremental increase of the applied K from 0 to maximum

The minimum stress profile, shown in Figure 50, defines an area ahead of the crack tip, where the stresses are negative. If these stresses are integrated over the distance ahead of the crack tip and the thickness, the result will be force. This is the clamping force (P_c) that the elastically deformed material away from the crack tip exerts on the plastically deformed region close to the crack tip. In order to determine the stress intensity factor corresponding to P_c, the next tensile loading is applied

incrementally. The stress distribution ahead of the crack is calculated for each applied level of the tensile stress intensity factor (Figure 50). Then these profiles are integrated over the negative stress distance x_1 and the thickness in order to find the force that would neutralize the clamping force. The stress intensity factor that corresponds to this force is called K_{int}.

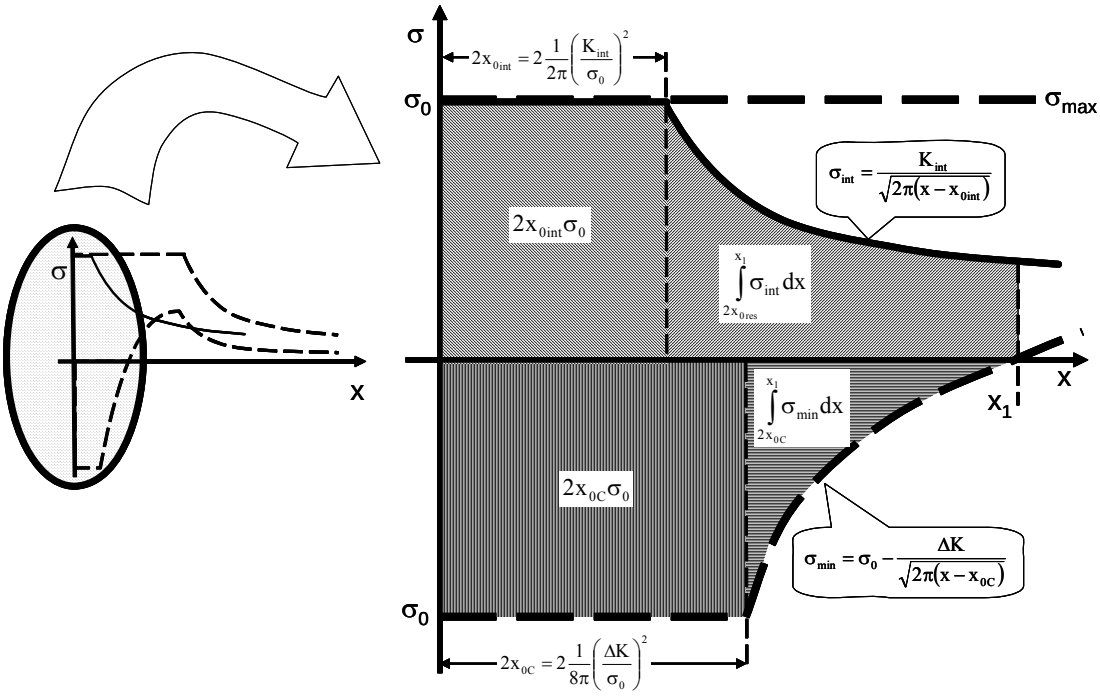

Figure 51 Calculation of the area below an arbitrary stress profile

The procedure outlined above can be applied for different load ratios. Instead, an analytical solution will be derived next, since it is much more practical (fast). The stress profiles ahead of the crack tip can be calculated for a known stress intensity factor, using the linear-elastic equations and σ_0 as shown in Figure 51. It can be seen that the profiles are modified to accommodate double the plastic zone than the one from the linear-elastic solution in order to account for the stress redistribution due to yielding. The clamping force, P_C, and the internal force, P_{int}, can be calculated as a

product of the corresponding stress profile areas and the thickness of the specimen (t):

$$\begin{aligned} P_{int} &= \left(2x_{0int}\sigma_0 + \int_{2x_{0int}}^{x_1} \frac{K_{int}}{\sqrt{2\pi(x - x_{0int})}} dx \right) t \\ P_C &= \left(2x_{0C}\sigma_0 + \int_{2x_{0C}}^{x_1} \sigma_0 - \frac{\Delta K}{\sqrt{2\pi(x - x_{0C})}} dx \right) t \end{aligned} \tag{2.11}$$

The upper boundary for the integrals in Eq. 2.11 can be determined from the condition that the minimum stress should be zero there. Beyond that point the stresses remain much lower than the yield stress and are not likely to affect the crack behavior:

$$\begin{aligned} \sigma_{min}(x_1) &= \sigma_0 - \frac{\Delta K}{\sqrt{2\pi(x_1 - x_{0C})}} = 0 \\ (x_1 - x_{0C}) &= \frac{1}{2\pi}\left(\frac{\Delta K}{\sigma_0}\right)^2 \\ (x_1 - x_{0C}) &= 4x_{0C} \\ x_1 &= 5x_{0C} \end{aligned} \tag{2.12}$$

Knowing the integral boundaries, Eq. 2.11 can be solved as follows:

$$\begin{aligned} P_{int} &= 2t\left(x_{0int}\sigma_0 + \frac{K_{int}}{\sqrt{2\pi}}\left(\sqrt{5x_{0C} - x_{0int}} - \sqrt{x_{0int}}\right)\right) \\ P_C &= \left(\sigma_0 x_{0C} - \Delta K\sqrt{\frac{2x_{0C}}{\pi}} \right) t \end{aligned} \tag{2.13}$$

These two forces must be in equilibrium, which can be used in order to find the internal stress intensity factor:

$$\left| \begin{aligned} P_{int} &= -P_C \\ x_{0int} &= \frac{1}{2\pi}\left(\frac{K_{int}}{\sigma_0}\right)^2 \\ x_{0C} &= \frac{1}{8\pi}\left(\frac{\Delta K}{\sigma_0}\right)^2 \end{aligned} \right. \tag{2.14}$$

The answer is a biquadratic equation giving the relation between the applied

and the internal stress intensity factor:

$$\frac{9}{16}\Delta K^4 - 5\Delta K^2 K_{int}^2 + 4K_{int}^4 = 0 \tag{2.15}$$

Equation 2.15 can be solved analytically to give a relation between K_{int} and the applied load ratio. For this purpose it will be normalized with respect to K_{max} and an additional relation between ΔK and R will be used:

$$\Delta K = (1-R)K_{max} \tag{2.16}$$

The result after the normalization/substitution is shown below:

$$\frac{9}{16}(1-R)^4 - 5(1-R)^2\left(\frac{K_{int}}{K_{max}}\right)^2 + 4\left(\frac{K_{int}}{K_{max}}\right)^4 = 0 \tag{2.17}$$

This is again a biquadratic equation and has four roots:

$$\left(\frac{K_{int}}{K_{max}}\right)_{1,2,3,4} = \pm\sqrt{\frac{5\pm 4}{8}}(1-R) \tag{2.18}$$

Obviously, the negative roots should be neglected. There are, however, two positive roots. In order to decide which one should be used, they are calculated at R = 0:

$$\begin{aligned}\left(\frac{K_{int}}{K_{max}}\right)_1 &= \sqrt{\frac{5+4}{8}}(1-R) = \frac{3}{2\sqrt{2}}(1-R) \approx 1.06(\text{when } R=0)\\ \left(\frac{K_{int}}{K_{max}}\right)_2 &= \sqrt{\frac{5-4}{8}}(1-R) = \frac{1}{2\sqrt{2}}(1-R) \approx 0.35(\text{when } R=0)\end{aligned} \tag{2.19}$$

The internal stress intensity factor cannot be bigger than K_{max}, therefore only the second root constitutes a legitimate solution:

$$\frac{K_{int}}{K_{max}} = \frac{1-R}{2\sqrt{2}} \tag{2.20}$$

It can be seen that the Eq. 2.20 is linear function of R (Figure 52). This makes the prediction of the internal stress intensity factor fast and easy, even cycle by cycle

in real time under variable amplitude loading.

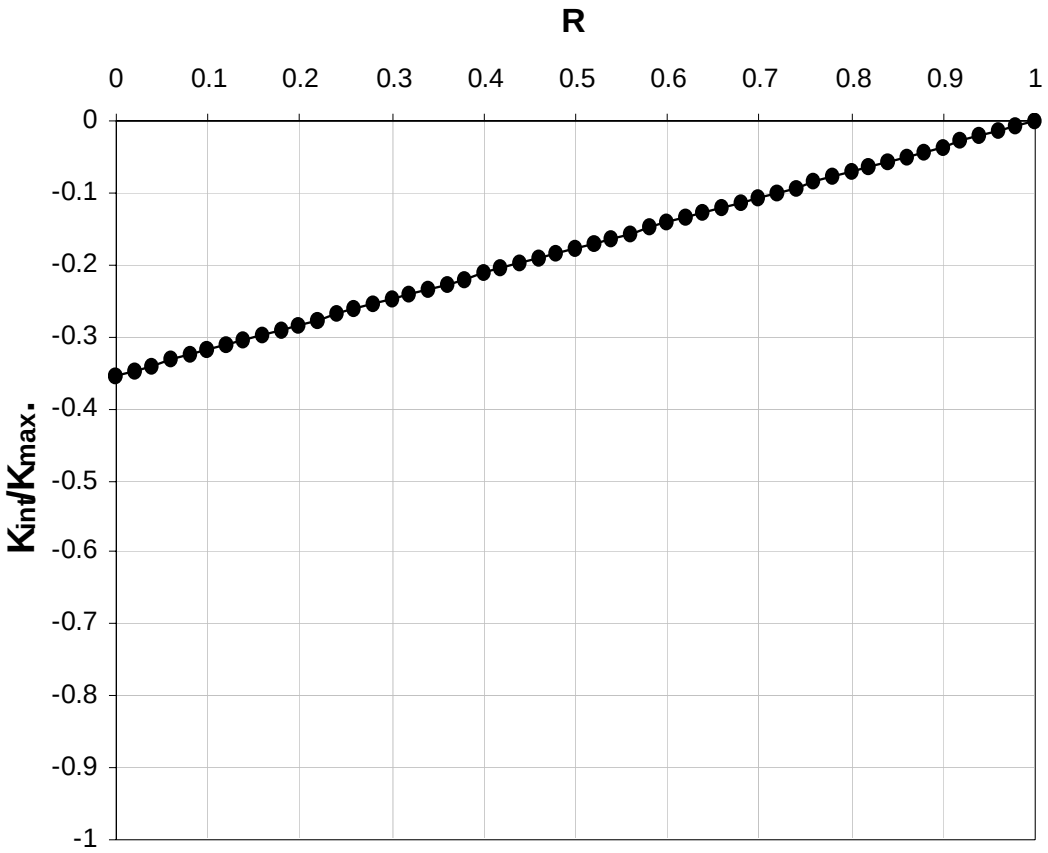

Figure 52 Internal stress intensity factor calculated using the clamping force method for different load ratios (constant amplitude loading)

The solution presented in this section uses one of the simplest material models, elastic-perfectly plastic. This is done in order to simplify the basics of the clamping force method. In fact, more realistic material models can be readily used. Therefore, in Appendix D two additional material models are considered. One of them uses kinematic and the other uses isotropic hardening law in the form of the Rice equation. The real material behavior is somewhere between these two models.

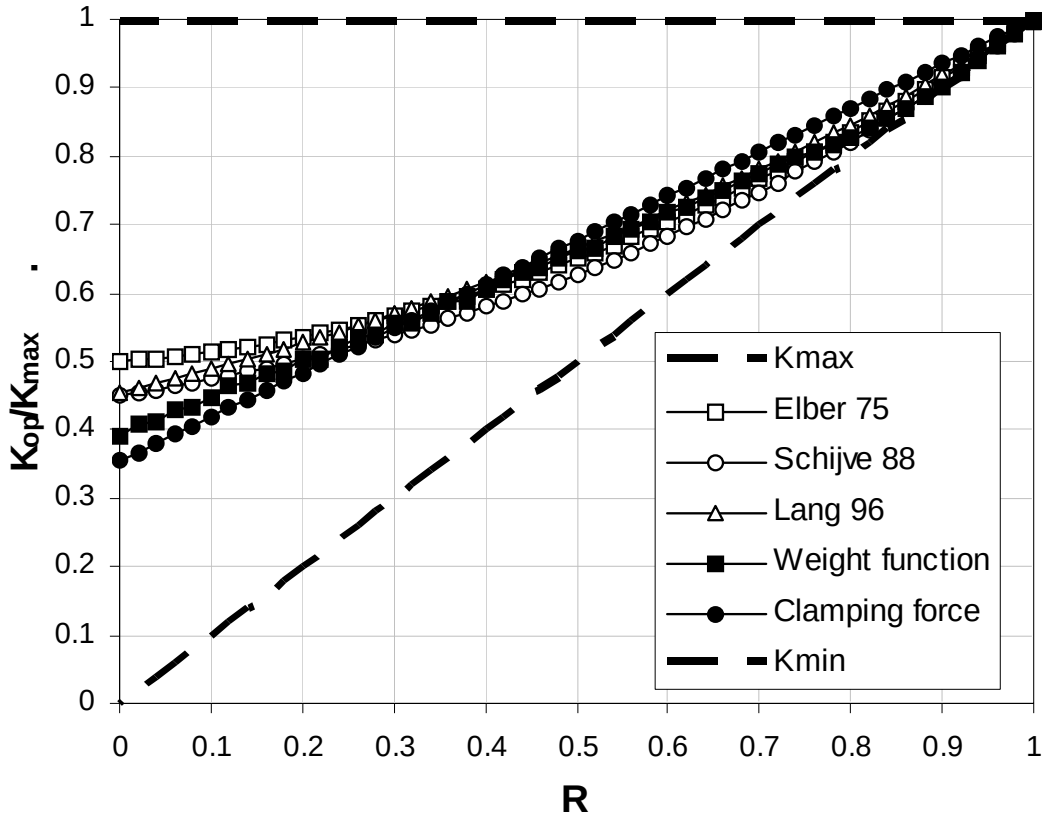

Figure 53 Comparison between the clamping force method and crack closure data from the literature

If the residual stress intensity factor, calculated using the weight function and clamping force procedures is applied to ΔK_{appl}, the results from previous studies on crack closure can be simulated using Eq. 2.21 very closely (Figure 53). This means that both crack closure measurements and internal stress calculations shall predict load history effects equally well. The internal stress calculations, however, have the advantage of being unambiguous and easy to apply. This is not true for the crack closure measurements as has been shown in part I.

$$\Delta K_{eff} = \Delta K^{appl} + K_{int}$$
$$K_{op} = K_{max}^{appl} - \Delta K_{eff} \qquad 2.21$$

Although the correlation in Figure 53 is very good, it is not the goal of the present investigation to simply follow the Elber crack closure model and reduce the applied ΔK. The internal stress intensity factor is present in the cracked specimens both under maximum and minimum load. Therefore, using the principle of superposition, K_{res} should be added to both the applied K_{max} and K_{min} (Figure 55). This means that K_{max} will change and ΔK should remain constant as shown in Figure 55.

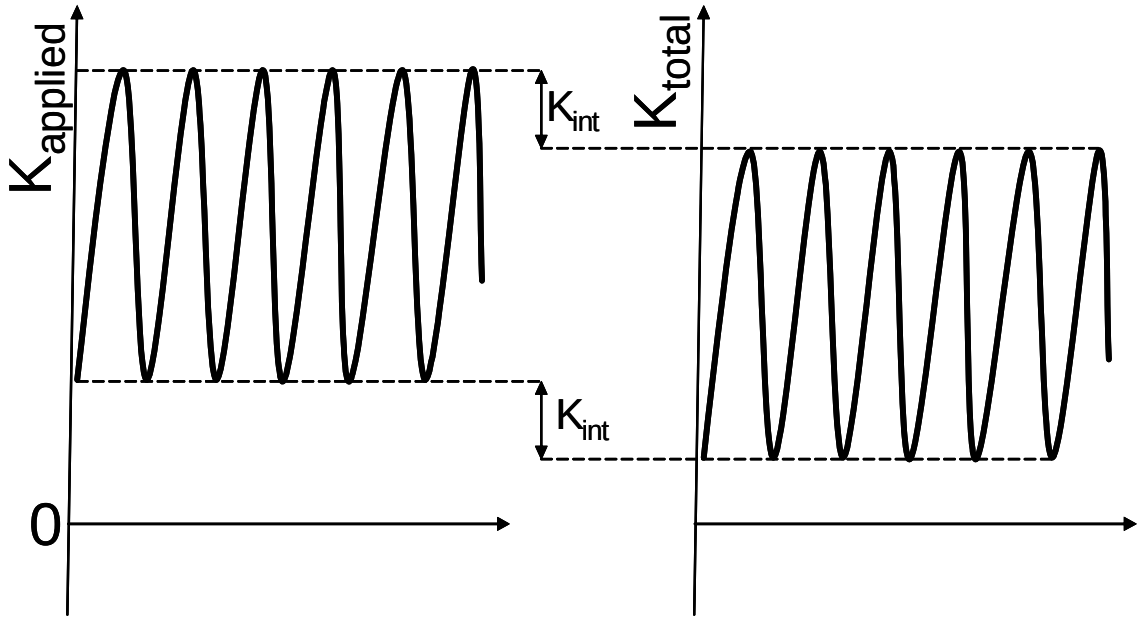

Figure 54 Estimation of the internal stress intensity factor at the crack tip for positive load ratios

Figure 55 also shows close agreement of the weight function and clamping force methods with the experimental data from Lang [126,127]. He originally plotted his results as a 'traditional' opening load values, but they can be also interpreted as internal stresses by using Eq. 2.21. The agreement between the theoretical models and the experiments in Figure 55 provides a level of confidence in the K_{int} estimations. Only positive load ratios are shown in the figure since K_{int} for $R < 0$ is dependent on

the applied values of stress and, therefore is not a unique value for a given R (it depends on the crack length).

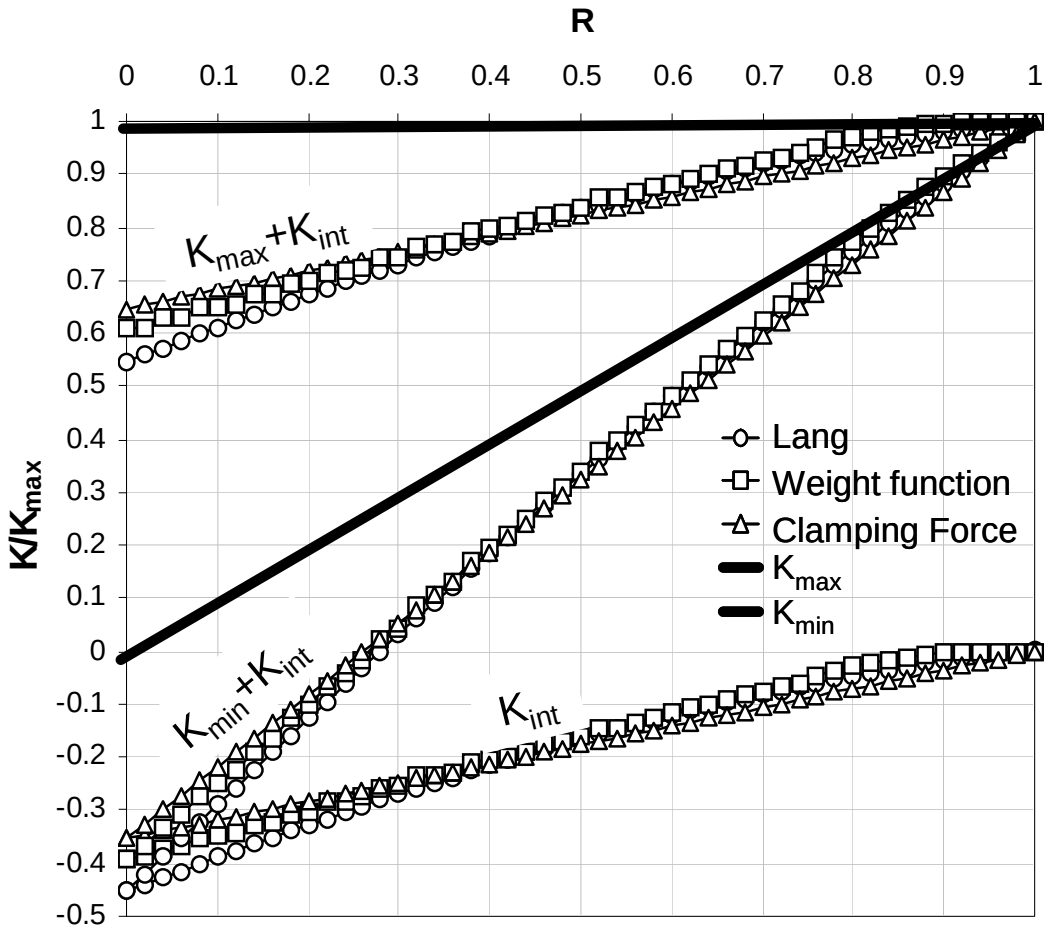

Figure 55 Effect of the internal stresses on the applied values of K_{max} and ΔK

Under negative load ratios the effect of the applied load is further reduced by the crack face contact (Figure 56). Therefore, the negative part of the applied K is almost eliminated ($\Delta K = K_{max}$). There is, however, some small contribution to the fatigue crack driving force form the negative part of the loading cycle which comes from the slightly different stress profiles at R=0 and R<0 as shown in Figure 46. This small contribution can be evaluated by subtracting the residual (for R=0) from the

internal (for the particular R<0) stress intensity factor. This difference has to be added to ΔK_{total} as shown in Figure 56.

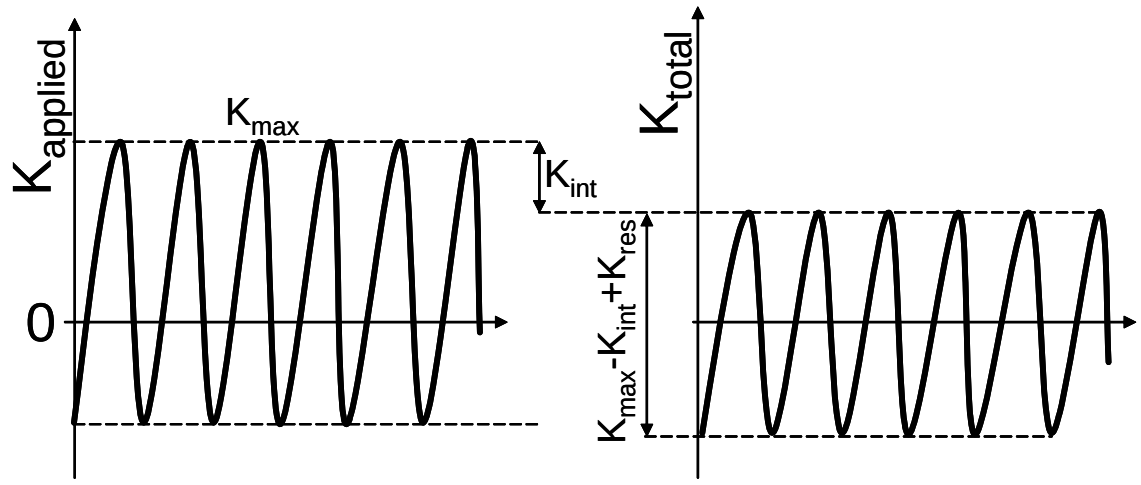

Figure 56 Estimation of the internal stress intensity factor at the crack tip for negative load ratios

Once the total values of the stress intensity factor are known they can be used to construct a local CP table for the crack tip that will incorporate the load ratio effect. The crack growth prediction for constant loading then becomes very easy. It can be done just by calculating the total values of K_{max} and ΔK for the particular loading and referencing the value of da/dN in the CP table.

To illustrate and also to confirm experimentally the 'process zone' CP table concept, experimental data from Donald [178] for Al 2324-T39 alloy will be used (Figure 57). First, all load ratios were digitized using 25 'standard' values of da/dN. Next, the internal stress intensity factor in the process zone is calculated using the weight function method and added to the applied K_{max} for every experimental point. ΔK remains unchanged for the positive load ratios and for R= -1 it is modified according to Figure 56.

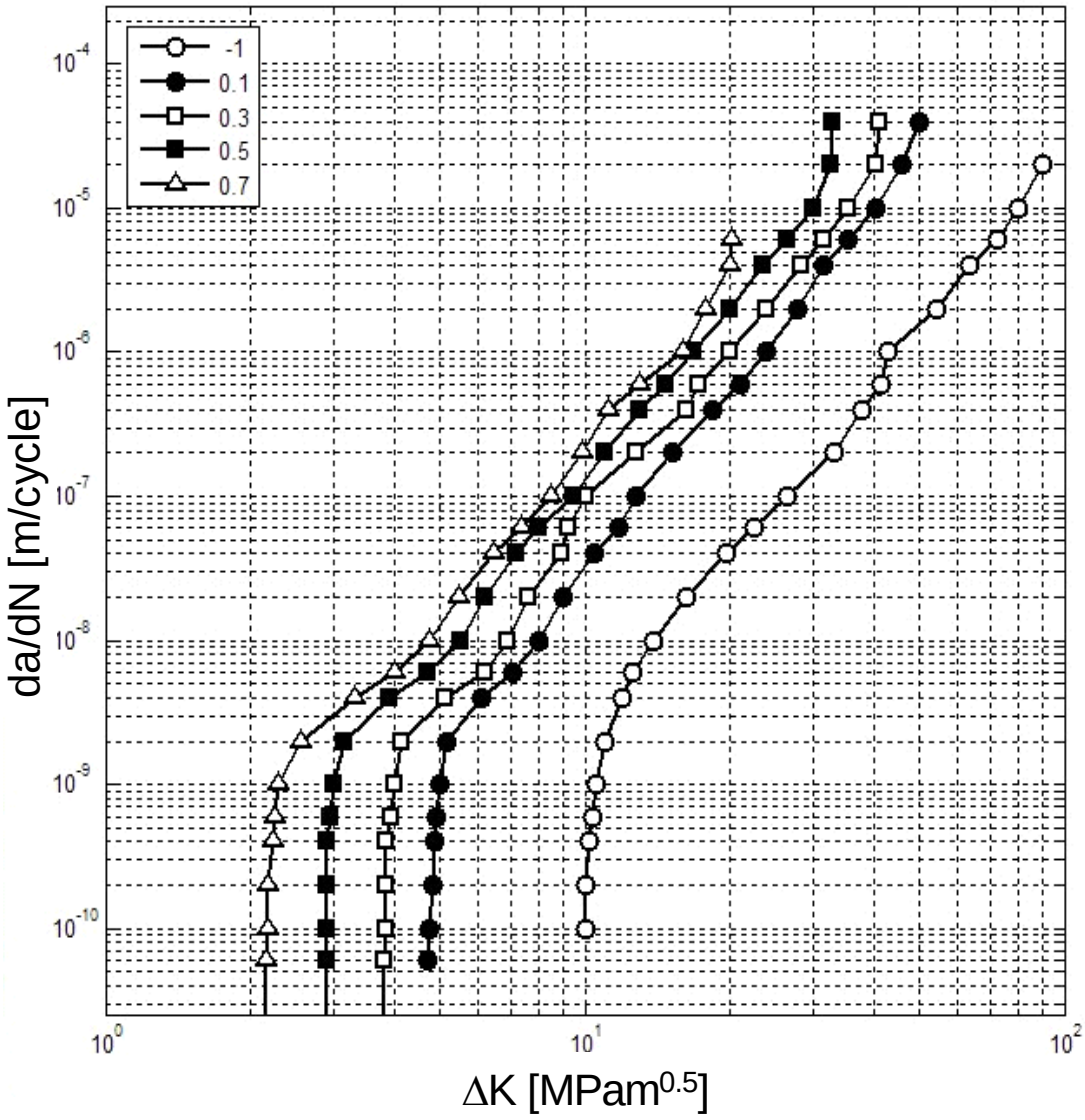

Figure 57 Experimental (Al 2324-T39 - data from [178])

Figure 58 shows both applied and the process zone crack propagation tables. It can be seen that the second one matches very well with the trends predicted from the analytical derivations shown in Figure 34. The $\Delta K - K_{max}$ relation in the process zone for any da/dN constitutes a straight line on the log-log plot. This means that a power law function (such as the two parameter driving force equation for example) can be used to simplify the crack growth predictions even more, by reducing the CP

table surface to a single line.

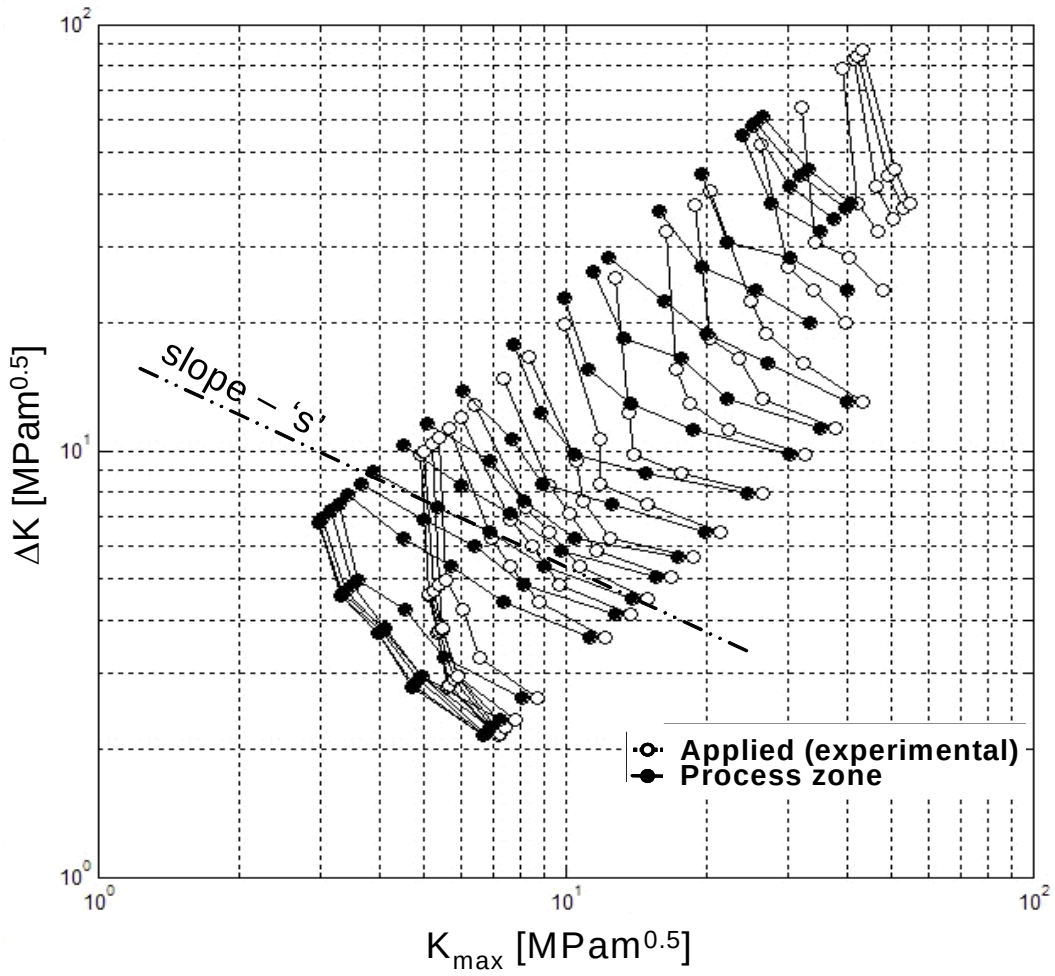

Figure 58 CP tables – applied and in the process zone (Al 2324-T39 - data from [178])

Fatigue crack growth predictions

In this section, experimental data for constant amplitude, block and overload load histories will be presented along with theoretical predictions of the crack growth behavior.

All experiments were done using the side edge notched specimen geometry

shown in Figure 13 with thickness of 2.54 mm. The material (Al 2324-T39) selected, based on the fact that this specimen-material combination gave the most stable results in terms of da/dN under the constant load ratio testing in Part I.

Figure 59 Front panel of the test control and data acquisition system

In order to improve the accuracy of the results, all tests were done using fully automated control and data acquisition system. Figure 59 shows the front panel of the programming interface. LabView programming language was used along with acquisition card from National Instruments to obtain a

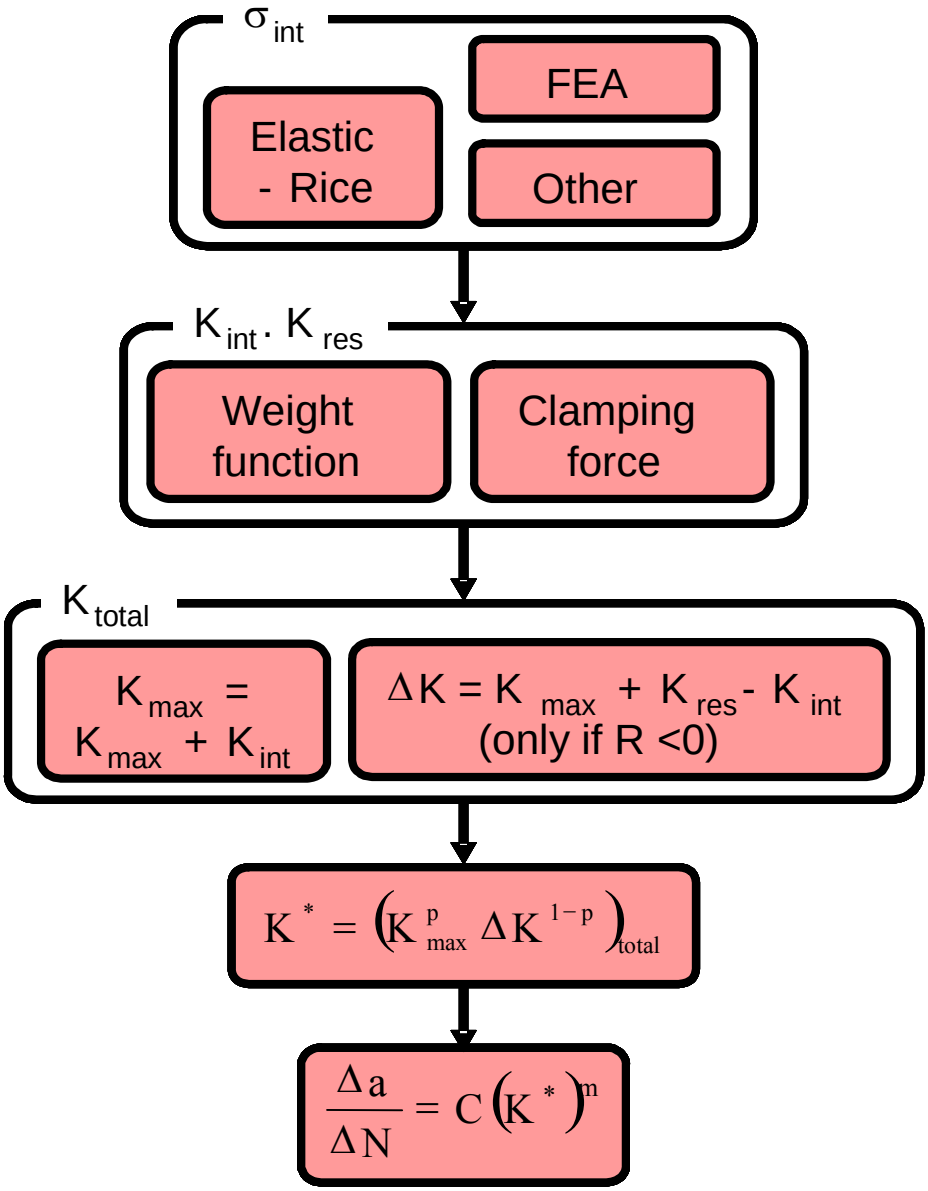

Figure 60 Block diagram for predicting crack growth rate under any type of loading

load displacement record from each cycle. Then the data were analyzed with a program written in MatLab. The crack length, K_{max} and ΔK were calculated from the specimen compliance according to the ASTM E647 recommendation. These feedback signals were passed back to the LabView program which provided control of the test on instrument level.

The system is capable of recording, analyzing and controlling any of the fracture mechanics parameters (ΔK, K_{max},, R etc.) on a cycle by cycle basis with test speed up to 30 Hz (see Appendix B for more details).

All crack growth rate predictions in the next sections were done in accordance with the block diagram in Figure 60. It was developed based on the analysis in the previous sections.

Constant amplitude loading

Both the analytical derivations and the crack propagation table in the process zone suggest a power law relation between ΔK and K_{max}. It will be used in this section in the form of the two-parameter crack driving force equation [160-163]:

$$\Delta K^{*} = K_{max}^{p} \Delta K^{1-p} \qquad (2.22)$$

For a given da/dN=constant, the corresponding crack driving force should be constant as well and Equation 2.22 can be represented as a straight line with slope 's' in Figure 58. This allows the coefficient 'p' to be determined directly from the CP table at the crack tip by using the following relationship:

$$\boldsymbol{p = \frac{s}{s-1}} \qquad (2.23)$$

In Equation 2.23, 's' is the slope on the log-log plot (Figure 58)

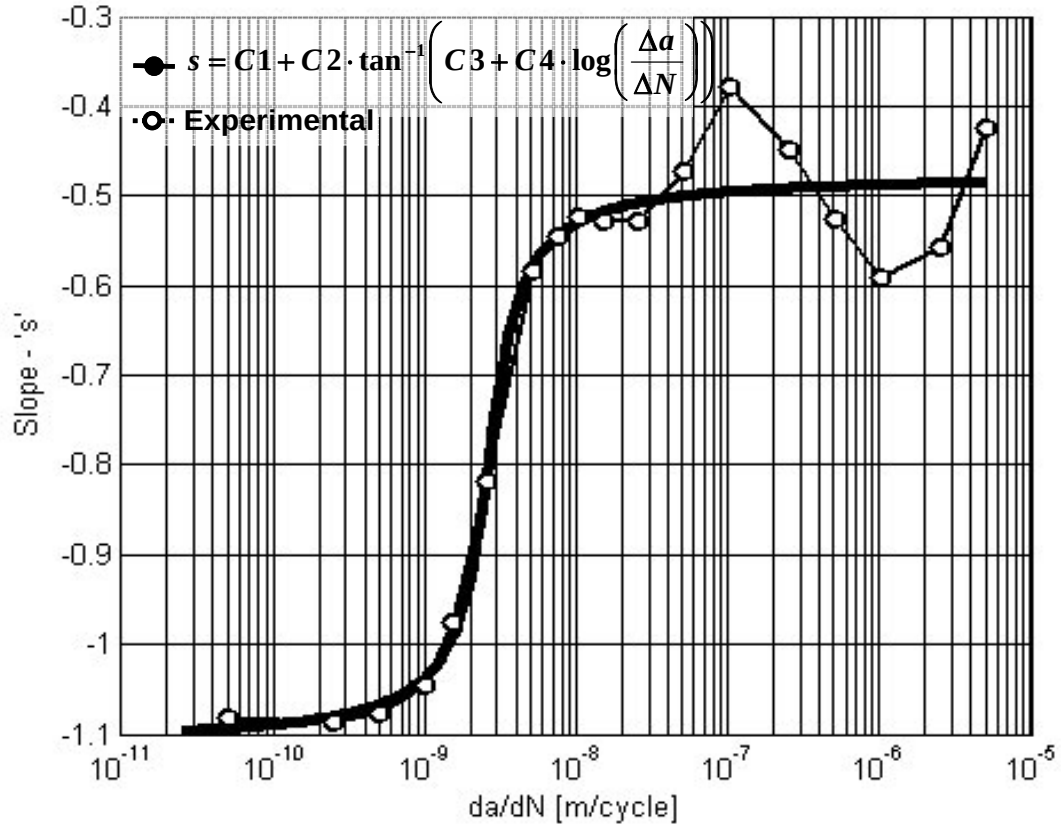

Figure 61 Function for interpolation/extrapolation of da/dN (Al 2324-T39 - data from [178])

The slope ‘s’ was found as a linear least squares fit for every particular crack growth rate. The results are shown on Figure 58. It can be seen that at low crack growth rates, where the plasticity at the crack tip is negligible, the slope is very close to the predicted (Figure 34) value of -1, based on smooth specimen analogy. At higher crack growth rates however, due to increased plasticity, the slope decreases but still deviates from the predicted value (n’= -0.107). The existence of a sharp transition between the values of the slope, characteristic for low and high da/dN, was also correctly predicted from the theoretical derivations. The significant variation at high crack growth rates cannot be explained with the current model and is either due to

experimental scatter, proximity to the specimen face or, less likely, due to material behavior.

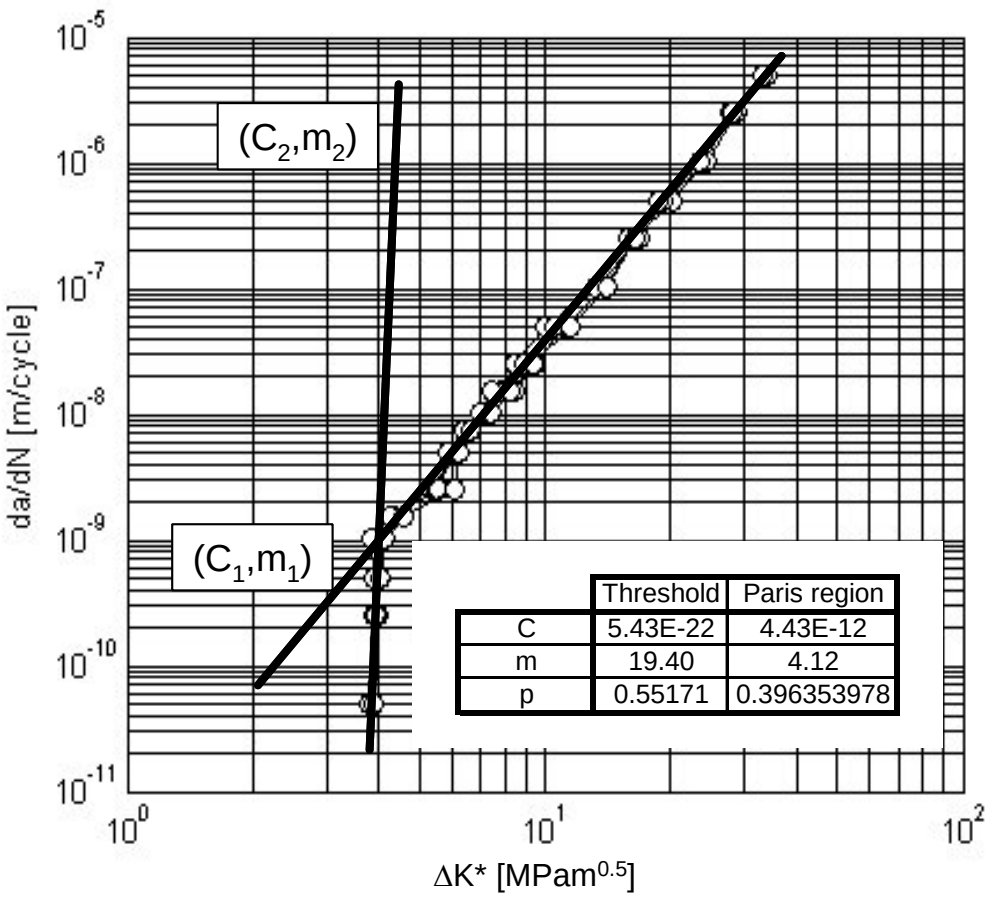

Figure 62 Two-parameter crack driving force (Al 2324-T39 - data from [178])

The relationship between 's' and 'da/dN' in Figure 61 can be fitted very well using inverse tangent function. This, unlike the polynomial fitting, allows extrapolation to higher, and more importantly, lower da/dN (to find the threshold for example).

Fatigue crack growth rate can be calculated then with the well-known Paris type equation, with two different sets of constants (C and m) for the Paris and threshold regions:

$$da / dN = C\left(\Delta K^{*}\right)^{m} \qquad (2.24)$$

Finally, all experimental data was plotted versus two-parameter driving force (Figure 62). The correlation is excellent, proving that ΔK* is indeed independent of the applied load ratio if a correction for the internal stress is done.

Two more aluminum alloys – 7055 and 6013 were also studied in this section and showed similar results. For clarity they are presented in Appendix E.

Block loading

Block loading history by definition consists of separate blocks with constant amplitudes. Crack growth rate for constant amplitude loading was already calculated in the previous section and can be readily obtained simply by CP table lookup. Therefore, only the transient effect, if any, will be modeled in this section.

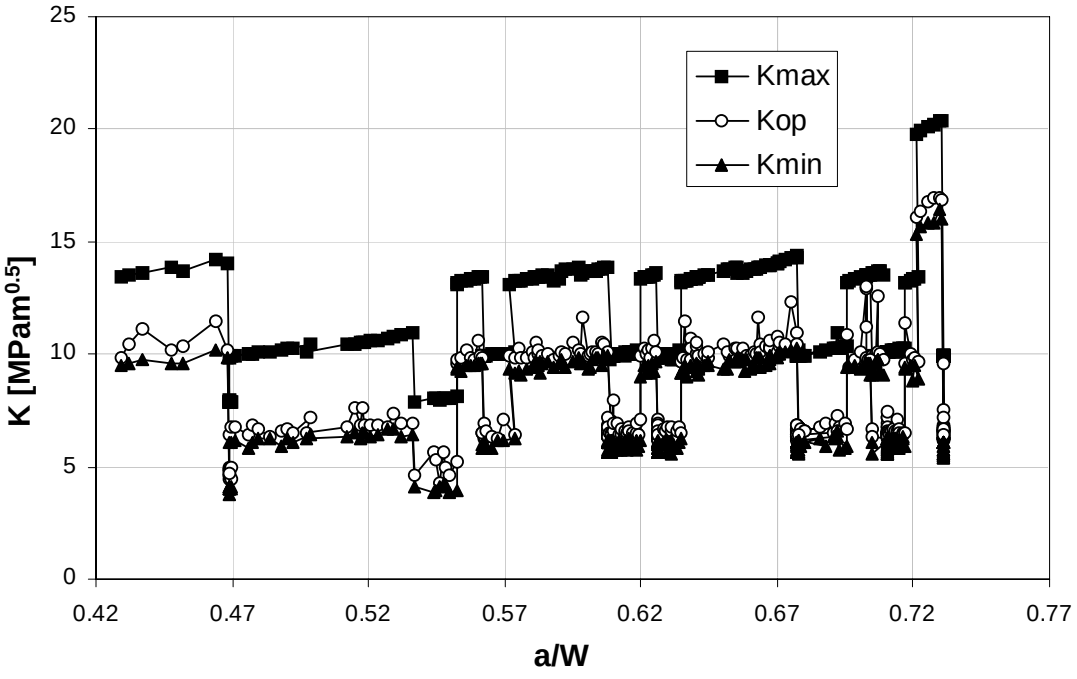

Figure 63 Block loading history

To avoid effects, associated with the questionable CC phenomena, all block loading experiments were done with high load ratio (R≥0.6), as shown in Figure 63. The opening load was calculated according to the ASTM E647 standard. It can be seen that the crack closure is negligible as expected and does not experience any systematic dependence on the load history.

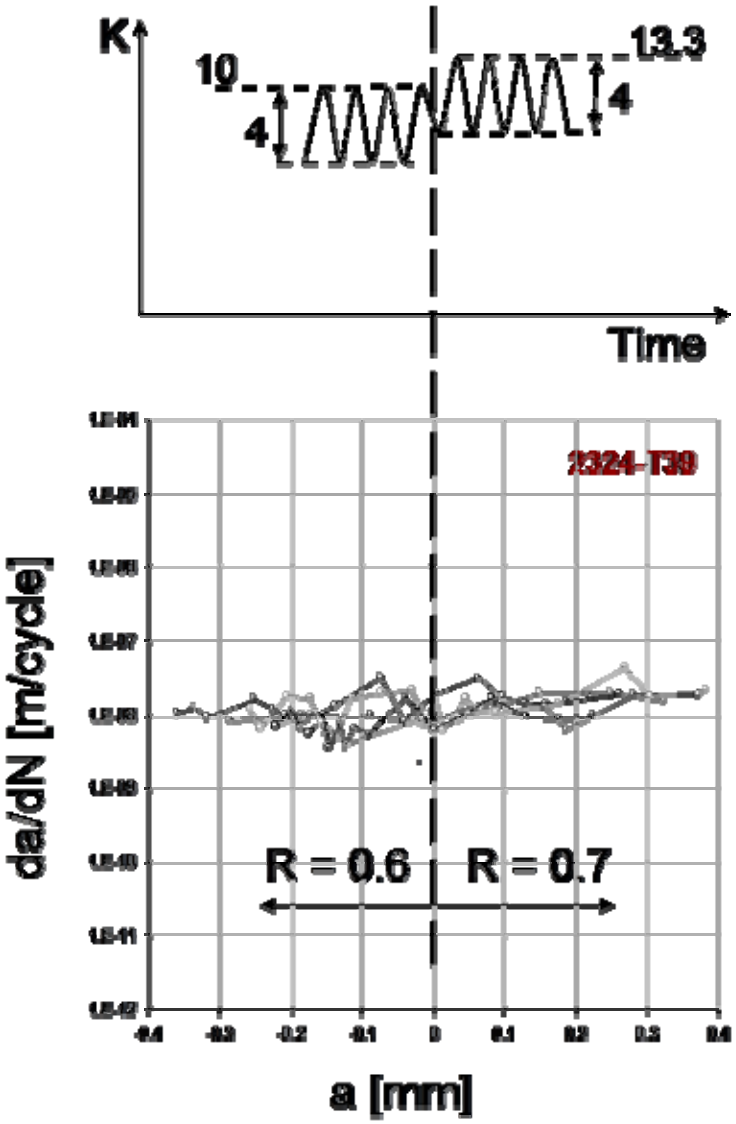

Figure 64 Effect of low to high load ratio transition on the observed crack growth rate

Portions of the test where the load ratio was changed from low (0.6) to high

(0.7) are plotted in Figure 64. It can be seen that the observed crack growth rate immediately assumes the slightly higher value, characteristic for the high load ratio. There are no transient effects (within the experimental accuracy). This means that, since both K_{max} and K_{min} of the new loading are bigger, they will erase all internal stresses left from the previous loading.

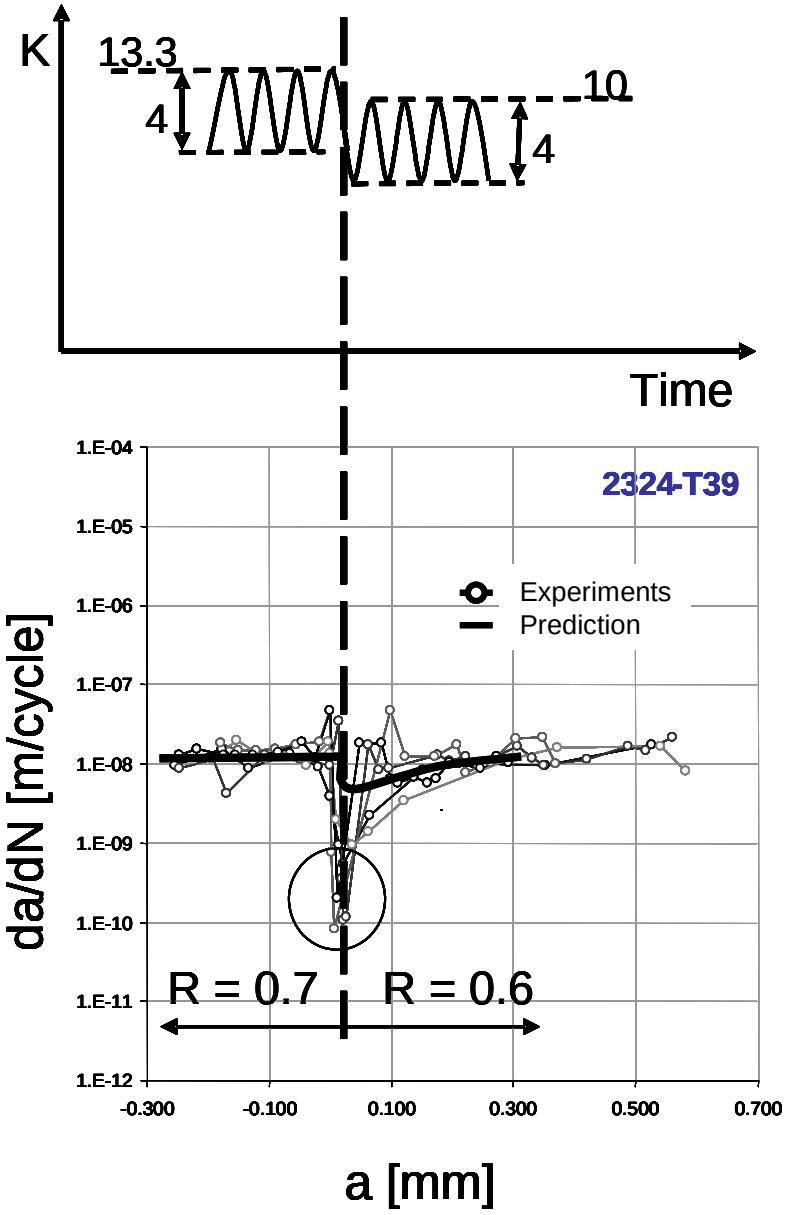

Figure 65 Effect of high to low load ratio transition on the observed crack growth rate

Figure 65 shows the block loading date for the opposite – high to low R sequence. Here the transient effect is obvious in all five tests, causing significant crack retardation. The points in the circle are questionable because the crack length was measured on the surface using a microscope and any crack growth in the interior of the specimen is unaccounted). The observed crack retardation cannot be predicted by the 'traditional crack closure' models simply because there is no crack closure.

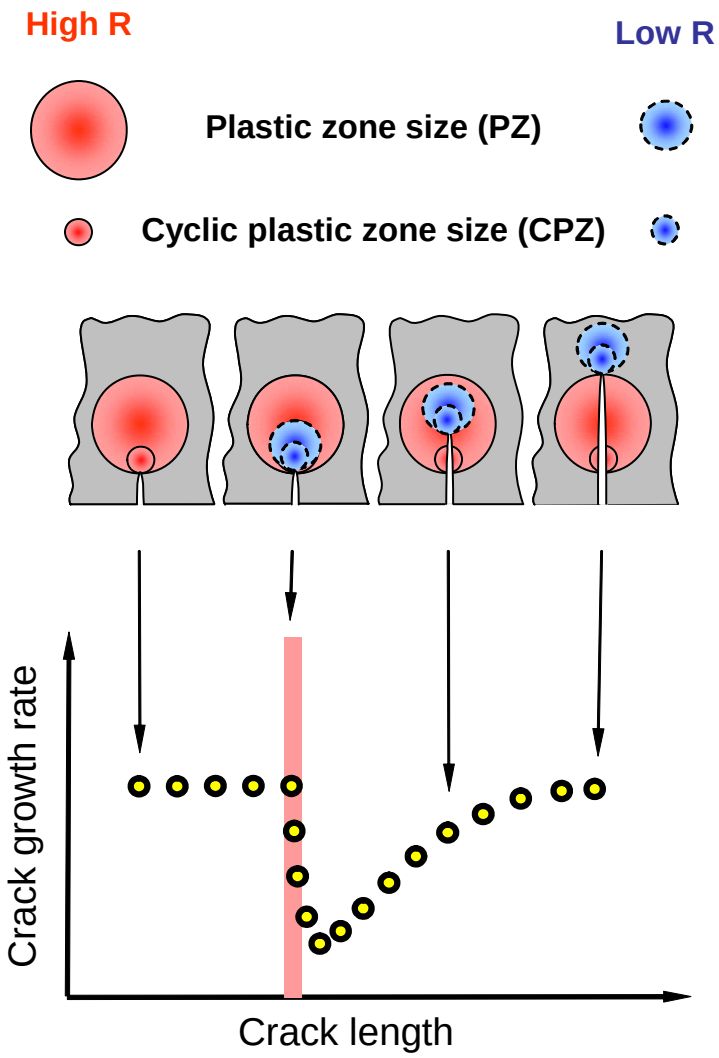

Figure 66 Trends in the experimental data for high to low load ratio block loading

Figure 66 shows analysis of the observed crack behavior under high-low R

block loading in terms of plastic zone sizes. It can be seen that the retardation occurs only when the crack grows through the internal stress field from the previous loadi, where R=0.7. This coincides with the area where K_{int} calculated with the weight function method is present (Figure 48).

The analysis of Figure 66 leads to the conclusion that K_{int}, calculated for R = 0.7 should be superimposed on the one for R = 0.6. This approach, however, proved to give insufficient retardation and therefore K_{res} was used instead of K_{int} for R = 0.7 (Figure 67). The dashed line represents the resultant internal stress intensity factor. Figure 67 also shows the equation used to calculate the total maximum stress intensity factor at the tip (stress intensity factor range remains the same).

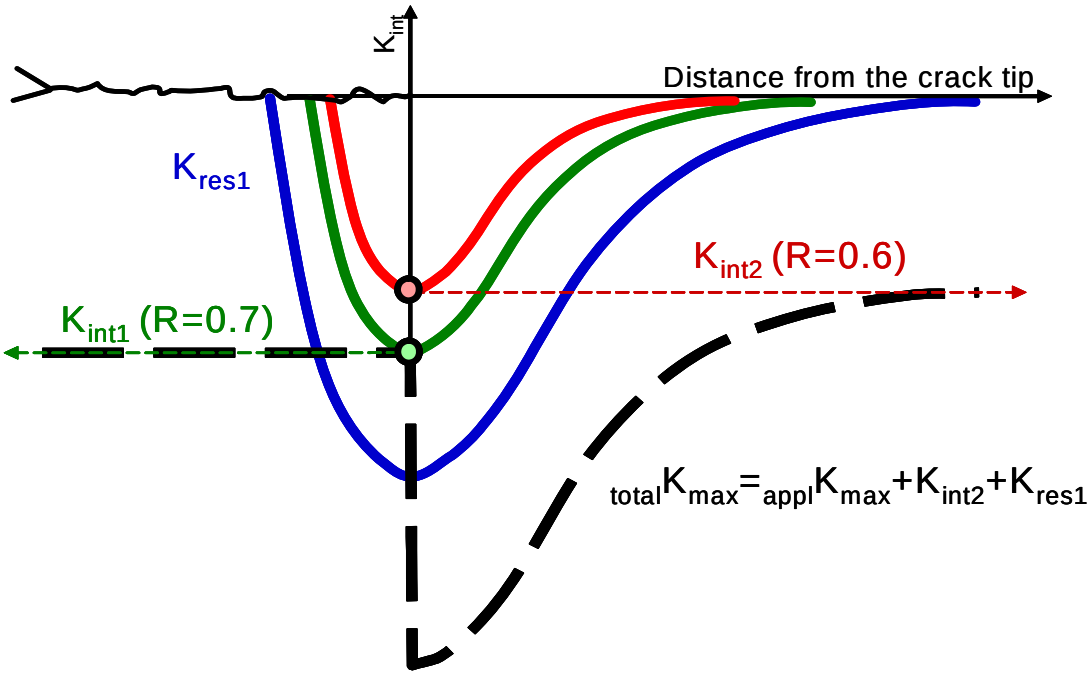

Figure 67 Calculation of the internal stress intensity factor in the transition region from high to low load ratio

The total values of K_{max} and ΔK were used to calculate the crack growth rate as shown in Figure 68. The straight lines represent the well-known Paris law (with

different constants for the threshold region.

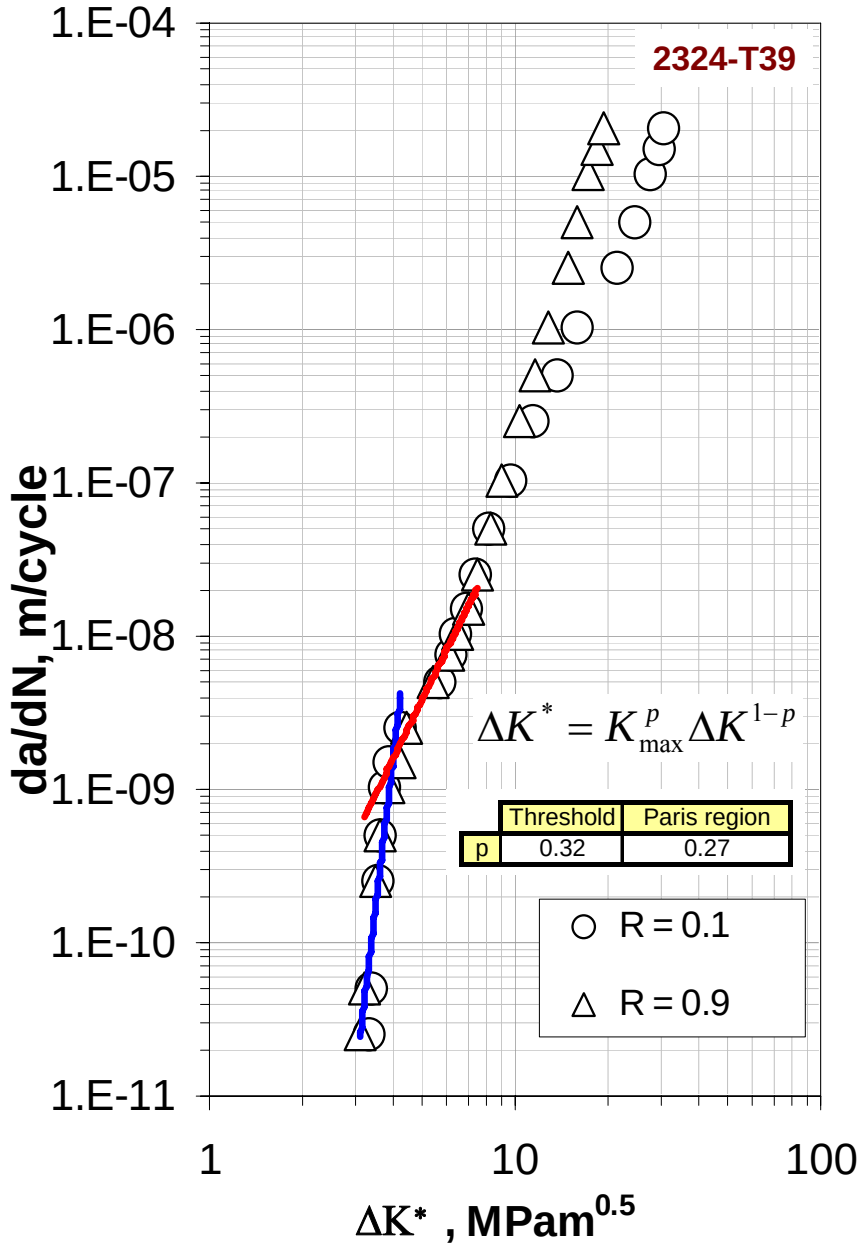

Figure 68 Crack driving force plot used to predict the crack growth rate

In order construct the plot in Figure 68 and to find the constant 'p' in the two-parameter crack driving force equation, constant amplitude experiments were done for two load ratios of 0.9 and 0.1 (Figure 69). These tests were performed using the

same material batch in lab air. Unfortunately, thr humidity varied between 20 and 70%, which can cause significant scatter in the crack growth rates!

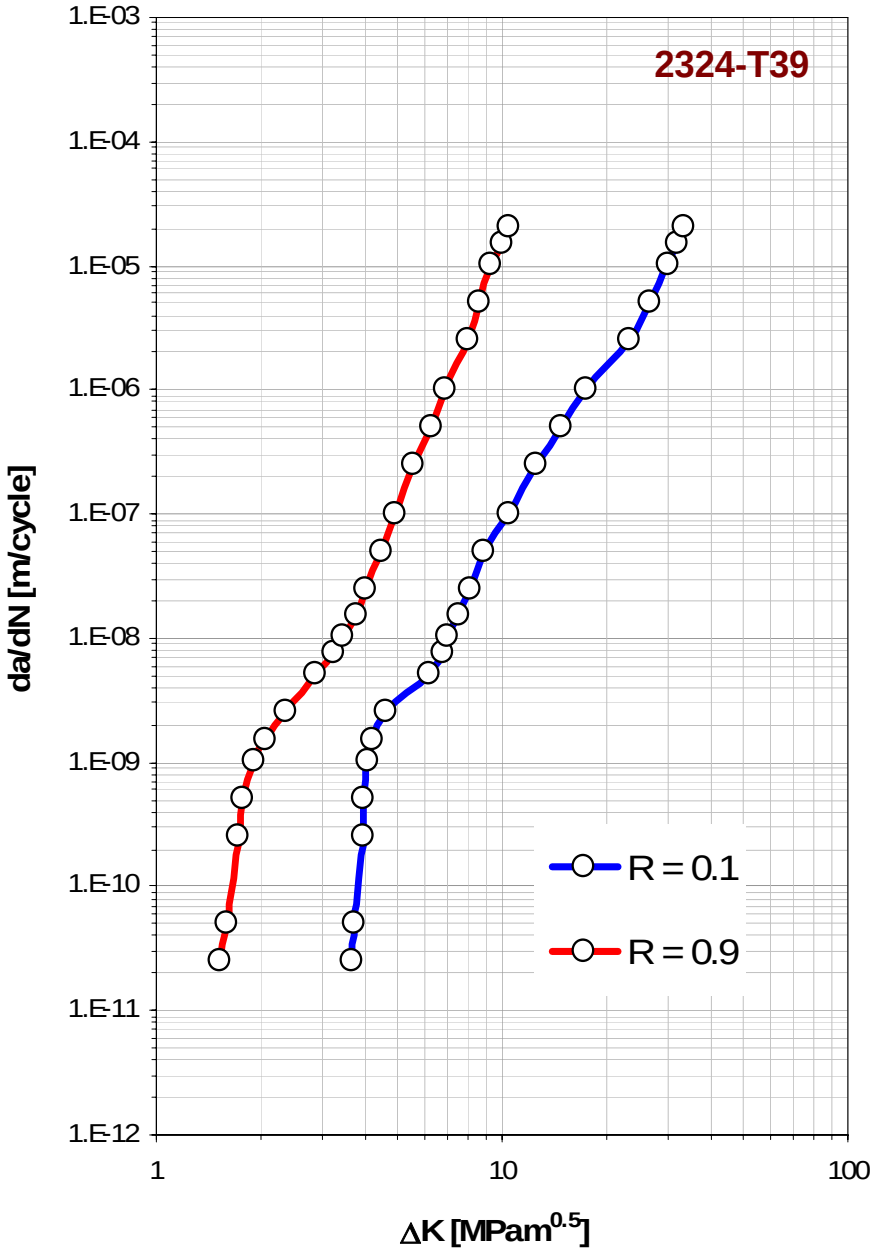

Figure 69 Constant amplitude tests used to plot the two-parameter crack driving force diagram

The only adjustable parameter in the model that is described in this section is

the process zone size, ρ*. In the present study process zone size was varied in order to find the sensitivity of the K_{int} calculation to this parameter (Figure 70). As a result, process zone size was chosen arbitrarily to be 10 micrometers since the sensitivity is very low.

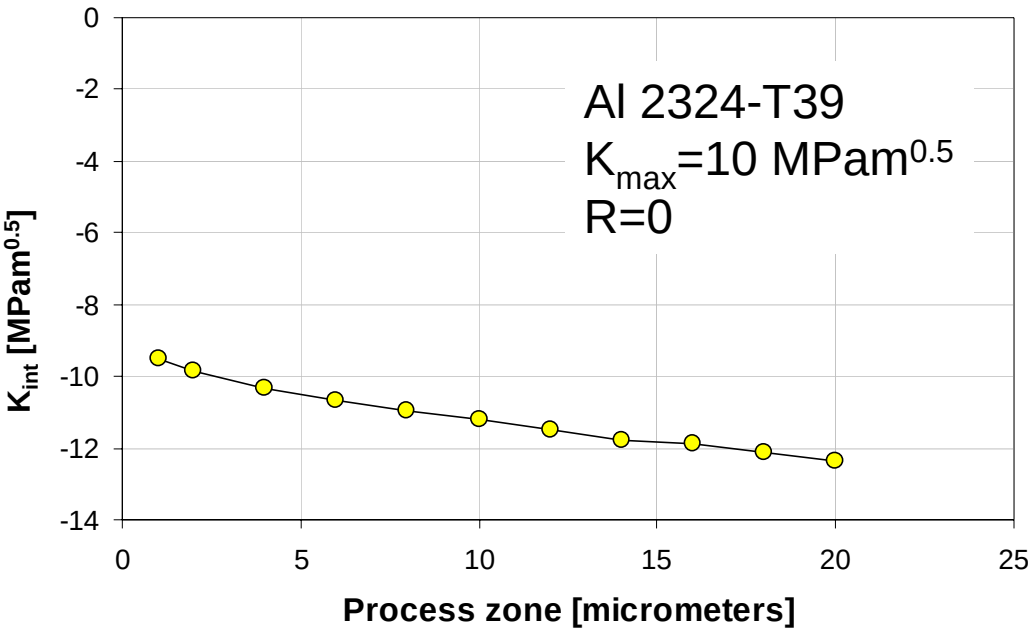

Figure 70 Sensitivity of the K_{int} estimation to the process zone size

Overloads

In this section, single overload histories with overload ratio ($OLR=K_{maxOL}/K_{maxBL}$) 1.5 and 2 are studied experimentally and the observed crack-growth behavior is predicted analytically using the two-parameter crack driving force. All tests were done with aluminum 2324-T39 at a load ratio of 0.1 for base loading. Figure 71 shows schematic load history of a test with OLR = 1.5. For modeling purposes this load history was divided in two parts – base loading, where K=1 to 10 $MPam^{0.5}$ and overload, where K=1 to 15 $MPam^{0.5}$.

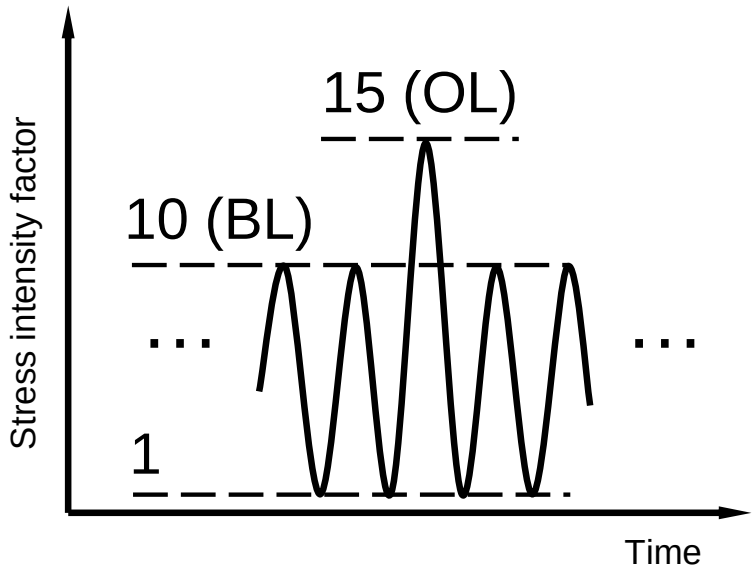

Figure 71 Load history of the experiments with OLR = 1.5

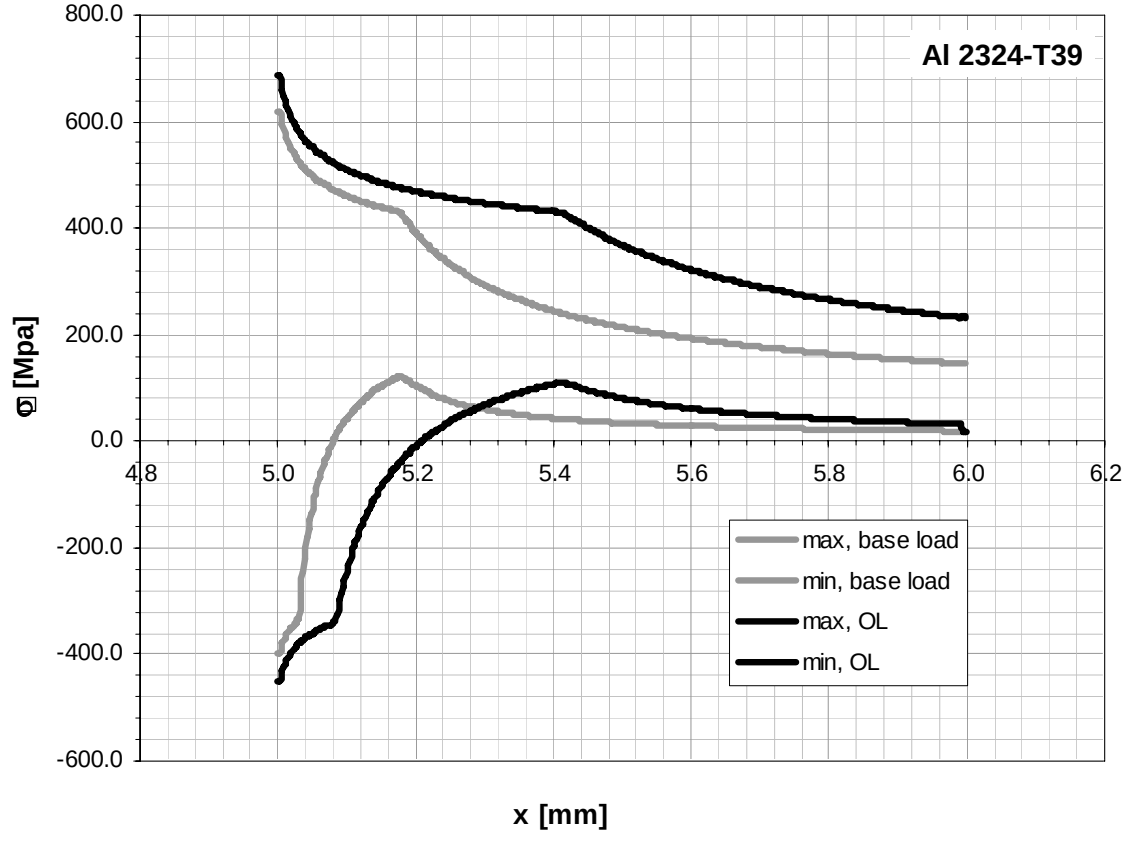

Figure 72 Stress profiles ahead of the crack tip for the base loading and for the overload (OLR = 1.5)

The stress profiles ahead of the crack tip for both overload (OL) and base load (BL) are shown in Figure 72. Both maximum and minimum profiles were estimated. The calculations were done using the same procedure that was used in the previous sections.

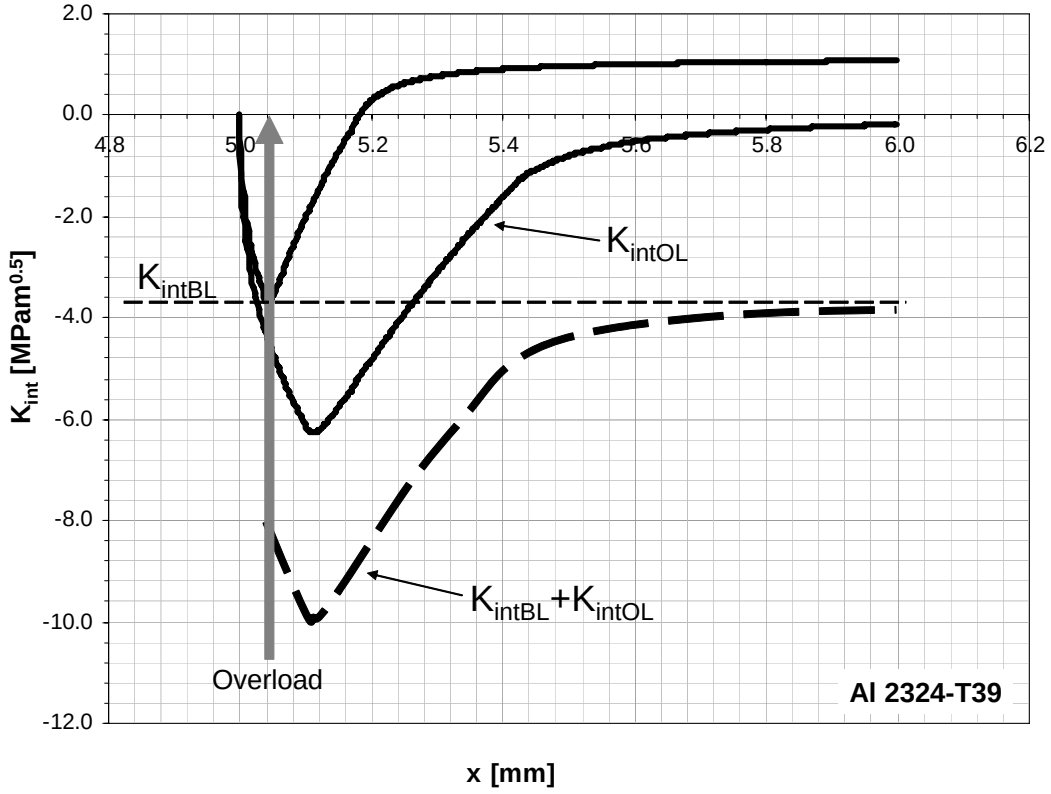

Figure 73 Internal stress intensity factor profiles used in the crack growth rate prediction for OLR = 1.5

In order to construct the internal stress intensity factor profiles in Figure 73, the minimum stress profiles from Figure 72 were multiplied by a weight function and integrated to the current crack length. As noted in the previous section, the whole stress/strain field is moving with the crack under constant amplitude loading (BL in this case) in such a way that the minimum of the internal stress intensity factor profile always stays at the crack tip. Therefore, the constant level of K_{int}, associated with the

block loading will be always present in the material, with or without overload (noted as a horizontal dashed line in Figure 73). The application of overload creates a bigger internal stress intensity factor (K_{intOL}) that should be added to K_{intBL} using the principle of superposition. The internal stresses created from the overload, however, are stationary and the crack is allowed to grow through them. In such a way the resultant K_{int} is increased by the K_{intOL} profile in the overload monotonic plastic zone and after that assumes again the value corresponding to the particular block loading.

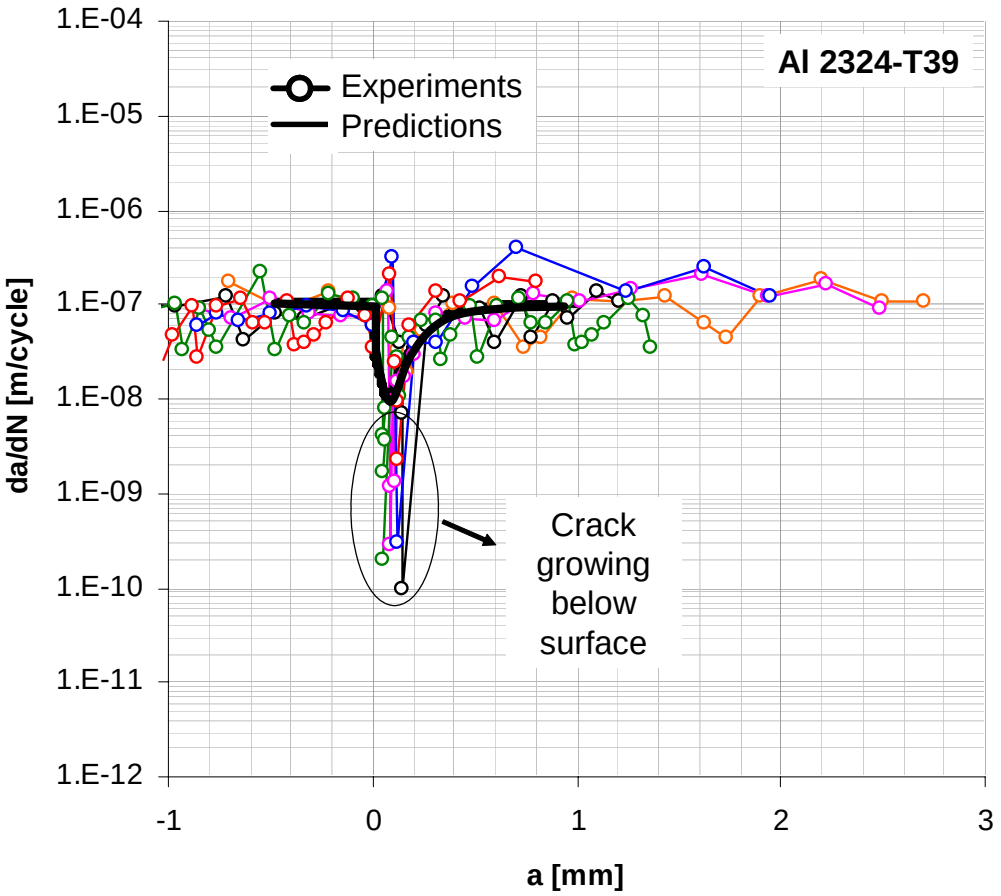

Figure 74 Experiments and prediction of da/dN vs. a (OLR = 1.5)

The internal stress intensity factor shown in Figure 72 with dashed line was used to predict the crack growth rate with the procedure outlined in the previous

section. The predictions are plotted in Figure 74. The zero on the x-axis corresponds to the OL application. It can be seen that the correlation with the experimental data is very good, except in the region immediately following the overload application. This discrepancy is probably caused by the fact that optical measurements of the crack length were used in order to calculate da/dN. This leaves any crack growth that may occur in the interior of the specimen unaccounted, which leads to unrealistically low experimental observations of the crack growth rate.

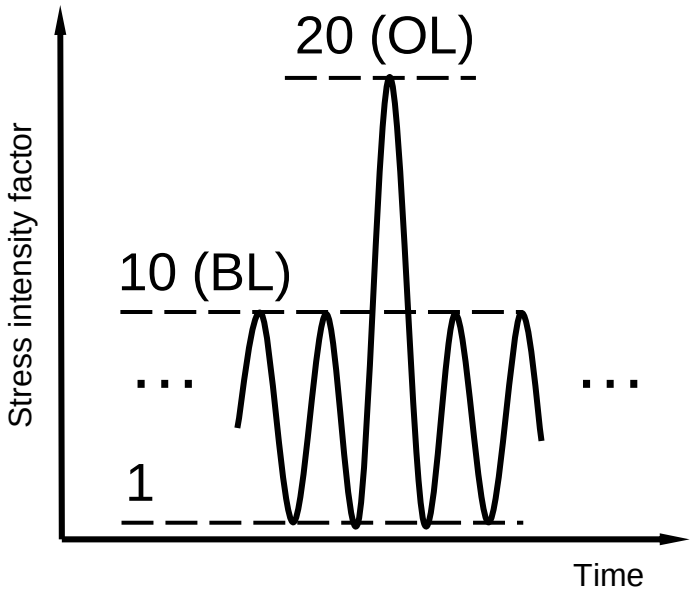

Figure 75 Load history of the experiments with OLR = 2

Next, a similar set of experiments was performed with overload ratio 2. A schematic of the load history is shown in Figure 75. The experimental results are plotted in Figure 76 along with the theoretical predictions. It can be seen that there is a significant discrepancy at the point of maximum crack growth retardation where the prediction indicated crack arrest. This problem can be solved by reducing the estimated value of K_{int} only by 7% (Figure 77). There are two possible explanations of this phenomena.

First – the material model that is used (linear-elastic, power law hardening) gives only approximate values of the stress/strain fields, particularly close to the crack tip. This problem can be corrected by using more accurate material models or finite element analysis.

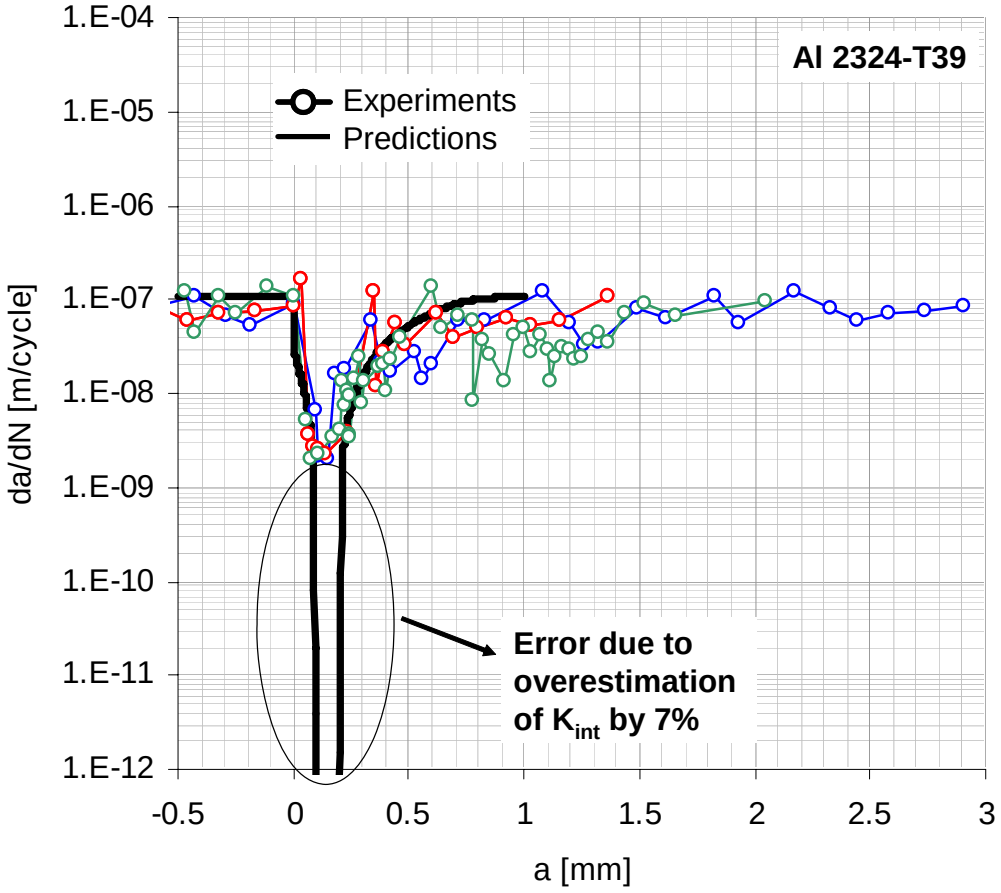

Figure 76 Experiments and prediction of da/dN vs. a (OLR = 2)

Second – the environmental conditions. All the material constants used in the prediction (most importantly the threshold values of ΔK) were obtained from a different set of data which was done in lab air with humidity varying as much as 30%. This can cause errors in the da/dN predictions, since the aluminum alloys are known to be very sensitive to changes in humidity.

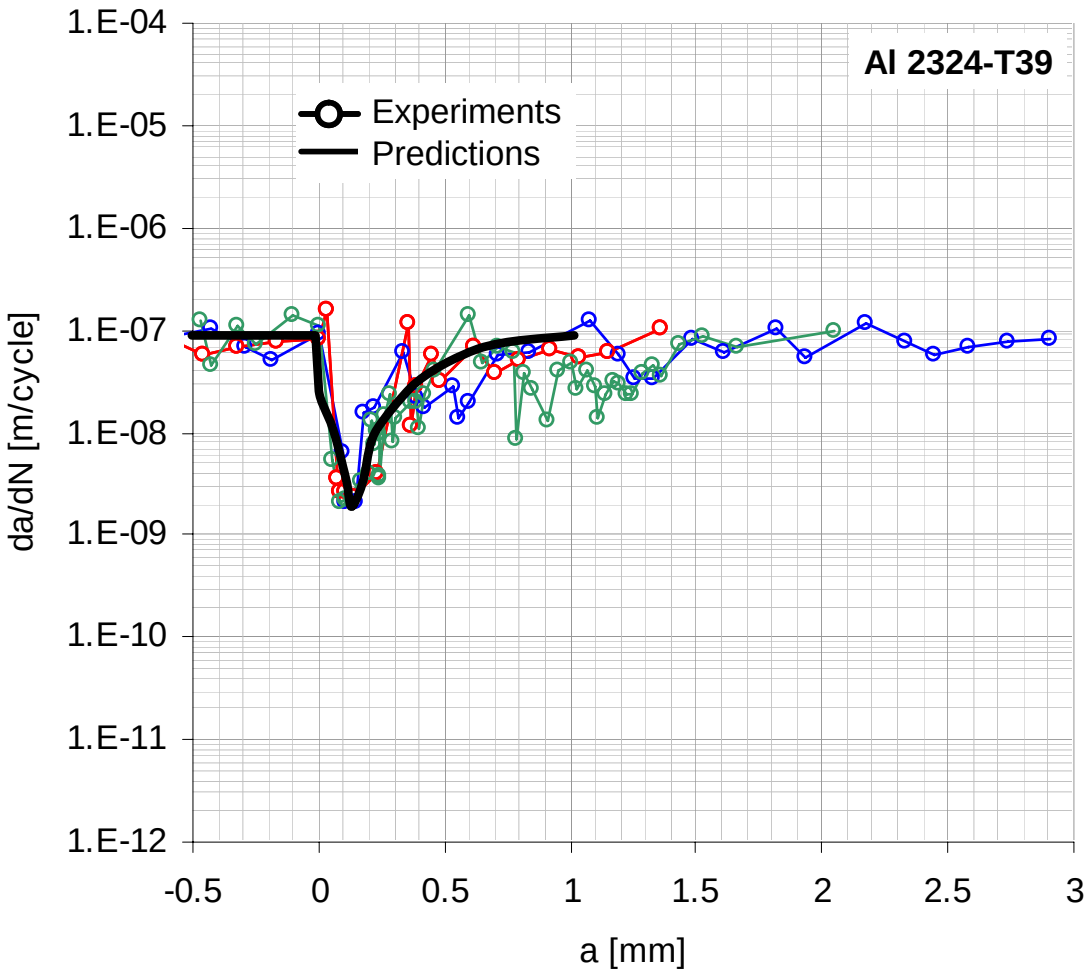

Figure 77 Experiments and prediction of da/dN vs. a (OLR = 2) with proper correction of K_{int}

Figure 77 clearly shows the potential of the two parameter crack driving force methods developed in this dissertation to predict the load history effects on fatigue crack growth. As an additional benefit, there is no need to calculate or estimate in any way the crack closure. This, along with the fact that practically there are no adjustment parameters in the model makes it straightforward and easy to implement in practice.

Conclusions

It was shown in Part I that the 'crack closure' concept, as defined by Elber 35 years ago, is not sufficient to explain the load interaction effects fully, despite the new methods for opening load determination that were developed in Part I. The two-parameter crack driving force model was identified in Part II as the most prominent alternative since it was derived analytically, using fundamental fatigue (ε-N curve) properties. The relationships that follow from such analysis constitute a basis for the newly developed crack propagation (CP) table concept. It proved to be very useful in representing and studying the fatigue crack growth in terms of ΔK and K_{max}.

Two methods for calculation of the internal stress intensity factor (K_{int}) were developed – weight function and clamping force. They both showed good correlation with the values estimated from experiments. The clamping force method is particularly promising because it has a sound theoretical basis and is faster than the weight function method. K_{int} was used together with ΔK and K_{max} applied values to construct local CP table corresponding to the crack tip process zone. It was used successfully for prediction of da/dN for constant R, block loading and single overloads.

Overall, the new theoretical models developed in this dissertation for fatigue crack growth prediction based on two parameters – ΔK and K_{max}, show good agreement with the experimental data. This was achieved without invoking the questionable crack closure phenomena. Therefore, further investigation of the two parameter crack driving force models is justified and needed in order to improve the general understanding of the load interaction effects on fatigue process and the fatigue crack growth predictions.

Future work

This study clearly demonstrates that there are many advantages in using the two parameter crack driving force models for fatigue crack growth predictions instead of the conventional crack closure methods.

Therefore, the next step in the development of the two parameter crack driving force models should be to incorporate finite element modeling in order to find the internal stresses. This will allow for more accurate calculation of the internal stress intensity factor, K_{int}. In addition, fatigue crack growth tests should be performed in vacuum in order to isolate the environment effects.

Another completely unexplored area is the underloads modeling. Once this is done, it will be possible to apply the two parameter crack driving force model to a real life problems where the loading is varying randomly.

Finally, there is a strong possibility that the models, developed in this dissertation will be applicable for micro and nano cracks, which will create a bridge between fracture mechanics and material science. Therefore, both analytical and experimental works in this area are strongly encouraged.

References

1. W. Elber (1970). 'Fatigue crack closure under cyclic tension'. Engineering Fracture Mechanics, 2, 37-45.

2. W. Elber (1971). 'The significance of fatigue crack closure'. Damage Tolerance in Aircraft Structures, ASTM STP 486, 230-242.

3. W. Elber (1975). 'Crack-closure and crack-growth measurements in surface – flawed titanium alloy Ti-6Al-4V'. NASA TN D-8010, NASA, Washington, DC.

4. Vasudevan A.K., Sadananda K., Louat N.A. A review of crack closure, fatigue crack threshold and related phenomena. Material Science Engineering, 1994, A188, pp 1-22.

Reviews on crack closure

5. D.E. Macha, D.M. Corbly, J.W. Jones (1979). 'On the variation of fatigue-crack-opening load with measurement location'. Experimental Mechanics, 19, 207-213.

6. S. Banerjee (1984). 'A review of crack closure'. Technical report AFWAL-TR-84-4031, AFWAL, Wright-Patterson AFB, OH.

7. J.E. Allison (1988). 'The measurement of crack closure during fatigue crack growth'. Fracture Mechanics: 18th Symposium, ASTM STP 945, 913-933.

8. J.E. Allison, R.C. Ku, M.A. Pompetzki (1998). 'A comparison of measurement methods and numerical procedures for the experimental characterization of fatigue crack closure'. Mechanics of Fatigue Crack Closure, ASTM STP 982, 171-185.

9. S.K. Ray, F. Alten, F. Grandt (1988). 'Comparison of methods for measuring fatigue crack closure in a thick specimen'. Mechanics of Fatigue Crack Closure, ASTM STP 982, 197-213.

10. J. Schijve (1988). 'Fatigue crack closure: Observations and technical significance'. Mechanics of Fatigue Crack Closure, ASTM STP 982, 5-34.

11. E.P. Phillips (1989). Results of the round robin on opening-load measurement. NASA Technical Memorandum 101601, Langley Research Center, Hampton, VA.

12. E.P. Phillips (1993). Results of the second round robin on opening-load measurement. NASA Technical Memorandum 109032, Langley Research Center, Hampton, VA.

13. X.Y. Huang, M. Lang, X.R. Wu, H. Doker (1998). 'Analysis of crack closure by different measurement methods'. Fracture and Strength of Solids, 637-642.

14. J.C. Newman Jr. (1999). 'An evaluation of plasticity-induced crack closure concept and measurement methods'. Advances in Fatigue Crack Closure

Measurement and Analysis, ASTM STP 1343, PA, 2, 128-144.

15. Y. Xu, P.J. Gregson, I. Sinclair (2000). 'Systematic assessment and validation of compliance-based crack closure measurements in fatigue'. Materials Science and Engineering, A284, 114-125.

Microscope, SEM observations and stereo imaging photography

[15], [55]

16. M. Jono (1999). 'SEM and AFM observation and mechanism of fatigue crack growth'. Fatigue '99: Proceedings of the Seventh International Fatigue Congress, Beijing, China, 57-68.

17. H. Nisitani, M. Kage (1977). Observation of crack closure phenomena at the tip of a fatigue crack by electron microscopy. Advance in Research on the Strength and Fracture of Materials, 4th International Conference on Fracture, Waterloo, Canada, 1099-1108.

18. D. Davidson, A. Nagy (1978). A low-frequency cyclic loading stage for the SEM Journal of Physics, Scientific Instruments, 11, 207-210.

19. D.L Davidson (1991). Fatigue crack closure. Eng. Fracture Mech., 38, 393-402.

20. S.J. Hudak Jr., D.L. Davidson (1988). The dependence of crack closure on fatigue loading variables. ASTM STP 982, ASTM, PA, 121-138.

21. D.L. Davidson, L.K. Austin (1991). Fatigue crack growth through ARALL-4 at ambient temperature. Fatigue and Fracture of Engineering Materials and Structures, 14, 939-951.

22. R.C. McClung, D.L. Davidson (1991). High resolution numerical and experimental studies of fatigue cracks. Engineering Fracture Mechanics, 39, 113-130.

23. N.A. Fleck (1984). 'An investigation of fatigue crack closure', PhD thesis, Cambridge University, Cambridge, UK.

24. N. Walker, C. Beevers (1979). A fatigue crack closure mechanism in titanium. Fatigue of Engineering Materials and Structures, 1, 135-148.

25. H. Sehitoglu (1985). 'Characterization of crack closure', Fracture Mechanics: 18th Symposium, STP 868, ASTM, PA, 445-456.

26. Ohta, M. Kosuge, E. Sasaki (1979). 'Change of fatigue crack closure level with gauge location along crack line'. International Journal of Fracture, 15, R53-R57.

27. H. Nisitani, K. Takao (1981). 'Significance of initiation, propagation and crack closure of micro cracks in high cycle fatigue of ductile materials'. Engineering Fracture Mechanics, 15, No.3-4, 445-456.

Photography

28. W.T. Riddell, R.S. Piascik, M.A. Sutton, W. Zhao, S.R. McNeill, J.D. Helm (1999). Advances in Fatigue Crack Closure Measurement and Analysis, Second Volume, ASTM STP 1343, ASTM, PA, 157-174.

29. H. Staal, J. Ellen (1979). Engineering Fracture Mechanics, 11, 275-283.

Optical and laser interferometry

[5], [9], [57]

30. R. Weller, M. Shepard (1948). 'Displacement measurement by mechanical interferometry'. Proceedings of Society for Experimental Stress Analysis, 6, No. 1, 35-38.

31. W.N. Sharpe (1982). 'Application of the interferometric Strain/Displacement gage'. Optical Engineering, 21, 483-488.

32. X. Su, W.N. Sharpe (1989). The effect of location in closure measurements after overloads. Engineering Fracture Mechanics, 34, 1249-1253.

33. J.J. Lee, W.N. Sharpe Jr. (1988). Closure measurements on short fatigue cracks. ASTM STP 982, ASTM, PA, 270-278.

34. W.N. Sharpe Jr., J.R. Jira, J.M. Larsen (1992). Real-time measurement of small-crack opening behavior using an interferometric strain/displacement gage. Small Crack Test Methods, ASTM STP 1149, ASTM, 92-115.

35. W.N. Sharpe (1989). 'An interferometric strain displacement measurement system'. NASA Technical Memorandum 101638.

36. L.J. Fellows, D. Nowell, D.A. Hills (1997). 'Advances in Fracture Research'. Proceedings of the 9th International Conference on Fracture, Sydney, Australia, 2552-2558.

37. K. Li (1995). 'Interferometric strain rosette for residual stress measurements'. Fatigue and Fracture at Elevated Temperatures, ASME, Aerospace Division (Publication), AD, 50, 135-143.

38. K. Li (1995). 'Interferometric 45 and 60 strain rosettes'. Journal of Applied Optics, 34, No. 28, 6376-6379.

39. W. Sharpe (1968), 'The interferometric strain gage'. Experimental Mechanics, 8, 164-170.

40. K. Li (1996), 'The interferometric strain rosette technique'. Experimental Mechanics, 36, No. 3, September, 199-203.

41. W. Sharpe, T. Payne, M. Smith (1978). 'A biaxial laser based displacement transducer'. Rev. Sci. Instruments., 49, 741-745.

42. K. Li (1996), ‘Out of plane displacement derivative measurements using interferometric strain/slope gage’. Journal of Applied Mechanics, 63, 1033-1038.

43. F. Bell (1956). ‘Determination of dynamic plastic strain through the use of diffraction grating’. Journal of Applied Physics, 27, No.10, 1109-1113.

44. J. Martinez, H. Kugler, S. Merino, H. Drude, A. Criado (1994). ‘Mechanical study of a hypo eutectoid steel weld’. Journal of Testing and Evaluation, 22, No. 5, 460-464.

45. Riemslag (1994). ‘Fatigue testing of high density polyethylene and polycarbonate with crack length measurement using image measurement using image processing techniques’. Journal of Testing and Evaluation, 22, No. 5, 410-419.

46. F. Tong, T. Gray (1996). ’Fatigue crack closure based on whole field displacements’. International Journal of Fatigue, 18, No. 8, 593-601.

Replica taking

[8], [15], [17], [23-27], [55]

47. S.L. Wong, P.E. Bold, M.W. Brown, R.J. Allen (2000). ‘Two measurement techniques for determining effective stress intensity factors’. Fatigue and Fracture of Engineering Materials and Structures, 659-666.

Surface strain

[9], [13], [15], [28], [77-81], [92], [101]

48. C.S. Shin, R.A. Smith (1985). International Journal of Fatigue, 7, 87-93.

49. G. Wanlin (1994). ‘Fatigue crack closure under triaxial stress constraint-I. Experimental investigation’. Engineering Fracture Mechanics, 49, No.2, 265-275.

50. H. Tsukuda, H. Ogiyama and T. Shiraishi (1995). ‘Fatigue crack growth and closure at high stress ratios’. Fatigue and Fracture of Engineering Materials and Structures, 18, No.4, 503-514.

51. D. Craig, D. Kujawski, F. Ellyn (1995). ‘An experimental technique to study the behavior of small corner cracks’. International Journal of Fatigue, 17, No. 4, 253-259.

52. D.H. Chen, H. Nisitani (1988). ‘Analytical and experimental study of crack closure behavior based on an s-shaped unloading curves’. Mechanics of Fatigue Crack Closure, ASTM STP 982, 475-488.

53. R. Garz, M. James (1989). ‘Observations on evaluating fatigue crack closure from compliance traces’. International Journal of Fatigue, 11, No. 6, 437-440.

54. Y. Kondo, T. Endo (1985). Automated Test Methods for Fracture and Fatigue Crack Growth, ASTM STP 877, ASTM, PA, 118-131.

55. W.J.D. Shaw, I. LeMay (1979). 'Crack closure during fatigue crack propagation'. Fracture Mechanics, STP677, ASTM, PA, 233-246.

56. R.S. Vecchio, J.S. Crompton, R.W. Hertzberg (1986). 'Anomalous aspects of crack closure'. International Journal of Fracture, 31, 29-33.

57. D.L. Chen, B. Weiss, R. Stickler (1992). 'Test procedures and a new concept for near threshold fatigue closure'. Theoretical Concepts and Numerical Analysis of Fatigue, Engineering Materials Advisory Services, Warley, 173-199.

58. K.A. Smith, P.C. Paris (1973). 'Threshold for fatigue crack propagation and the effects of load ratio and frequency'. ASTM STP 536, 79-94.

59. M. Ghate (1983). 'Crack closure measurements in fatigue', B. Tech. Project Report, Indian Institute of Technology, Bombay, India.

60. S. Kawa (1982). 'The effect of stress ratio on FCG in a 3% NaCl solution'. Engineering Fracture Mechanics, 16, No. 6, 857-870.

61. D. Can, J. Weertman (1981). 'Crack closure and crack propagation rates in 7050 Al.' Engineering Fracture Mechanics, 15, No. 1-2, 87-106.

62. W.D. Dover, F.E.W. Charlesworth (1981). 'The use of the plastic crack tip opening displacement to correlate fatigue crack growth data for a structural steel'. Advances in Fracture Research, ICF-5, 2, D. Francois ed., Pergamon Press, 933-941.

X-Ray tomography

63. Guvenilir, T.M. Breunig, J.H. Kinney, S.R. Stock (1997). Direct observation of crack opening as a function of applied load in the interior of a notched tensile sample of Al-Li 2090. Acta Mater., 45, 1977-1987.

64. J. H. Kinney, T. M. Breunig, T. L. Starr, D. Haupt, M. C. Nichols, S. R. Stock, M. D. Butts and R. A. Saroyan (1993). X-ray tomographic study of chemical vapor infiltration processing of ceramic composites. Science, 260, 789-798.

65. T. M. Breunig (1992). PhD Thesis, Georgia Institute of Technology.

66. E. Zywicz, J. H. Kinney, M. L. Sattler, T. M. Breunig and M. C. Nichols (1993). Heterogeneous fibre microstructures and their influence on failure. J. Microscopy, 169, 247-253.

67. T. M. Breunig, S. R. Stock, S. D. Antolovich, J. H. Kinney, W. N. Massey and M. C. Nichols (1992). Fracture Mechanics: Twenty-Second Symposium, ASTM STP 1311, ASTM, Philadelphia, 1, 749-761.

68. S. R. Stock, A. Guvenilir, T. M. Breunig, J. H. Kinney and M. C. Nichols

(1995). J. Metals, 47, 19-26.

69. G. T. Herman (1980). 'Image Reconstruction from Projections: The Fundamentals Computerized Tomography'. Academic Press, Orlando.

70. C. Kak and M. Slaney (1998). 'Principles of Computerized Tomography Imaging'. IEEE Press, New York.

Caustics

71. P. Manogg (1966). 'Investigation of the rupture of a Plexiglas plate by means of an optical method involving high speed filming of the shadows originating around holes drilled in the plate'. International Journal of Fracture Mechanics, 2, 604-613.

72. P.S. Teocharis (1981). 'Elastic stress intensity factors, evaluated by caustics'. Mechanics of Fracture, 7, 190-252.

73. I.R. Wallhead, L. Edwards (1994). 'High accuracy stress intensity factor measurements using the optical method of reflective caustics'. Engineering Fracture Mechanics, 49, 699-709.

74. I.R. Wallhead, L. Edwards, P. Poole (1998). 'A study of crack closure using the optical method of caustics and consequences for the use of ΔK_{eff} as a fatigue crack driving force'. Engineering Fracture Mechanics, 60, No. 3, 291-302.

75. J. Beinert, J.F. Kalthoff (1981). 'Experimental determination of dynamic stress intensity factors by shadow patterns'. Mechanics of Fracture, 281-330.

76. C. Smith (1987). 'The role of optical stress analysis in fatigue fracture'. SPIE, Photomechanics and Speckle Metrology, 814, 648-654.

Back face strain

[8], [9], [13], [15], [28], [49], [52-54]

77. N.A. Fleck, R.A. Smith (1982). 'Crack closure – is it just a surface phenomenon', International Journal of Fatigue, Vol. 4, , pp. 157-160.

78. R.S. Vecchio, J.S. Crompton, R.W. Hertzberg (1986). 'Anomalous aspects of crack closure'. International Journal of Fracture, 31, 29-33.

79. N.A. Fleck (1975). 'Compliance methods for measurement of crack length'.

80. C.S. Lee, C.G. Park, Y.M. Chang (1996). Precise determination of fatigue crack closure in Al alloys. Mater. Sci. Eng., A216, 131-138.

81. J.K. Donald, G.M. Connelly, P.C. Paris, H. Tada (2000). 'Crack wake influence theory and crack closure measurement'. National Symposium on Fatigue and Fracture Mechanics, ASTM STP 1360, ASTM, 30, 185-200.

Crack mouth opening displacement

[5], [8], [9], [15], [28], [48], [49], [53], [55], [77-81]

82. U. Singh, S. Banerjee (1989). 'Crack closure and fatigue crack growth rate in three point bend specimens of different widths'. Fatigue and Fracture of Engineering Materials and Structures, 12, No. 1, 47-58.

83. R. Sunder (1985). 'System for automated fatigue crack growth testing under random loading'. International Journal of Fatigue, 7, 3-12.

84. J.E. Allison, C.P. You (1990). 'Problems associated with the quantification of fatigue crack closure'. Fatigue '90, UK, Materials and Components Engineering Publications, 1249-1255.

85. R.W. Hertzberg, C.H. Newton, R. Jaccard (1998). 'Crack closure – correlation and confusion'. Mechanics of Fatigue Crack Closure, ASTM STP 982, 139-148.

86. L.J. Roberson, M.T. Kirk (1988). 'A statistical approach to crack closure determination'. ASTM STP 982, 230-246.

87. K.K Brahma, P.K. Dash, B. Dattaguru (1989). Observation of crack closure using a crack mouth opening displacement gauge. International Journal of Fatigue, 11, 37-41.

88. V.S. Sarma, G. Jaeger, A. Koethe (2001). 'On the comparison of crack closure evaluation using dynamic and static compliance measurements'. International Journal of Fatigue, 23, 741-745.

89. S. Seetharam, P. Dash (1992). 'Load-CMOD data analysis for crack closure'. International Journal of Fracture, 53, R53-R58.

90. J.K. Donald, G.H. Bray, R.W. Busch (1999). 'An evaluation of the adjusted compliance ratio technique for determining the effective stress intensity factor'. 29th National Symposium on Fatigue and Fracture Mechanics, ASTM STP 1332, ASTM, 675-695.

91. J.K. Donald, P.C. Paris (1999). 'An evaluation of K_{eff} estimation procedures on 6061-T6 and 2024-T3 aluminum alloys'. International Journal of Fatigue, 21, S47-S57.

92. J.K. Donald (1997). 'Introducing the compliance ratio concept for determining effective stress intensity'. International Journal of Fatigue, 19, 191-195.

Near crack tip gage

[5], [15], [48], [49], [57], [2], [78], [79], [101], [81], [90], [92]

93. C.S. Oh, Y.Y. Earmme, J.H. Song (1997). 'Automated real-time measurements of fatigue crack length and crack opening load using unloading compliance method'. International Journal of Fatigue, 19, 169-176.

94. C.Y. Kim, J.H. Song (1993). 'An automated procedure for determining crack opening level from differential displacement signal data'. International Journal of Fatigue, 15, 301-309.

95. W. Yisheng, J. Schijve (1995). 'Fatigue crack closure measurements on 2024-T3 sheet specimens'. Fatigue and Fracture of Engineering Materials and Structures, 18, No.9, 917-921.

96. C.D. Carman, C.C. Turner, B.M. Hilberry (1988). 'A method for determining crack opening load from load-displacement data'. Mechanics of Fatigue Crack Closure, ASTM STP 982, 214-221.

Push Rod

[23], [77]

Eddy current

97. S. Burke (1994). Eddy-current inversion in the thin-skin limit: determination of depth and opening for a long crack. Journal of Applied Physics, 76, No.5, 3072-3080.

98. J. Moulder, W. Ward (1998). Low frequency, pulsed eddy currents for deep penetration. Review of Progress in Quantitative Nondestructive Evaluation; New York, NY, USA : Plenum, 2, xxviii+2128, 291-8 vol.1

Potential drop

[13]

99. R.H. VanStone, T.L. Richardson (1985). Potential drop monitoring of cracks in surface-flawed specimens. Automated Test Methods for Fracture and Fatigue Crack Growth, ASTM STP 877, ASTM, PA, 148-166.

100. V. Bachmann, D. Munz (1976). Unusual potential drop during the application of the electrical potential method in a fracture mechanics test. Journal of Testing and Evaluation, 4, 257-260.

101. T.T. Shih, R.P. Wei (1974). 'A study of crack closure in fatigue'. Engineering Fracture Mechanics, 6, 19-32.

Acoustic emission

[5], [80]

102. K. Hirano, H. Kobayashi, A. Hayashi (1987). 'Monitoring of surface fatigue crack growth and crack tip closure behavior by the ultrasonic isoscanning

technique'. JSME Int. J., 30, 1707-1713.

103. R.K. Abbott, P. Doig (1984). Single specimen fracture toughness testing of low strength steel plate using the direct current electrical potential method. Journal of Testing and Evaluation 12, No.5, 297-304

Other methods for determination of opening load

104. G.S. Booth, S.J. Maddox (1988). 'Correlation of fatigue crack growth data obtained at different stress ratios'. Mechanics of Fatigue Crack Closure, ASTM STP 982, 516-527.

105. ASTM (2000) Standard Test Method Measurement of Fatigue Crack Growth Rates. In: *2000 Annual Book of ASTM Standards*, E647-00, Vol.03.01, ASTM, W. Conshohocken, PA, p.603.

106. J.K. Donald (1988). 'A procedure for standardizing crack closure levels'. Mechanics of Fatigue Crack Closure, ASTM STP 982, ASTM, 222-229.

107. C.W. Dunnett (1964). 'New tables for multiple comparisons with a control'. Biomechanics, 20, No.3, 482-491.

108. R.S. Blandford, S.R. Daniewiz, J.D. Skinner (2001). 'Determination of the opening load for a growing fatigue crack: evaluation of experimental data reduction techniques and analytical models'. Fatigue and Fracture of Engineering Materials and Structures, 25, 17-25.

109. Schijve (1991). 'Regression analysis to find the transition from linear to non-linear function. Application to results of crack closure measurements', Document B2-91-06, Faculty of Aerospace Engineering, Delft University of Technology.

110. Joyce, G.E. Sutton (1985). 'An automated method of computer controlled low cycle fatigue crack growth testing using he elastic-plastic parameter cyclic J'. in Automated Test Methods for Fracture and Fatigue Crack Growth, ASTM STP 877, ASTM, 227-247.

111. M. Scorupa, S. Beretta, M. Carboni and T. Machiniewicz (2001). 'An algorithm for evaluating crack closure from local compliance measurements'. Fatigue and Fracture of Engineering Materials and Structures, 25, 261-273.

112. M. Toyosada, T. Niwa (1999). 'The significance of RPG load for fatigue crack propagation and the development of a compliance measurement system'. International Journal of Fatigue, 67, 217-230.

113. J.D Dougherty (1997). Engineering Fracture Mechanics, 56, 189-212.

114. S.R. Daniewicz (1999). 'Smoothing and differentiating load-displacement data using a low-pass filter for improved crack opening estimates'. Fatigue and Fracture of Engineering Materials and Structures, 22, 273-279.

115. D.L. Chen, B. Weiss, R. Stickler (1996). 'Contribution of the cycling loading portion below the opening load to fatigue crack growth'. Materials Science and Engineering, A208, 181-187.

116. A.K. Vasudevan, K. Sadananda, N. Louat (1994). 'A review of crack closure, fatigue crack threshold and related phenomena'. Materials Science and Engineering, A188, 1-22.

117. H. Tada, P. Paris, G. Irwin (1985). 'The stress analysis of cracks handbook', Paris Productions Inc.

118. J.K. Donald, E. Phillips (1999). 'Analysis of the second ASTM round robin program on opening –load measurement using the adjusted compliance ratio technique'. ASTM STP 1343, 79-93.

119. D. Kujawski (2001). 'Enhanced model of partial crack closure for correlation of R-ratio effects in aluminum alloys'. International Journal of Fatigue, 23, 95-102.

120. D. Kujawski (2000). 'Correlation of long and physically short cracks growth in aluminum alloys'. Engineering Fracture Mechanics, 68, 1357-1369.

121. J. Pellas, G. Baudin, M. Roberts (1977). 'Fatigue crack growth model prediction with two coupled differential equations'. ICF4, 2, 1353-1360.

122. G. Marci, K. Hartmann, V. Bachmann (1990). 'Experimentelle bestimmung des ΔK_{eff} fur Ermitidungssrisfortschritt'. Materialwiss. U. Werkstoffech, 21, 174-184.

123. G. Marci (1996). 'Determination of the partitioning point dividing K into K_{eff}'. Engineering Fracture Mechanics, 53, No.1, 23-36.

124. G. Marci (1996). 'The K_{eff}-concept: a unique and complete description of fatigue crack propagation'. Engineering Fracture Mechanics, 55, No.1, 95-114.

125. H. Doker, V. Bachmann (1988). 'Determination of crack opening load by use of crack threshold behavior'. Mechanics of Fatigue Crack Closure, ASTM STP 982.

126. M. Lang (1998). 'A model for fatigue crack growth, part I: phenomenology'. Fatigue and Fracture of Engineering Materials and Structures, 23, 587-601.

127. M. Lang (1998). 'A model for fatigue crack growth, part II: modeling'. Fatigue and Fracture of Engineering Materials and Structures, 23, 603-617.

128. J. Schijve (1976). 'The effect of pre-strain on fatigue crack growth and crack closure'. Engineering Fracture Mechanics, 8, 575-581.

129. U. De Koning (1981). 'A study of cyclic crack tip plasticity and crack closure under variable amplitude loading'. NLR TR 81141 L, National Aerospace Laboratory NLR, Amsterdam, the Netherlands.

130. R.M. Pelloux, M. Faral, W.M. McGee (1979). Assessment of crack tip closure in an aluminum alloy by electron fractography. Fatigue and Fracture of Engineering Materials and Structures, No.1, 21-35.

131. R. Sunder, P.K. Dash (1982). 'Measurement of fatigue crack closure through electron microscopy'. International Journal of Fatigue, 4, 97-105.

132. Kujawski, D. and Stoychev S. (2004). A New Method for Opening Load Determination from Compliance Measurements. Fatigue and Fracture Mechanics: 34th Volume, ASTM STP 1461, S. R. Daniewicz, J. C. Newman and K.-H. Schwalbe, Eds., ASTM International, West Conshohocken, PA, (in press).

Krak Gage

133. H. Fitzgerald and M. D. Griffith (1980). 'Preliminary Evaluation of Optical Crack Measurements vs. FRACTOMAT Measurements and Automated, Computerized, FRACTOMAT Measurements', Support Services Laboratories, Northrop Corporation Aircraft Division, Hawthorne, CA 90250.

134. H. S. Pearson, G. J. Gilbert (1981). 'Automated Crack Growth Testing—Evaluation of a Bonded Foil Crack—Gage System', ASTM Spring Meeting, New Orleans.

135. H. R. Hartman, R. W. Churchill (1981). 'KRAK—GAGE, a New Transducer for Crack Growth Measurements', SESA Fall Meeting, Keystone, CO, Oct..

136. Anon., Micro-Measurements Manual. P.O. Box 27777, Raleigh, NC 27611.

137. P. Lilaw, H. Hartman, E. Helm (1983). 'Corrosion fatigue crack propagation testing with the crack gage in salt water'. Engineering Fracture Mechanics, 18, No. 1, 121-131.

138. P. Paris, B. Hayden (1979). 'A new system for fatigue crack growth measurement and control', ASTM Symposium on Fatigue Crack Growth.

139. K. Jen, J. Scardina, D. Smith (1984). 'Bonded-resistance gages for fatigue – crack lengths in nodular iron'. Experimental Techniques, 8, No. 4, 26-29.

Other

140. R.C. McClung (1991). 'The influence of applied stress, crack length and Stress intensity Factor on crack closure'. Metallurgical Transactions, 22A, 1559-1571.

141. W.J. Shaw, W. Zhao (1994). 'Back face strain calibration for crack length measurements', Journal of Testing and Evaluation, 22, No. 6, 512-516.

142. J. Schijve (1972). 'The accumulation of fatigue damage in aircraft materials and structure'. AGARD, No. 157.

143. J. Schijve (1979). 'Four lectures on fatigue crack growth'. Engineering Fracture Mechanics, 11, 167-221.

144. H. Tada, P. Paris (2002). 'Theoretical analysis of load-displacement relations associated with crack surface interferences'. International Conference on Fatigue

Damage of Structural Materials IV, Hyannis, MA.

145. D. Kujawski, S. Stoychev (2002). 'Parametric study on variability of P_{op} determination'. International Conference on Fatigue Damage of Structural Materials IV, Hyannis, MA.

146. Forth S C, Newman J C, Forman RG. (2002) 'On Generating Fatigue Crack Growth Thresholds'. International Journal of Fatigue, Vol. 25, No. 1, pp. 9-15.

147. Paris, P. C., Tada, H. and Donald, J. K. (1999) 'Service Load Fatigue Damage - A Historical Perspective' International Journal of Fatigue, Vol. 21, pp. S35-S46.

148. Memorandum 109032, Langley Research Center, Hampton, VA, (1993).

149. Kujawski D. and Stoychev S. Parametric Study on the Variability of Opening Load Determination. International Journal of Fatigue, (2003), Vol. 25, pp. 1181-1187.

154. Stoychev S. and Kujawski D. Methods for Crack Opening Load and Crack Tip Shielding Determination: A Review. Fatigue and Fracture of Engineering Materials and Structures, (2003), Vol. 26, pp. 1053-1067.

155. Sadananda K, Vasudevan AK. A unified framework for fatigue crack growth. In: Lutjering G. Nowack H, editors. Fatigue 96, vol. 1. Berlin: Pergamon, 1996:375–80.

156. Vasudevan A.K, Sadananda K. Application of unified fatigue damage approach to compression–tension region. International Journal of Fatigue 21 (1999), S263–S273.

157. Sadananda K., Vasudevan A.K., Holtz R.L. Extension of the Unified Approach to fatigue crack growth to environmental interactions. International Journal of Fatigue (2001), 23, S277–S286.

158. Vasudevan A.K., Sadananda K., and Glinka G. Critical Parameters for Fatigue Damage. International Journal of Fatigue (2001), 23S, S39-S53.

159. Sadananda K., Vasudevan A.K. Crack tip driving forces and crack growth representation under fatigue. International Journal of Fatigue (2004), 26, 39– 47.

160. Kujawski D. A new $(\Delta K K_{max})^{0.5}$ driving force parameter for crack growth in aluminum alloys. International Journal of Fatigue, (2001), Vol. 23, pp. 733–740.

161. Kujawski D. ΔK_{eff} Parameter Under Re-examination, International Journal of Fatigue, (2003), Vol. 25, pp. 793-800.

162. Dinda S. Correlation and prediction of fatigue crack growth for different R-ratios using K_{max} and ΔK^{+} parameters, Master's Thesis, (2002). Dept. of Mech./Aeronautical Eng., College of Eng./App. Sci., Western Michigan University, Kalamazoo, MI.

163. Dinda S. and Kujawski D. Correlation and Prediction of Fatigue Crack Growth

for Different R-ratios using K_{max} and ΔK^{+} Parameters, Engineering Fracture Mechanics, (2004), Vol. 71, Issue 12, pp. 1779-1790.

164. Head A.K. The growth of fatigue cracks, Philosophical Magazine, (1953), Vol. 44, pp. 925-938.

165. Liu H.W and Iino N. A mechanical model for fatigue crack propagation, Proc. 2nd Int. Conf. on Fracture, (1969), Paper 71, pp. 812-823, Chapman-Hall.

166. Anatolovich S.D., Saxena, A. and Chanani, G.R. A model for fatigue crack propagation, Engineering Fracture Mechanics, (1975), Vol. 7, pp. 649-652.

167. Majumdar S. and Morrow J. Correlation between fatigue crack propagation and low cycle fatigue properties, Fracture toughness and slow-stable cracking, ASTM STP 559, (1974), pp. 159-182.

168. Glinka G. Cumulative model of fatigue crack growth, International Journal of Fatigue, (1982), Vol. 4, pp.59-67.

169. Kujawski D. and Ellyn F. A fatigue crack propagation model, Engineering Fracture Mechanics, (1984), Vol. 20, No. 5/6, pp. 695-704.

170. Kujawski D. and Ellyn F. A fatigue crack growth model with load ratio effects, Engineering Fracture Mechanics, (1987), Vol. 28, No. 4, pp. 367-378.

171. Pandey K.N., Chand S. Fatigue crack growth model for constant amplitude loading, Fatigue and Fracture of Engineering Materials and Structures, (2003), Vol. 27, pp. 459-472.

172. Smith K.N., Watson P., Topper T.H. A stress-strain function for the fatigue of metals, Journal of Materials, ASTM, (1970), Vol. 5, No. 4, pp. 767-778.

173. Glinka G. (May 2004) Private communication.

174. Rice J. R. Stress due to a sharp notch in a work–hardening elastic–plastic material loaded by longitudinal shear. Journal of applied Mechanics, (1967), 34, 387-298.

175. McClintock, Discussion of fracture testing of high strength materials. Mater. Res. Standards, (1969), 1, 277-279.

176. Donald J.K., Bray G.H., Bush R.W. Introducing the K_{max} sensitivity concept for correlating fatigue crack growth data. *In High Cycle Fatigue of Structural Materials,* Edited by Soboyejo W.O. and Srivatsan T.S. The Minerals, Metals and Materials Society, 1997, pp 123-141

177. Barber C. B., Dobkin D.P. and Huhdanpaa H.T. The Quickhull Algorithm for Convex Hulls. ACM Transactions on Mathematical Software, Dec. 1996, Vol. 22, No. 4, pp 469-483. (see also http://www.qhull.org)

178. Bray, G. H., Donald, J. K. Separating the Influence of Kmax from Closure-Related Stress Ratio Effects Using the Adjusted Compliance Ratio Technique.

Advances in Fatigue Crack Closure Measurement and Analysis: Second Volume, ASTM STP 1343, R. C. McClung, J. C. Newman, Jr., Eds., American Society for Testing and Materials, 1998

Appendix A

This appendix contains all the test data that was generated during the dissertation writing process. Data tables along with plots of the experimental data are included for each test. Some of the results were not discussed for brevity in the main text, but all of them were analyzed and agreed with the trends, shown in Part I and II (there are no ‘outliers’).

Overloads with OLR=1.5

Material – al.2324-T39
Base load – K_{min}=1 Mpam$^{0.5}$; K_{max}=10 Mpam$^{0.5}$
Overload - K_{min}=1 Mpam$^{0.5}$; K_{max}=15 Mpam$^{0.5}$

Specimen 3								
OLR 1.5			OLR 1.5			OLR 1.5		
a [mm]	dadN [m/cycle]	N [cycles]	a [mm]	dadN [m/cycle]	N [cycles]	a [mm]	dadN [m/cycle]	N [cycles]
-0.8603	5.90078E-08	-11002	-0.8438	8.89388E-08	-10000	-0.6991	1.70926E-07	-6000
-0.7602	8.21401E-08	-10000	-0.6843	7.05458E-08	-8000	-0.436	9.21937E-08	-4000
-0.6506	6.84588E-08	-8000	-0.4999	1.13938E-07	-6000	-0.2102	1.33649E-07	-2000
-0.5006	8.15352E-08	-6000	-0.3066	7.93237E-08	-4000	0	7.65071E-08	0
-0.3251	9.39103E-08	-4000	-0.1503	7.70162E-08	-2000	0.08208	9.21769E-08	121
-0.1453	8.59581E-08	-2000	0	7.3238E-08	0	0.11968	3.2018E-08	2121
0	5.92962E-08	0	0.07997	1.40219E-07	96	0.17112	1.94126E-08	4122
0.09843	3.16228E-07	2	0.08785	1.1538E-09	2096	0.24304	5.24979E-08	6122
0.12766	3.01726E-10	3914	0.08833	2.8845E-10	8096	0.39861	1.03073E-07	8122
0.20631	3.91713E-08	7915	0.09679	9.32655E-09	12096	0.60511	1.03429E-07	10122
0.30977	3.82257E-08	9228	0.10747	1.3461E-09	14096	0.74412	3.55755E-08	12122
0.49226	1.57398E-07	11228	0.12372	1.49032E-08	16096	0.82354	4.38444E-08	14122
0.70386	4.08417E-07	15228	0.15612	1.74993E-08	18096	0.98102	1.13635E-07	16122
1.24657	1.34293E-07	17228	0.20208	2.84604E-08	20096	1.20417	1.09515E-07	18122
1.62209	2.41226E-07	19228	0.309	7.84584E-08	22096	1.43701	1.23332E-07	20122
1.94347	1.23992E-07	20521	0.45848	7.10265E-08	24096	1.62477	6.44205E-08	22122
			0.59585	6.63435E-08	26096	1.73446	4.52725E-08	24122
			0.78854	1.26341E-07	28096	1.90117	1.21437E-07	26122
			1.02196	1.07083E-07	30096	2.20507	1.82464E-07	28122
			1.27074	1.41697E-07	32096	2.49394	1.0641E-07	30122
			1.6156	2.03165E-07	34096	2.70602	1.05669E-07	32122
			1.94075	1.21986E-07	36096			
			2.22716	1.64417E-07	38096			
			2.48193	9.03527E-08	40096			

Specimen 4								
OLR 1.5			OLR 1.5			OLR 1.5		
a [mm]	dadN [m/cycle]	N [cycles]	a [mm]	dadN [m/cycle]	N [cycles]	a [mm]	dadN [m/cycle]	N [cycles]
-1.3477	xxx	-16000	-1.2277	xxx	-15004	-1.0517	xxx	-16000
-1.1481	9.98037E-08	-14000	-1.1566	7.1151E-08	-14004	-1.0265	2.51913E-08	-15000
-0.9597	9.41987E-08	-12000	-1.0673	8.9227E-08	-13004	-0.9785	4.8075E-08	-14000
-0.7166	1.21534E-07	-10000	-0.9641	1.0316E-07	-12003	-0.882	9.6478E-08	-13000
-0.6347	4.09458E-08	-8000	-0.932	3.2082E-08	-11002	-0.8551	2.6922E-08	-12000
-0.4759	7.94199E-08	-6000	-0.843	8.9007E-08	-10002	-0.7587	9.63423E-08	-11000
-0.3347	7.05599E-08	-4000	-0.7916	5.1316E-08	-9002	-0.6441	1.14611E-07	-10000
-0.1161	1.09323E-07	-2000	-0.7565	3.5191E-08	-8002	-0.582	6.20846E-08	-9000
0	5.80463E-08	0	-0.5418	2.1461E-07	-7002	-0.5172	6.48051E-08	-8000
0.04981	1.23895E-07	402	-0.4775	3.2196E-08	-5002	-0.4105	1.06726E-07	-7000
0.12961	3.99022E-08	2402	-0.4001	7.7227E-08	-4001	-0.3736	3.69216E-08	-6000
0.14346	6.9228E-09	4402	-0.3365	6.3588E-08	-3000	-0.3353	3.82677E-08	-5000
0.14365	9.615E-11	6402	-0.208	1.2846E-07	-2000	-0.2895	4.57674E-08	-4000
0.26134	5.88438E-08	8402	-0.0944	1.1365E-07	-1000	-0.2257	6.38436E-08	-3000
0.34518	1.22577E-07	9086	0	9.4391E-08	0	-0.1117	1.13977E-07	-2000
0.52707	9.09438E-08	11086	0.0502	1.1639E-07	431	-0.035	7.67277E-08	-1000
0.60514	3.90369E-08	13086	0.0542	4.0343E-09	1432	0	3.49986E-08	0
0.73008	1.24938E-07	14086	0.0636	7.8392E-09	2634	0.08923	2.09454E-07	426
0.77508	4.49982E-08	15086	0.0527	-1.0961E-08	3634	0.11307	2.38452E-08	1426
0.88276	1.07688E-07	16086	0.0544	1.7307E-09	4634	0.1223	9.2304E-09	2426
0.95526	7.24971E-08	17086	0.058	3.6537E-09	5634	0.12192	-3.846E-10	3426
1.09564	1.40379E-07	18086	0.0504	-7.692E-09	6634	0.12423	2.3076E-09	4426
1.20308	1.07439E-07	19086	0.0505	1.923E-10	7634	0.18268	5.84592E-08	5426
			0.0948	4.4229E-08	8634	0.31729	1.3461E-07	6426
			0.1229	2.8076E-08	9634	0.42765	1.10352E-07	7426
			0.1336	1.0769E-08	10634	0.62665	1.99002E-07	8426
			0.1788	4.5191E-08	11634	0.80357	1.76916E-07	9426
			0.2465	6.769E-08	12634			
			0.3153	6.8843E-08	13634			
			0.3405	2.5191E-08	14634			
			0.3886	4.8075E-08	15634			
			0.4851	9.6478E-08	16634			
			0.512	2.6922E-08	17634			
			0.6084	9.6342E-08	18634			
			0.723	1.1461E-07	19634			
			0.785	6.2085E-08	20634			
			0.8499	6.4805E-08	21634			
			0.9566	1.0673E-07	22634			
			0.9935	3.6922E-08	23634			
			1.0318	3.8268E-08	24634			
			1.0775	4.5767E-08	25634			
			1.1414	6.3844E-08	26634			
			1.2554	1.1398E-07	27634			
			1.3321	7.6728E-08	28634			
			1.3671	3.4999E-08	29634			

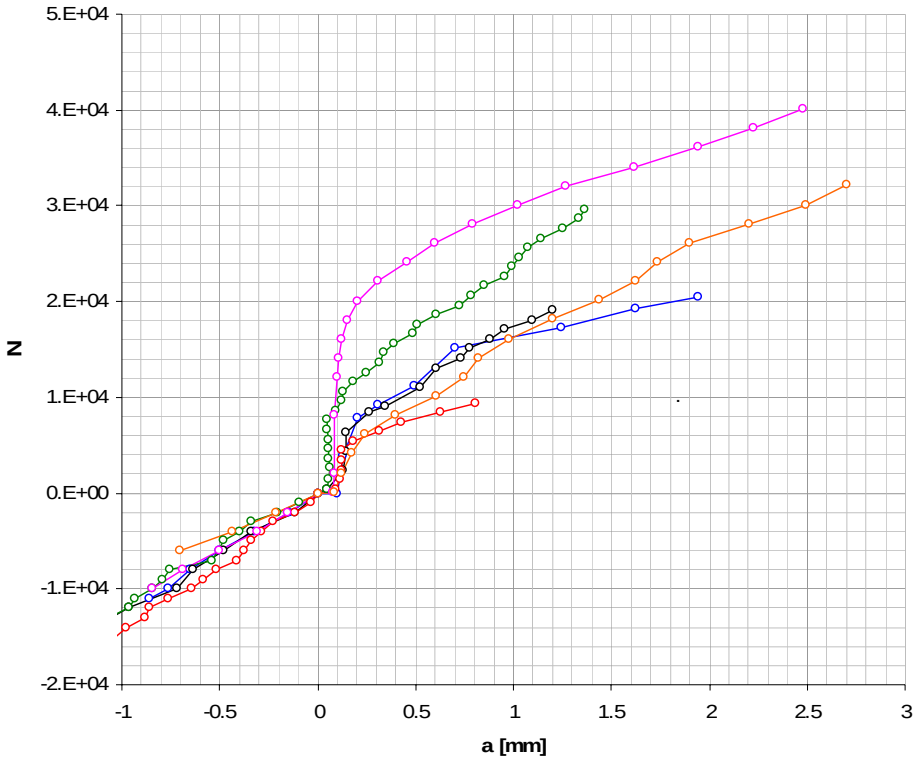
5.E+04
4.E+04
3.E+04
2.E+04
1.E+04
0.E+00
-1.E+04
-2.E+04
N
-1
-0.5
0
0.5
1
1.5
2
2.5
3
a [mm]

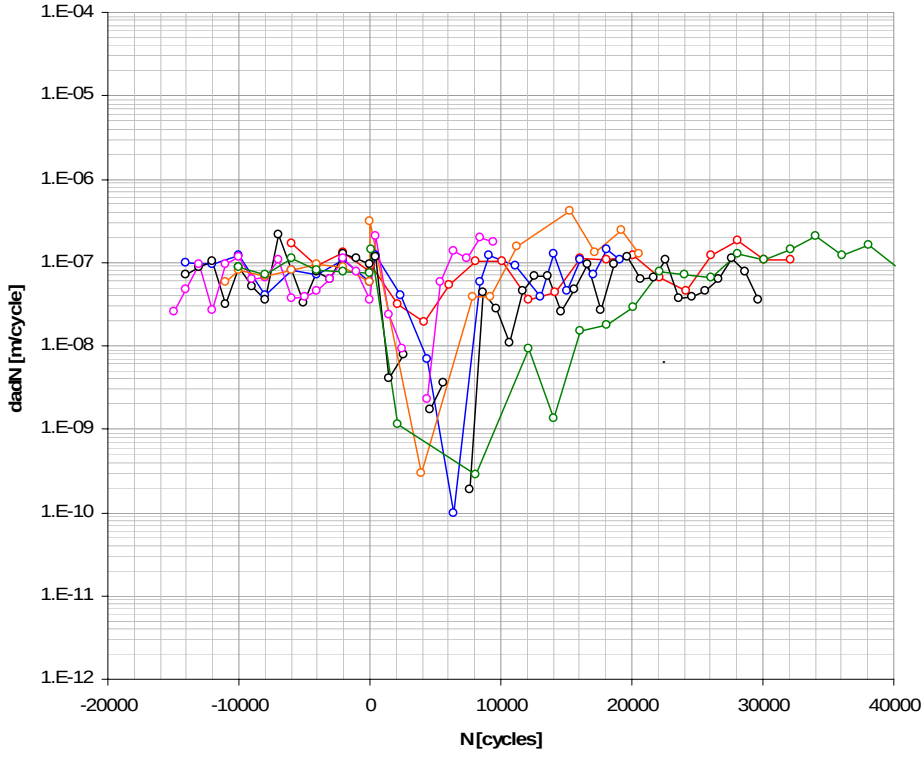
1.E-04
1.E-05
1.E-06
1.E-07
1.E-08
1.E-09
1.E-10
1.E-11
1.E-12
da/dN [m/cycle]
-20000
-10000
0
10000
20000
30000
40000
N [cycles]

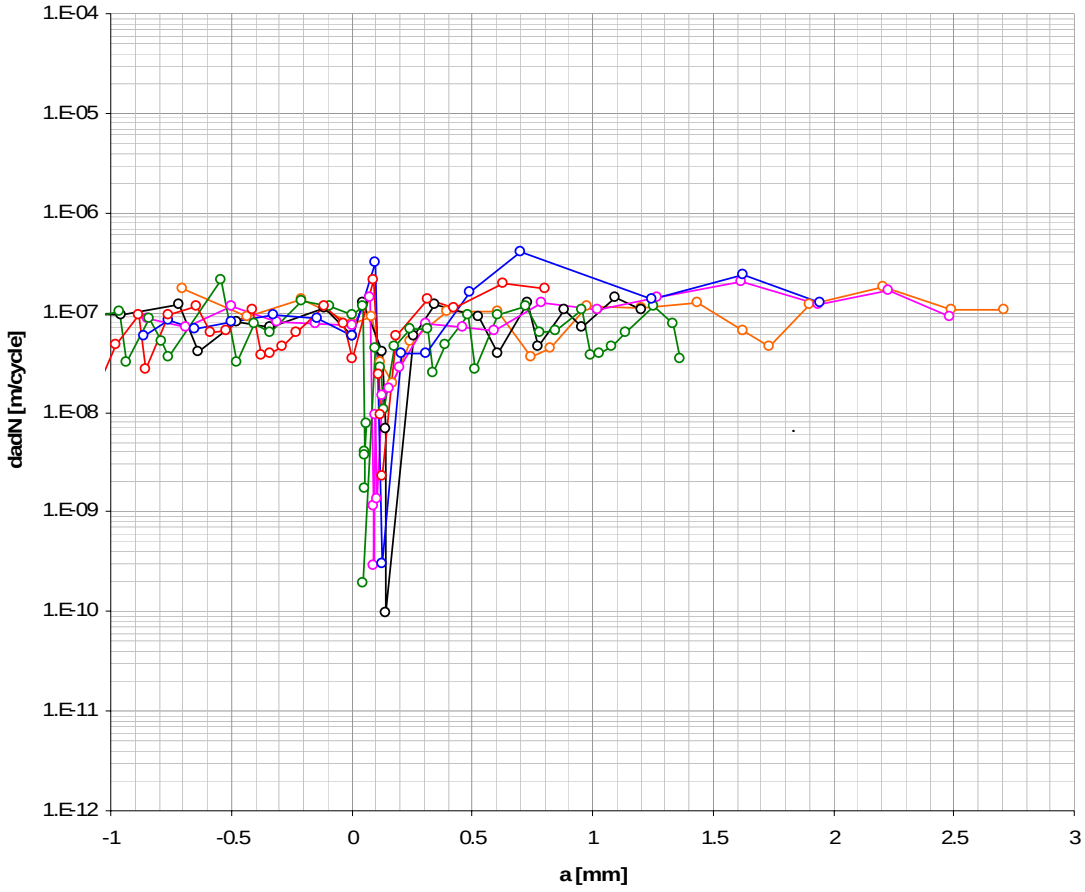
1.E-04
1.E-05
1.E-06
1.E-07
1.E-08
1.E-09
1.E-10
1.E-11
1.E-12
dadN [m/cycle]
-1
-0.5
0
0.5
1
1.5
2
2.5
3
a [mm]

Overloads with OLR=2

Material – al.2324-T39
Base load – K_{min}=1 Mpam$^{0.5}$; K_{max}=10 Mpam$^{0.5}$
Overload - K_{min}=1 Mpam$^{0.5}$; K_{max}=2 Mpam$^{0.5}$

Specimen 4								
OLR2			OLR2			OLR2		
a [mm]	dadN [m/cycle]	N [cycles]	a [mm]	dadN [m/cycle]	N [cycles]	a [mm]	dadN [m/cycle]	N [cycles]
-1.766	xxxxx	-22000	-1.709	xxxxx	-24002	-0.598	xxxxx	-6000
-1.5028	1.31615E-07	-20000	-1.643	3.27871E-08	-22002	-0.473	1.24938E-07	-5000
-1.3892	5.68105E-08	-18000	-1.575	3.41191E-08	-20002	-0.428	4.49982E-08	-4000
-1.2321	7.85404E-08	-16000	-1.412	8.14391E-08	-18002	-0.32	1.07688E-07	-3000
-1.1358	4.8157E-08	-14000	-1.289	6.13295E-08	-16002	-0.248	7.24971E-08	-2000
-1.0485	4.36521E-08	-12000	-1.078	1.05861E-07	-14002	-0.107	1.40379E-07	-1000
-0.797	1.25764E-07	-10000	-0.967	5.54644E-08	-12002	0	1.07439E-07	0
-0.6358	8.05737E-08	-8000	-0.731	1.17866E-07	-10002	0.0588	5.30985E-09	11082
-0.4234	1.06232E-07	-6000	-0.574	7.85404E-08	-8002	0.0813	2.04537E-09	22082
-0.2886	6.7387E-08	-4000	-0.457	5.8363E-08	-6002	0.1063	2.27264E-09	33082
-0.1847	5.1921E-08	-2000	-0.319	6.931E-08	-4002	0.1702	3.36019E-09	52082
0	9.23719E-08	0	-0.165	7.67855E-08	-2001	0.1986	4.06577E-09	59082
0.0931	6.46342E-09	14400	0	8.24413E-08	0	0.2119	1.32687E-08	60082
0.1096	2.0818E-09	22344	0.0344	1.5936E-07	216	0.2194	7.4997E-09	61082
0.151	2.06924E-09	42346	0.0698	3.53761E-09	10218	0.2298	1.03842E-08	62082
0.1831	1.60348E-08	44346	0.083	2.70281E-09	15100	0.2394	9.615E-09	63082
0.2192	1.80762E-08	46346	0.106	2.61304E-09	23902	0.2431	3.6537E-09	64082
0.34	6.03822E-08	48346	0.136	2.30698E-09	36906	0.2465	3.4614E-09	65082
0.3846	2.22926E-08	50346	0.2338	3.91285E-09	61910	0.261	1.44225E-08	66082
0.4196	1.74993E-08	52346	0.3517	1.1788E-07	62910	0.285	2.40375E-08	67082
0.5296	2.74989E-08	56346	0.3634	1.16737E-08	63910	0.2931	8.0766E-09	68082
0.5578	1.41199E-08	58346	0.3913	2.78556E-08	64911	0.3065	1.3461E-08	69082
0.5984	2.02877E-08	60346	0.4476	5.62876E-08	65912	0.3658	1.97428E-08	72082
0.7153	5.84592E-08	62346	0.4803	3.2691E-08	66912	0.3859	2.01915E-08	73082
0.8347	5.9695E-08	64346	0.6203	6.99972E-08	68912	0.3967	1.07688E-08	74082
1.0778	1.21534E-07	66346	0.6982	3.89266E-08	70912	0.4202	2.34606E-08	75082
1.1931	5.76182E-08	68348	0.7982	4.9998E-08	72912	0.46	3.98061E-08	76082
1.2587	3.27871E-08	70348	0.9256	6.37475E-08	74912	0.5982	1.38235E-07	77082
1.3269	3.41191E-08	72348	1.0317	5.30465E-08	76912	0.6467	4.84596E-08	78082
1.4898	8.14391E-08	74348	1.1519	6.00938E-08	78912	0.7146	6.78819E-08	79082
1.6125	6.13295E-08	76348	1.3633	1.05669E-07	80912	0.7749	6.03539E-08	80082
1.8242	1.05861E-07	78348				0.7834	8.4612E-09	81082
1.9351	5.54644E-08	80348				0.8203	3.69216E-08	82082
2.1708	1.17866E-07	82348				0.8468	2.65374E-08	83082
2.3279	7.85404E-08	84348				0.9124	1.31092E-08	88082
2.4446	5.8363E-08	86348				0.9535	4.11522E-08	89082
2.5833	6.931E-08	88348				1.0026	4.90365E-08	90082
2.7369	7.67855E-08	90349				1.0297	2.71143E-08	91082
2.9019	8.24413E-08	92350				1.0704	4.07676E-08	92082
						1.0995	2.90373E-08	93082
						1.1133	1.38456E-08	94082
						1.1374	2.40375E-08	95082
						1.1685	3.11526E-08	96082
						1.1978	2.92296E-08	97082
						1.2212	2.34606E-08	98082
						1.2452	2.39809E-08	99082
						1.2825	3.73062E-08	100082
						1.3271	4.46136E-08	101082
						1.3629	3.57678E-08	102082
						1.434	7.1151E-08	103082
						1.5233	8.92272E-08	104082
						1.6586	6.7622E-08	106084
						2.0488	9.753E-08	110084

Specimen 2					
OLR2			OLR2		
a [mm]	dadN [m/cycle]	N [cycles]	a [mm]	dadN [m/cycle]	N [cycles]
-1.19459	xxxxx	-11000	-2.103343	xxxxx	-10114
-1.56054	-3.65947E-07	-10000	-1.706436	1.98454E-07	-8114
-1.50304	1.14995E-07	-9500	-1.280933	2.12752E-07	-6114
-1.45881	8.8458E-08	-9000	-1.176571	9.36825E-08	-5000
-1.424	6.96126E-08	-8500	-0.907927	2.68643E-07	-4000
-1.39708	5.3844E-08	-8000	-0.668514	2.39414E-07	-3000
-1.25093	2.92296E-07	-7500	-0.612968	5.55464E-08	-2000
-1.18344	1.34995E-07	-7000	-0.194964	4.18004E-07	-1000
-1.14465	7.7576E-08	-6500	0	1.94964E-07	0
-0.9412	4.06907E-07	-6000	-0.043652	-2.78571E-08	1567
-0.75563	3.71139E-07	-5500	-0.016538	5.58022E-09	6426
-0.18397	1.1433E-06	-5000	0.079035	9.55731E-10	106426
-0.59992	-8.3189E-07	-4500	0.017499	-1.02313E-09	166571
-0.50012	1.99607E-07	-4000	0.272681	3.06415E-08	174899
-0.42262	1.54994E-07	-3500	0.396302	1.23621E-07	175899
-0.3657	1.13842E-07	-3000	0.852025	2.27861E-07	177899
-0.05766	6.16073E-07	-2500	1.086959	7.83113E-08	180899
-0.25823	-4.01138E-07	-2000	1.271951	4.62481E-08	184899
-0.25285	1.07688E-08	-1500	1.628227	7.12551E-08	189899
-0.13516	2.35375E-07	-1000			
0.18557	6.41456E-07	-500			
0	-3.71139E-07	0			
0.06577	1.31533E-07	500			
0.09807	6.46128E-08	1000			
0.10788	1.96146E-08	1500			
0.11192	8.0766E-09	2000			
0.12711	1.51765E-08	3001			
0.1273	1.923E-10	4001			
0.13096	3.6537E-09	5001			
0.1273	-3.65005E-09	6002			
0.1273	0	7002			
0.12711	-9.615E-11	9002			
0.12403	-1.5384E-09	11002			
0.1273	1.63455E-09	13002			
0.12769	7.692E-11	18002			
0.1273	-7.692E-11	23002			
0.12307	-4.2306E-11	123002			
0.1273	4.2306E-11	223002			
0.12346	-4.37006E-11	311010			
0.12346	0	311154			
0.12346	0	411154			
0.13442	1.42559E-10	488042			
0.13307	-1.3461E-11	588042			
0.13365	5.769E-12	688042			
0.13423	5.769E-12	788042			
0.13538	1.1538E-11	888042			
0.13519	-1.923E-12	988042			
0.12288	-1.23072E-10	1088042			
0.12923	6.3459E-11	1188042			
0.15596	2.67297E-10	1288042			
0.08903	-6.69204E-10	1388042			
0.15499	6.59589E-10	1488042			
0.11615	-3.88446E-10	1588042			
0.11596	-1.923E-12	1688042			
0.12884	1.28841E-10	1788042			
0.12557	-3.2691E-11	1888042			
0.26903	1.14444E-08	1900577			
0.69818	1.53079E-08	1928612			
1.1616	7.37452E-08	1934896			
2.66692	1.5298E-07	1944736			
3.43664	2.45603E-07	1947870			
4.02933	3.61396E-07	1949510			
4.59857	2.70937E-07	1951611			
4.64395	3.17362E-07	1951754			
5.24571	3.00878E-07	1953754			
5.79052	2.72408E-07	1955754			

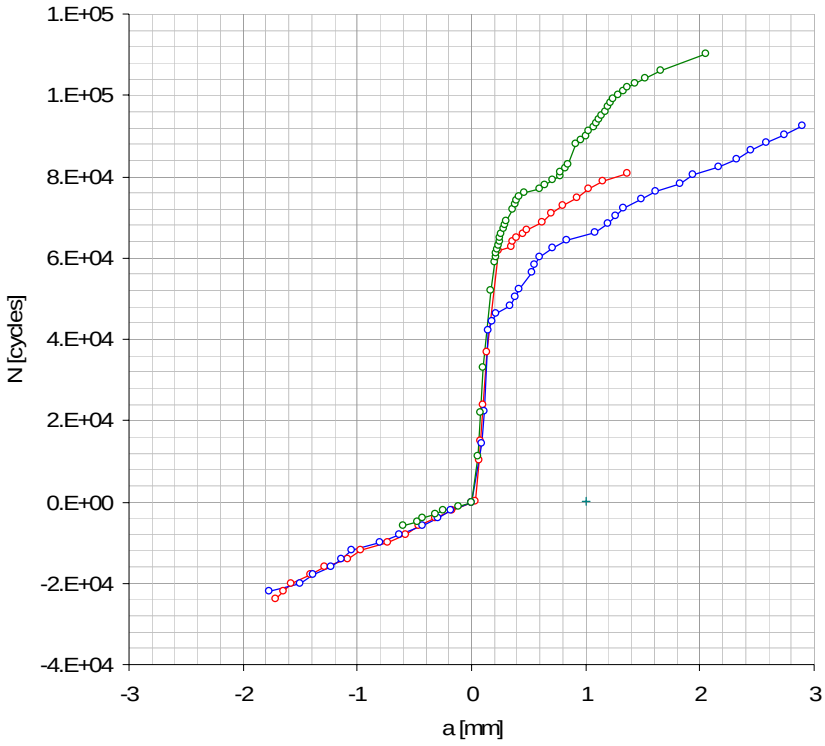
1.E+05
1.E+05
8.E+04
6.E+04
4.E+04
2.E+04
0.E+00
-2.E+04
-4.E+04
N [cycles]
-3
-2
-1
0
1
2
3
a [mm]

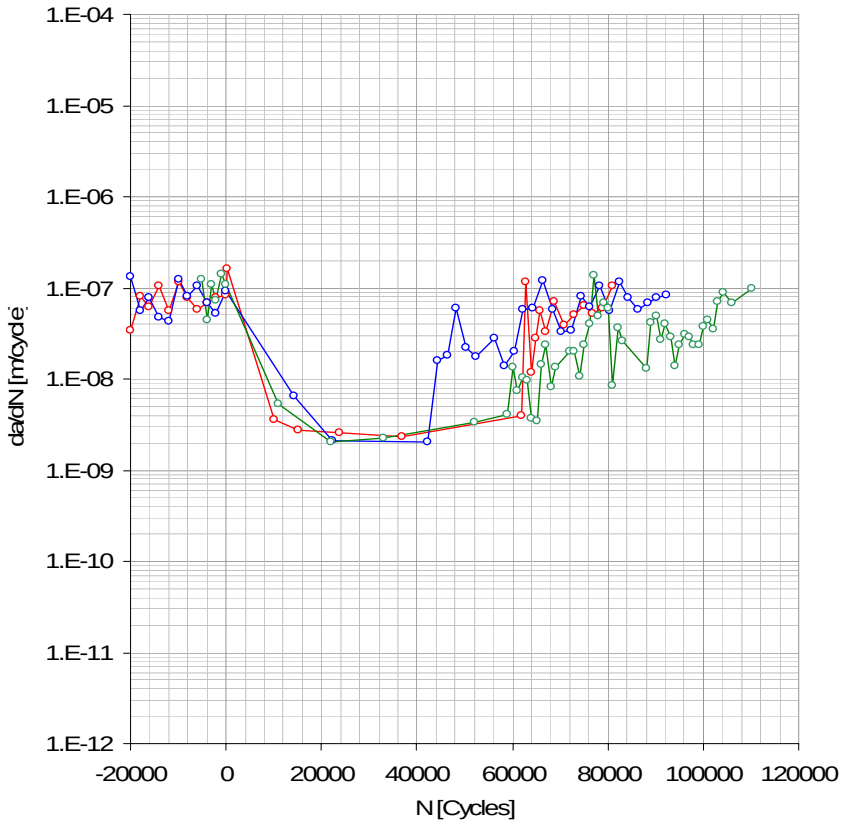
1.E-04
1.E-05
1.E-06
1.E-07
1.E-08
1.E-09
1.E-10
1.E-11
1.E-12
da/dN [m/cycle]
-20000
0
20000
40000
60000
80000
100000
120000
N [Cycles]

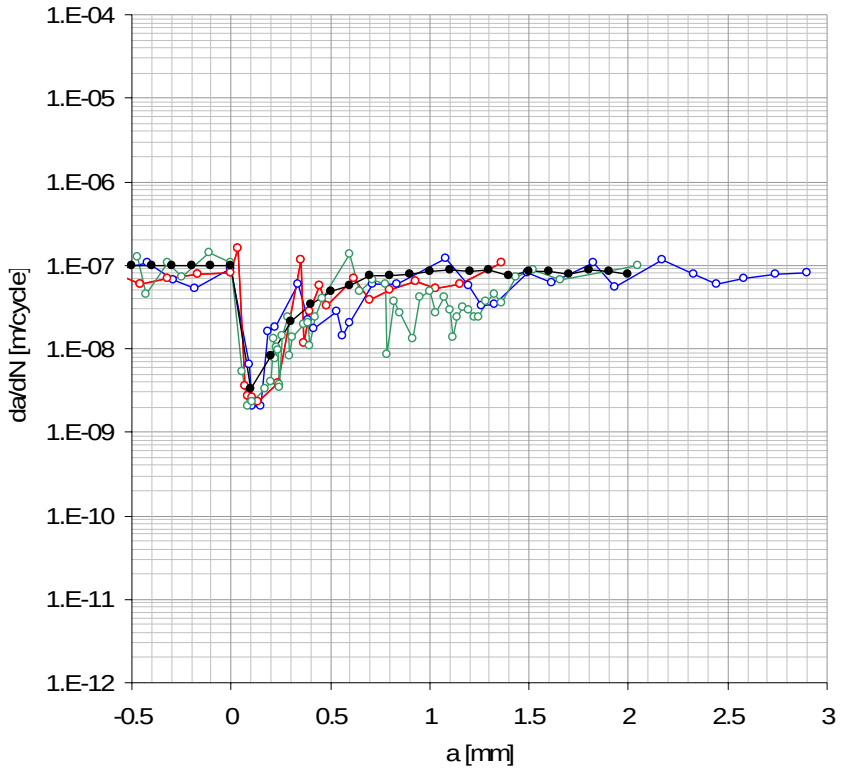
1.E-04
1.E-05
1.E-06
1.E-07
1.E-08
1.E-09
1.E-10
1.E-11
1.E-12
da/dN [m/cycle]
-0.5
0
0.5
1
1.5
2
2.5
3
a [mm]

Block loading – R=0.1,0.7-0.1

Material – al.2324-T39

$\Delta K=4$ Mpam$^{0.5}$ (starts from the notch)

0.1 - 0.7 - 0.1 (arrest)		
a [mm]	dadN	N [cycles]
-3.96	XXXXXX	0
-3.89	1.94E-09	33496
-3.86	1.19E-09	60992
-3.83	1.46E-09	83694
-3.62	4.02E-09	133694
-3.50	2.48E-09	183694
-3.45	1.04E-09	233694
-3.41	7.94E-10	283694
-3.37	7.46E-10	333694
-3.30	7.30E-10	433694
-3.22	1.54E-09	483694
-3.12	9.81E-10	583694
-3.06	4.33E-10	733694
-3.04	1.80E-10	833694
-2.90	2.66E-09	884884
-2.82	1.75E-09	934884
-2.64	3.53E-09	984884
-2.41	2.35E-09	1084884
-2.21	3.96E-09	1134884
-1.98	4.57E-09	1184884
-1.83	3.04E-09	1234884
-1.64	3.78E-09	1284884
-1.49	2.92E-09	1334884
-1.38	2.27E-09	1384885
-1.21	3.30E-09	1434886
-1.03	3.70E-09	1484886
-0.83	3.94E-09	1534886
-0.68	2.95E-09	1584887
-0.52	3.19E-09	1634887
-0.35	3.39E-09	1684888
-0.18	3.55E-09	1734888
0.00	3.53E-09	1784888
0.06	7.27E-08	1785732
0.25	4.80E-08	1789588
0.31	1.73E-08	1793350
0.42	2.56E-08	1797562
0.51	1.26E-08	1804858
0.64	1.29E-08	1814744
0.72	1.72E-08	1819217
0.83	1.85E-08	1825543
0.94	2.00E-08	1830633
1.25	2.00E-08	1846446
1.54	1.13E-08	1872334
1.82	1.79E-08	1887644
2.43	3.73E-08	1904048
2.69	1.92E-08	1917666
2.92	1.38E-08	1934175
3.23	1.91E-08	1950428
3.49	2.07E-08	1963250
3.51	1.00E-11	4214352

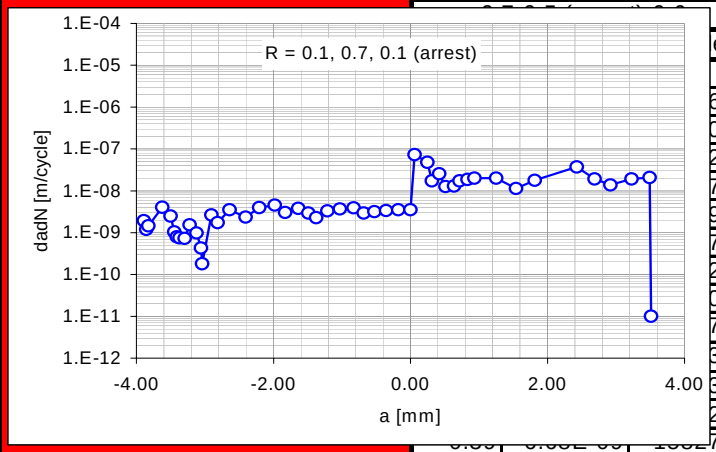

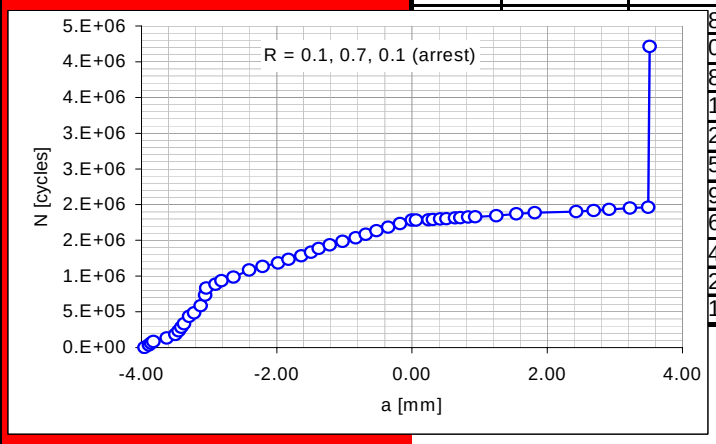

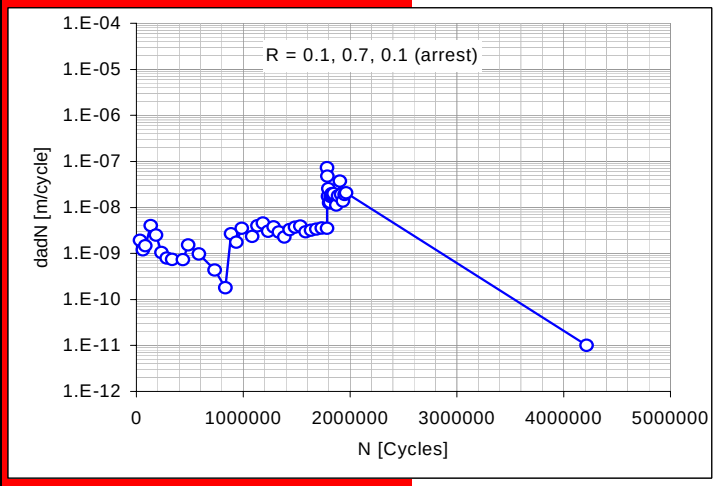

Block loading – R=0.7-0.6

Material – al.2324-T39

ΔK=4 Mpam$^{0.5}$

0.7-0.5 (arrest)-0.6			0.7-0.6			0.7-0.6		
a [mm]	dadN	N [cycles]	a [mm]	dadN	N [cycles]	a [mm]	dadN	N [cycles]
-2.22	XXXXXX	0	-0.351	XXXXXX	-35001	-0.29095	XXXXXX	-30000
-2.03	1.30E-08	14656	-0.255	9.65E-09	-25001	-0.247298	8.73E-09	-25000
-1.79	1.38E-08	32066	-0.178	1.54E-08	-20001	-0.191146	1.12E-08	-20000
-1.65	1.92E-08	39263	-0.134	8.81E-09	-15001	-0.169609	4.31E-09	-15000
-1.45	1.77E-08	50732	-0.066	1.37E-08	-10001	-0.105765	1.28E-08	-10000
-0.95	2.12E-08	73977	-0.020	9.18E-09	-5001	-0.04846	1.15E-08	-5000
-0.78	1.29E-08	87717	0.000	3.92E-09	0	0	9.69E-09	0
-0.23	1.57E-08	122298	0.015	9.44E-10	15881	0.013844	3.43E-08	404
-0.04	1.45E-08	136065	0.020	5.38E-10	25881	0.01769	3.50E-10	11404
0.00	2.64E-11	1467714	0.066	2.27E-09	45881	0.021344	1.07E-10	45404
0.04	6.50E-10	1526308	0.152	8.58E-09	55881	0.026578	1.14E-10	91406
0.08	4.23E-09	1536347	0.253	1.02E-08	65881	0.061577	1.75E-08	93406
0.32	6.64E-09	1572290	0.351	9.79E-09	75881	0.078692	8.56E-09	95406
0.39	6.68E-09	1582764	0.527	1.75E-08	85881	0.096191	8.75E-09	97406
0.48	1.02E-08	1591820				0.174649	1.31E-08	103406
0.65	1.54E-08	1603022				0.195995	1.07E-08	105406
0.95	9.79E-09	1632864				0.220994	1.25E-08	107406
1.33	6.95E-09	1688134				0.240031	9.52E-09	109406
2.19	1.36E-08	1751292				0.306154	1.65E-08	113406
2.31	8.58E-09	1765551				0.330192	1.20E-08	115406
2.45	1.13E-08	1777912				0.349614	9.71E-09	117406
2.60	1.33E-08	1788644				0.419034	1.16E-08	123408
2.70	9.58E-09	1799458				0.487109	1.70E-08	127408
2.83	1.10E-08	1811218				0.516338	1.46E-08	129408
3.03	1.72E-08	1823110				0.55977	2.17E-08	131408

0.7-0.6			0.7-0.6			0.7-0.6		
a [mm]	dadN	N [cycles]	a [mm]	dadN	N [cycles]	a [mm]	dadN	N [cycles]
-0.216	XXXXXX	-12372	-0.222	XXXXXX	-17000	-0.298614	XXXXXX	-20512
-0.180	1.79E-08	-10372	-0.193	1.12E-08	-14400	-0.247462	1.28E-08	-16512
-0.150	1.49E-08	-8372	-0.153	2E-08	-12400	-0.217078	1.52E-08	-14512
-0.122	1.44E-08	-6372	-0.105	1.14E-08	-8200	-0.174772	1.28E-08	-11200
-0.091	1.54E-08	-4372	-0.073	1.23E-08	-5600	-0.154	1.3E-08	-9600
-0.056	1.73E-08	-2372	-0.040	9.71E-09	-2200	-0.127274	1.27E-08	-7500
-0.017	1.94E-08	-371	-0.004	1.89E-08	-300	-0.085	1.41E-08	-4512
0.000	4.66E-08	0	0.000	1.33E-08	0	-0.047306	1.88E-08	-2512
0.002	7.69E-10	2000	0.010	1.94E-09	5001	-0.024	1.17E-08	-512
0.006	8.24E-11	58000	0.035	9.28E-10	32196	0	4.69E-08	0
0.098	4.59E-08	60000	0.063	1.41E-09	52197	0.012115	2.02E-10	60004
0.122	1.22E-08	62000	0.121	3.43E-09	69198	0.047883	1.79E-08	62004
0.172	1.24E-08	66000	0.292	1.14E-08	84198	0.084997	1.86E-08	64004
0.206	1.72E-08	68000	0.371	1.57E-08	89198	0.098265	6.63E-09	66004
0.222	7.88E-09	70000	0.541	1.7E-08	99198	0.109611	5.67E-09	68004
0.264	1.05E-08	74000	0.581	7.96E-09	104198	0.136918	6.83E-09	72004
0.305	2.04E-08	76000				0.159994	5.77E-09	76004
0.348	2.18E-08	78000				0.173262	6.63E-09	78004
0.368	1.00E-08	80000				0.194223	1.05E-08	80004
						0.2465	8.71E-09	86006
						0.271307	1.24E-08	88006
						0.292268	1.05E-08	90006

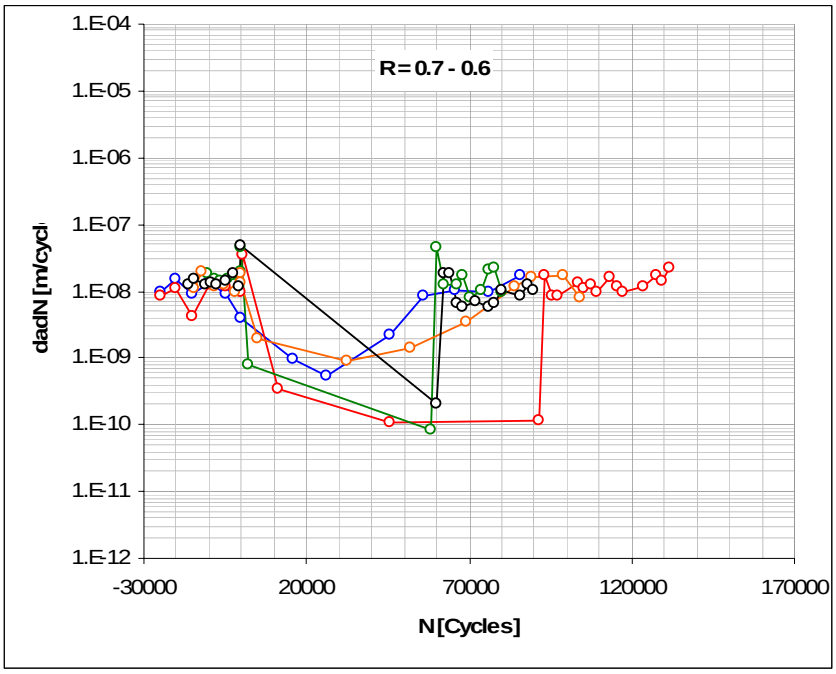

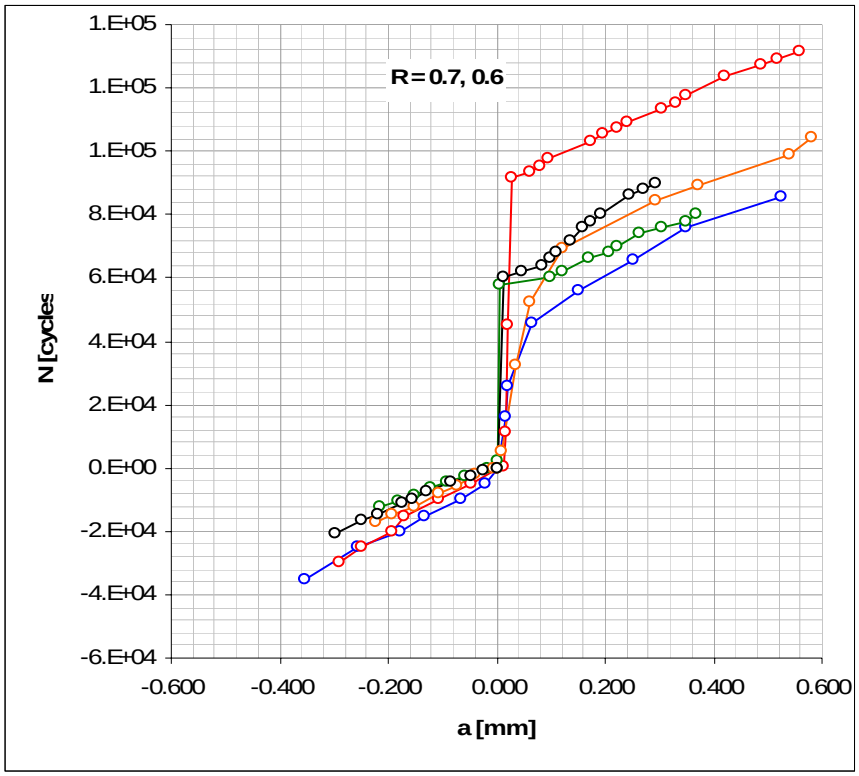
R=0.7, 0.6
N [cycles]
a [mm]
1.E+05
1.E+05
1.E+05
8.E+04
6.E+04
4.E+04
2.E+04
0.E+00
-2.E+04
-4.E+04
-6.E+04
-0.600
-0.400
-0.200
0.000
0.200
0.400
0.600

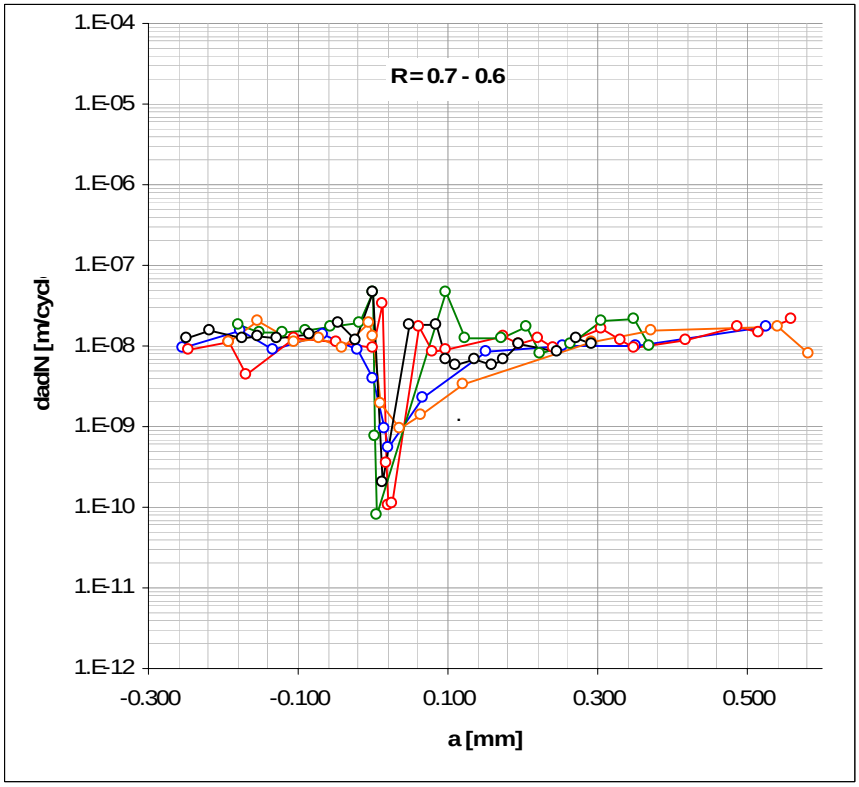
R=0.7 - 0.6
dadN [m/cycl
a [mm]
1.E-04
1.E-05
1.E-06
1.E-07
1.E-08
1.E-09
1.E-10
1.E-11
1.E-12
-0.300
-0.100
0.100
0.300
0.500

Block loading – R=0.6-0.7

Material – al.2324-T39

ΔK=4 Mpam$^{0.5}$

0.6 - 0.7		
a [mm]	dadN	N [cycles]
-0.3732543	XXXXXX	-40602
-0.2874885	8.577E-09	-30602
-0.1857618	1.017E-08	-20602
-0.0878811	9.788E-09	-10602
0	8.289E-09	0
0.0907373	1.815E-08	5000
0.156	1.305E-08	10001
0.1878488	6.37E-09	15001
0.2795129	1.833E-08	20001
0.3729707	1.869E-08	25001

0.6 - 0.7		
a [mm]	dadN	N [cycles]
-0.3828127	XXXXXX	-28240
-0.3614674	1.067E-08	-26240
-0.3364684	1.25E-08	-24240
-0.3174307	9.519E-09	-22240
-0.2513078	1.653E-08	-18240
-0.2272703	1.202E-08	-16240
-0.207848	9.711E-09	-14240
-0.1922717	7.784E-09	-12239
-0.1384277	1.346E-08	-8238
-0.0749687	3.173E-08	-6238
-0.0411239	8.461E-09	-2238
0	1.838E-08	0
0.061536	3.077E-08	2000
0.0973038	1.788E-08	4000
0.1271103	1.49E-08	6000
0.1559553	1.442E-08	8000
0.1867233	1.538E-08	10000
0.2213373	1.731E-08	12000
0.2601536	1.94E-08	14001

0.6 - 0.7		
a [mm]	dadN	N [cycles]
-0.2805091	XXXXXX	-20492
-0.256087	1.221E-08	-18492
-0.2428183	6.634E-09	-16492
-0.2064736	1.817E-08	-14492
-0.1720519	1.721E-08	-12492
-0.1562833	7.884E-09	-10492
-0.1486479	3.818E-09	-8492
-0.1144185	1.711E-08	-6492
-0.0736509	2.038E-08	-4492
-0.0299988	2.183E-08	-2492
-0.0099996	1E-08	-492
0	2.032E-08	0
0.0128841	6.442E-09	2000
0.0451905	1.615E-08	4000
0.0678819	1.135E-08	6000
0.0890349	1.058E-08	8000
0.1771083	1.468E-08	14000
0.2690277	4.596E-08	16000
0.3051801	1.808E-08	18000
0.3826204	2.151E-08	21600

0.6 - 0.7		
a [mm]	dadN	N [cycles]
-0.259605	XXXXXX	-35450
-0.2232603	7.269E-09	-30450
-0.172	1.025E-08	-25450
-0.142	6E-09	-20450
-0.1224951	3.901E-09	-15450
-0.027	8.565E-09	-4300
0	6.279E-09	0
0.0514798	1.03E-08	5000
0.150322	1.977E-08	10000
0.2493565	1.981E-08	15000
0.3245458	1.504E-08	20000

0.6 - 0.7		
a [mm]	dadN	N [cycles]
-0.236	XXXXXX	-32058
-0.222	7E-09	-30058
-0.1994	1.13E-08	-28058
-0.1862	6.6E-09	-26058
-0.1748	5.7E-09	-24058
-0.1546	1.01E-08	-22058
-0.1475	3.55E-09	-20058
-0.1319	7.8E-09	-18058
-0.1243	3.8E-09	-16058
-0.1111	6.6E-09	-14058
-0.0899	5.3E-09	-10058
-0.0725	8.696E-09	-8057
-0.0379	1.729E-08	-6056
0	6.258E-09	0
0.082	1.64E-08	5000
0.1295	9.5E-09	10000
0.1739	8.88E-09	15000
0.2235	9.918E-09	20001

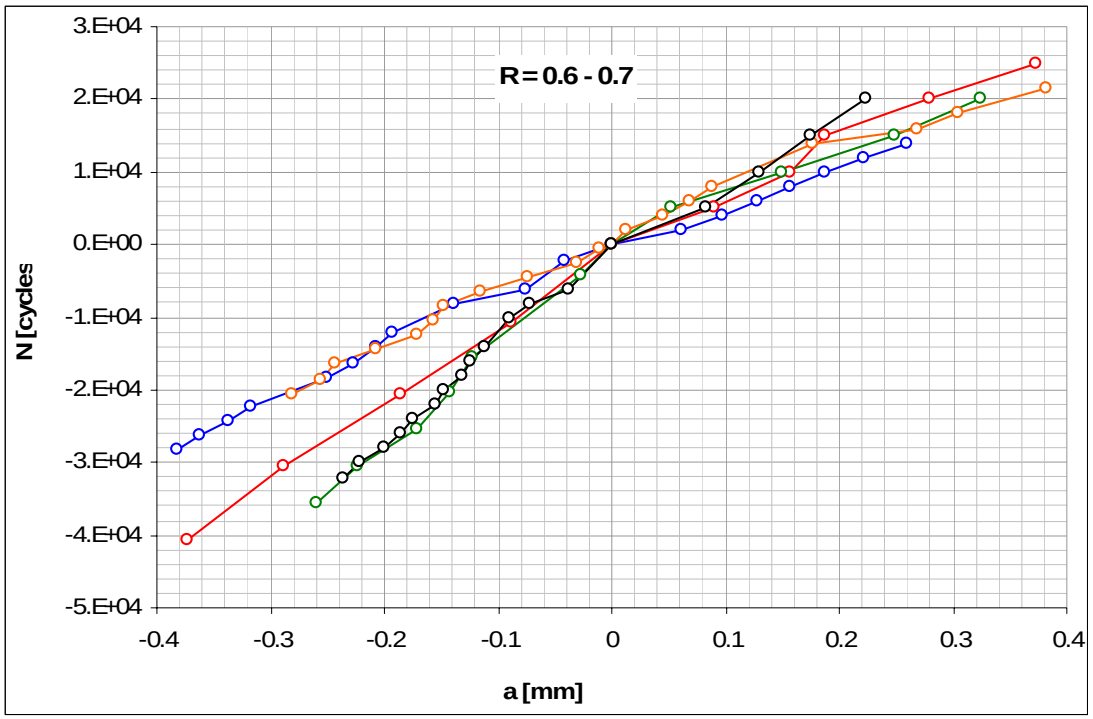
R = 0.6 - 0.7
N [cycles
3.E+04
2.E+04
1.E+04
0.E+00
-1.E+04
-2.E+04
-3.E+04
-4.E+04
-5.E+04
-0.4
-0.3
-0.2
-0.1
0
0.1
0.2
0.3
0.4
a [mm]

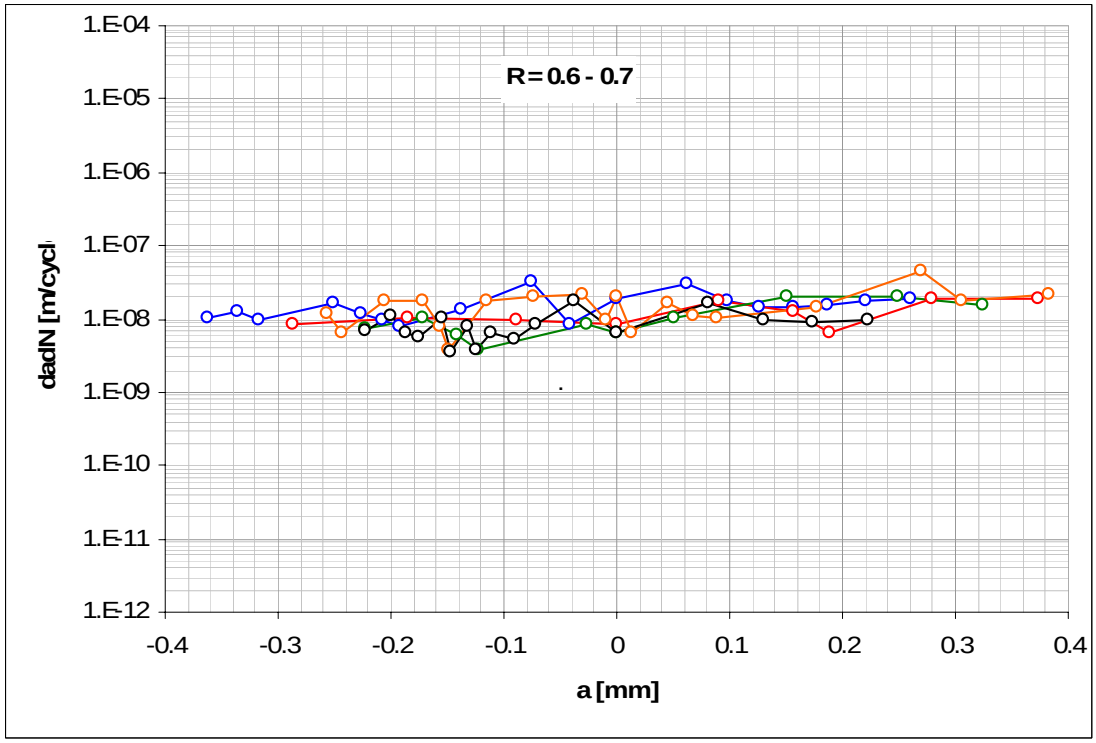
R = 0.6 - 0.7
dadN [m/cycl
1.E-04
1.E-05
1.E-06
1.E-07
1.E-08
1.E-09
1.E-10
1.E-11
1.E-12
-0.4
-0.3
-0.2
-0.1
0
0.1
0.2
0.3
0.4
a [mm]

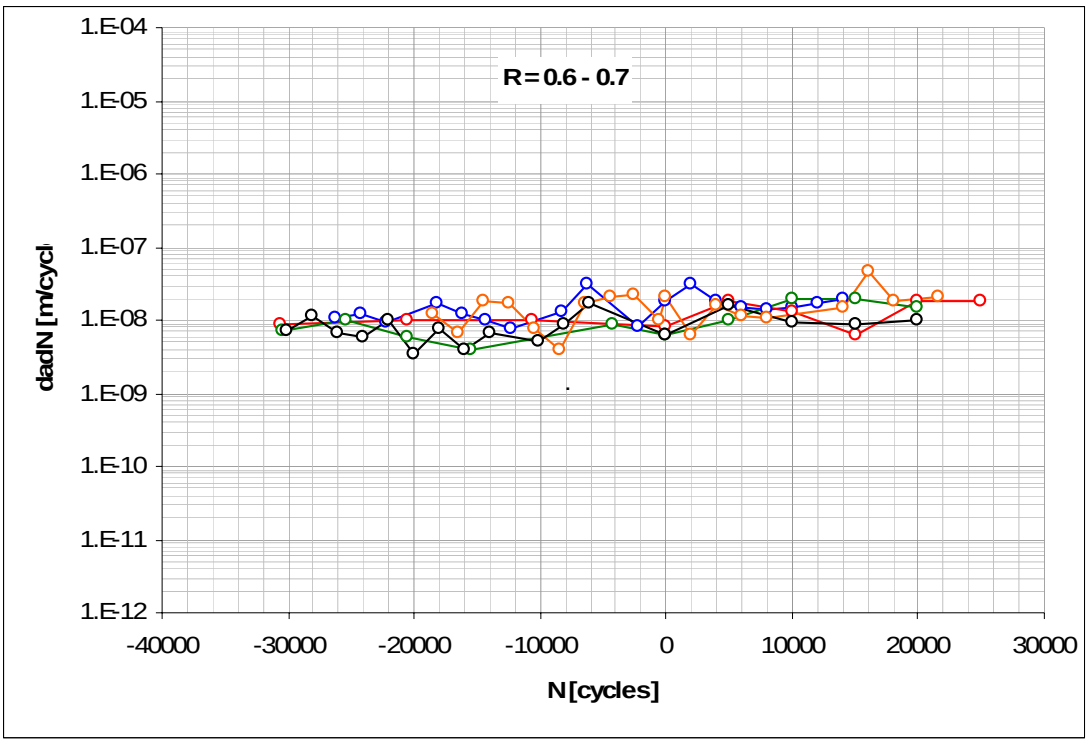
R = 0.6 - 0.7
1.E-04
1.E-05
1.E-06
1.E-07
1.E-08
1.E-09
1.E-10
1.E-11
1.E-12
dadN [m/cycl
-40000
-30000
-20000
-10000
0
10000
20000
30000
N [cycles]

Block loading – R=0.6-0.5

Material – al.2324-T39

ΔK=4 Mpam$^{0.5}$

0.6 - 0.5		
a [mm]	dadN	N [cycles]
-0.72005	XXXXXX	-57559
-0.580113	1.13E-08	-45198
-0.437234	1.33E-08	-34466
-0.333584	9.58E-09	-23652
-0.204358	1.1E-08	-11892
0	1.72E-08	0
0.012115	7.59E-09	1596
0.337679	3.63E-09	91212
0.376523	8.65E-09	95704
0.434762	5.75E-09	105826
0.486298	7.56E-09	112644
0.536681	7.05E-09	119792
0.590304	6.55E-09	127978
0.738375	5.62E-09	154327

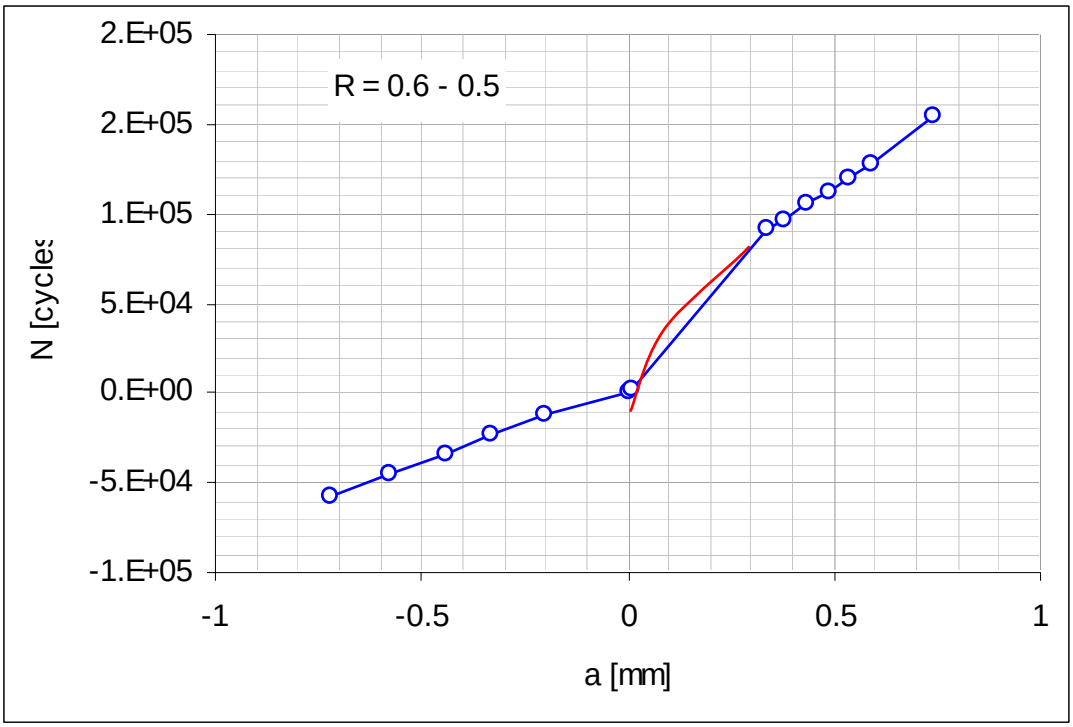

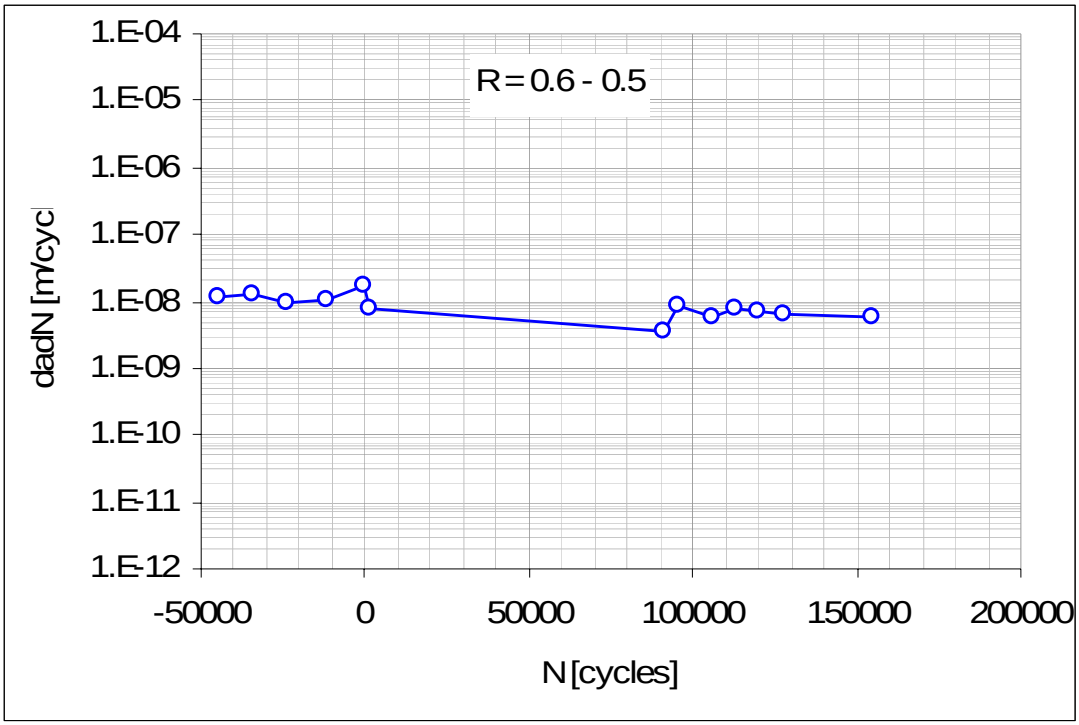
R = 0.6 - 0.5
dadN [m/cyc]
1.E-04
1.E-05
1.E-06
1.E-07
1.E-08
1.E-09
1.E-10
1.E-11
1.E-12
-50000
0
50000
100000
150000
200000
N [cycles]

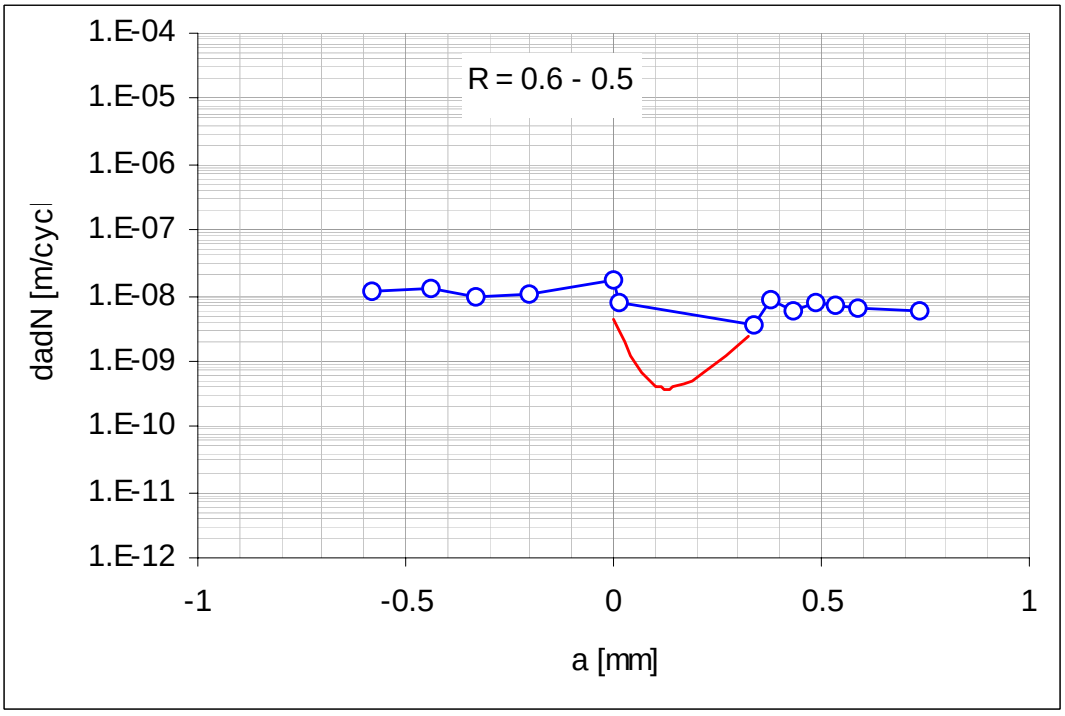
R = 0.6 - 0.5
dadN [m/cyc]
1.E-04
1.E-05
1.E-06
1.E-07
1.E-08
1.E-09
1.E-10
1.E-11
1.E-12
-1
-0.5
0
0.5
1
a [mm]

Block loading – R=0.5-0.7

Material – al.2324-T39
ΔK=4 Mpam$^{0.5}$

0.5 - 0.7		
a [mm]	dadN	N [cycles]
-0.400697	XXXXXX	-63115
-0.361852	8.65E-09	-58623
-0.303613	5.75E-09	-48501
-0.252077	7.56E-09	-41683
-0.201694	7.05E-09	-34535
-0.148071	6.55E-09	-26349
0	5.62E-09	0
0.017708	5.26E-09	3367
0.074821	7.9E-09	10597
0.171327	9.65E-09	20597
0.248247	1.54E-08	25597
0.292284	8.81E-09	30597
0.360743	1.37E-08	35597
0.406646	9.18E-09	40597

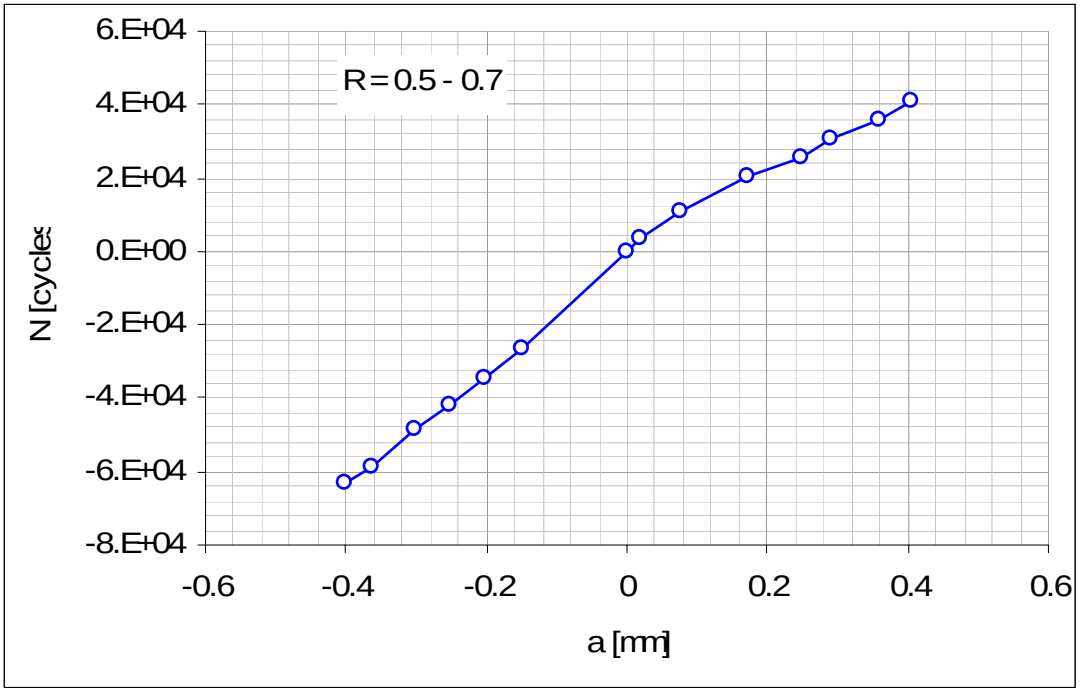

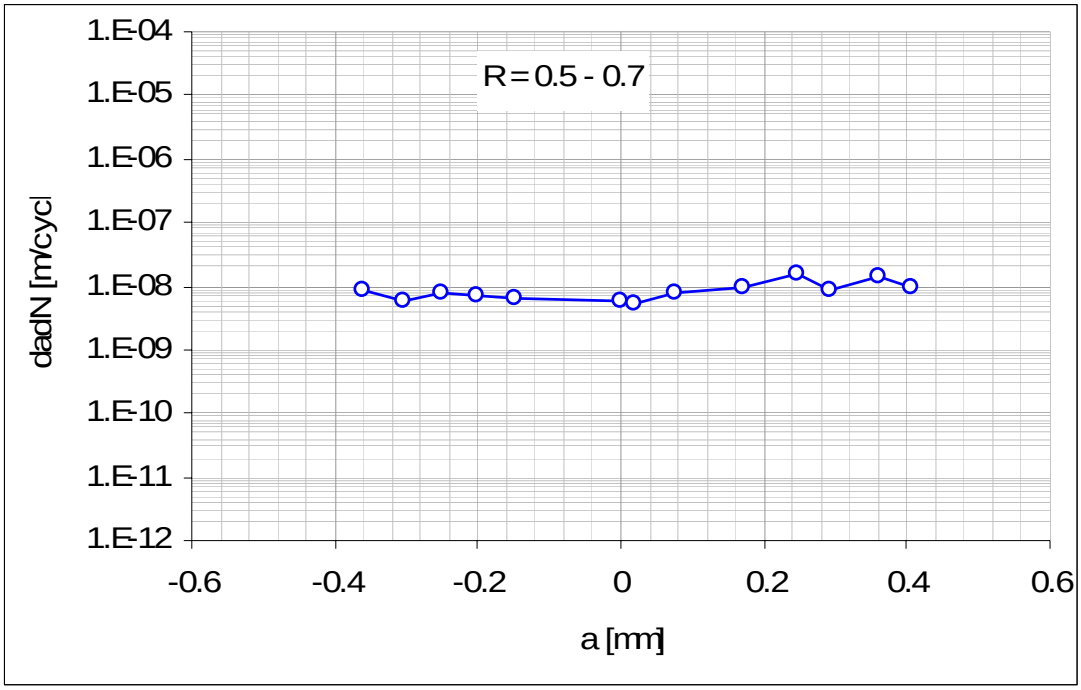
R = 0.5 - 0.7
1.E-04
1.E-05
1.E-06
1.E-07
1.E-08
1.E-09
1.E-10
1.E-11
1.E-12
dadN [m/cyc]
-0.6
-0.4
-0.2
0
0.2
0.4
0.6
a [mm]

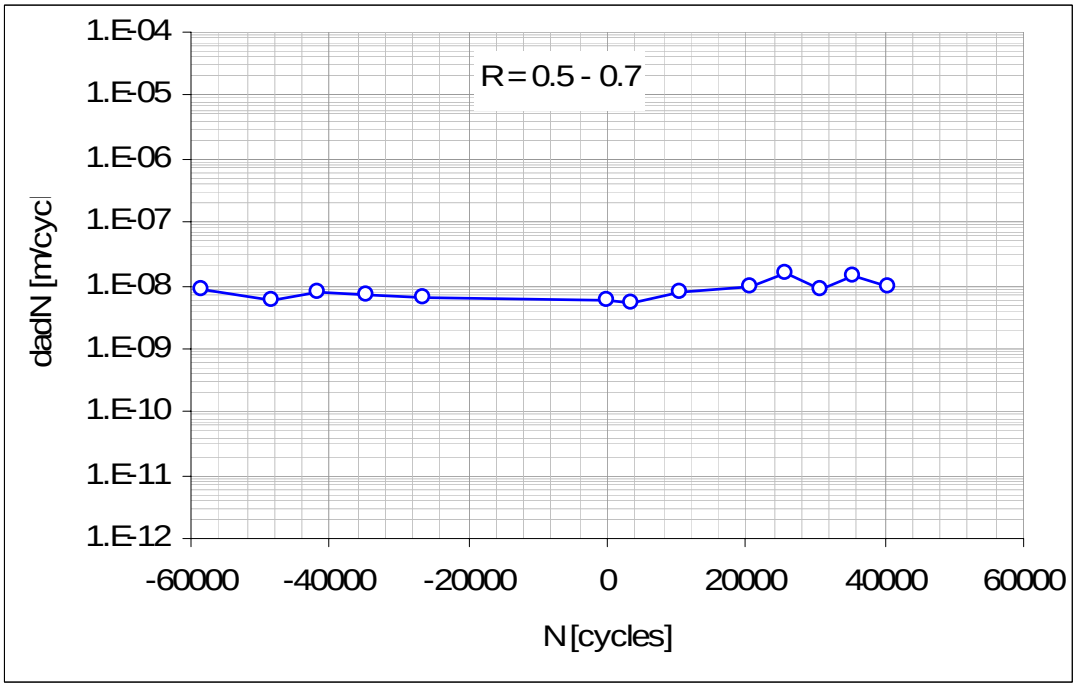
R = 0.5 - 0.7
1.E-04
1.E-05
1.E-06
1.E-07
1.E-08
1.E-09
1.E-10
1.E-11
1.E-12
dadN [m/cyc]
-60000
-40000
-20000
0
20000
40000
60000
N [cycles]

Block loading – R=0.7-0.8

Material – al.2324-T39

ΔK=4 Mpam$^{0.5}$

0.7 - 0.8		
a [mm]	dadN	N [cycles]
-0.192	XXXXXX	-22001
-0.176	8E-09	-20001
-0.129	9.4E-09	-15001
-0.094006	7E-09	-10001
-0.049585	8.88E-09	-5001
0	9.92E-09	0
0.080975	1.6E-08	5069
0.182701	2.03E-08	10069
0.279044	1.93E-08	15069
0.378599	1.99E-08	20069

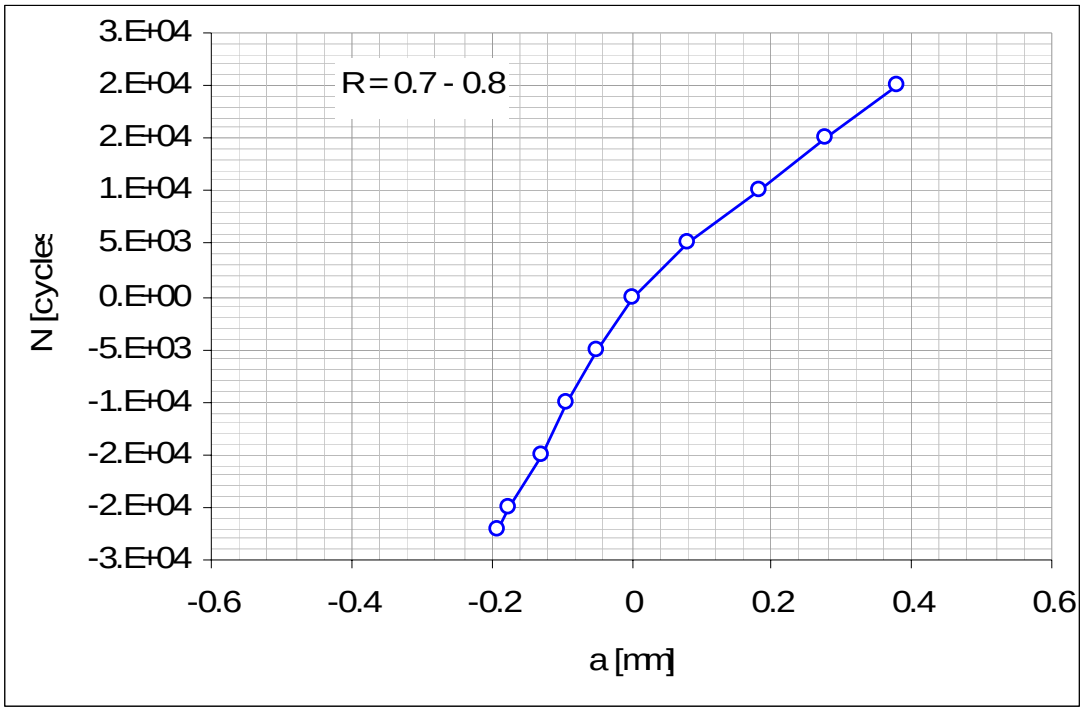

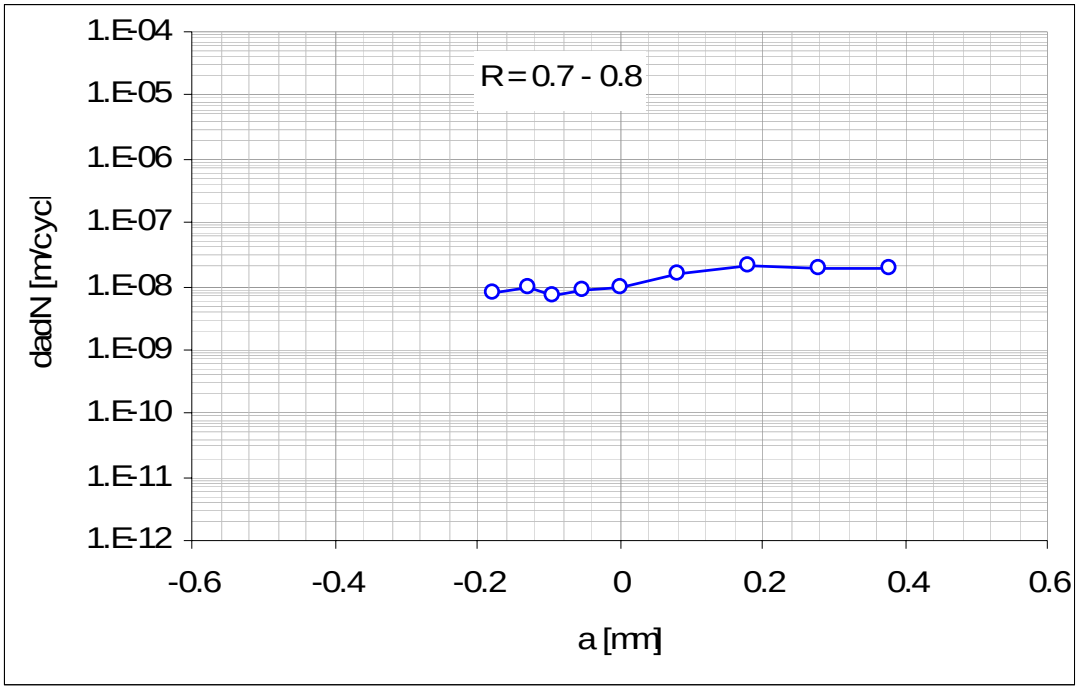
R = 0.7 - 0.8
dadN [m/cyc]
1.E-04
1.E-05
1.E-06
1.E-07
1.E-08
1.E-09
1.E-10
1.E-11
1.E-12
-0.6
-0.4
-0.2
0
0.2
0.4
0.6
a [mm]

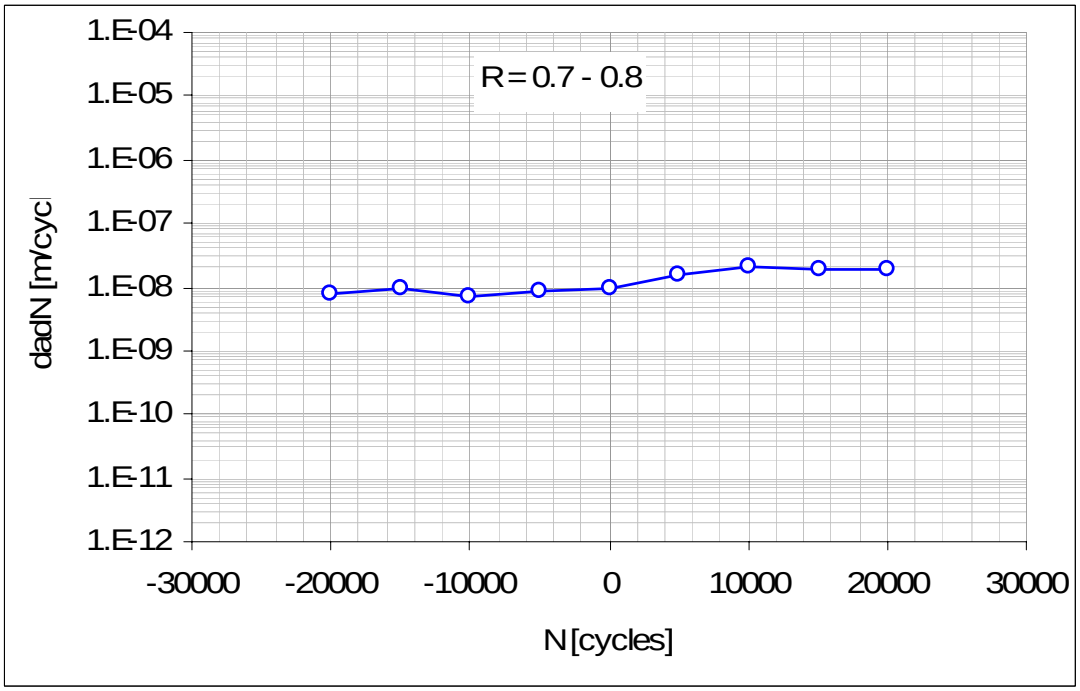
R = 0.7 - 0.8
dadN [m/cyc]
1.E-04
1.E-05
1.E-06
1.E-07
1.E-08
1.E-09
1.E-10
1.E-11
1.E-12
-30000
-20000
-10000
0
10000
20000
30000
N [cycles]

Constant R loading – al. 7475-T7351

Precracked under compression

	7475									
	R=0.1				R=0.9					
	Thin		Thick						Thin	
	Summer						Winter			
	dadn [m/cycle]	□□ [MPam0.5]	dadn [m/cycle]	□□ [MPam0.5]	dadn [m/cycle]	□□ [MPam0.5]	dadn [m/cycle]	□□ [MPam0.5]	dadn [m/cycle]	□□ [MPam0.5]
0										
1	1.31618E-11	0.883	3.21724E-09	3.829	1.18219E-11	0.963	4.5801E-11	1.052	[illegible]2E-24	1.077
2	1.157E-10	1.079	5.55318E-09	4.580	5E-11	1.041	3.01694E-11	[illegible]	[illegible]62E-24	1.218
3	6.87419E-11	1.279	5.19379E-09	4.754	3.5E-10	1.057	6.9353[illegible]	1.174	0	1.386
4	5.55191E-11	2.241	5.226E-09	4.909	3E-10	1.069	4[illegible]11	1.297	3.33506E-10	1.428
5	1.1972E-11	2.441	6.24102E-09	5.066	3E-10	1.080	0	1.302	5.16797E-10	1.526
6	8.47619E-12	2.675	7.37789E-09	5.239	1E-10	1.088	9.06821E-11	1.312	7.00376E-10	1.635
7	2.09799E-11	2.677	7.11958E-09	5.409	1.8E-10	1.098	2.48403E-10	1.405	7.24308E-10	1.736
8	2.11905E-11	2.944	1.40908E-08	5.636	2E-10	1.115	2.13223E-10	1.452	9.9457E-10	1.841
9	2.11905E-11	3.467	1.95436E-08	5.965	3.4E-10	1.138	6.33604E-10	1.522	1.0478E-09	1.947
10	8.09476E-11	3.949	3.39832E-08	6.273	3E-10	1.165	5.27044E-10	1.604	1.77196E-09	2.067
11	2.97514E-09	4.521	4.40381E-08	6.441	1.6E-10	1.184	7.21311E-10	1.685	2.23E-09	2.203
12	1.06825E-08	5.516	4.69475E-08	6.527	6.2E-10	1.215	1.31706E-09	1.776	2.56526E-09	2.310
13	1.39373E-08	6.163	3.57187E-08	6.607	3E-10	1.250	1.05077E-09	1.834	3.24141E-09	2.373
14	2.01966E-08	6.616	4.76532E-08	6.689	5E-10	1.268	1.4755E-09	1.875	3.00194E-09	2.413
15	3.29281E-08	7.006	5.73075E-08	6.794	7.5E-10	1.286	1.57022E-09	1.911	3.17754E-09	2.453
16	6.21432E-08	7.410	5.38196E-08	6.908	4E-10	1.299	1.3283E-09	1.936	2.9455E-09	2.494
17	8.62071E-08	7.752	6.58261E-08	7.035	6.5E-10	1.311	1.08742E-09	1.963	4.35275E-09	2.543
18	9.55225E-08	7.954	6.90068E-08	7.184	6E-10	1.327	2.14692E-09	1.998	4.73421E-09	2.609
19	1.16951E-07	8.208	7.59594E-08	7.352	4.5E-10	1.341	1.88197E-09	2.039	7.21196E-09	2.689
20	9.32074E-08	8.483	9.76076E-08	7.564	1.15E-09	1.362	2.10922E-09	2.078	9.12119E-09	2.776
21	1.21747E-07	8.754	9.46197E-08	7.815	9.05492E-10	1.387	2.27679E-09	2.119	7.83509E-09	2.853
22	1.27175E-07	8.980	1.11112E-07	8.103	7.44508E-10	1.407	2.44749E-09	2.161	8.60592E-09	2.912
23	1.24219E-07	9.141	1.35886E-07	8.482	1.5E-09	1.433	3.0172E-09	2.208	1.16016E-08	2.963
24	1.30088E-07	9.310	1.67762E-07	8.910	1.35226E-09	1.465	2.18148E-09	2.250	1.6261E-08	3.010
25	1.33172E-07	9.493	1.87731E-07	9.304	2.04774E-09	1.501	3.04723E-09	2.291	1.12925E-08	3.046
26	1.54415E-07	9.700	2.25017E-07	9.725	1.2086E-09	1.534	3.13591E-09	2.338	9E-09	3.080
27	1.32833E-07	9.917	2.85855E-07	10.305	1.5414E-09	1.560	2.94775E-09	2.384	1.44063E-08	3.145
28	1.44742E-07	10.135	3.30868E-07	10.748	2.85E-09	1.600	4.32282E-09	2.437	1.00083E-08	3.215
29	1.84082E-07	10.405	4.10777E-07	10.880	2.2E-09	1.644	3.87491E-09	2.483	1.72092E-08	3.266
30	2.32083E-07	10.766	4.17347E-07	10.970	2.50154E-09	1.672	2.93517E-09	2.508	1.53015E-08	3.328
31	2.2339E-07	11.187	4.17876E-07	11.051	2.48734E-09	1.691	5.28808E-09	2.538	1.93214E-08	3.384
32	2.77405E-07	11.685	3.56E-07	11.136	2.71112E-09	1.711	5.71254E-09	2.580	1.93404E-08	3.437
33	2.21154E-07	12.223	2.84618E-07	11.244	2E-09	1.725	6.51549E-09	2.626	3.26168E-08	3.511
34	3.31483E-07	12.876	3.49982E-07	11.405	2.6E-09	1.733	7.33793E-09	2.681	6.73961E-09	3.568
35	3.59687E-07	13.544	4.04865E-07	11.635	3E-09	1.743	9.43668E-09	2.730	2.20927E-08	3.611
36	4.61698E-07	14.134	2.95268E-07	11.856	2.8E-09	1.753	8.56669E-09	2.756	1.37737E-08	3.656
37	4.21118E-07	14.659	4.04484E-07	12.086	1.8E-09	1.761	9.87703E-09	2.776	1.47912E-08	3.678
38	5.49003E-07	15.063	4.895E-07	12.394	3.2E-09	1.770	8.09432E-09	2.799	2.89438E-08	3.713
39	6.20118E-07	15.584	4.80558E-07	12.746	2.2E-09	1.779	1.05566E-08	2.824	2.46819E-08	3.756
40	6.73349E-07	16.205	5.69854E-07	13.151	2E-09	1.786	9.68147E-09	2.851	2.72913E-08	3.798
41	7.57221E-07	16.958	6.51734E-07	13.656	1.8E-09	1.793	1.15713E-08	2.880	2.3657E-08	3.841
42	8.26535E-07	17.880	6.80066E-07	14.250	3.2E-09	1.801	9.9515E-09	2.910	2.79656E-08	3.885
43	1.41095E-06	18.876	7.58111E-07	14.950	2.2E-09	1.810	1.13572E-08	2.940	4.88191E-08	3.952
44	7.55059E-07	19.649	9.12335E-07	15.849	3E-09	1.819	1.36891E-08	2.977	4.83219E-09	4.001
45	6.82291E-07	20.468	1.36115E-06	17.240	2.7E-09	1.832	1.28047E-08	3.016	4.6146E-08	4.048
46	1.07571E-06	21.494	1.03503E-06	18.559	2.1E-09	1.848	1.41359E-08	3.058	3.17465E-08	4.121
47	1.53161E-06	22.700	1.25545E-06	19.447	3.7E-09	1.866	1.85707E-08	3.110	3.34019E-08	4.185
48	1.17336E-06	24.085	1.57481E-06	20.785	3.4E-09	1.888	1.85904E-08	3.172	3.62453E-08	4.293
49	1.84082E-06	25.153	2.57648E-06	22.418	4.2E-09	1.911	2.221E-08	3.242	4.45218E-08	4.419
50	1.30872E-06	25.901	4.20539E-06	24.615	2.7E-09	1.932	2.48003E-08	3.328	6.06347E-08	4.538
51	2.31909E-06	26.809	4.70929E-05	33.097	2.8E-09	1.952	2.59399E-08	3.426	6.09243E-08	4.685
52	2.93297E-06	28.217			4.82367E-09	1.986	3.55848E-08	3.503	5.20721E-06	8.319
53	7.01458E-06	31.217			5.62268E-09	2.025	3.48967E-08	3.553		
54					4.48362E-09	2.048	4.00157E-08	3.607		
55					5.4E-09	2.063	4.10166E-08	3.668		
56					4.6E-09	2.078	4.14011E-08	3.732		
57					4.83422E-09	2.100	5.21776E-08	3.808		
58					4.36578E-09	2.129	5.24614E-08	3.897		
59					6.1E-09	2.162	5.03288E-08	3.988		
60					9.31891E-09	2.197	5.83805E-08	4.062		
61					6.08109E-09	2.223	6.49841E-08	4.121		
62					7.2E-09	2.245	6.15415E-08	4.184		
63					6.2E-09	2.268	7.75128E-08	4.255		
64					9.2E-09	2.296	6.49204E-08	4.331		
65					6.6E-09	2.324	7.09915E-08	4.406		
66					9E-09	2.354	7.97974E-08	4.492		
67					6.6E-09	2.383				

BAD DATA

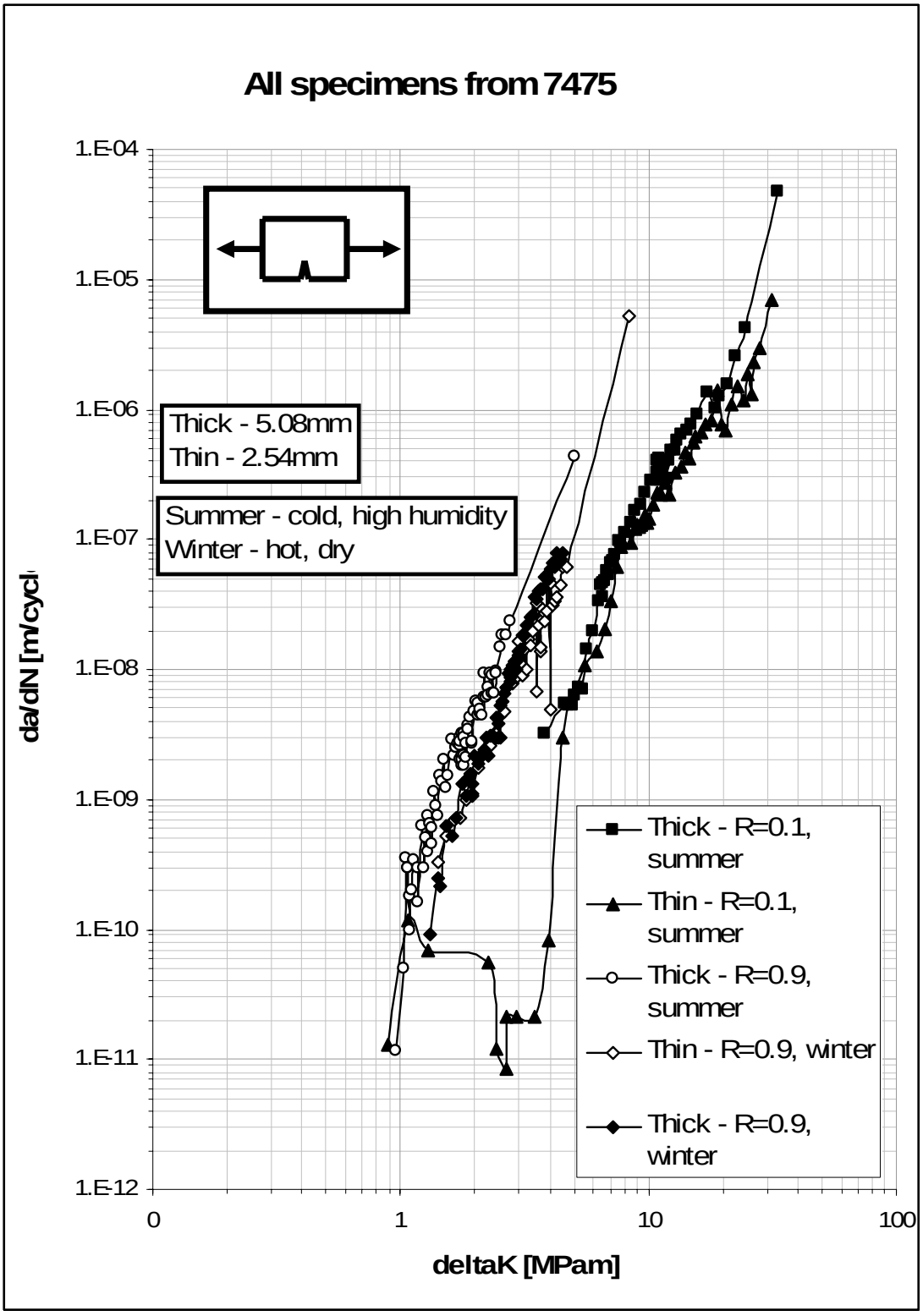
All specimens from 7475
1.E-04
1.E-05
1.E-06
1.E-07
1.E-08
1.E-09
1.E-10
1.E-11
1.E-12
da/dN [m/cycl
Thick - 5.08mm
Thin - 2.54mm
Summer - cold, high humidity
Winter - hot, dry
Thick - R=0.1, summer
Thin - R=0.1, summer
Thick - R=0.9, summer
Thin - R=0.9, winter
Thick - R=0.9, winter
0
1
10
100
deltaK [MPam]

Constant R loading – al. 2324-T39

Precracked under compression

	2324											
	R=0.1						R=0.9				R=0.7	
	Thin				Thick				Thin			
	Winter		Summer									
	dadn	□□	dadn	□□	dadn	□□	dadn	□□	dadn	□□	dadn	□□
	[m/cycle]	[MPam0.5]	[m/cycle]	[MPam0.5]	[m/cycle]	[MPam0.5]	[m/cycle]	[MPam0.5]	[m/cycle]	[MPam0.5]	[m/cycle]	[MPam0.5]
0												
1	0	3.49524816	1.9873E-09	4.092	1.749E-10	2.877	9.53572E-10	1.707	7.62857E-12	0.944	1.93E-11	1.401
2	0	4.18939052	5.18419E-11	3.701	4E-11	3.130	6.57329E-10	1.730	6.53726E-11	0.947	1.68E-11	1.406
3	0	4.90727776	4.37681E-11	3.441	1.78E-11	3.370	9.17972E-10	1.753	2.58524E-11	1.117	1.72E-11	1.449
4	0	5.58954767	4.54254E-10	3.728	6.73E-11	3.613	2.19533E-10	1.769	6.99286E-12	1.211	1.66E-11	1.454
5	0	6.33197131	4.84424E-10	3.759	2.6271E-09	3.947	7.73029E-10	1.782	5.68964E-11	1.309	1.53E-11	1.551
6	0	7.04431808	2.20965E-11	3.776	6.95E-10	4.050	4.69581E-10	1.799	5.19167E-12	1.312	5.24E-12	1.552
7	0	7.04431808	4.88673E-11	3.867	6.255E-09	4.081	2.66152E-10	1.809	3.51762E-12	1.313	3.02E-11	1.556
8	5.83673E-09	7.28777413	5.29467E-10	4.075	1.251E-09	4.107	3.36081E-10	1.817	1.02562E-11	1.400	5.08E-11	1.662
9	5.60922E-09	7.68631205	3.78191E-10	4.106	1.251E-09	4.116	3.53475E-10	1.835	1.33924E-11	1.496	3.89E-10	1.738
10	1.07451E-08	8.14324568	8.29045E-10	4.148	3.753E-09	4.133	5.30822E-10	1.861	5.29762E-11	1.594	1.21E-11	1.789
11	1.11587E-08	8.6722591	1.08401E-09	4.212	2.502E-09	4.155	1.28308E-09	1.907	2.51033E-10	1.707	1.21E-11	1.793
12	1.93712E-08	9.30565743	2.2326E-09	4.319	2.919E-09	4.173	1.39179E-09	1.971	5.0391E-10	1.765	3.15E-11	1.800
13	3.88447E-08	10.27742	1.91815E-09	4.446	3.753E-09	4.209	2.18643E-09	2.028	5.88883E-10	1.820	8.25E-11	1.817
14	2.95458E-07	12.2964495	2.78076E-09	4.582	3.475E-09	4.268	1.16887E-09	2.065	8.32786E-10	1.860	1.61E-10	1.852
15	2.51389E-06	15.1264747	2.29889E-09	4.720	2.2518E-09	4.339	2.30425E-09	2.102	6.63686E-10	1.901	7.16E-11	1.881
16	1.04127E-06	16.8978119	1.87906E-09	4.828	1.5846E-09	4.400	1.26126E-09	2.139	1.45324E-09	1.957	1.52E-10	1.912
17	8.66796E-07	17.4452247	1.75582E-09	4.917	3.1692E-09	4.473	1.2032E-09	2.163	1.27694E-09	2.024	1.05E-10	1.943
18	1.67705E-06	17.8914175	2.62328E-09	5.019	3.50121E-09	4.574	1.85756E-09	2.193	1.89083E-09	2.096	7.96E-11	1.965
19	6.05675E-07	18.2811446	1.96234E-09	5.121	2.88959E-09	4.667	1.68973E-09	2.227	2.56649E-09	2.188	8.38E-12	1.974
20	4.45093E-07	18.5720591	2.13189E-09	5.208	1.61471E-09	4.730	2.52379E-09	2.265	3.47969E-09	2.300	2.86E-11	1.979
21	7.01132E-07	19.2023568	5.46507E-09	5.358	2.63459E-09	4.789	3.20358E-09	2.316	2.6806E-09	2.399	4.58E-11	2.075
22			3.6625E-09	5.524	2.37963E-09	4.857	1.97707E-09	2.359	2.69077E-09	2.458	4.74E-11	2.064
23			4.22341E-09	5.655	2.71898E-09	4.924	2.65411E-09	2.397	3.59984E-09	2.500	2.97E-10	2.286
24			4.33602E-09	5.786	3.90939E-09	5.059	2.30807E-09	2.435	3.35233E-09	2.545	1.71E-09	2.559
25			4.18453E-09	5.895	3.05952E-09	5.226	3.10992E-09	2.476	3.6668E-09	2.586	2.39E-09	2.711
26			4.83043E-09	5.991	4.4618E-09	5.396	2.86495E-09	2.519	3.52313E-09	2.627	3.41E-09	2.768
27			4.06449E-09	6.080	4.75925E-09	5.590	3.27266E-09	2.562	4.24445E-09	2.668	2.85E-09	2.840
28			6.26139E-09	6.178	4.75925E-09	5.731	3.09254E-09	2.604	4.57312E-09	2.712	2.8E-09	2.911
29			4.68888E-09	6.286	5.86408E-09	5.831	2.88572E-09	2.642	4.89415E-09	2.756	3.66E-09	2.992
30			4.23659E-09	6.380	5.77909E-09	5.986	3.42692E-09	2.681	4.57079E-09	2.799	3.32E-09	3.062
31			6.21338E-09	6.485	5.78598E-09	6.268	3.08406E-09	2.719	4.40465E-09	2.837	3.45E-09	3.128
32			7.0199E-09	6.612	4.50429E-09	6.504	4.11752E-09	2.760	5.1887E-09	2.877	4.02E-09	3.200
33			1.43071E-08	6.809	7.06749E-09	6.754	4.11265E-09	2.806	5.82548E-09	2.922	4E-09	3.268
34			1.2747E-08	7.023	1.39793E-08	7.104	3.74393E-09	2.848	6.00326E-09	2.969	6.8E-09	3.327
35			1.17336E-08	7.186	1.72465E-08	7.466	5.2349E-09	2.894	6.65508E-09	3.019	5.6E-09	3.376
36			2.01741E-08	7.369	2.52487E-08	7.804	4.57291E-09	2.943	5.8384E-09	3.070	7.2E-09	3.436
37			1.72463E-08	7.569	3.12802E-08	8.041	4.39999E-09	2.987	8.63832E-09	3.125	6.4E-09	3.495
38			2.19719E-08	7.794	3.61931E-08	8.244	3.84565E-09	3.027	7.86993E-09	3.191	4.9E-09	3.545
39			2.73062E-08	8.069	4.155E-08	8.490	4.43474E-09	3.066	8.71141E-09	3.267	8.1E-09	3.613
40			1.97265E-08	8.326	6.61162E-08	8.854	5.04037E-09	3.111	1.22069E-08	3.351	6.3E-09	3.685
41			2.43083E-08	8.585	8.99117E-08	9.231	6.52752E-09	3.165	1.09861E-08	3.436	1.04E-08	3.777
42			3.42049E-08	8.902	8.09874E-08	9.556	5.62183E-09	3.222	1.19605E-08	3.525	1.15E-08	3.904
43			7.86711E-08	9.294	9.85155E-08	9.888	6.08167E-09	3.278	1.49834E-08	3.620	1.14E-08	4.050
44			1.17061E-07	9.749	4.90692E-08	10.104	9.11445E-09	3.352	1.79763E-08	3.725	1.01E-08	4.204
45			1.01164E-07	10.194	8.49761E-08	10.309	1.22208E-08	3.459	2.07484E-08	3.857	1.63E-08	4.392
46			1.23307E-07	10.549	6.74794E-08	10.512	9.74338E-09	3.577	2.68458E-08	4.034	2.65E-08	4.680
47			3.25026E-07	11.077	1.62483E-07	10.927	1.12093E-08	3.696	4.33896E-08	4.176	2.62E-08	5.010
48			3.44637E-07	11.864	2.26755E-07	11.517	1.58976E-08	3.854	3.06441E-08	4.297	2.63E-08	5.277
49			3.00598E-07	12.444	1.31219E-07	11.881	2.58984E-08	4.076	9.97182E-08	4.475	4.15E-08	5.501
50			1.91769E-07	12.754	2.63597E-07	12.311	4.77775E-08	4.327	6.81783E-08	4.638	6.15E-08	5.723
51			2.97581E-07	13.078	1.81478E-07	12.950	4.4615E-08	4.611	2.03573E-06	8.438	4.42E-08	5.960
52			3.30612E-07	13.641	4.09976E-07	13.724	2.81115E-07	5.091			7.81E-08	6.035
53			3.79735E-07	14.483	5.21765E-07	14.794	1.72346E-05	9.380			8.36E-08	6.155
54			2.14142E-07	15.277	1.05831E-06	15.966					5.96E-08	6.282
55			3.48573E-07	16.119	9.66361E-07	17.549					6.87E-08	6.382
56			5.41918E-07	17.330	9.80576E-07	19.405						
57			8.55272E-07	19.226	1.20589E-06	21.049						
58			7.39108E-07	21.932	1.982E-06	23.916						
59			1.37993E-06	24.985	6.25948E-06	27.526						
60			6.57673E-06	38.017	5.56303E-05	38.380						

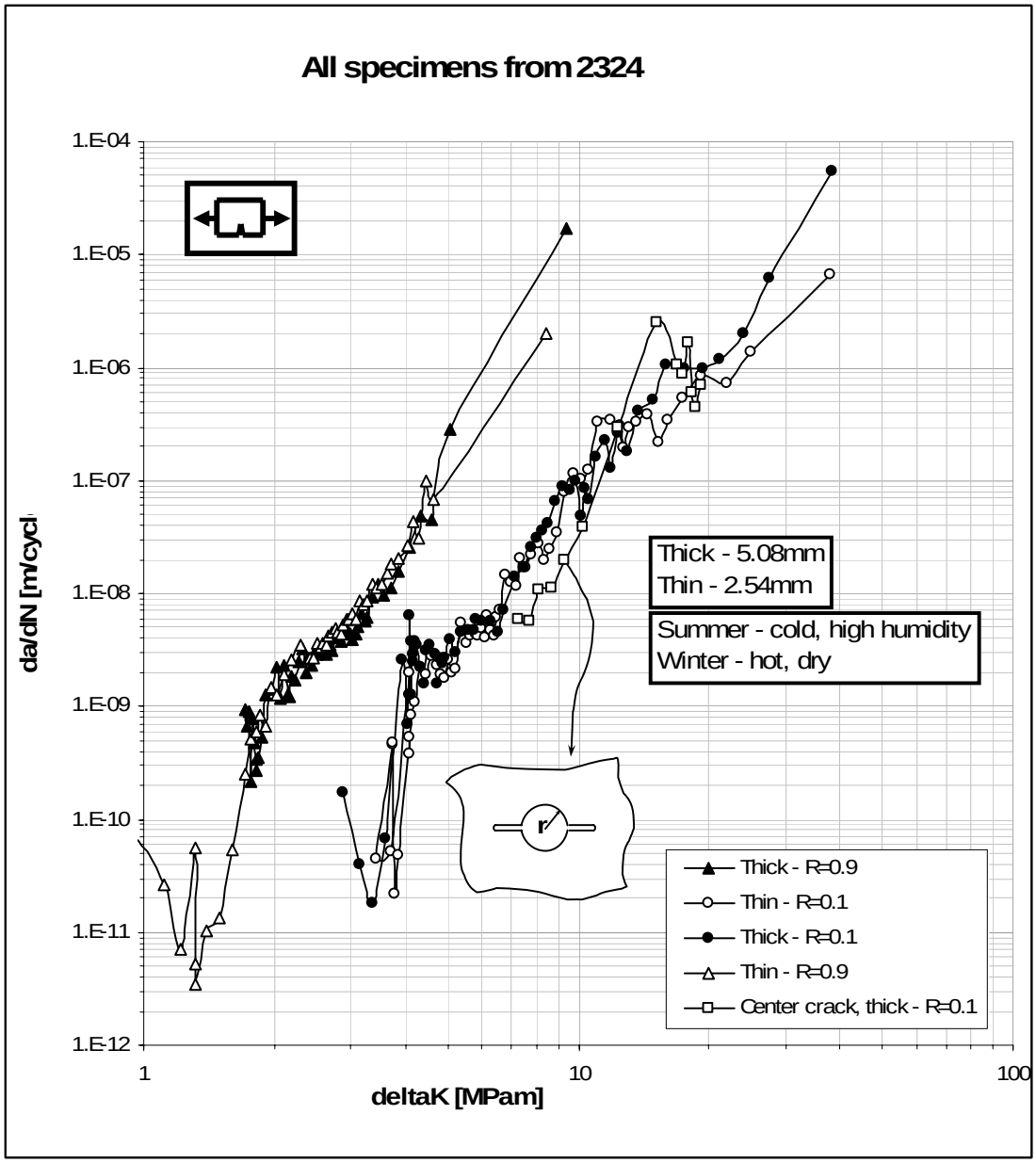
All specimens from 2324
da/dN [m/cycl
1.E-04
1.E-05
1.E-06
1.E-07
1.E-08
1.E-09
1.E-10
1.E-11
1.E-12
1
10
100
deltaK [MPam]
Thick - 5.08mm
Thin - 2.54mm
Summer - cold, high humidity
Winter - hot, dry
r
Thick - R=0.9
Thin - R=0.1
Thick - R=0.1
Thin - R=0.9
Center crack, thick - R=0.1

Monotonic and cyclic stress-strain curve – al. 2324-T39

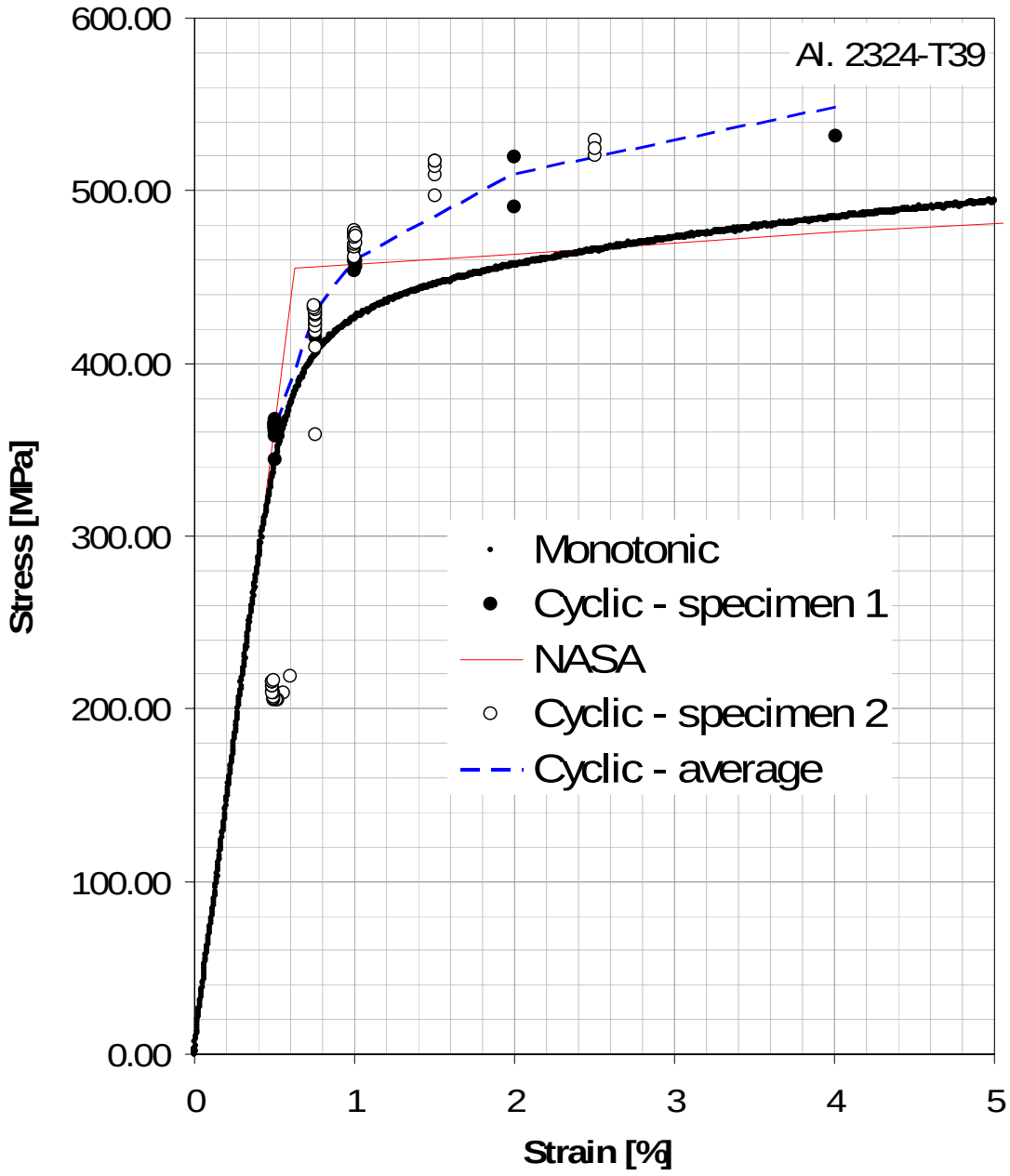

Monotonic and cyclic stress-strain curve – al. 2024-T351

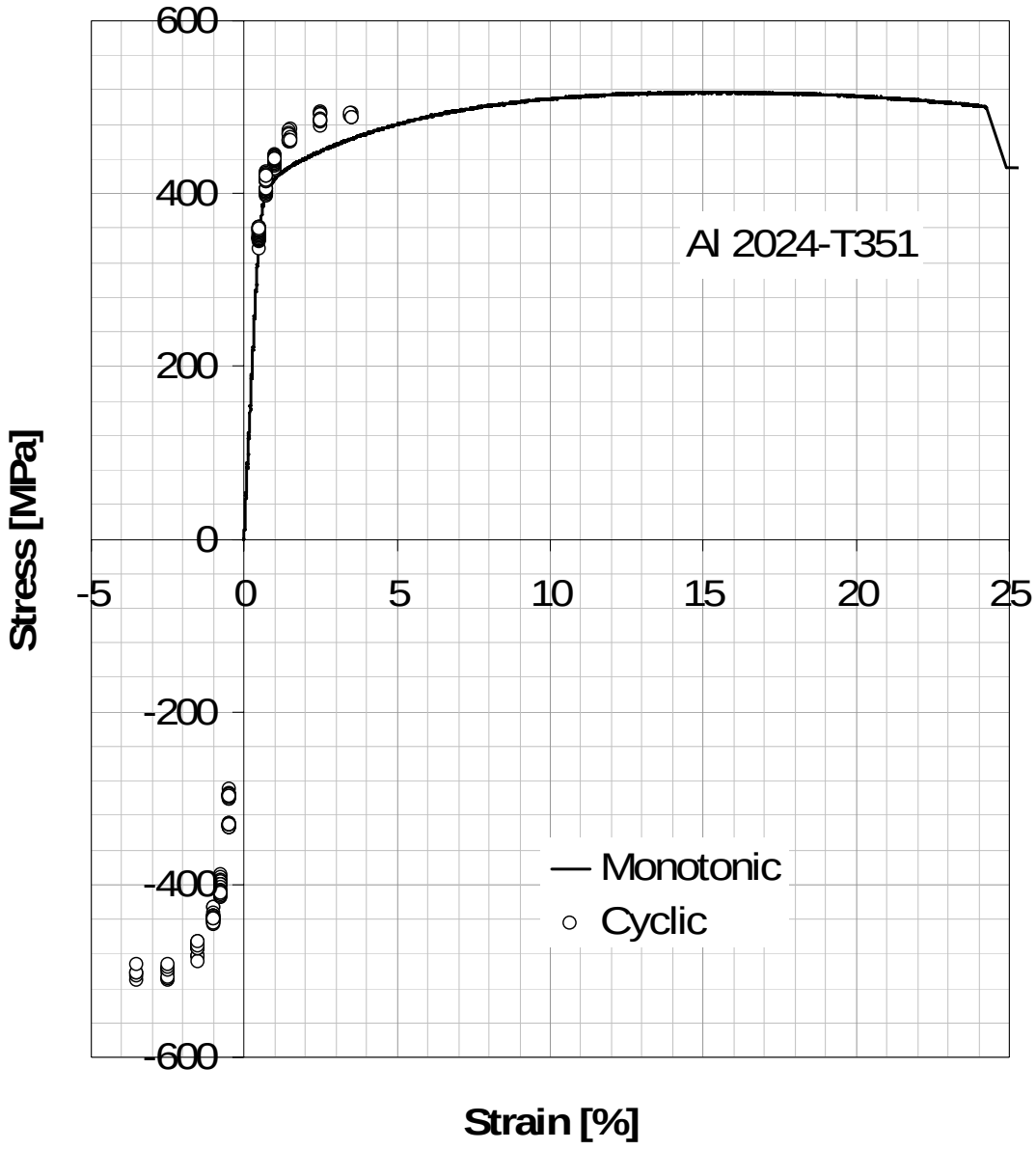

Monotonic stress-strain curve – al. 7475-T7351

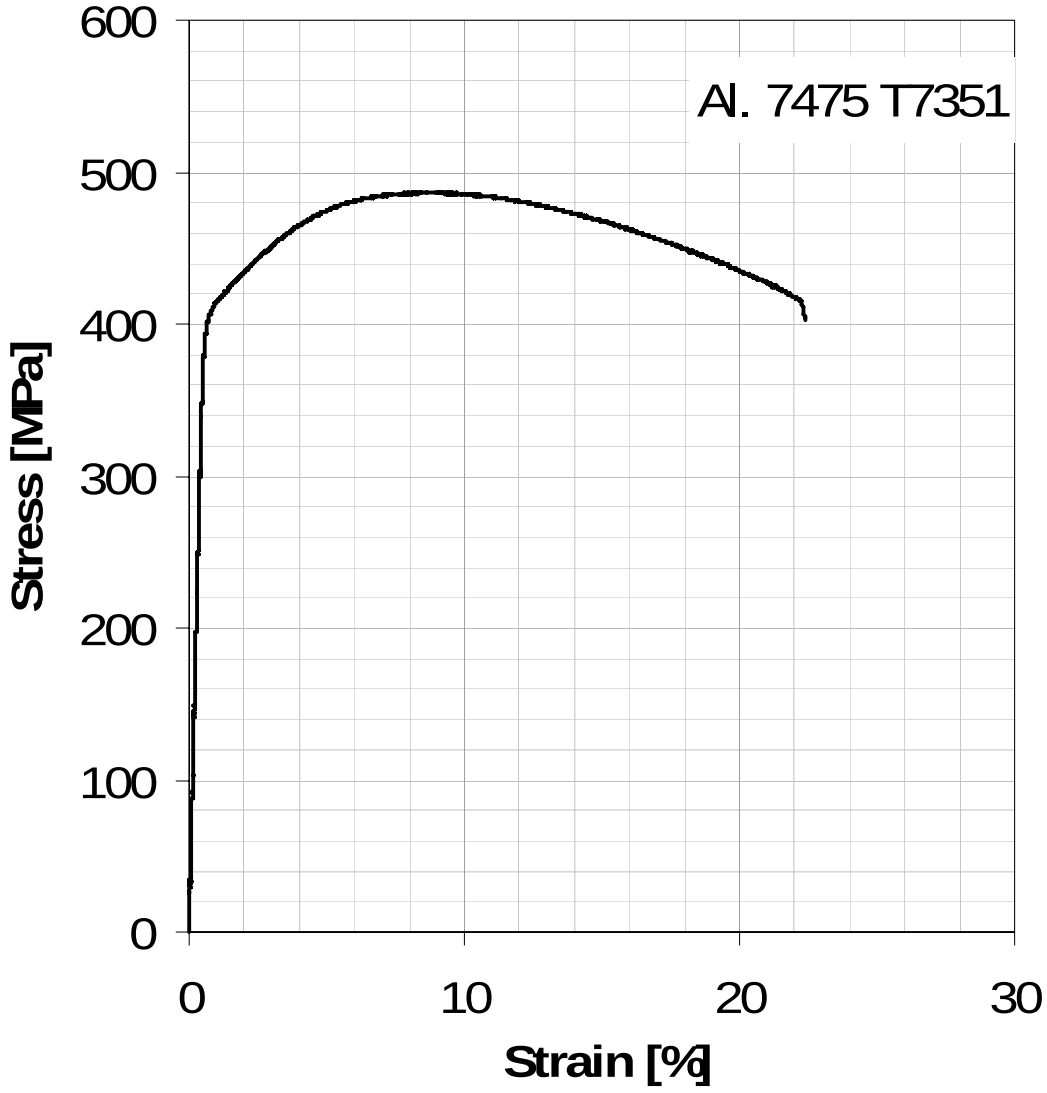

Appendix B

This appendix contains the full documentation of the automated test control software, written in LabView.

The data acquisition is handled by a separate vi (virtual instrument), which is not shown in order to make the Appendix more concise. The load and displacement data are supplied using the global variables.

Control panel

Current Revision: 1084

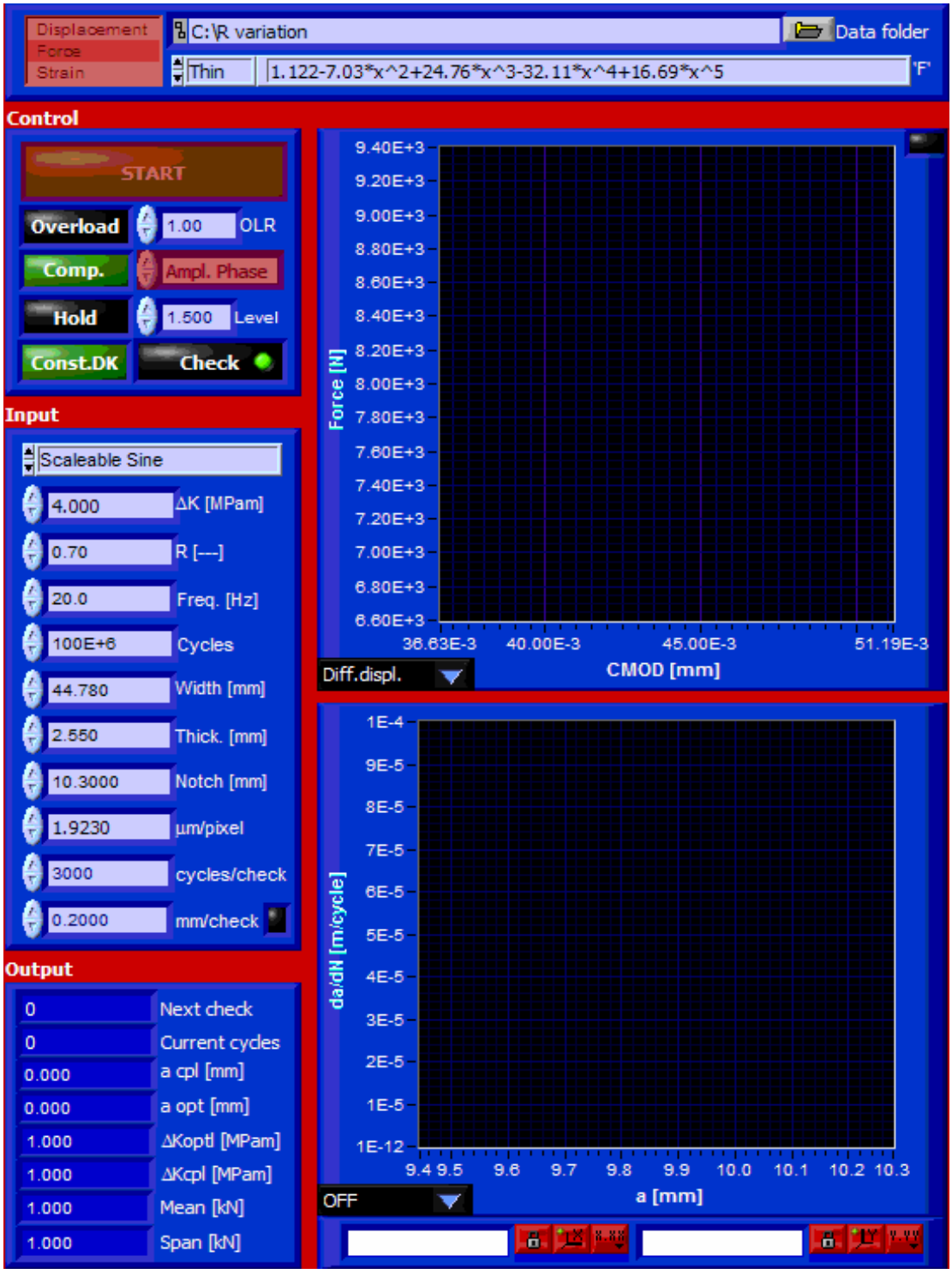

Block Diagram

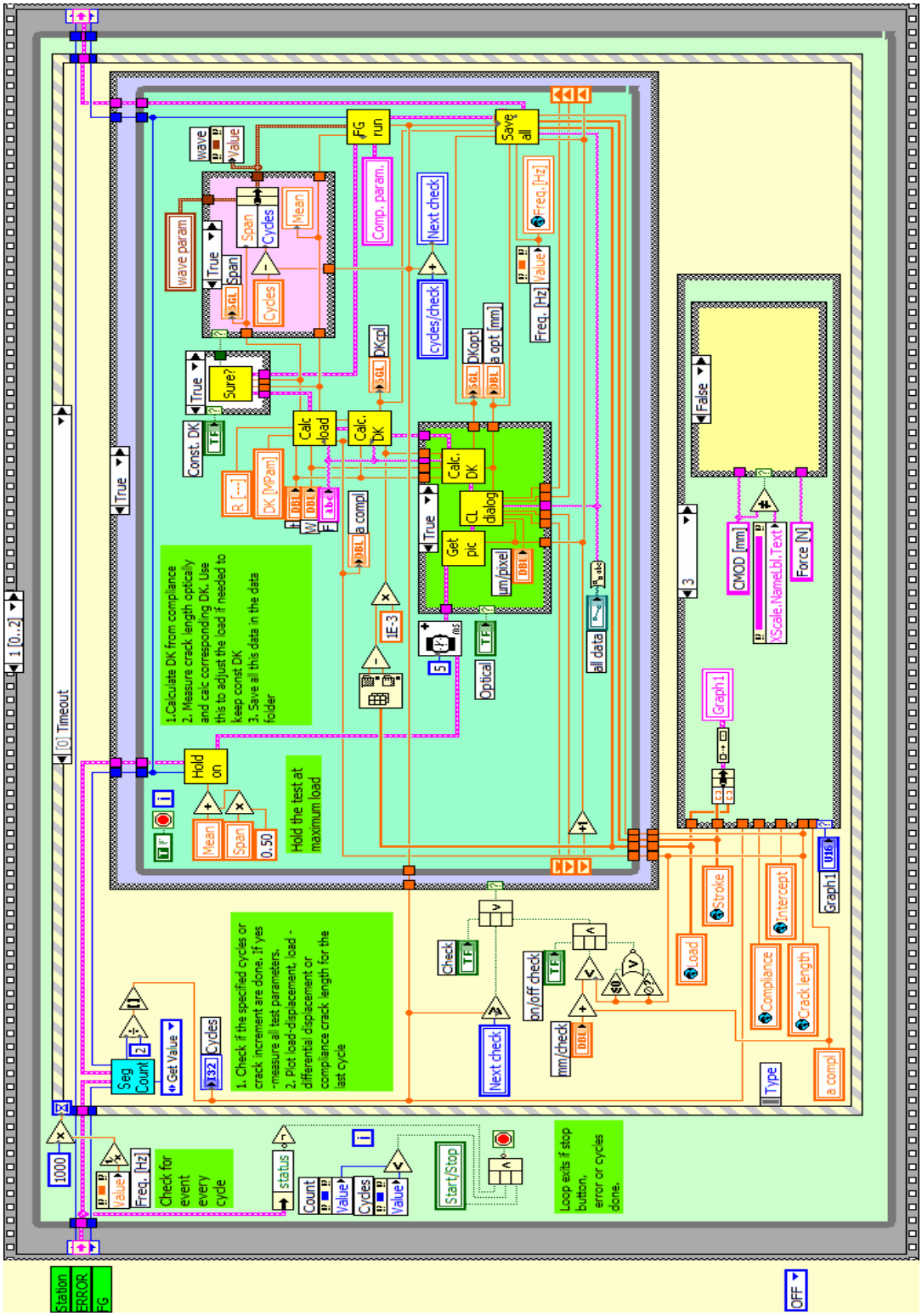

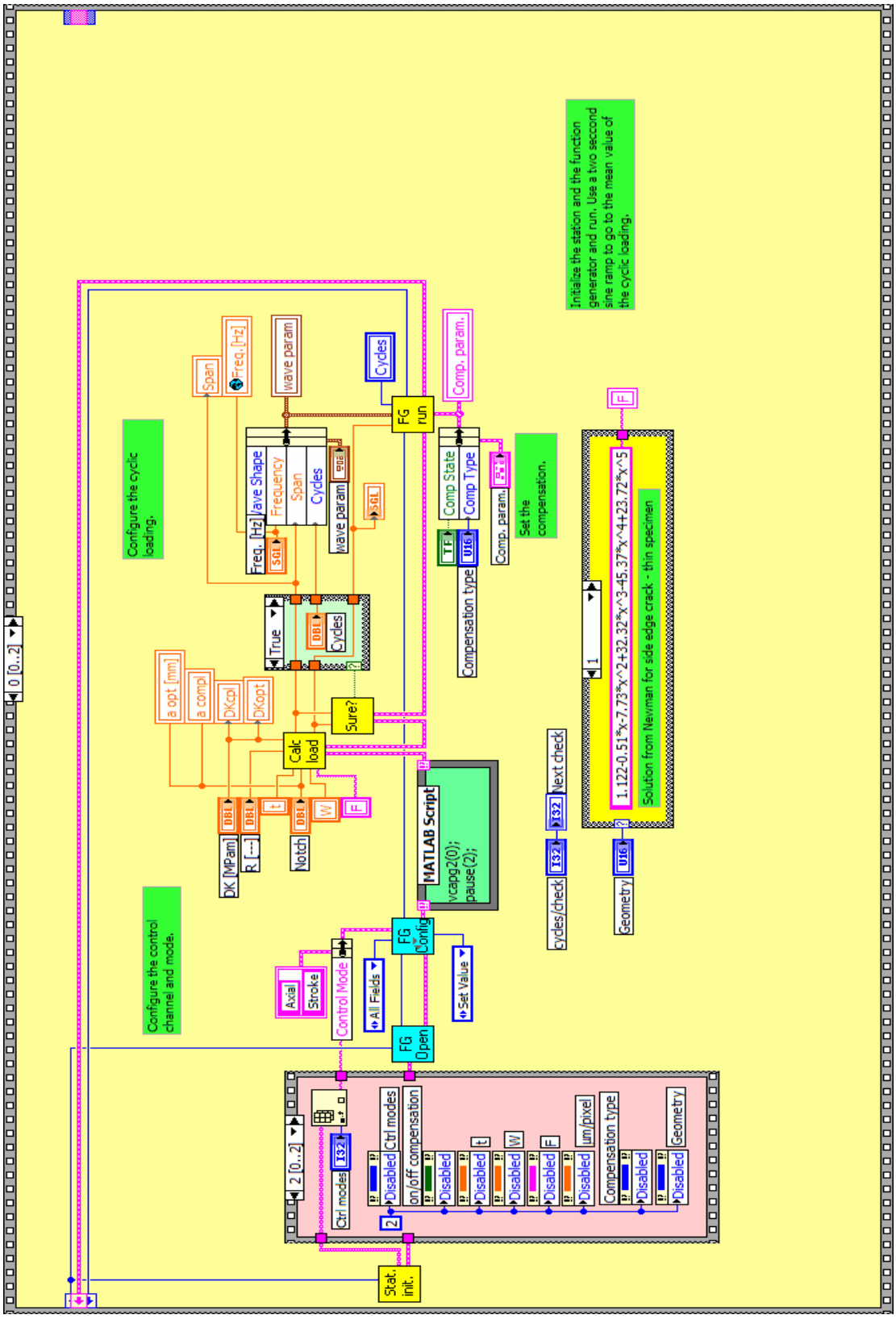
Initialize the station and the function generator and run. Use a two second sine ramp to go to the mean value of the cyclic loading.
Configure the cyclic loading.
Configure the control channel and mode.
Set the compensation.
Solution from Newman for side edge crack - thin specimen
1.122-0.51*x-7.73*x^2+32.32*x^3-45.37*x^4+23.72*x^5
MATLAB Script
vcapg2(0);
pause(2);
Stat. Init.
FG Open
FG Config
FG run
Control Mode
Axial
Stroke
All Fields
Set Value
Calc load
Sure?
Cycles
Wave Shape
Frequency
Span
Wave param
Freq. [hz]
Comp. param.
Comp State
Comp Type
Compensation type
Next check
cycles/check
Geometry
DK [MPam]
R [---]
Notch
a opt [mm]
a comp
DKcpl
DKopt
Ctrl modes
on/off compensation
um/pixel
Compensation type
Disabled
0 [0..2]
1
2

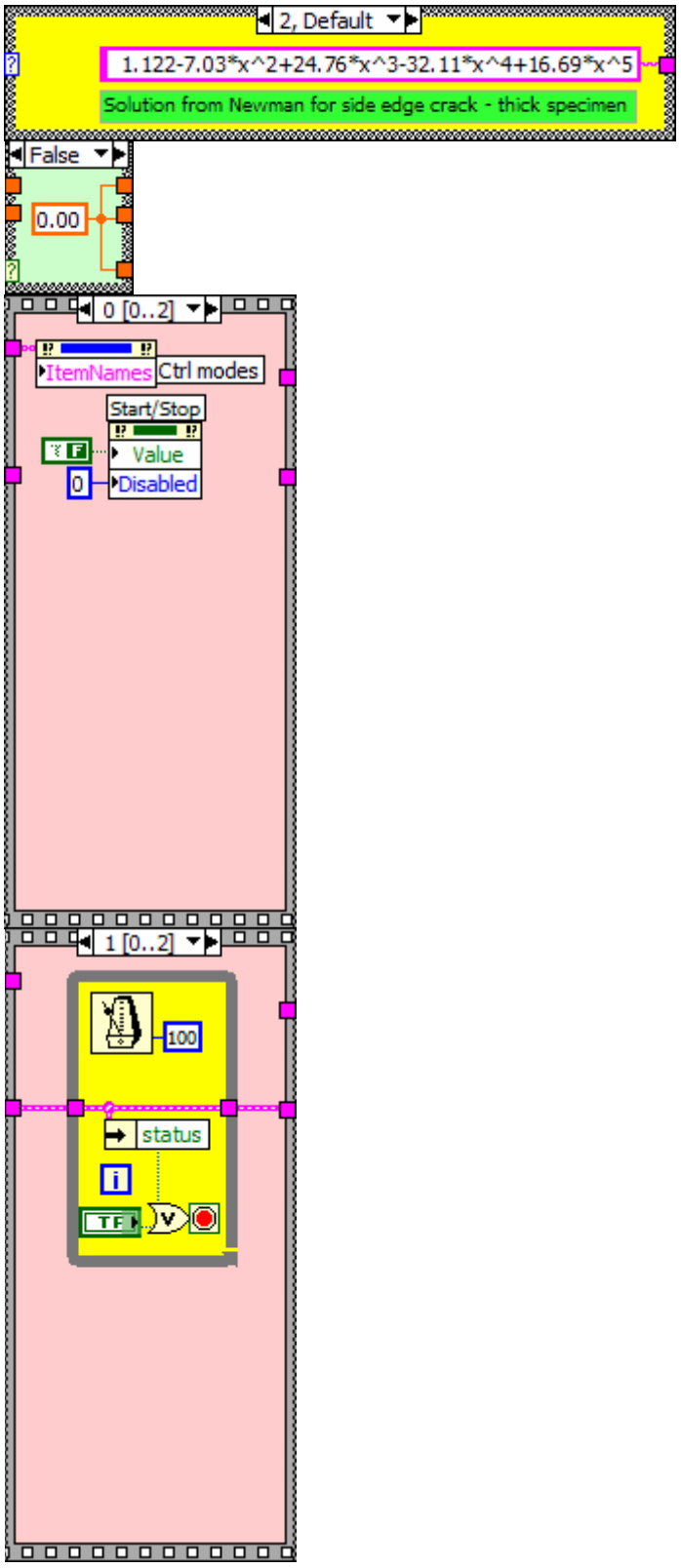
2, Default
1.122-7.03*x^2+24.76*x^3-32.11*x^4+16.69*x^5
Solution from Newman for side edge crack - thick specimen
False
0.00
0 [0..2]
ItemNames
Ctrl modes
Start/Stop
Value
0
Disabled
1 [0..2]
100
status
i
TF

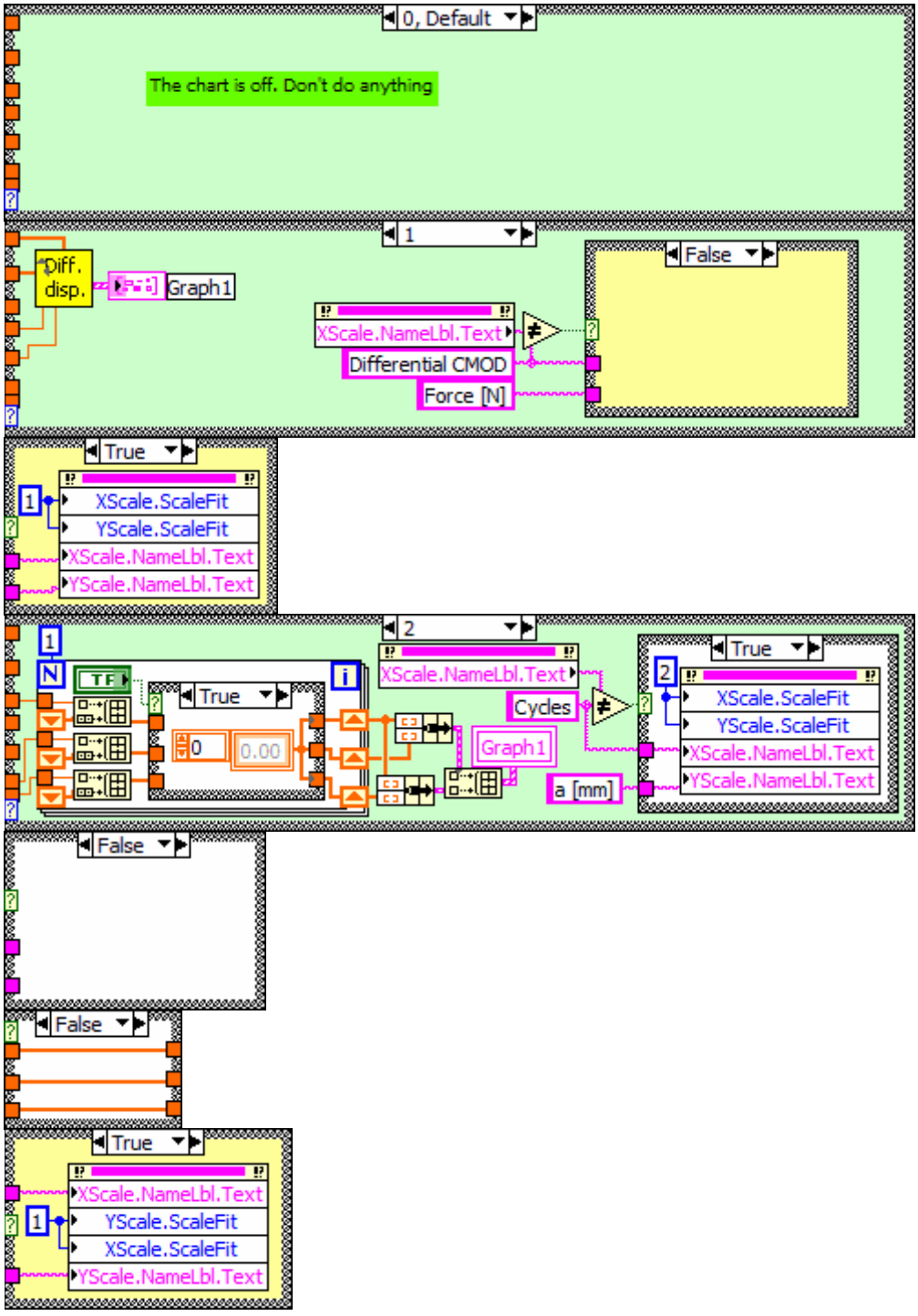
0, Default
The chart is off. Don't do anything
1
Diff. disp.
Graph1
False
XScale.NameLbl.Text
Differential CMOD
Force [N]
True
XScale.ScaleFit
YScale.ScaleFit
XScale.NameLbl.Text
YScale.NameLbl.Text
2
True
0
0.00
Cycles
Graph1
a [mm]
False
False
True
XScale.NameLbl.Text
YScale.ScaleFit
XScale.ScaleFit
YScale.NameLbl.Text

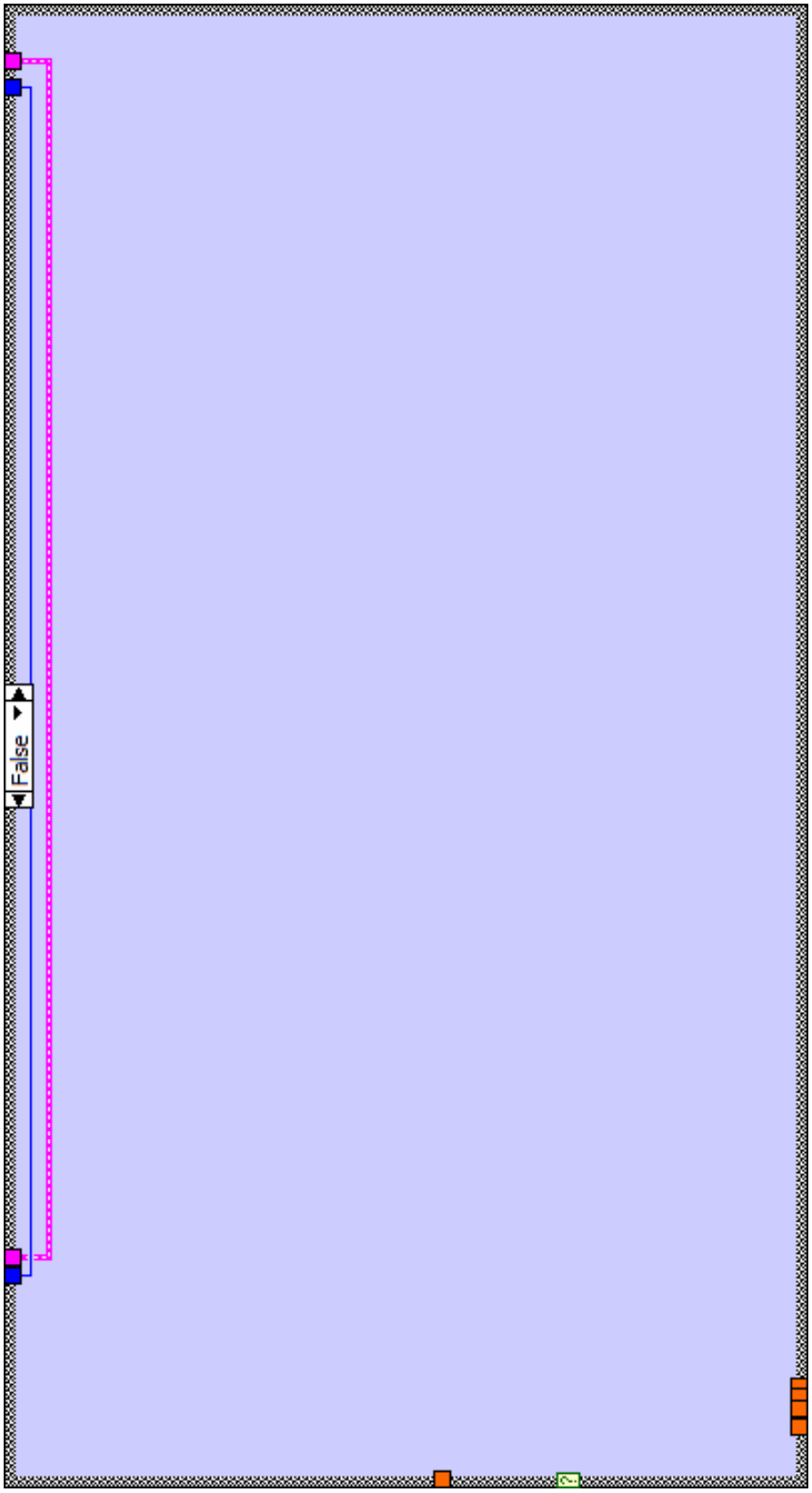
False

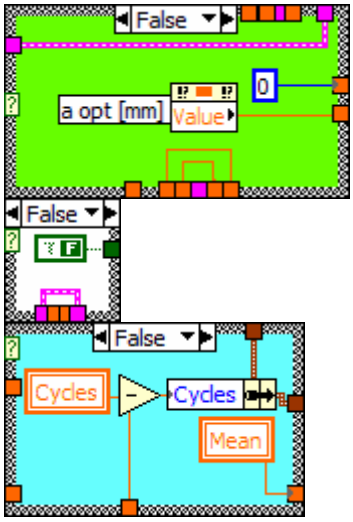
False
a opt [mm]
Value
0
False
False
Cycles
Cycles
Mean

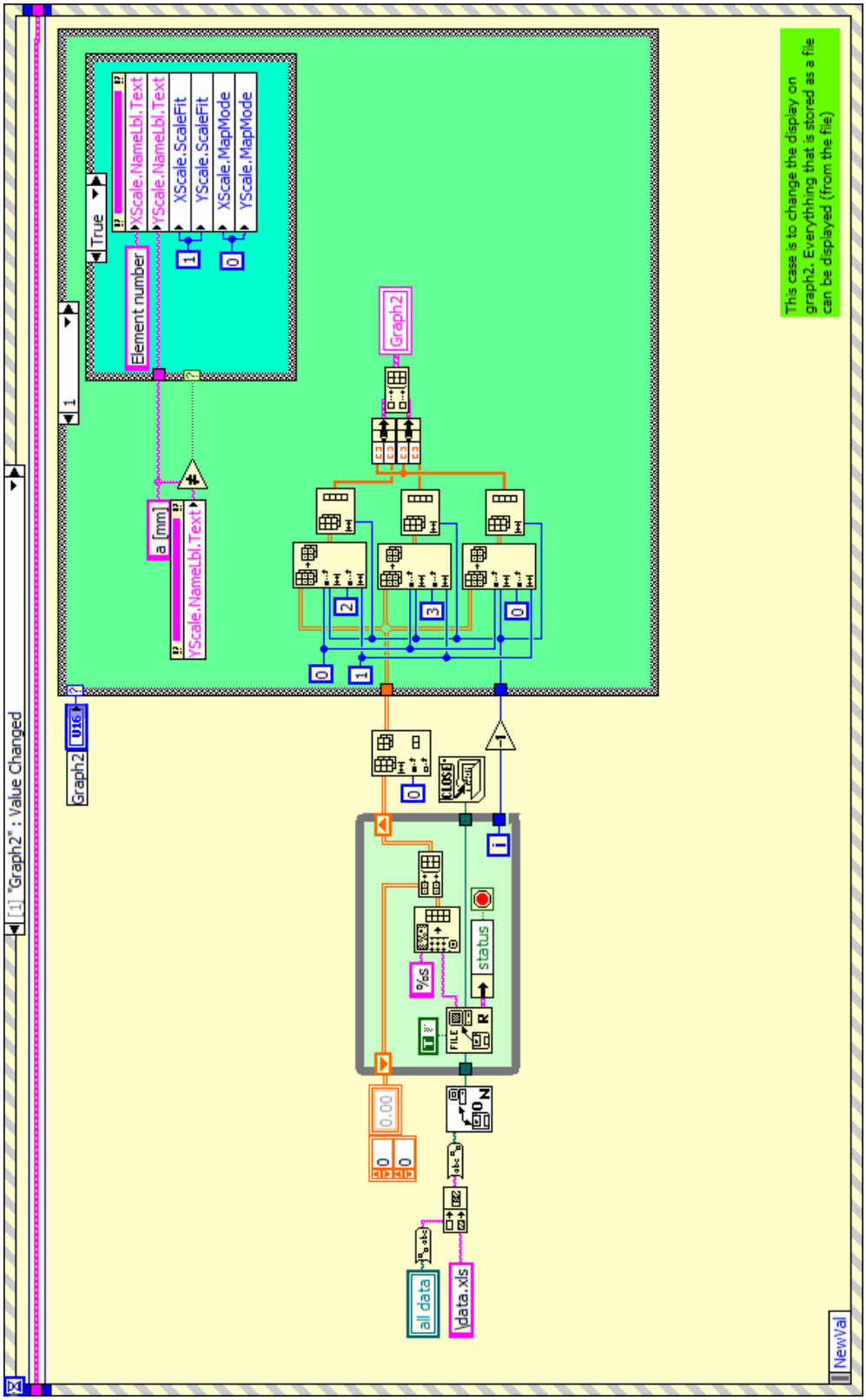
[1] "Graph2" : Value Changed
This case is to change the display on graph2, Everythhing that is stored as a file can be displayed (from the file)
Graph2
Element number
True
XScale.NameLbl.Text
YScale.NameLbl.Text
XScale.ScaleFit
YScale.ScaleFit
XScale.MapMode
YScale.MapMode
a [mm]
YScale.NameLbl.Text
status
%s
all data
\data.xls
NewVal

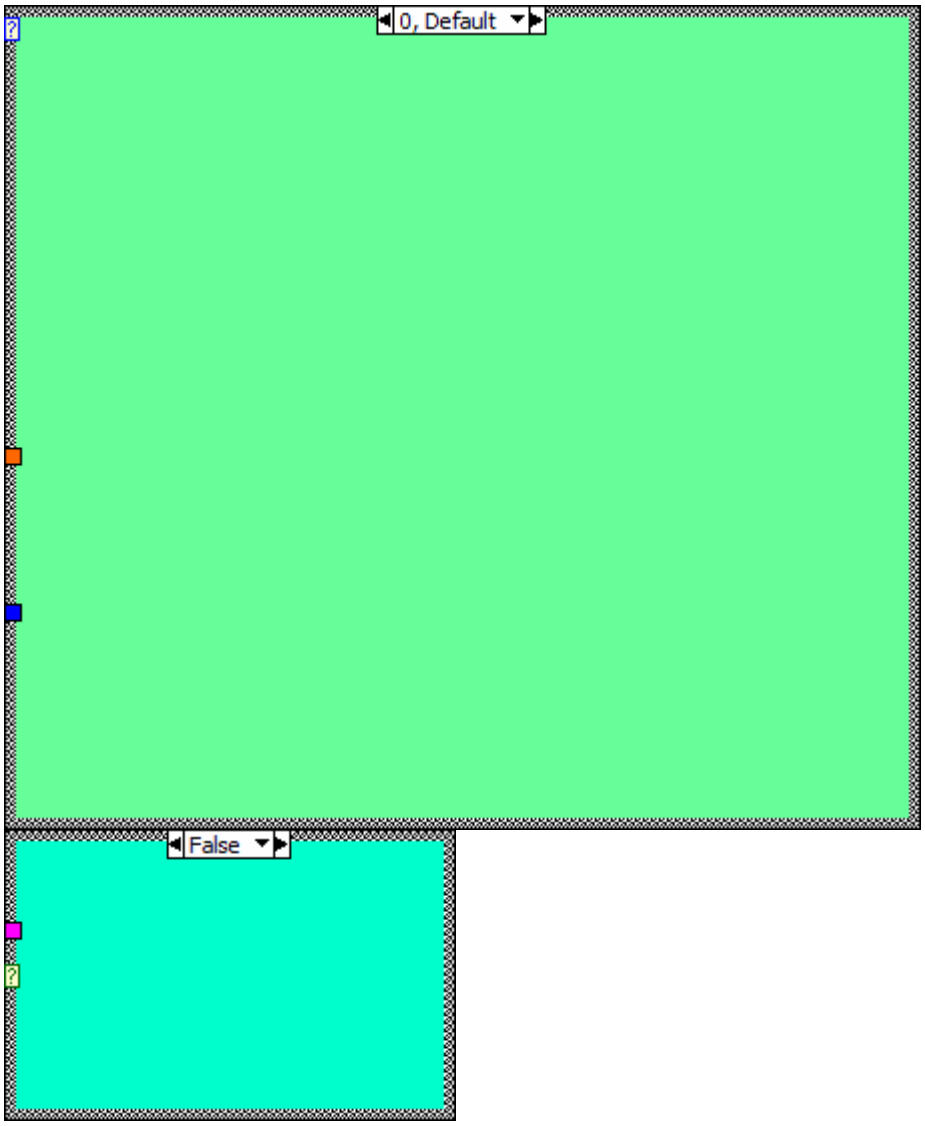
0, Default
False

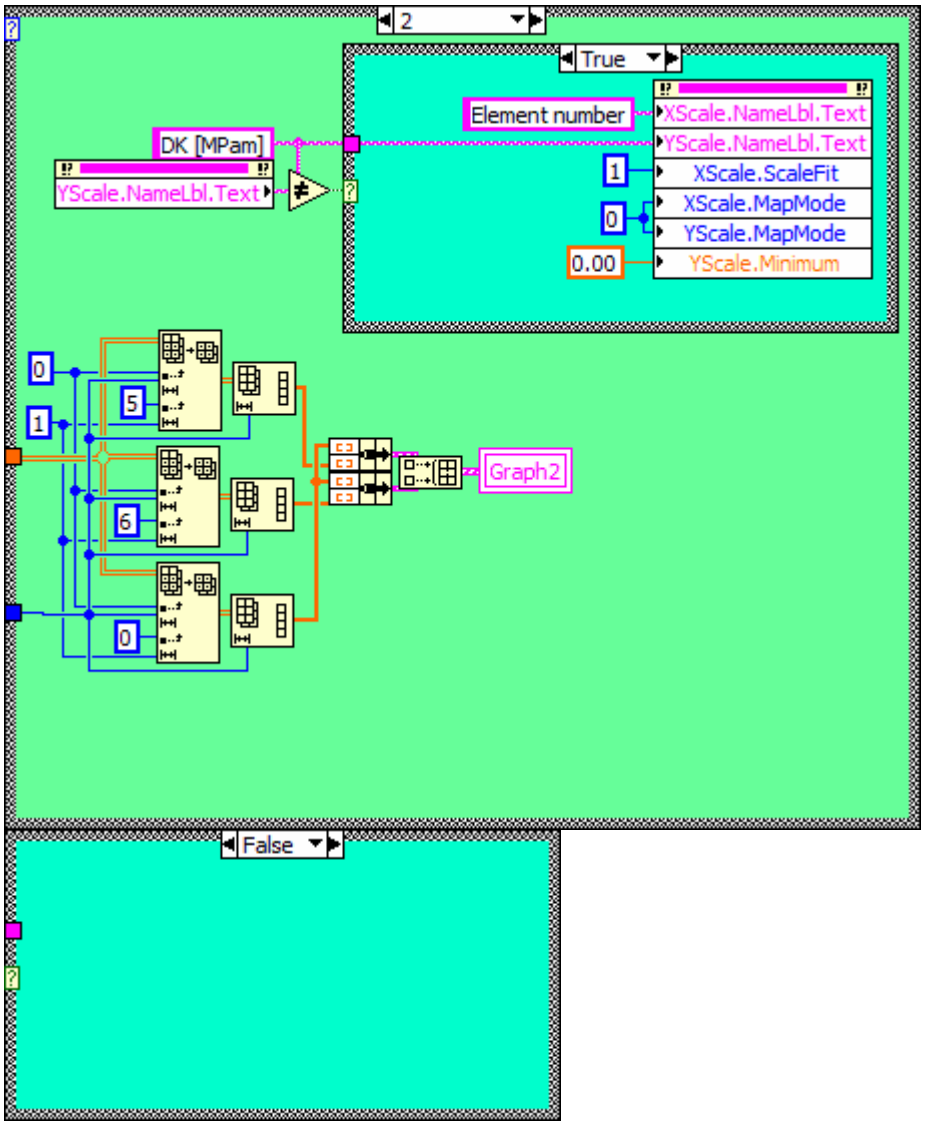
2
True
Element number
DK [MPam]
YScale.NameLbl.Text
XScale.NameLbl.Text
YScale.NameLbl.Text
1
XScale.ScaleFit
0
XScale.MapMode
YScale.MapMode
0.00
YScale.Minimum
0
1
5
6
0
Graph2
False

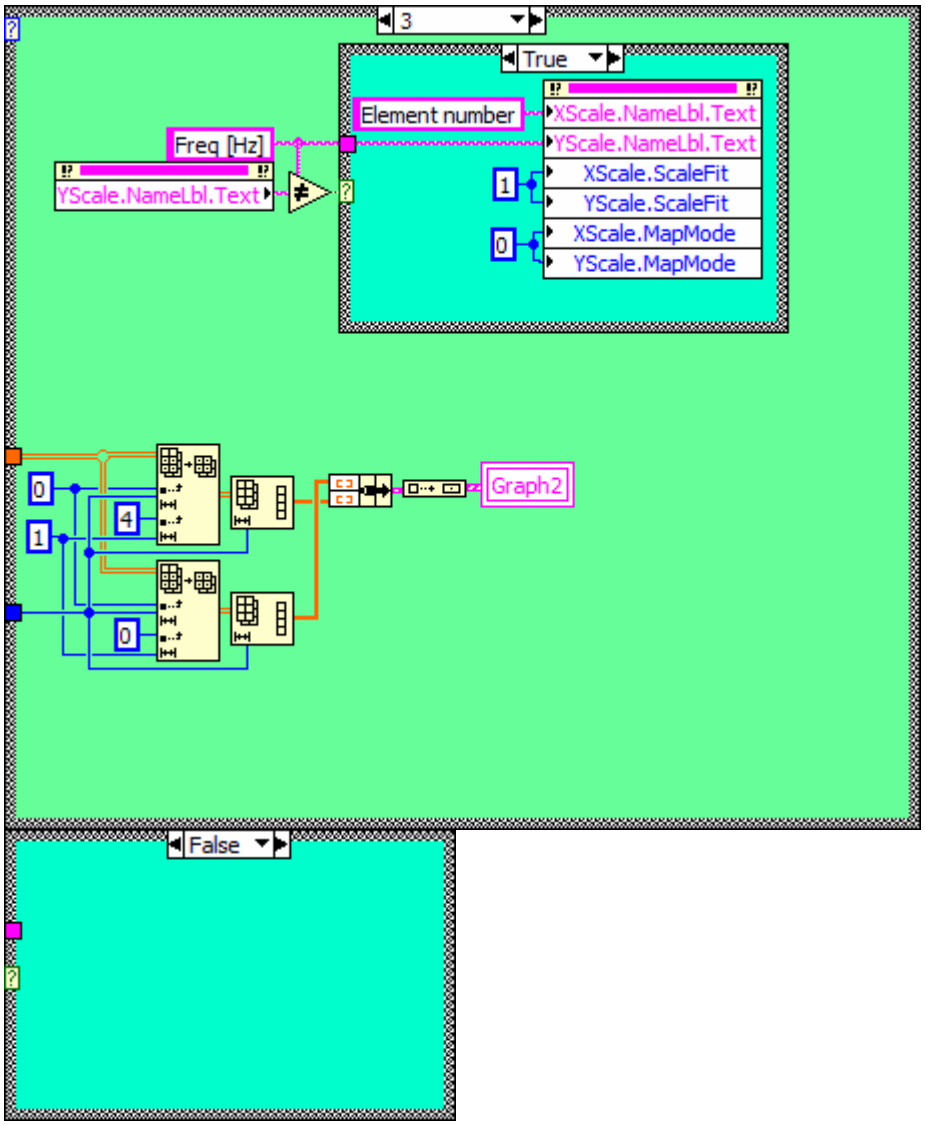
3
True
Element number
Freq [Hz]
YScale.NameLbl.Text
XScale.NameLbl.Text
YScale.NameLbl.Text
XScale.ScaleFit
YScale.ScaleFit
XScale.MapMode
YScale.MapMode
1
0
0
1
4
0
Graph2
False

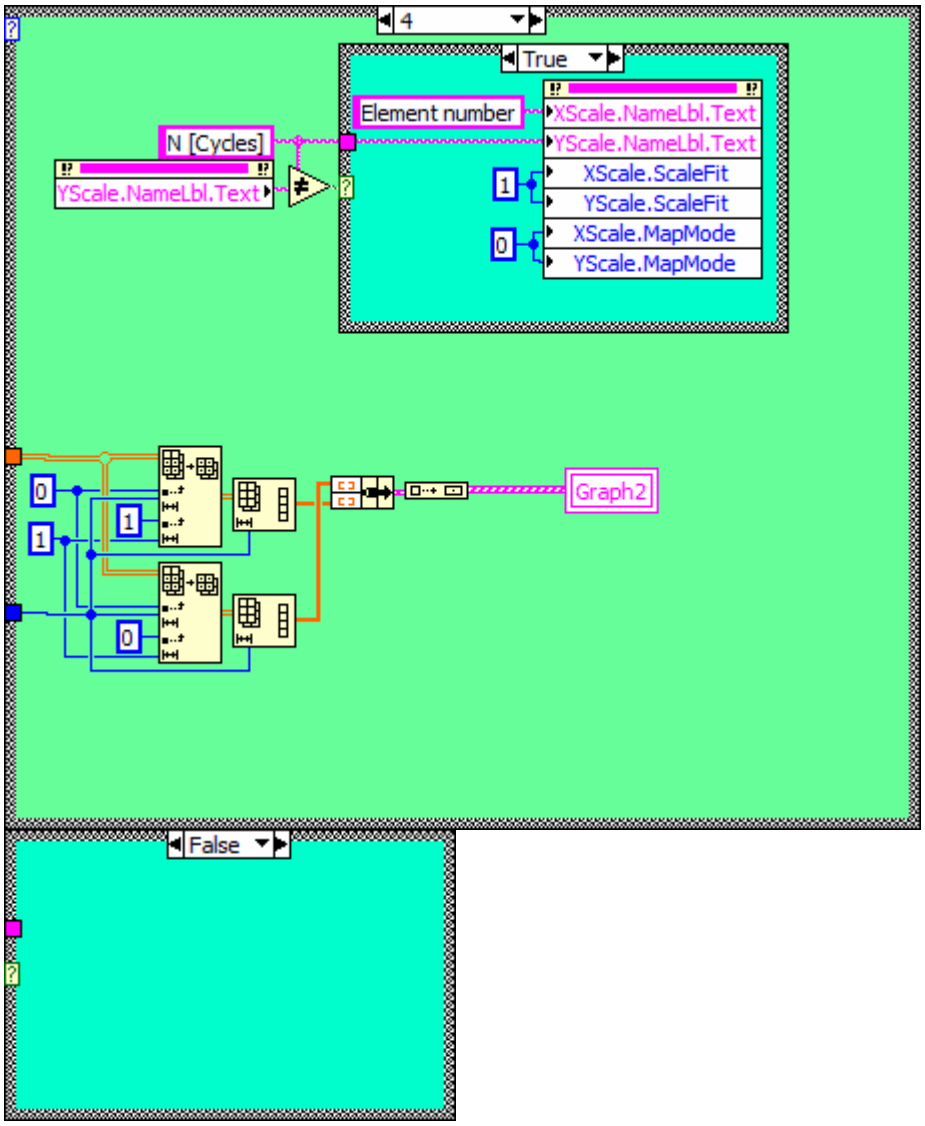
4
True
Element number
N [Cycles]
YScale.NameLbl.Text
XScale.NameLbl.Text
YScale.NameLbl.Text
XScale.ScaleFit
YScale.ScaleFit
XScale.MapMode
YScale.MapMode
1
0
Graph2
False

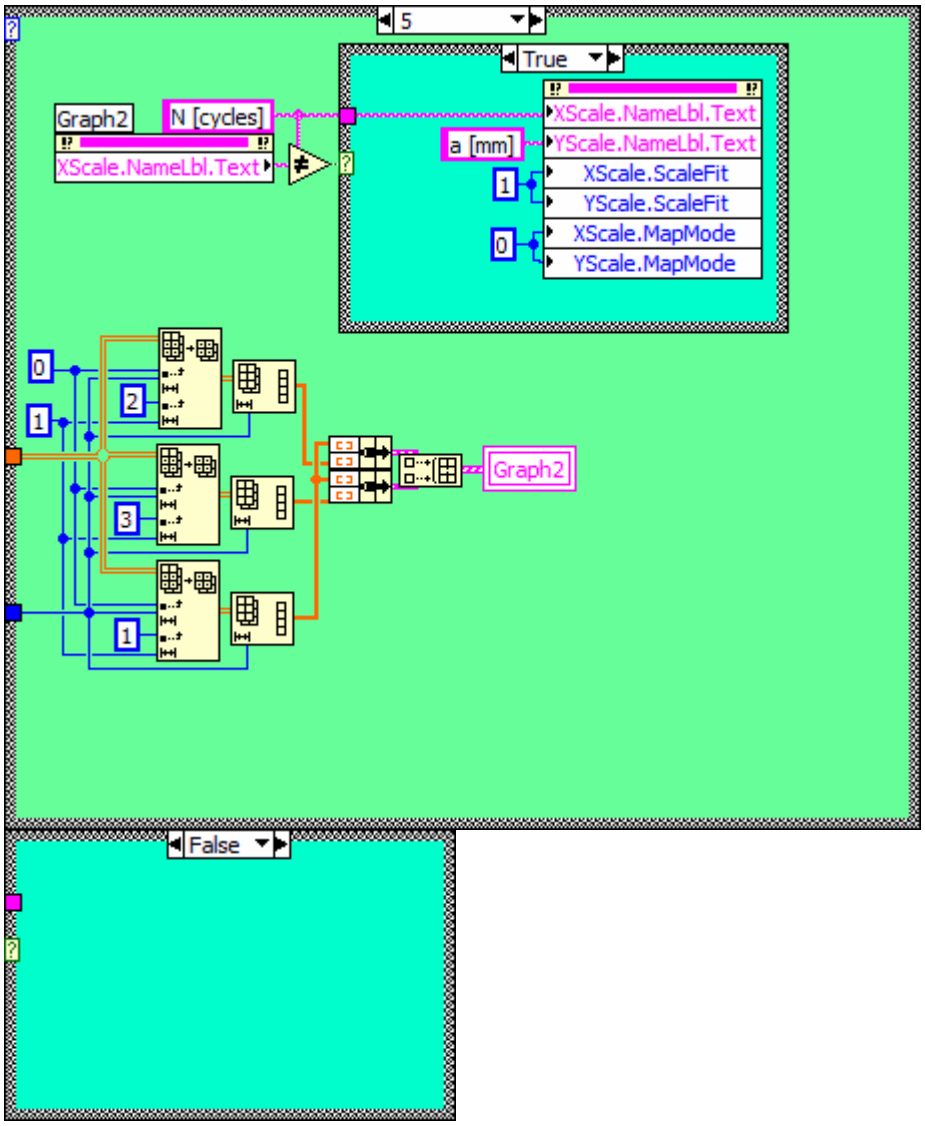
5
True
Graph2
N [cycles]
XScale.NameLbl.Text
a [mm]
YScale.NameLbl.Text
XScale.ScaleFit
YScale.ScaleFit
XScale.MapMode
YScale.MapMode
1
0
2
3
Graph2
False

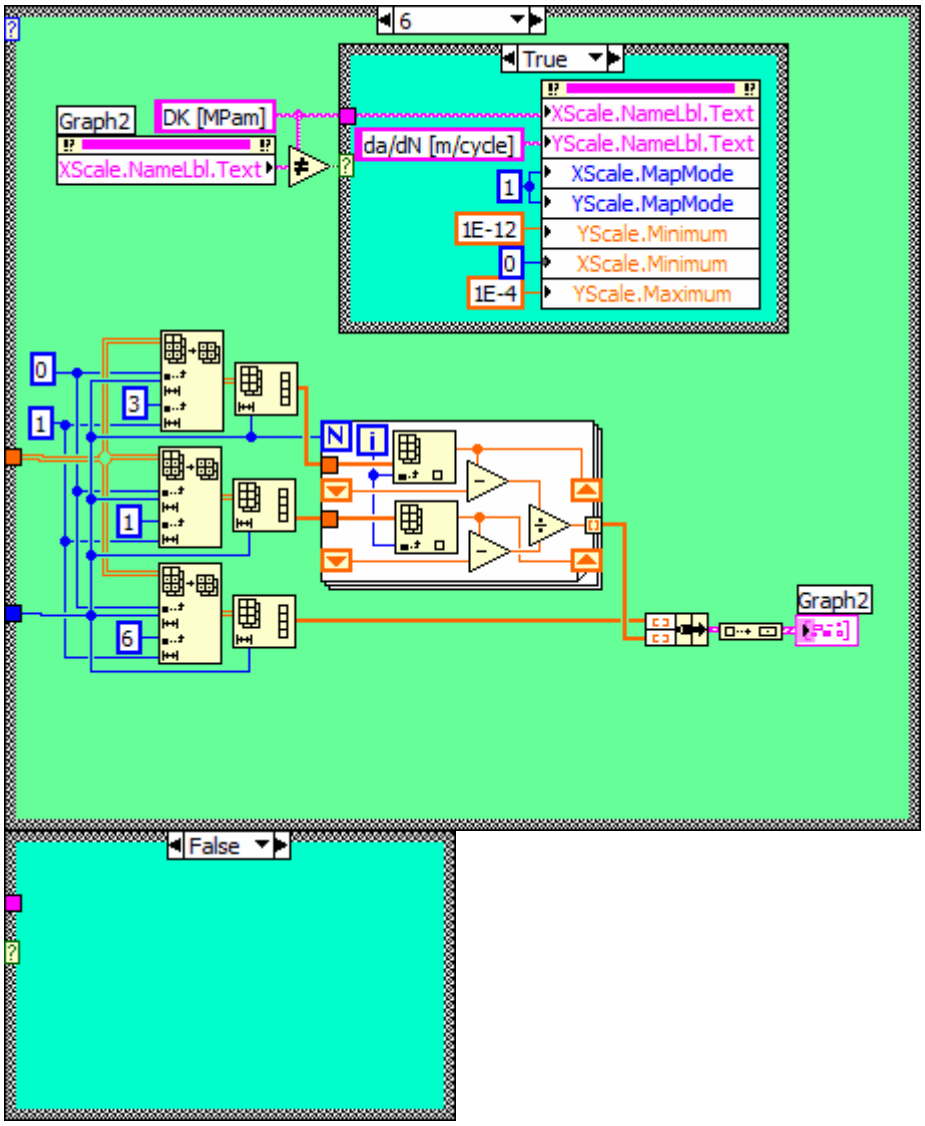
6
True
Graph2
DK [MPam]
XScale.NameLbl.Text
da/dN [m/cycle]
XScale.NameLbl.Text
YScale.NameLbl.Text
XScale.MapMode
YScale.MapMode
YScale.Minimum
XScale.Minimum
YScale.Maximum
1
1E-12
0
1E-4
0
1
3
1
6
N
i
Graph2
False

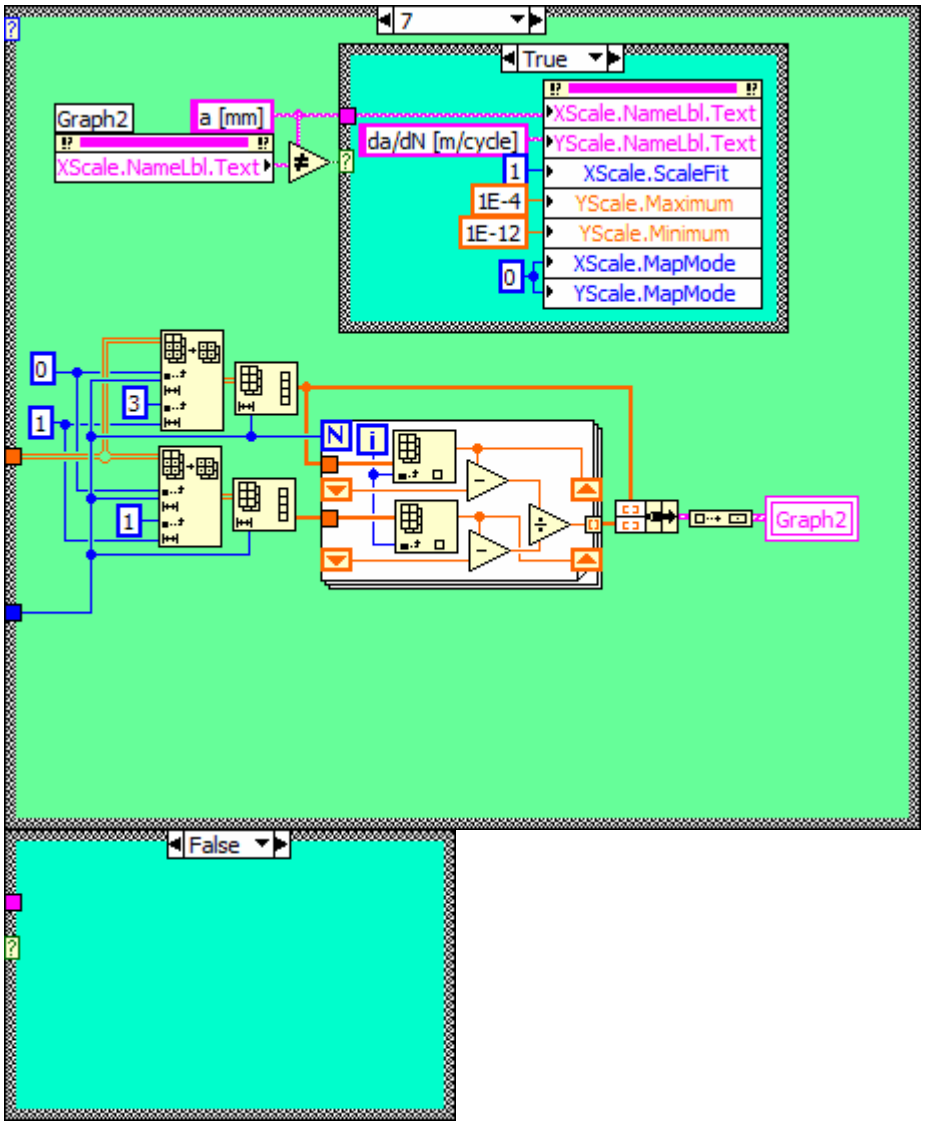
7
True
Graph2
a [mm]
XScale.NameLbl.Text
da/dN [m/cycle]
1
1E-4
1E-12
0
XScale.NameLbl.Text
YScale.NameLbl.Text
XScale.ScaleFit
YScale.Maximum
YScale.Minimum
XScale.MapMode
YScale.MapMode
0
1
3
1
N
i
Graph2
False

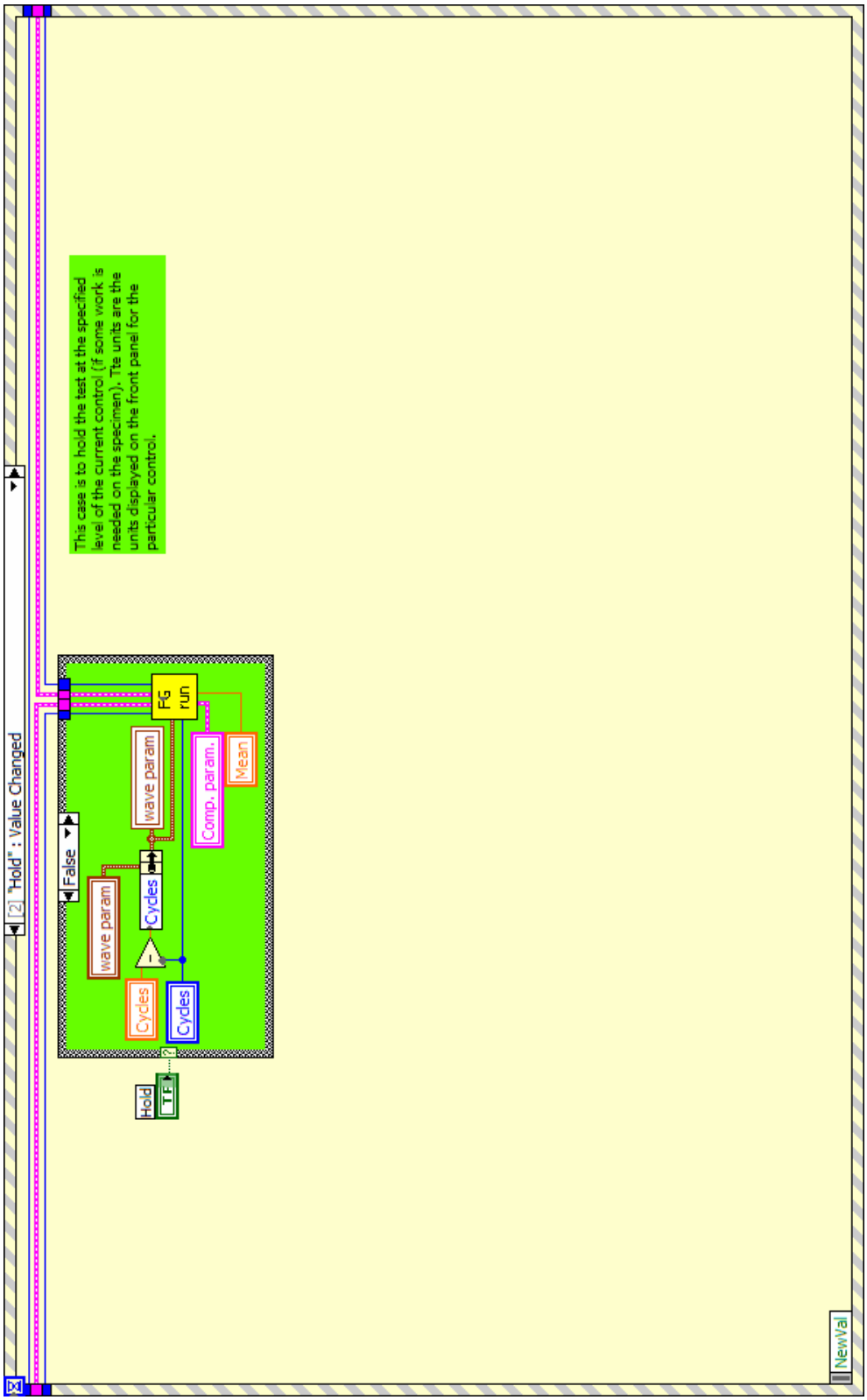
[2] "Hold" : Value Changed
This case is to hold the test at the specified level of the current control (if some work is needed on the specimen). The units are the units displayed on the front panel for the particular control.
False
wave param
Cycles
i
wave param
Cycles
FG run
Comp. param.
Mean
Cycles
Hold
TF
NewVal

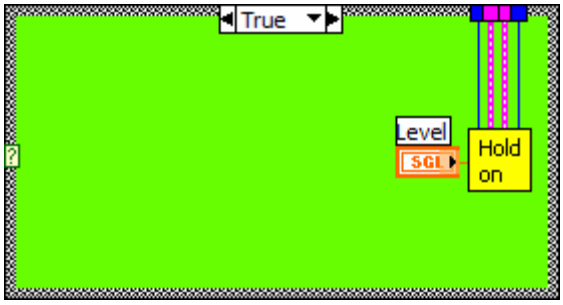
True
Level
SGL
Hold
on

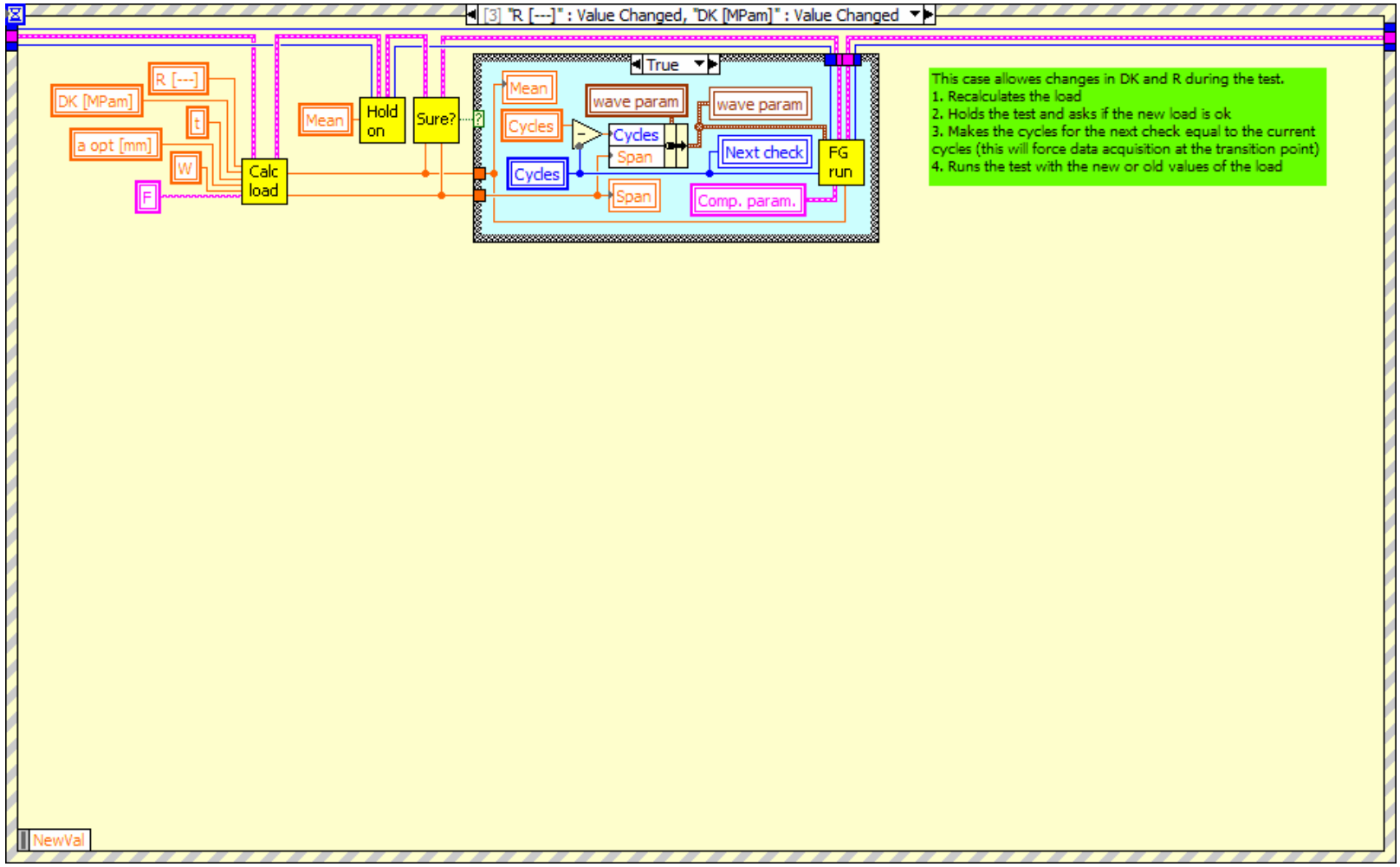
[3] "R [---]" : Value Changed, "DK [MPam]" : Value Changed
R [---]
DK [MPam]
t
a opt [mm]
W
F
Calc load
Mean
Hold on
Sure?
True
Mean
Cycles
wave param
wave param
Cycles
Span
Next check
Cycles
Span
Comp. param.
FG run
This case allowes changes in DK and R during the test.
1. Recalculates the load
2. Holds the test and asks if the new load is ok
3. Makes the cycles for the next check equal to the current cycles (this will force data acquisition at the transition point)
4. Runs the test with the new or old values of the load
NewVal

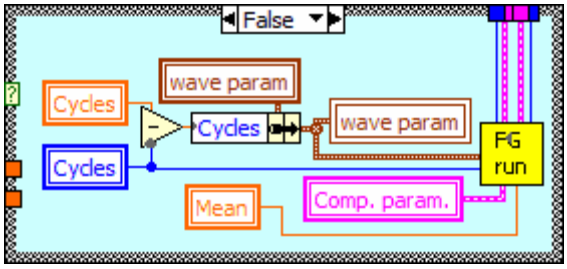
False
wave param
Cycles
Cycles
wave param
Cycles
FG
run
Mean
Comp. param.

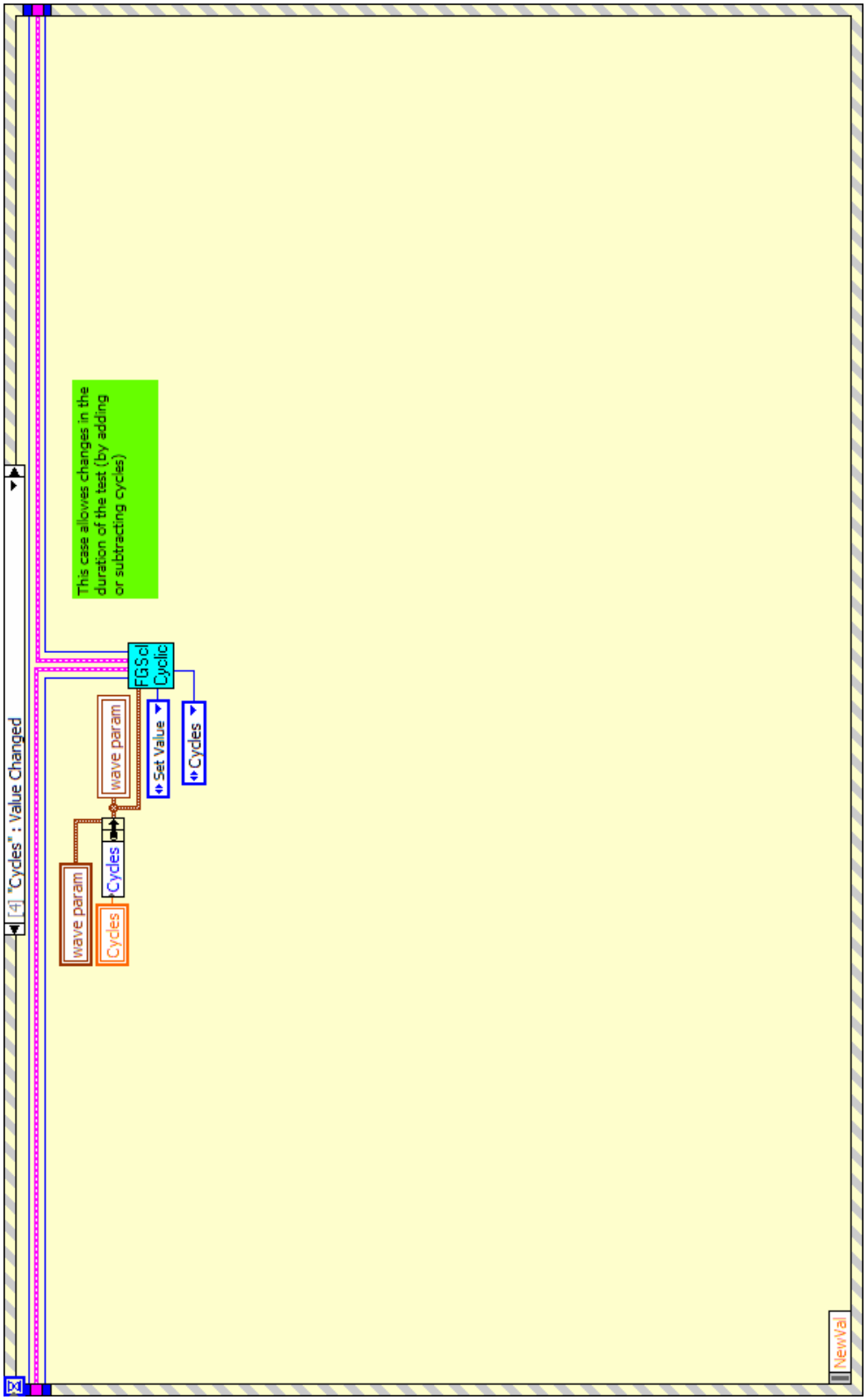
"Cycles" : Value Changed
This case allowes changes in the duration of the test (by adding or subtracting cycles)
wave param
Cycles
Cycles
wave param
FGSc Cyclic
Set Value
Cycles
NewVal


[5] "Freq. [Hz]" : Value Changed
Pretty obvious
wave param
Freq.
wave param
NewVal

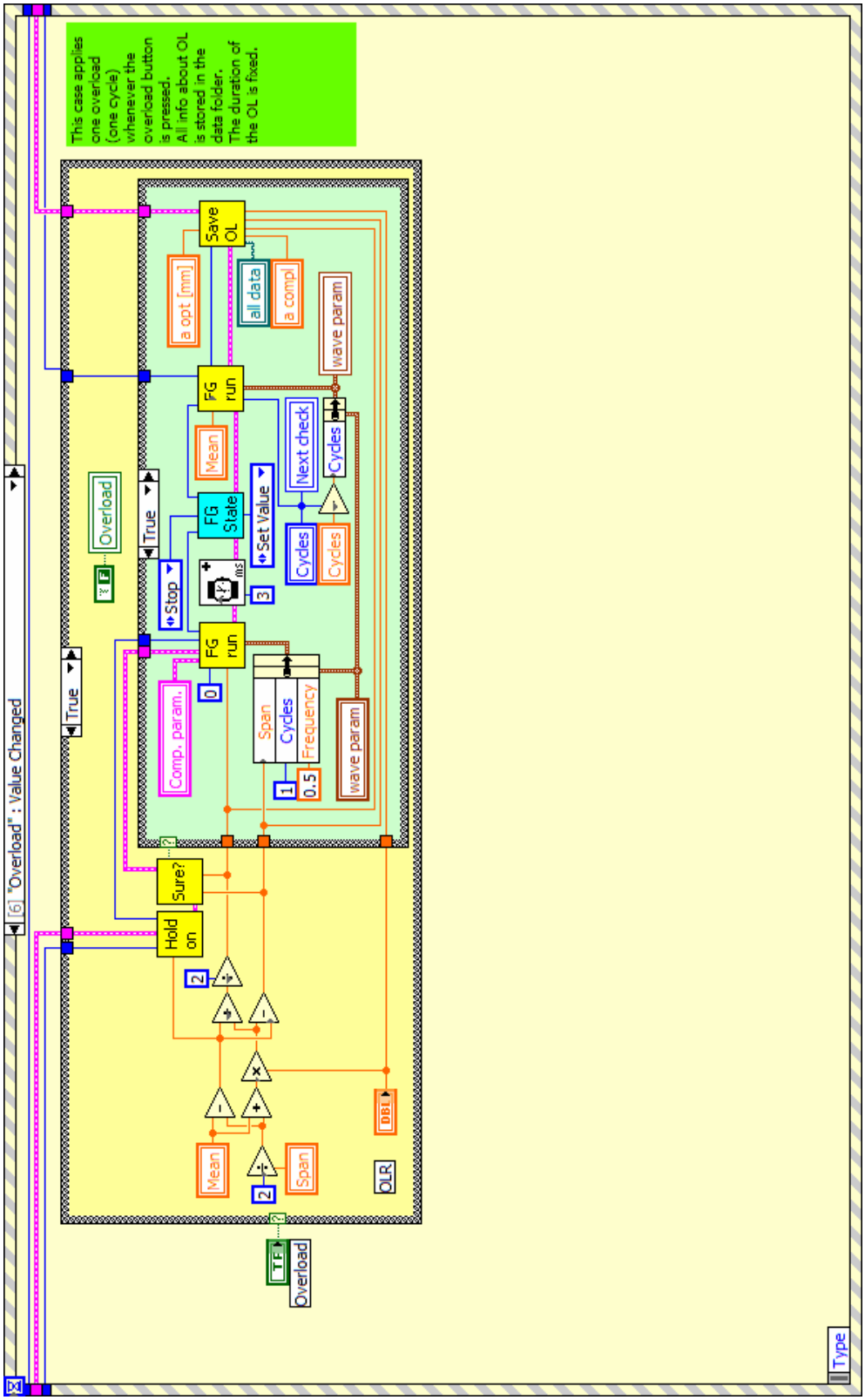
[6] "Overload" : Value Changed
This case applies one overload (one cycle) whenever the overload button is pressed. All info about OL is stored in the data folder. The duration of the OL is fixed.
Overload
True
Stop
FG State
Set Value
FG run
Mean
Save OL
a opt [mm]
all data
a compl
wave param
Next check
Cycles
Comp. param.
Span
Frequency
0.5
Sure?
Hold on
DBL
OLR
Type

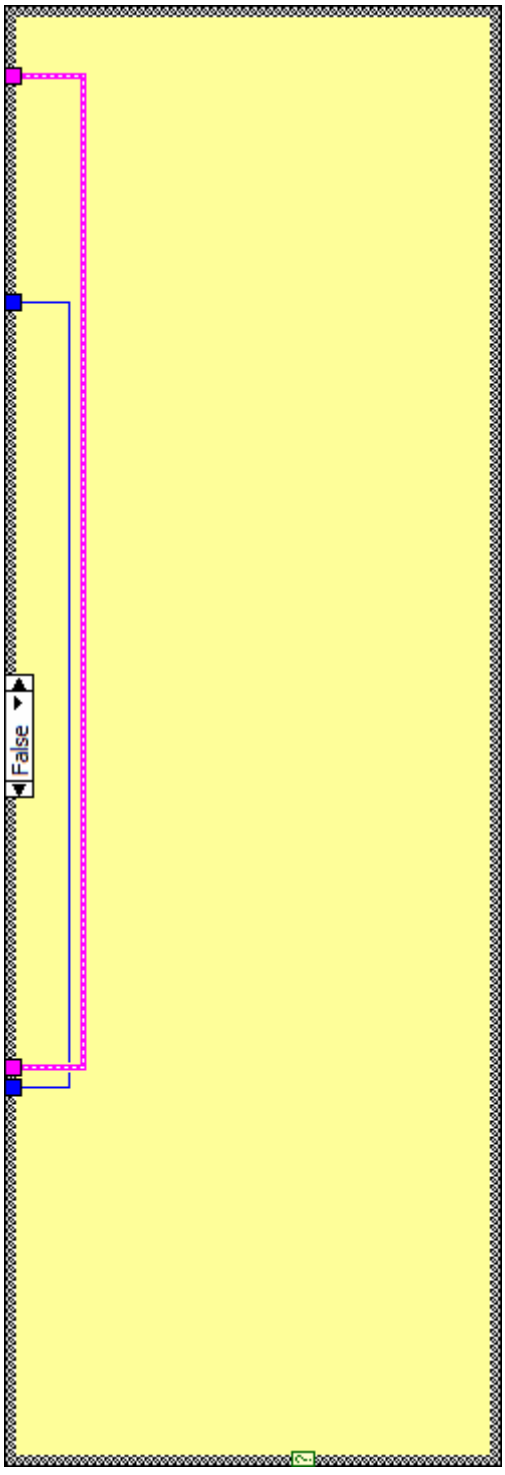
False

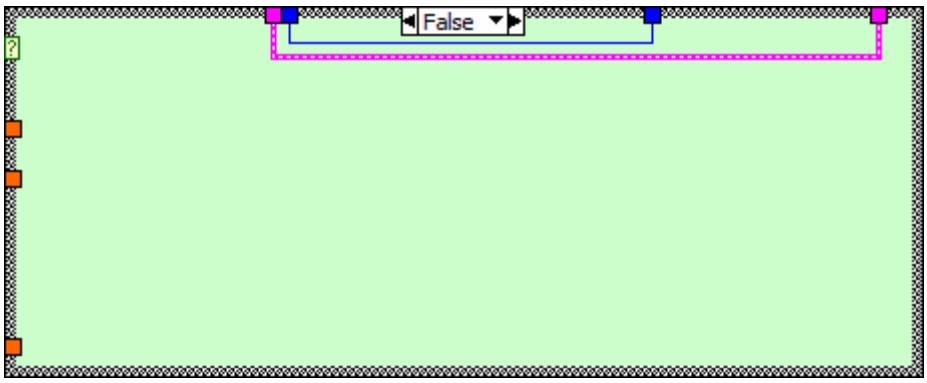
False

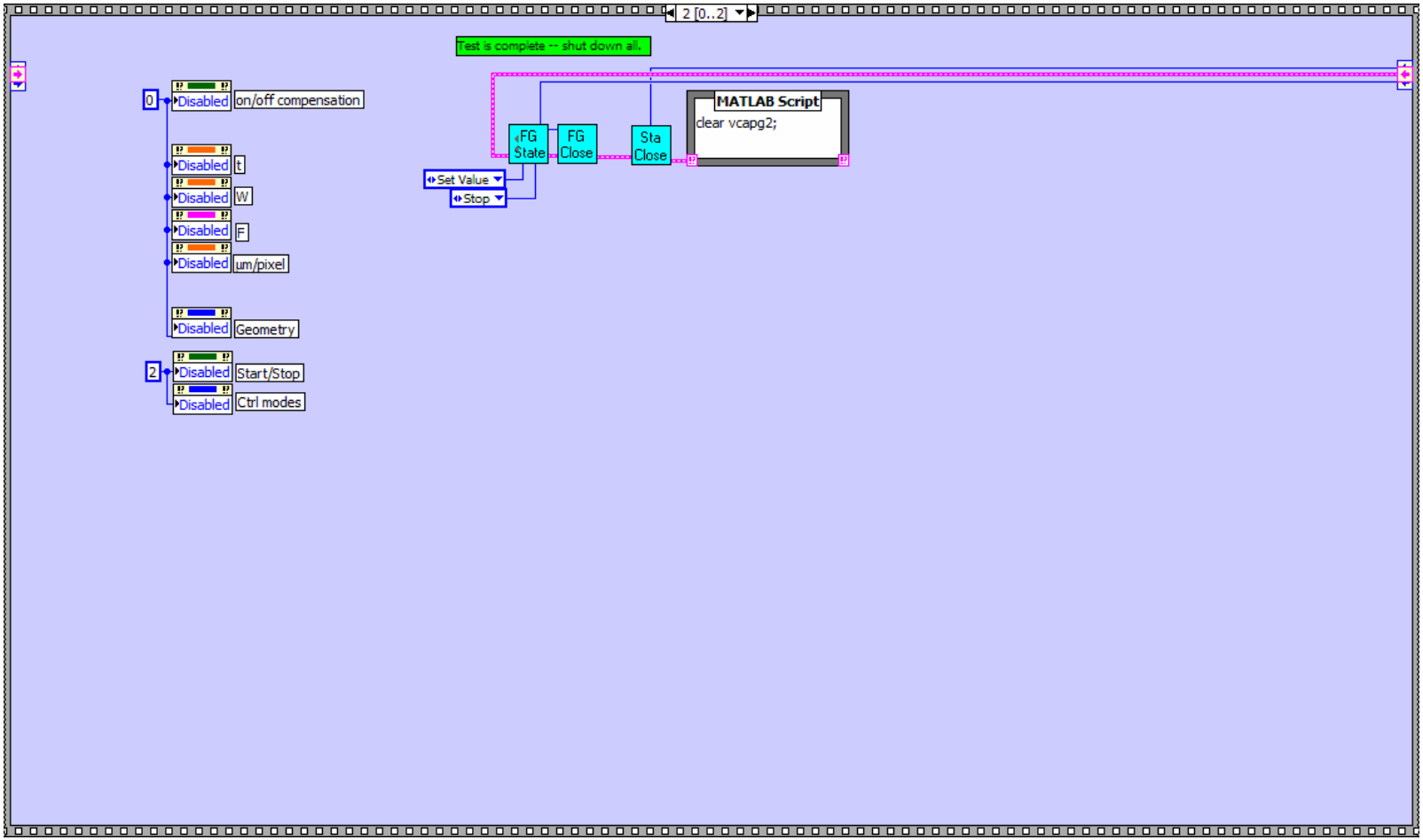
2 [0..2]
Test is complete -- shut down all.
0
Disabled
on/off compensation
Disabled
t
Disabled
W
Disabled
F
Disabled
um/pixel
Disabled
Geometry
2
Disabled
Start/Stop
Disabled
Ctrl modes
FG State
FG Close
Sta Close
MATLAB Script
clear vcapg2;
Set Value
Stop

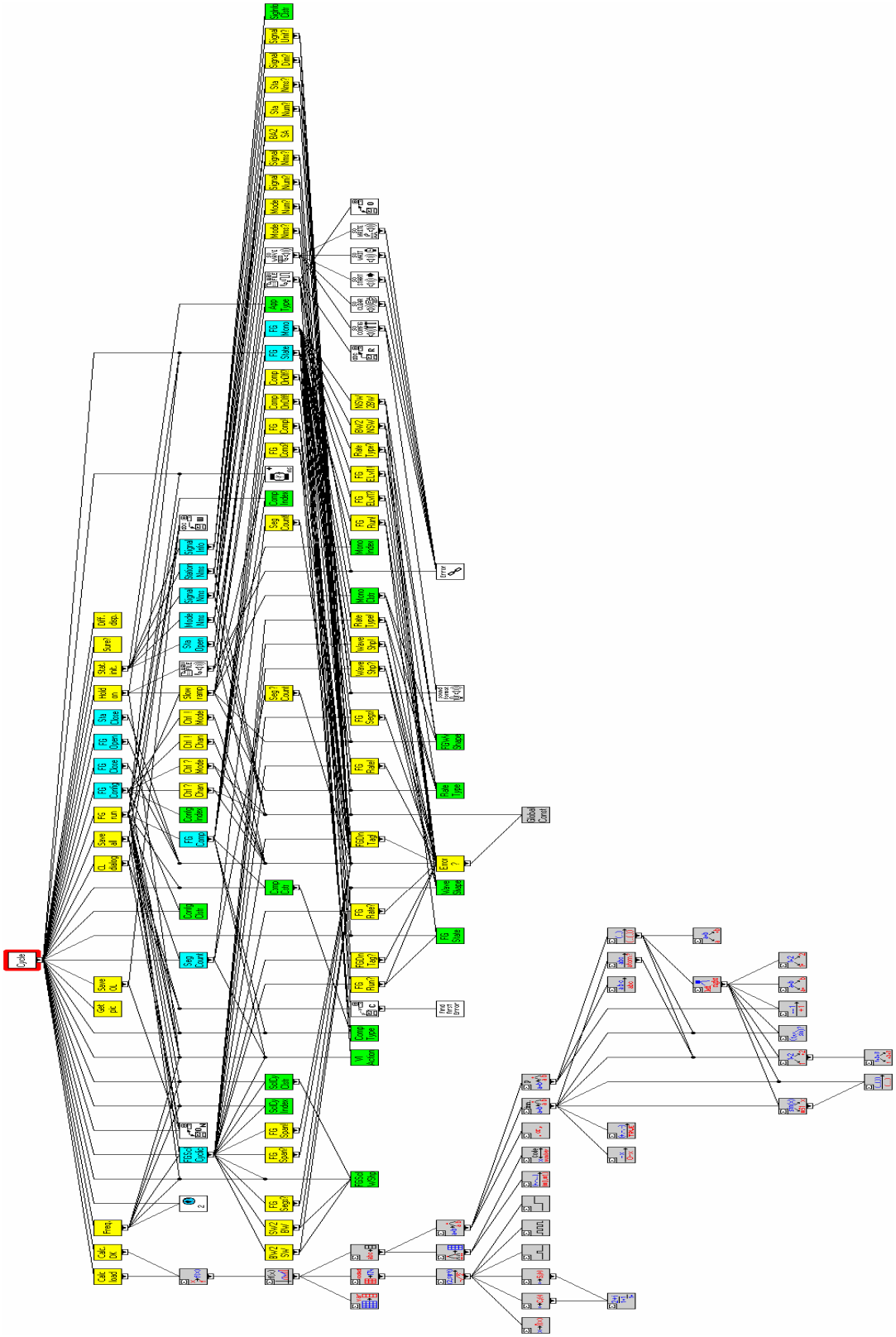

Appendix C

This appendix contains various programs, written in MatLab, that were used in the dissertation. In the beginning of each function there is a brief explanation of the input and output variables along with description of the algorithm that are used.

```
Calculation of the internal stress profile
function [MaxStrs,MinStrs,X,CPZ]=...
   rice(a_init,ProcessZone,dX,DK,Kmax,n,H,E,Sy,Width,option,Smin);
%=============================================================
% This function will calculate the stress distribution (minimum and
% maximum) ahead of crack tip for the full width of the specimen
% It does not work in te proces zone
% Power hardening + Hooke's law was used instead of Ramberg-Osgood equation
% E is the elastic modulus [Pa]
% a is the crack length [m]
% H is the strength coefficient [Pa]
% n is the strain hardening exponent
% Sy is the yield stress [Pa]
% Kmax is the maximum stres intensity factor [Pam0.5]
% DK is the stress intensity factor range [Pam0.5]
% X is the distance from the crack tip [m]
% DX is the increment of the distance from the crack tip for the next
%   stress calcuation [m]
% ProcessZone is the size of the process zone in [m]
% Width is the width of the specimen in [m]
% Smin is required for option 1, this is the applied minimum stress at
%   negative load ratios (negative as well) [Pa].
% OPTION=1
% This option will add the minimum applied stress to residual strs profile
% ahead of the crack tip. In the plastic region stresses are added by
% preserving the slope of Rice equation, statring from the intersection
% of elastic profile and yield stress
% The output is in [Pa] and [m]
%=============================================================
%Calculate the process zone (limited from strain)
ed=0.30; %plastic (or total) strain limit
sd=H*ed^n; %corresponding stress limit
maxPZ=1/(1+n)/pi*(Sy/sd)^((1+n)/n)*(Kmax/Sy)^2; %Process zone under Pmax
dSy=2*Sy; sd=2*sd;
dPZ=1/(1+n)/pi*(dSy/sd)^((1+n)/n)*(Kmax/dSy)^2; %Process zone for dP
mPZ=min([dPZ,maxPZ]);
X=mPZ:(Width-a_init)/500:(Width-a_init);% dX is obsolete here
L=length(X);
% First - calculate the maximum stress profile
%=============================================================
% Rice solution:
Const=Sy*(((Kmax/Sy)^2)/(pi*(1+n)))^(n/(1+n));
for i=1:L
   MaxStrs(i)=Const/(X(i)^(n/(1+n)));
```

```
   if MaxStrs(i)<=Sy; break; end;
end
% This is the offset for the elastic solution:
MaxOffset=X(i)-1/(2*pi)*(Kmax/MaxStrs(i))^2;
% Elactic solution:
for i=(i+1):length(X)
   MaxStrs(i)=Kmax/sqrt(2*pi*(X(i)-MaxOffset));
end
% adjust the strersses in the process zone
if X(1)<maxPZ
   q=find(X<=maxPZ);
   MaxStrs(q)=MaxStrs(q(end)+1);
end
%=============================================================
% Next - do the same for the ranges, but with twice higher Sy:
%=============================================================
Sy=Sy*2;
StrsOffset=0; % this is the default value (positive R)
if (option==1)&(Kmax-DK)<0 % means negative load ratio
   StrsOffset=Smin;
   DK=Kmax; %in order to calculate the residual stresses
end
% Do the Rice solution until stress drops below yield point
Const=Sy*(((DK/Sy)^2)/(pi*(1+n)))^(n/(1+n)); % all that is const in Rice
for i=1:L
   DeltaStrs(i)=Const/(X(i)^(n/(1+n)));
   if DeltaStrs(i)<=Sy; break; end;
end
% Find the offset for el. solution to match with Rice
DeltaOffset=X(i)-1/(2*pi)*(DK/DeltaStrs(i))^2;
% and use it:
DeltaStrs(i+1:L)=DK./sqrt(2*pi*(X(i+1:end)-DeltaOffset))-StrsOffset;
MinStrs=MaxStrs-DeltaStrs;
% Next make the offset of the stresses in the plastic zone for negative R
%   find the point where yielding occurs (analytically)
Xo=1/(2*pi)*(DK/(Sy+StrsOffset))^2+DeltaOffset;
So=Sy;
% Find the offset to use with 'n'slope to get rice solution in plastic zone
C=So.*Xo.^(n/(1+n));
i=max(find(DeltaStrs>=Sy)); % This is the new yield point numerically
X(i)=Xo; % in order to calculate stress exactly on the plastic transition
DeltaStrs(1:i)=C.*X(1:i).^(-n/(1+n));
MinStrs(1:i)=MaxStrs(1:i)-DeltaStrs(1:i);
% adjust the strersses in the process zone
```

```
if X(1)<dPZ
   q=find(X<=dPZ);
   MinStrs(q)=MinStrs(q(end)+1);
end
% Keep stresses constant in the process zone
X(2:end+1)=X;
MaxStrs(2:end+1)=MaxStrs;
MinStrs(2:end+1)=MinStrs;
X(1)=0;
MaxStrs(1)=MaxStrs(2);
MinStrs(1)=MinStrs(2);
X=X+a_init;
%offset=MaxOffset; %how much the elastic solution was offset to match Rice
CPZ=Xo;
Calculation of the internal stress intensity factor
function [Kres] = WeightFun(ResStrs,X,Width,Geometry);
% Strs and X define the points of the residual stress profile
% The units are [Pa] and [m], accordingly
% Width is the width of the specimen in [m]
% These points will be connected with straight lines and the Kres will be
% calc for every point (make shure, that you have ENOUGH POINTS)
% The units are [Pam0.5]
% Then Kres for all points will be added to form Kres at the last element of
% Dist array.
% This is assumed to be the point, where residual stress is
% close to zero.
% The first element of Dist array is assumed to be the initial crack length
% (important for calculating the geometry function)
% DO NOT ASSUME, THAT IT IS ZERO BY DEFAULT!!!!!

% Geometry can be one of the following :
%       3 - center crack plate (a=a/2 ; b=b/2)
%       1 - single edge crack
%       2 - double edge crack (a=a/2 ; b=b/2)
% All these geometries refer to a through thickness cracks
% The output is in [Pam0.5]
%============================================================
K(1)=0;
Kres(1)=0;
% Create new x scale with only 500 points to speed up the calculation:
%Xnew=X(1):(X(length(X))-X(1))/100:X(length(X));
Xnew=X;
for j=2:length(Xnew)
   u=Xnew(1:j)/Xnew(j);
```

```
   % Now evaluate the SIF for each sub interval up to the
   % crack tip
   for i=2:length(u)
      alpha=Xnew(i)/Width;
      if Geometry==3
         M1 = (0.06987+ 0.40117*(alpha)- 5.5407*(alpha).^2+...
            50.0886*(alpha).^3- 200.699*(alpha).^4+...
            395.552*(alpha).^5- 377.939*(alpha).^6+ 140.218*(alpha).^7);
         M2 = (-0.09049- 2.14886*(alpha)+ 22.5325*(alpha).^2-
89.6553*(alpha).^3+...
            210.599*(alpha).^4- 239.445*(alpha).^5+ 111.128*(alpha).^6);
         M3 = (0.247216+ 2.56001*(alpha)- 29.6349*(alpha).^2+ 138.4*(alpha).^3-...
            347.255*(alpha).^4+ 457.128*(alpha).^5- 295.882*(alpha).^6+ ...
            68.1575*(alpha).^7);
      elseif Geometry==1
         M1 = 0.08502-(0.02230*alpha)-(1.41028*(alpha).^2)+...
            (4.64559*(alpha).^3)+(19.6924*(alpha).^4)...
            -(148.266*(alpha).^5)+(336.837*(alpha).^6)-(336.591*(alpha).^7)+...
            (127.009*(alpha).^8);
         M2 = 0.2234-(0.6146*alpha)+(11.1687*(alpha).^2)-(56.5326*(alpha).^3)...
            +(151.937*(alpha).^4)-(182.634*(alpha).^5)+(86.4731*(alpha).^6);
         M3 = 0.4983+(0.7512*alpha)-(10.5597*(alpha).^2)+(47.9251*(alpha).^3)...
            -(115.933*(alpha).^4)+(131.976*(alpha).^5)-(59.8893*(alpha).^6);
      elseif Geometry==2
         M1 = ((-0.029207+alpha*(0.213074+alpha*(-3.029553+alpha*(5.901933+...
            alpha*(-2.657820)))))/(1+alpha*(-1.259723+alpha*(-0.048475+...
            alpha*(.48125+alpha*(-.526796+alpha*(.345012)))))));
         M2 = ((.451116+alpha*(3.462425+alpha*(-1.078459+alpha*(3.558573+...
            alpha*(-7.553533)))))/(1+alpha*(-1.496612+alpha*(.764586+...
            alpha*(-.659316+alpha*(.258506+alpha*(.114568)))))));
         M3 = ((.427195+alpha*(-3.730114+alpha*(16.276333+alpha*(-18.799956+...
            alpha*(14.112118)))))/(1+alpha*(-1.129189+alpha*(.033758+...
            alpha*(.192114+alpha*(-.658242+alpha*(.554666)))))));
      end
      A= ((ResStrs(i)-ResStrs(i-1))/(u(i)-u(i-1)));
      B= ResStrs(i-1)-(A*u(i-1));
      F1= (X(j)/((2*pi*X(j)).^0.5)).*(A*((-4*(1-u(i)).^0.5)-...
         (2*M1*(1-u(i)))+(4/3*(1-u(i)).^1.5)-(4/3*M2*(1-u(i)).^1.5)+...
         (M1*(1-u(i)).^2)-(M3*(1-u(i)).^2)+(4/5*M2*(1-u(i)).^2.5)+...
         (2/3*M3*(1-u(i)).^3))-B*((4*(1-u(i)).^0.5)...
         +(2*M1*(1-u(i)))+(4/3*M2*(1-u(i)).^1.5)+(M3*(1-u(i)).^2)));
      F2= (X(j)/((2*pi*X(j)).^0.5)).*(A*((-4*(1-u(i-1)).^0.5)-...
         (2*M1*(1-u(i-1)))+(4/3*(1-u(i-1)).^1.5)-(4/3*M2*(1-u(i-1)).^1.5)+...
         (M1*(1-u(i-1)).^2)-(M3*(1-u(i-1)).^2)+(4/5*M2*(1-u(i-1)).^2.5)+...
```

```
        (2/3*M3*(1-u(i-1)).^3))-B*((4*(1-u(i-1)).^0.5)+(2*M1*(1-u(i-1)))+...
        (4/3*M2*(1-u(i-1)).^1.5)+(M3*(1-u(i-1)).^2)));
      K(i)=F1-F2;
   end
   Kres(j)=sum(K);
end
% Interpolate the Kres results to get results matching the rest of the
% arrays:
Kres=interp1(Xnew,Kres,X);
Analytical simulation of the CP table
function varargout = Rtransition(varargin)
% RTRANSITION M-file for Rtransition.fig
%      RTRANSITION, by itself, creates a new RTRANSITION or raises the existing
%      singleton*.
%     H = RTRANSITION returns the handle to a new RTRANSITION or the
%      handleto
%      the existing singleton*.
%      RTRANSITION('CALLBACK',hObject,eventData,handles,...) calls the local
%      function named CALLBACK in RTRANSITION.M with the given input
arguments.
%      RTRANSITION('Property','Value',...) creates a new RTRANSITION or raises
the
%      existing singleton*.  Starting from the left, property value pairs are
%      applied to the GUI before Rtransition_OpeningFunction gets called.  An
%      unrecognized property name or invalid value makes property application
%      stop.  All inputs are passed to Rtransition_OpeningFcn via varargin.
%      *See GUI Options on GUIDE's Tools menu.  Choose "GUI allows only one
%      instance to run (singleton)".
% See also: GUIDE, GUIDATA, GUIHANDLES
% Edit the above text to modify the response to help Rtransition
% Last Modified by GUIDE v2.5 30-Jun-2004 16:18:59
% Begin initialization code - DO NOT EDIT
gui_Singleton = 1;
gui_State = struct('gui_Name',       mfilename, ...
                   'gui_Singleton',  gui_Singleton, ...
                   'gui_OpeningFcn', @Rtransition_OpeningFcn, ...
                   'gui_OutputFcn',  @Rtransition_OutputFcn, ...
                   'gui_LayoutFcn',  [] , ...
                   'gui_Callback',   []);
if nargin & isstr(varargin{1})
   gui_State.gui_Callback = str2func(varargin{1});
end
if nargout
   [varargout{1:nargout}] = gui_mainfcn(gui_State, varargin{:});
```

```
else
   gui_mainfcn(gui_State, varargin{:});
end
% End initialization code - DO NOT EDIT
% --- Executes just before Rtransition is made visible.
function Rtransition_OpeningFcn(hObject, eventdata, handles, varargin)
set(handles.figure1,'color',[1,1,0.502]);
clc;
% Choose default command line output for Rtransition
handles.output = hObject;
% Update handles structure
guidata(hObject, handles);
% UIWAIT makes Rtransition wait for user response (see UIRESUME)
% uiwait(handles.figure1);
% --- Outputs from this function are returned to the command line.
function varargout = Rtransition_OutputFcn(hObject, eventdata, handles)
% varargout  cell array for returning output args (see VARARGOUT);
% hObject    handle to figure
% eventdata  reserved - to be defined in a future version of MATLAB
% handles    structure with handles and user data (see GUIDATA)
% Get default command line output from handles structure
varargout{1} = handles.output;

%==========================================================
function [SWTSa]=SWT_button_Callback(hObject, eventdata, handles)
% This function calculates the stress amplitude, according to
% Smith-Watson-Topper parameter (for a fixed Nf)
clc;
E=str2num(get(handles.E_edit,'string'));
H=str2num(get(handles.H_edit,'string'));
n=str2num(get(handles.n_edit,'string'));
b=str2num(get(handles.b_edit,'string'));
c=str2num(get(handles.c_edit,'string'));
sf=str2num(get(handles.sf_edit,'string'));
ef=str2num(get(handles.ef_edit,'string'));
Nf=str2num(get(handles.Nf_edit,'string'));
minKmax=str2num(get(handles.min_edit,'string'));
maxKmax=str2num(get(handles.max_edit,'string'));
SWT=num2str(sf*ef*(2*Nf)^(b+c)+(sf^2)/E*(2*Nf)^(2*b));
d=str2num(get(handles.d_edit,'string'));
H=num2str(H);
% n=num2str(n);
% E=num2str(E);
Schoice=get(handles.RO_button,'value');
```

```
deltaKmax=(maxKmax-minKmax)/100;
% if Schoice==1
% %use Romberg-Osgood equation to calculate the stresses at the crack tip
%     Sm=Sm_min;
%     deltaSm=(Sm_max-Sm_min)/100;
%     for j=1:100
%         sm=num2str(Sm(j));
%         fx=(['(',sm,'+x)*(x/',E,'+(x/',H,')^(1/',n,'))-',SWT]);
%         fx1=(['x/',E,'+(x/',H,')^(1/',n,')+(',sm,'+x)*(1/',E,'+(x/',H,...
%             ')^(1/',n,')/(',n,'*x))']);
%         [x]=Newton(fx,fx1,4000e6,1,1000);
%         SWTSa(j)=x(end);
%         Sm(j+1)=Sm_min+j*deltaSm;
%     end
% end
N=logspace(1,5,50);
for q=1:50
   Nf=N(q);
   if Schoice==0
      %Use Rice and elastic equations to calculate stresses at the crack
      %tip
      Kmax=logspace(log10(minKmax),log10(maxKmax),200);
      s0=645e6;
      e0=s0/E;
      SWT=(sf^2)/E*(2*Nf)^(2*b)+sf*ef*(2*Nf)^(b+c);
      Ec=sqrt(2*pi*d);
      Rc=(1+n)*pi*(s0^2)*d;
      Cee=2*Ec^2*E*SWT;
      % Constants for SWT
      Cpp=2*(Rc/s0^2*E*SWT)^((1+n)/2);
      Cep=(SWT*Ec*(4*Rc)^(1/(1+n))/e0)^((1+n)/2);
      Cpe=SWT*2*Ec*Rc^(n/(1+n))/e0;
      % Constants for inverse SWT
%       Cpp=2*(Rc/s0^2*E*SWT)^((1+n)/(2*n));
%       Cep=(SWT*Ec*(4*Rc)^(n/(1+n))/e0)^((1+n)/(2*n));
%       Cpe=SWT*2*Ec*Rc^(1/(1+n))/e0;
      dKtr=e0*2*E*Ec;
      Kmaxtr=s0*Ec;
      for j=1:200
         %SWT
         dKee(j)=Cee/Kmax(j);
         dKpp(j)=Cpp*Kmax(j)^(-n);
         dKep(j)=Cep*Kmax(j)^(-(1+n)/2);
         dKpe(j)=Cpe*Kmax(j)^(-2*n/(1+n));
```

```
        dKe(j)=min([dKep(j),dKee(j)]);
        if dKee(j)>dKep(j); dKee(j)=nan; else dKep(j)=nan; end;
        dKp(j)=min([dKpp(j),dKpe(j)]);
        if dKpe(j)>dKpp(j); dKpe(j)=nan; else dKpp(j)=nan; end;
        if dKp(j)>dKe(j); dKep(j)=nan; dKee(j)=nan; else dKpp(j)=nan; dKpe(j)=nan;
end;
%
        % Inverse SWT
%           dKee(j)=Cee/Kmax(j);
%           dKpp(j)=Cpp*Kmax(j)^(-1/n);
%           dKpe(j)=Cep*Kmax(j)^(-2/(1+n));
%           dKep(j)=Cpe*Kmax(j)^(-(1+n)/(2*n));
%
%           dKe(j)=max([dKep(j),dKee(j)]);
%           if dKee(j)>dKep(j); dKep(j)=nan; else dKee(j)=nan; end;
%
%           dKp(j)=max([dKpp(j),dKpe(j)]);
%           if dKpe(j)>dKpp(j); dKpp(j)=nan; else dKpe(j)=nan; end;
%
%           if dKp(j)<dKe(j); dKep(j)=nan; dKee(j)=nan; else dKpp(j)=nan;
dKpe(j)=nan; end;
      end
   end
   hold on;
   loglog(Kmax/1e6,dKee/1e6,'k.-');
   loglog(Kmax/1e6,dKpp/1e6,'k.-');
   loglog(Kmax/1e6,dKep/1e6,'r.-');
   loglog(Kmax/1e6,dKpe/1e6,'b.-');

   % loglog(Kmax/1e6,dK/1e6,'k-');
   % loglog(Kmax/1e6,dKe/1e6,'r.');
   % loglog(Kmax/1e6,dKp/1e6,'b.');
   xlabel('Kmax [MPam^{0.5}]');
   ylabel('{\Delta}K [MPam^{0.5}]');
   grid on;
   xlim([1,100]); ylim([1,100]);
   drawnow;
end
%=========================================================
function [MorrowSa]=Morrow_button_Callback(hObject, eventdata, handles)
% This function calculates the stress amplitude, according to
% mod. Morrow parameter (for a fixed Nf)
clc;
E=str2num(get(handles.E_edit,'string'));
```

```
H=str2num(get(handles.H_edit,'string'));
n=str2num(get(handles.n_edit,'string'));
b=str2num(get(handles.b_edit,'string'));
c=str2num(get(handles.c_edit,'string'));
sf=str2num(get(handles.sf_edit,'string'));
ef=str2num(get(handles.ef_edit,'string'));
Nf=str2num(get(handles.Nf_edit,'string'));
minKmax=str2num(get(handles.min_edit,'string'));
maxKmax=str2num(get(handles.max_edit,'string'));
d=str2num(get(handles.d_edit,'string'));
C1=num2str(-ef*(2*Nf)^c-sf/E*(2*Nf)^b);
C2=num2str(((2*Nf)^b)/E);
H=num2str(H);
n=num2str(n);
E=num2str(E);
Schoice=get(handles.RO_button,'value');
deltaKmax=(maxKmax-minKmax)/100;
if Schoice==1
   %use Romberg-Osgood equation to calculate the stresses at the crack tip
   Sm=Sm_min;
   deltaSm=(Sm_max-Sm_min)/100;
   for j=1:100
      sm=num2str(Sm(j));
      fx=(['(x/',E,'+(x/',H,')^(1/',n,'))+',C1,'+',sm,'*',C2]);
      fx1=(['1/',E,'+x^((1-',n,')/',n,')/(',n,'*',H,'^(1/',n,'))']);
      [x]=Newton(fx,fx1,4000e6,1,1000);
      MorrowSa(j)=x(end);
      Sm(j+1)=Sm_min+j*deltaSm;
   end
end
if Schoice==0
% Use Rice equations to calculate stresses at the crack tip
   n=str2num(n);
   H=str2num(H);
   Kmax=minKmax;
   e0=0.002;
   s0=H*e0^n;
   Cp=(ef/e0*(2*Nf)^c)^((1+n)/2)*sqrt(4*(1+n)*pi*d*s0^2);
   Ce1=2*(2*Nf)^b/(1-(2*Nf)^b);
   Ce2=Ce1*sf*sqrt(2*pi*d);
   for j=1:100
      dKe=-Ce1*Kmax(j)+Ce2;
      dKp=Cp;
      dK(j)=dKp;
```

```
        if dKe<=dKp; dK(j)=dKe; end;
        Kmax(j+1)=minKmax+j*deltaKmax;
    end
end
hold on;
loglog(Kmax(1:end-1)/1e6,dK/1e6,'r.-');
xlabel('Kmax [MPam^{0.5}]');
ylabel('{\Delta}K [MPam^{0.5}]');
grid on;
%=================================================================
function Rtransition_button_Callback(hObject, eventdata, handles)
% This function will calculate and plot the intersection between Morrow and
% SWT in terms of load ratio
Nf=str2num(get(handles.Nf_edit,'string'));
Nf=logspace(log10(Nf),6,21);
Sm_min=str2num(get(handles.min_edit,'string'));
Sm_max=str2num(get(handles.max_edit,'string'));
deltaSm=(Sm_max-Sm_min)/100;
Sm=Sm_min:deltaSm:Sm_max-1;
i=find(Sm>1000);
%WaitMess=waitbar(0,['Nf = ',num2str(Nf)]);
for k=1:20
    [MorrowSa]=Morrow_button_Callback(hObject, eventdata, handles);
    [SWTSa]=SWT_button_Callback(hObject, eventdata, handles);
    [Smin,j]=min(abs(MorrowSa(i)-SWTSa(i)));
    pause(1);
    Smax(k)=MorrowSa(j)+Sm(j);
    DS(k)=2*MorrowSa(j);
    set(handles.Nf_edit,'string',num2str(Nf(k+1)));
    %waitbar(k/1e22,['Nf = ',num2str(Nf(k+1))]);
end
%close(WaitMess);
hold off;
plot(Smax/1e6,DS/1e6,'k.-');
xlabel('DS [MPa]');
ylabel('Smax [MPa]');
axis equal;
set(handles.Nf_edit,'string',num2str(Nf(1)));
%=================================================================
function X_button_Callback(hObject, eventdata, handles)
% This button clears the axes
cla;
reset(gca);
set(gca,'color',[.502,1,.502],'xscale','log','yscale','log');
```

```
grid on;
CP table
function varargout = cpt(varargin)
% Begin initialization code - DO NOT EDIT
gui_Singleton = 1;
gui_State = struct('gui_Name',       mfilename, ...
                   'gui_Singleton',  gui_Singleton, ...
                   'gui_OpeningFcn', @cpt_OpeningFcn, ...
                   'gui_OutputFcn',  @cpt_OutputFcn, ...
                   'gui_LayoutFcn',  [] , ...
                   'gui_Callback',   []);
if nargin & isstr(varargin{1})
   gui_State.gui_Callback = str2func(varargin{1});
end
if nargout
   [varargout{1:nargout}] = gui_mainfcn(gui_State, varargin{:});
else
   gui_mainfcn(gui_State, varargin{:});
end
% End initialization code - DO NOT EDIT
%==========================================================
% --- Executes just before cpt is made visible.
function cpt_OpeningFcn(hObject, eventdata, handles, varargin)
handles.output = hObject;
% Update handles structure
guidata(hObject, handles);
matDir=uigetdir('C:\MATLAB\work\CPT\Materials',...
   'Where are the material datafiles?');
mats=dir([matDir,'\*.txt']);
for i=1:length(mats)
   matFiles{i}=mats(i).name;
end
set(handles.material,'string',matFiles);
setappdata(handles.CPT,'matDir',matDir);
bgim=ones(100,100,3);
bgim(:,:,2:3)=0;
set(findobj('tag','X'),'cdata',bgim);
X_Callback(hObject, eventdata, handles);
%==========================================================
% --- Outputs from this function are returned to the command line.
function varargout = cpt_OutputFcn(hObject, eventdata, handles)
% varargout  cell array for returning output args (see VARARGOUT);
% Get default command line output from handles structure
varargout{1} = handles.output;
```

```
%==========================================================
function material_Callback(hObject, eventdata, handles)
clc;
matDir=getappdata(gcbf,'matDir');
matFiles=get(handles.material,'string');
matNum=get(handles.material,'value');
fileName=[matDir,'\',matFiles{matNum}];
r=dlmread(fileName,'\t',0,1);
r=r(1,:);
dk=dlmread(fileName,'\t',1,1);
dadn=dlmread(fileName,'\t',1,0);
dadn=dadn(:,1);
for n=1:length(r)
   for i=1:length(dadn)
      kmax(i,n)=dk(i,n)/(1-r(n));
   end
end
lspec=['ko-';'ks-';'kx-';'k>-';'k<-';'k^-';...
   'kv-';'kd-';'k*-';'k+-';'kp-';'kh-';...
   'ro-';'rs-';'rx-';'r>-';'r<-';'r^-';...
   'rv-';'rd-';'r*-';'r+-';'rp-';'rh-';'bo-'];
%Fit da/dNconst with a straight lines
for n=1:length(dadn);
   m=find(isnan(dk(n,:))==0);
   L=length(m);
   X=log10(kmax(n,m));
   Y=log10(dk(n,m));
   if L>=3%check for insufficient data
      for i=2:L-1%switch x and y depending on the slope in this loop
         p1(i,:)=polyfit(Y(1:i),X(1:i),1);% Kmax stuff
         p2(i,:)=polyfit(X(i:L),Y(i:L),1);% DK stuff
         rsd1=abs(10.^X(1:i)-10.^(polyval(p1(i,:),Y(1:i))));
         rsd2=abs(10.^Y(i:L)-10.^(polyval(p2(i,:),X(i:L))));
         rsd(i)=sum([rsd1,rsd2]);
      end
      [rsd1,i]=min(rsd(2:L-1));
      i=i+1;%since the search started from seccond element
      p(n,:)=[p1(i,:),p2(i,:)];
   else p(n,1:4)=nan;
   end
end
%find the intersection points
for i=1:length(p(:,1))
   itrKmax(i)=(p(i,1)*p(i,4)+p(i,2))/(1-p(i,1)*p(i,3));
```

```
    itrdK(i)=(p(i,3)*p(i,2)+p(i,4))/(1-p(i,1)*p(i,3));
    Ritr(i)=(10^itrKmax(i)-10^itrdK(i))/(10^itrKmax(i));
end
set(handles.CPTcorrection_label,'visible','off');
setappdata(gcbf, 'itrKmax', itrKmax);
setappdata(gcbf, 'itrdK', itrdK);
setappdata(gcbf, 'Ritr', Ritr);
setappdata(gcbf, 'p', p);
setappdata(gcbf, 'lspec', lspec);
setappdata(gcbf, 'kmax', kmax);
setappdata(gcbf, 'dk', dk);
setappdata(gcbf, 'dadn', dadn);
setappdata(gcbf, 'r', r);
%=========================================================
function plotChoice_Callback(hObject, eventdata, handles)
clc;
plotChoice=get(handles.plotChoice,'value');
hold on;
if plotChoice==1%Plot dk versus dadn
    dadNdK_Callback(hObject, eventdata, handles);
elseif plotChoice==2%Plot kmax versus dk
    dKKmax_Callback(hObject, eventdata, handles);
elseif plotChoice==3%Plot CPT (crack propagation table)
    cpt_Callback(hObject, eventdata, handles);
elseif plotChoice==4%Plot the slopes on dk-kmax graph
    Slopes_Callback(hObject, eventdata, handles);
elseif plotChoice==5%Plot the transitional load ratio
    Rtransition_Callback(hObject, eventdata, handles);
elseif plotChoice==6%Plot the transitional Kmax vs DK points
    Ktransition_Callback(hObject, eventdata, handles);
elseif plotChoice==7%Plot the angles of the constant dadn
                %contours in the kmax dominated region
    SlopeKmax_Callback(hObject, eventdata, handles);
elseif plotChoice==8%Same as 7, but for dk dominated region
    SlopeDK_Callback(hObject, eventdata, handles);
elseif plotChoice==9%Calculate the prediction for a,N,Kres
    Prediction_Callback(hObject, eventdata, handles);
elseif plotChoice==10%Calculate CPT at the crack tip
    CPT_tip(hObject, eventdata, handles);
elseif plotChoice==11%Calculate the crack driving force - K* for all R
    Kstar_Callback(hObject, eventdata, handles);
end
%=========================================================
function dadNdK_Callback(hObject, eventdata, handles)
```

```
dadn = getappdata(gcbf, 'dadn');
dk = getappdata(gcbf, 'dk');
r = getappdata(gcbf, 'r');
lspec = getappdata(gcbf, 'lspec');
set(handles.axes1,'xscale','log','yscale','log',...
   'ylim',[2.54E-11,2.54E-4]);
for i=1:length(dk(1,:))
   loglog(dk(:,i),dadn,lspec(i,:));
end
legend(num2str(r(:)),2);
xlabel('DK [MPam^{0.5}]');
ylabel('da/dN [m/cycle]');
%=========================================================
function dKKmax_Callback(hObject, eventdata, handles)
dadn =  getappdata(gcbf, 'dadn');
dk =    getappdata(gcbf, 'dk');
r =     getappdata(gcbf, 'r');
lspec = getappdata(gcbf, 'lspec');
kmax =  getappdata(gcbf, 'kmax');
p =     getappdata(gcbf, 'p');
itrKmax=getappdata(gcbf, 'itrKmax');
itrdK=getappdata(gcbf, 'itrdK');
maxKmax=str2num(get(handles.maxKmax,'string'));
maxDK = str2num(get(handles.maxDK,'string'));
set(handles.axes1,'xscale','log','yscale','log');
for i=1:length(dadn)
   loglog(kmax(i,:),dk(i,:),lspec(i,:));
   if isnan(p(i,1))==0
      loglog(10.^polyval(p(i,1:2),[itrdK(i),log10(maxDK)]),...
         [10^itrdK(i),maxDK],'k:');
      loglog([10^itrKmax(i),maxKmax],...
         10.^polyval(p(i,3:4),[itrKmax(i),log10(maxKmax)]),'kx:');
   end
end
minKmax=str2num(get(handles.minKmax,'string'));
minDK = str2num(get(handles.minDK,'string'));
ylabel('DK [MPam^{0.5}]');
xlabel('Kmax [MPam^{0.5}]');
set(gca,'xlim',[minKmax,maxKmax]);
set(gca,'ylim',[minDK,maxDK]);
%=========================================================
function Rtransition_Callback(hObject, eventdata, handles)
Rtr=getappdata(gcbf,'Ritr')';
dadn=getappdata(gcbf,'dadn');
```

```
fitorder=str2num(get(handles.fitorder,'string'));
mapping=get(handles.mapping,'value');
%get rid of the NaN's (otherwise polyfit gives NaN sa well)
i=find(isnan(Rtr)==0);
Rtr=Rtr(i);
dadn=dadn(i);
%do the fit
if mapping==1 %do log-log fitting
   p=polyfit(log10(dadn),log10(Rtr),fitorder);
   Rcorr=10.^polyval(p,log10(dadn));
   set(gca,'yscale','log','xscale','log');
elseif mapping==2 %do semilog fitting
   p=polyfit(log10(dadn),Rtr,fitorder);
   Rcorr=polyval(p,log10(dadn));
   set(gca,'yscale','log','xscale','linear');
else %nonsense
   funny=imread('bluechickenbg.gif');
   imagesc(funny);
end
hold on;
plot(Rtr,dadn,'ko-');
plot(Rcorr,dadn,'r-','linewidth',2);
ylabel('da/dN [m/cycle]');
xlabel('R transition');
clear
%=========================================================
function Ktransition_Callback(hObject, eventdata, handles)
hold on;
maxKmax =   str2num(get(handles.maxKmax,'string'));
maxdK =     str2num(get(handles.maxDK,'string'));
minKmax =   str2num(get(handles.minKmax,'string'));
mindK =     str2num(get(handles.minDK,'string'));
itrKmax=getappdata(gcbf,'itrKmax');
itrdK=getappdata(gcbf,'itrdK');
fitorder=str2num(get(handles.fitorder,'string'));
mapping=get(handles.mapping,'value');
%get rid of the NaN's (otherwise polyfit gives NaN sa well)
i=find(isnan(itrKmax)==0);
itrKmax=itrKmax(i);
itrdK=itrdK(i);
%do the fit
if mapping==1 %do log-log fitting
   p=polyfit(itrKmax,itrdK,fitorder);
   Kcorr=10.^polyval(p,itrKmax);
```

```
   set(gca,'yscale','log','xscale','log');
elseif mapping==2 %nonsense
   funny=imread('bluechickenbg.gif');
   imagesc(funny);
else %do linear fitting
   p=polyfit(10.^itrKmax,10.^itrdK,fitorder);
   Kcorr=polyval(p,10.^itrKmax);
   set(gca,'yscale','linear','xscale','linear');
end
plot([minKmax,maxKmax],[minKmax,maxKmax],'r-','linewidth',2);
plot(10.^itrKmax,10.^itrdK,'ko-','markerfacecolor','y');
plot(10.^itrKmax,Kcorr,'b-','linewidth',2);
set(gca,'xlim',[minKmax,maxKmax],'ylim',[mindK,maxdK]);
ylabel('DK [MPam^{0.5}]');
xlabel('Kmax [MPam^{0.5}]');
clear;
%=========================================================
function SlopeKmax_Callback(hObject, eventdata, handles)
P=getappdata(gcbf,'p');
dadn=getappdata(gcbf,'dadn');
fitorder=str2num(get(handles.fitorder,'string'));
mapping=get(handles.mapping,'value');
angleKmax=unwrap(atan(1./P(:,1))*2)/2*180/pi;
% angleKmax=atan(1./P(:,1))*180/pi;
%get rid of the NaN's (otherwise polyfit gives NaN sa well)
i=find(isnan(angleKmax)==0);
angleKmax=angleKmax(i);
dadn=dadn(i);
%do the fit
if mapping==1 %do log-log fitting
   pA=polyfit(log10(dadn),log10(-angleKmax),fitorder);
   Acorr=10.^polyval(pA,log10(dadn));
   angleKmax=-angleKmax;%make it positive for the log axis
   set(gca,'yscale','log','xscale','log');
elseif mapping==2 %do semilog fitting
   pA=polyfit(log10(dadn),angleKmax,fitorder);
   Acorr=polyval(pA,log10(dadn));
   set(gca,'yscale','log','xscale','linear');
else %nonsense
   funny=imread('bluechickenbg.gif');
   imagesc(funny);
end
hold on;
plot(angleKmax,dadn,'ko-','markerfacecolor','y');
```

```
plot(Acorr,dadn,'bx-','linewidth',2);
set(gca,'ylim',[2.54E-11,2.54E-4]);
ylabel('da/dN [m/cycle]');
xlabel('Angles of the const. da/dN contours in the Kmax dominated region');
% calculate the corresponding poly. coeff.:
itrKmax=getappdata(gcbf,'itrKmax');
itrdK=getappdata(gcbf,'itrdK');
P(i,1)=1./tan(Acorr*pi/180);
%P(i,1)=mean(P(i,1));
P(i,2)=itrKmax(i)'-P(i,1).*itrdK(i)';
setappdata(gcbf, 'p', P);
set(handles.CPTcorrection_label,'visible','on');
clear;
%=========================================================
function SlopeDK_Callback(hObject, eventdata, handles)
P=getappdata(gcbf,'p');
dadn=getappdata(gcbf,'dadn');
fitorder=str2num(get(handles.fitorder,'string'));
mapping=get(handles.mapping,'value');
angleDK=unwrap(atan(P(:,3))*2)/2*180/pi;
%get rid of the NaN's (otherwise polyfit gives NaN sa well)
i=find(isnan(angleDK)==0);
angleDK=angleDK(i);
dadn=dadn(i);
%do the fit
if mapping==1 %do log-log fitting
   pA=polyfit(log10(dadn),log10(-angleDK),fitorder);
   Acorr=10.^polyval(pA,log10(dadn));
   angleDK=abs(angleDK);%make it positive for the log axis
   set(gca,'yscale','log','xscale','log');
elseif mapping==2 %do semilog fitting
   pA=polyfit(log10(dadn),angleDK,fitorder);
   Acorr=polyval(pA,log10(dadn));
   set(gca,'yscale','log','xscale','linear');
else %nonsense
   funny=imread('bluechickenbg.gif');
   imagesc(funny);
end
hold on;
plot(angleDK,dadn,'ko-','markerfacecolor','y');
plot(Acorr,dadn,'b-','linewidth',2);
set(gca,'ylim',[2.54E-11,2.54E-4]);
ylabel('da/dN [m/cycle]');
xlabel('Angles of the const. da/dN contours in the Kmax dominated region');
```

```
% calculate the corresponding poly. coeff.:
itrKmax=getappdata(gcbf,'itrKmax');
itrdK=getappdata(gcbf,'itrdK');
P(i,3)=1./tan(Acorr*pi/180);
%P(i,3)=mean(P(i,1));
P(i,3)=-0.106;
P(i,4)=itrKmax(i)'-P(i,3).*itrdK(i)';
setappdata(gcbf, 'p', P);
set(handles.CPTcorrection_label,'visible','on');
clear;
%============================================================
function Slopes_Callback(hObject, eventdata, handles)
dadn=getappdata(gcbf,'dadn');
itrKmax=getappdata(gcbf,'itrKmax');
itrdK=getappdata(gcbf,'itrdK');
P=getappdata(gcbf,'p');
angleKmax=unwrap(atan(1./P(:,1))*2)/2*180/pi;
angleDK=unwrap(atan(P(:,3))*2)/2*180/pi;
n=find(isnan(angleKmax)==0);
angleKmax=angleKmax(n);
angleDK=angleDK(n);
dadn=dadn(n);
slopeKtr=diff(itrdK(n))./diff(itrKmax(n));
angleKtr=atan(slopeKtr)*180/pi;
%unwrapping the atan function
i=find(diff(angleKtr)>180);
angleKtr(i)=angleKtr(i)-180;
i=find(diff(angleKtr)<-180);
angleKtr(i)=angleKtr(i)+180;
%----------------------------
angleKtr(length(angleKtr)+1)=nan;
angleKtr(:)=45;
alpha=angleKtr'-angleDK;
beta=180-(angleKtr'-angleKmax);
plot(angleKtr,dadn,'k-','linewidth',3);
plot(alpha,dadn,'ro-','markerfacecolor','r');
plot(beta,dadn,'bo-','markerfacecolor','b');
plot(alpha+beta,dadn,'ko-','markerfacecolor','k');
set(gca,'yscale','log','ylim',[2.54E-11,2.54E-4]);
xlabel('Angles [deg]');
ylabel('da/dN [m/cycle]');
%============================================================
function Prediction_Callback(hObject, eventdata, handles);
% Predict all every 'dN' cycles
```

```
dN=str2num(get(handles.dN_edit,'string'));
% Calculate the stress profile (and Kres) every dX process zones
dX=str2num(get(handles.dX_edit,'string'));
cpt=getappdata(gcbf,'cpt');
Balance_button=get(handles.Balance_button,'value');
StrsDecay_button=get(handles.StrsDecay_button,'value');
n=str2num(get(handles.n_edit,'string'));
H=str2num(get(handles.H_edit,'string'));
Sy=str2num(get(handles.Sy_edit,'string'));
ProcessZone=str2num(get(handles.d_edit,'string'));
E=str2num(get(handles.E_edit,'string'));
DK_edit=get(handles.DK_edit,'string');
Kmax_edit=get(handles.Kmax_edit,'string');
Cycles_edit=get(handles.Cycles_edit,'string');
for i=1:length(DK_edit)
   DK(i)=str2num(DK_edit{i});
   Kmax(i)=str2num(Kmax_edit{i});
   Cycles(i)=str2num(Cycles_edit{i});
end;
a_init=str2num(get(handles.ainit_edit,'string'));
Width=str2num(get(handles.W_edit,'string'));
Geometry=get(handles.Geometry_menu,'value');
N=0:dN:Cycles(1);
i=1:length(N); % Index for the first block
DKd(i)=DK(1);
Kmaxd(i)=Kmax(1);
dadN(i)=griddata(cpt(:,:,3),cpt(:,:,2),cpt(:,:,1),...
   Kmaxd(1),DKd(1)); %Interpolate da/dN from CPT
a=a_init+N*dadN(1);
% iKres(i)=0;
Transitions(1)=1; % This will be used later to annotate graphs
for i=2:length(DK) % i is the number of load changes
   Transitions(i)=length(a);
   a_init=a(length(a));
   % Calculate the stress and the resulting residual
   % stress profiles from the first cycle in the block
   % and the last cycle of the previous block
   ResStrs_menu=get(handles.ResStrs_menu,'value');
   if ResStrs_menu==1 %Residual(means DK = Kmax)
      [MaxStrs1,ResStrs1,X,offset1]=...
         rice(a_init,ProcessZone,dX,Kmax(i-1)*1e6,Kmax(i-1)*1e6,n,H,E,Sy,Width);
      [MaxStrs2,ResStrs2,X,offset2]=...
         rice(a_init,ProcessZone,dX,Kmax(i)*1e6,Kmax(i)*1e6,n,H,E,Sy,Width);
   elseif ResStrs_menu==2 %Minimum
```

```
      [MaxStrs1,ResStrs1,X,offset1]=...
         rice(a_init,ProcessZone,dX,DK(i-1)*1e6,Kmax(i-1)*1e6,n,H,E,Sy,Width);
      [MaxStrs2,ResStrs2,X,offset2]=...
         rice(a_init,ProcessZone,dX,DK(i)*1e6,Kmax(i)*1e6,n,H,E,Sy,Width);
   end
   if Balance_button==1
      % Balance the positive and negative area in the residual stress
      % profiles:
      [ResStrs1]=BalanceK(ProcessZone,dX,X,ResStrs1);
      [ResStrs2]=BalanceK(ProcessZone,dX,X,ResStrs2);
   end
   % Calculate Kres using weight function:
   Kres_menu=get(handles.Kres_menu,'value');
   PZ=1/pi*(max(Kmax)*1e6/Sy)^2; % Plastic zone size
   Xk=find(X<=a_init+3*PZ);
   Xk=X(Xk); % Where the residual K will be calculated (to reduce calc)
   % Residual K from stresses behind the tip
   rKb=WeightFun(ResStrs1,Xk,Width,Geometry);
%    % Residual K from stresses ahead of the crack tip (elastic or Rice)
%    for iK=1:length(ResStrs1)
%       % Elstic
%       rKae=abs(ResStrs1(iK))*sqrt(2*pi*ProcessZone);
%       % Rice
%       rKap=sqrt(((abs(ResStrs1(iK))./Sy).^(n/(1+n)))*(1+n)*pi*...
%          (Sy^2)*ProcessZone);
%       rKa(iK)=min([rKae,rKap]);
%    end
%    iK=max(find(ResStrs1<=0));
%    rKa(1:iK)=-rKa(1:iK);
%    rKa=interp1(X,rKa,Xk);
   Kres1=rKb;% +rKa;
   if Kres_menu==1 % Block1 - Kres is only from the res stress in Block1
      Kres=Kres1;
      ResStrs=ResStrs1;
   elseif Kres_menu==2 % ???? - Reserved for trying new stuff
      % Residual K from stresses behind the tip
      rKb=WeightFun(ResStrs2,Xk,Width,Geometry);
%       % Residual K from stresses ahead of the crack tip (elastic or Rice)
%       for iK=1:length(ResStrs2)
%          % Elstic
%          rKae=abs(ResStrs2(iK))*sqrt(2*pi*ProcessZone);
%          % Rice
%          rKap=sqrt(((abs(ResStrs2(iK))./Sy).^(n/(1+n)))*(1+n)*pi*...
%             (Sy^2)*ProcessZone);
```

```
%           rKa(iK)=min([rKae,rKap]);
%       end
%       iK=max(find(ResStrs2<=0));
%       rKa(1:iK)=-rKa(1:iK);
%       rKa=interp1(X,rKa,Xk);
      Kres2=rKb;% +rKa;
      Kres(find(Kres>0))=0;
      ResStrs=ResStrs1; % just to make the program working
   end
   Kres(length(Xk)+1:length(X))=0; % To speed up the calc
%    if StrsDecay_button==1
%       %Stresses decay as the crack goes through the positive res.strs. area
%       [Kres]=WeightFunDecay(ResStrs,X,Width,Geometry);
%    else
%       [Kres]=WeightFun(ResStrs,X,Width,Geometry);
%    end;
   % See what is done by now
   figure(10);
   hold on;
   subplot(2,1,1);plot(X*1e3,ResStrs*1e-6,'ko-',...
      X*1e3,MaxStrs1*1e-6,'rx-',...
      X*1e3,ResStrs1*1e-6,'rx-',...
      X*1e3,MaxStrs2*1e-6,'bx-',...
      X*1e3,ResStrs2*1e-6,'bx-');
   xlabel('Distance from the specimen edge [mm]');
   ylabel('[MPam^{0.5}]');
   legend('ResStrs','MaxStrs1','ResStrs1','MaxStrs1','ResStrs2',0);
   subplot(2,1,2);plot(X*1e3,Kres*1e-6,'kx-');
   xlabel('Distance from the specimen edge [mm]');
   ylabel('Kres [MPam^{0.5}]');
   figure(handles.CPT);
   % Number of equally spaced predictions for the given load level
   p=Cycles(i)/dN;
   % Do the crack growth simulation:
   L=length(a)+p-1;
   MaxX=max(X);
   WaitMess=waitbar(0,[num2str(a_init*1e3),' mm   ',num2str(N(end)),' cycles']);
   for j=length(a):L
      % Digitized Cycles (over the current load level)
      N(j+1)=N(j)+dN;
      % Digitized DK (over the current load level)
      DKd(j+1)=DK(i);
      % Digitized Kmax (over the current load level)
      Kmaxd(j+1)=Kmax(i);
```

```
        % Find Kres for the current crack length
        if a(j)<=MaxX % Crack is in the overload zone
           iKres(j+1)=interp1(X,Kres,a(j)); % Interpolate Kres
        else
           iKres(j+1)=0; % No Kmax modification is needed
        end
        Kmaxd(j+1)=Kmaxd(j+1)+iKres(j+1)*1e-6;
        dadN(j+1)=griddata(cpt(:,:,3),cpt(:,:,2),cpt(:,:,1),...
           Kmaxd(j+1),DKd(j+1),'v4'); %Interpolate da/dN from CPT
        a(j+1)=a(j)+dadN(j)*dN; %This works for dN cycles
        if a(end)>=Width; break; end;
        waitbar(j/L,WaitMess,[num2str(a(end)*1e3),' mm   ',num2str(N(end)),' cycles']);
     end
     close(WaitMess);
end
Transitions(i+1)=length(a);
MaxStrs1=interp1(X,MaxStrs1,a);
MaxStrs2=interp1(X,MaxStrs2,a);
ResStrs1=interp1(X,ResStrs1,a);
ResStrs2=interp1(X,ResStrs2,a);
ResStrs=interp1(X,ResStrs,a);
setappdata(gcbf,'Predicted_MaxStrs1',MaxStrs1);
setappdata(gcbf,'Predicted_MaxStrs2',MaxStrs2);
setappdata(gcbf,'Predicted_ResStrs1',ResStrs1);
setappdata(gcbf,'Predicted_ResStrs2',ResStrs2);
setappdata(gcbf,'Predicted_ResStrs',ResStrs);
setappdata(gcbf,'Predicted_dadN',dadN);
setappdata(gcbf,'Predicted_Kres',iKres);
setappdata(gcbf,'Predicted_a',a);
setappdata(gcbf,'Predicted_N',N);
setappdata(gcbf,'Predicted_DK',DKd);
setappdata(gcbf,'Predicted_Kmax',Kmaxd);
setappdata(gcbf,'Predicted_Transitions',Transitions);
Prediction_Plot_Callback(hObject, eventdata, handles);
%=========================================================
function [ResStrs]=BalanceK(ProcessZone,dX,X,ResStrs);
neg=find(ResStrs<0);
NegArea=trapz(X(neg),ResStrs(neg));
pos=neg(end):length(X);
PosArea=trapz(X(pos),ResStrs(pos));
Scale=abs(NegArea/PosArea);
ResStrs(pos)=ResStrs(pos)*Scale;
% [i,M]=max(ResStrs);
% PosArea=sum(ResStrs(length(neg):M))*dX*ProcessZone;
```

```
% for i=(M+1):(length(ResStrs)-1)
%     PosArea=PosArea+dX*ProcessZone*ResStrs(i);
%     Slope=(ResStrs(i+1)-ResStrs(i))/(dX*ProcessZone);
%     Intercept=ResStrs(i)-Slope*X(i);
%     Xmax=-Intercept/Slope;
%     TriArea=ResStrs(i)*(Xmax-X(i))/2;
%     TotalPosArea=PosArea+TriArea;
%     if abs(TotalPosArea)>=abs(NegArea); break; end;
% end
% % Round Xmax to the closest element in ResStrs profile:
% Xmax=find(X<Xmax);
% Xmax=Xmax(length(Xmax));
% ResStrs(i:Xmax)=Slope*X(i:Xmax)+Intercept;
% % Make everything else zero:
% ResStrs(Xmax+1:length(X))=0;
%=========================================================
function Prediction_Plot_Callback(hObject, eventdata, handles);
PlotChoice=get(handles.Prediction_menu,'value');
%X_Callback(hObject, eventdata, handles);
hold on;
if PlotChoice==3 % Plot da/dN vs. a
   Plot_dadN_a_Callback(hObject, eventdata, handles);
elseif PlotChoice==2 % Plot Kres vs. a
   Plot_Kres_a_Callback(hObject, eventdata, handles);
elseif PlotChoice==1 %Plot a vs. N
   Plot_a_N_Callback(hObject, eventdata, handles);
elseif PlotChoice==4 % Plot da/dN on the CPT
   Plot_dadN_CPT_Callback(hObject, eventdata, handles);
elseif PlotChoice==5 % Plot the residual stresses
   Plot_Residual_Stresses_Callback(hObject, eventdata, handles);
elseif PlotChoice==6 % Export all data to Excel
   Excel_Export_Callback(hObject, eventdata, handles);
end
%=========================================================
function Plot_dadN_a_Callback(hObject, eventdata, handles);
Transitions=getappdata(gcbf,'Predicted_Transitions');
dadN=getappdata(gcbf,'Predicted_dadN');
a=getappdata(gcbf,'Predicted_a')*1e3;
hold on;
plot(a,dadN,'k.-');
for i=1:length(Transitions)
   text(a(Transitions(i)),dadN(Transitions(i)),...
      ['\bf\bullet\leftarrow Tr.\fontsize{6}',num2str(i)]);
end
```

```
set(gca,'yscale','log','ylim',[2.54E-11,2.54E-4]);
xlabel('Crack length [mm]');
ylabel('da/dN [m/cycle]');
%=============================================================
function Plot_Kres_a_Callback(hObject, eventdata, handles);
Transitions=getappdata(gcbf,'Predicted_Transitions');
Kres=getappdata(gcbf,'Predicted_Kres');
a=getappdata(gcbf,'Predicted_a')*1e3;
plot(a,Kres,'k.-');
for i=1:length(Transitions)
   text(a(Transitions(i)),Kres(Transitions(i)),...
      ['\bf\bullet\leftarrow Tr.\fontsize{6}',num2str(i)]);
end
set(gca,'yscale','linear','xscale','linear');
xlabel('Crack length [mm]');
ylabel('Residual stress intensity factor [MPam^{0.5}]');
%=============================================================
function Plot_a_N_Callback(hObject, eventdata, handles);
Transitions=getappdata(gcbf,'Predicted_Transitions');
N=getappdata(gcbf,'Predicted_N');
a=getappdata(gcbf,'Predicted_a')*1e3;
plot(N,a,'k.-');
for i=1:length(Transitions)
   text(N(Transitions(i)),a(Transitions(i)),...
      ['\bf\bullet\leftarrow Tr.\fontsize{6}',num2str(i)]);
end
set(gca,'yscale','linear','xscale','linear');
ylabel('Crack length [mm]');
xlabel('N [cycles]');
%=============================================================
function Plot_dadN_CPT_Callback(hObject, eventdata, handles);
DK=getappdata(gcbf,'Predicted_DK');
Kmax=getappdata(gcbf,'Predicted_Kmax');
a=getappdata(gcbf,'Predicted_a');
cpt=getappdata(gcbf,'cpt');
maxKmax=str2num(get(handles.maxKmax,'string'));
maxdK=str2num(get(handles.maxDK,'string'));
minKmax=str2num(get(handles.minKmax,'string'));
mindK=str2num(get(handles.minDK,'string'));
cptsize=str2num(get(handles.cptsize,'string'));
y=logspace(log10(mindK),log10(maxdK),cptsize);
x=logspace(log10(minKmax),log10(maxKmax),cptsize);
z=logspace(log10(2.54e-11),log10(2.54e-4),cptsize);
% Digitize DK and Kmax with the precision of the CPT
```

```
DK=interp1(1:length(DK),DK,y);
Kmax=interp1(1:length(Kmax),Kmax,x);
for i=1:length(DK); Z(:,i)=z'; end
for i=1:length(z); X(i,:)=Kmax(:)'; Y(i,:)=DK(:)'; end
wireOut_Callback(hObject, eventdata, handles);%plot the cpt as a mesh
delete(findobj('type','surface','facecolor','r'));%delete the exp. data
mesh(X,Y,Z,'edgecolor','w','facecolor','b');%plot the loading plane
%=============================================================
function Plot_Residual_Stresses_Callback(hObject, eventdata, handles);
ResStrs=getappdata(gcbf,'Predicted_ResStrs')*1e-6;
MaxStrs1=getappdata(gcbf,'Predicted_MaxStrs1')*1e-6;
MaxStrs2=getappdata(gcbf,'Predicted_MaxStrs2')*1e-6;
ResStrs1=getappdata(gcbf,'Predicted_ResStrs1')*1e-6;
ResStrs2=getappdata(gcbf,'Predicted_ResStrs2')*1e-6;
Transitions=getappdata(gcbf,'Predicted_Transitions');
a=getappdata(gcbf,'Predicted_a')*1e3;
plot(a,MaxStrs1,'b-','markerfacecolor','y','linewidth',3);
plot(a,ResStrs1,'b-','markerfacecolor','y','linewidth',3);
plot(a,MaxStrs2,'r-','markerfacecolor','y','linewidth',3);
plot(a,ResStrs2,'r-','markerfacecolor','y','linewidth',3);
plot(a,ResStrs,'w-','markerfacecolor','y','linewidth',1);
for i=1:length(Transitions)
   text(a(Transitions(i)),0,...
      ['\bf\bullet\leftarrow Tr.\fontsize{6}',num2str(i)]);
end
set(gca,'yscale','linear','xscale','linear');
xlabel('Crack length [mm]');
ylabel('Stress [MPa]');
legend('MaxStrs1','ResStrs1','MaxStrs2','ResStrs2','ResStrs',0);
%=============================================================
function Excel_Export_Callback(hObject, eventdata, handles);
ResStrs=getappdata(gcbf,'Predicted_ResStrs')*1e-6;
MaxStrs1=getappdata(gcbf,'Predicted_MaxStrs1')*1e-6;
MaxStrs2=getappdata(gcbf,'Predicted_MaxStrs2')*1e-6;
ResStrs1=getappdata(gcbf,'Predicted_ResStrs1')*1e-6;
ResStrs2=getappdata(gcbf,'Predicted_ResStrs2')*1e-6;
DK=getappdata(gcbf,'Predicted_DK');
Kmax=getappdata(gcbf,'Predicted_Kmax');
a=getappdata(gcbf,'Predicted_a')*1e3;
Transitions=getappdata(gcbf,'Predicted_Transitions');
N=getappdata(gcbf,'Predicted_N');
Kres=getappdata(gcbf,'Predicted_Kres')*1e-6;
dadN=getappdata(gcbf,'Predicted_dadN');
c=clock;
```

```
c=num2str(c(6));
FileName=['C:\Documents and Settings\stoyan\Desktop\',c,'.txt'];
d=[N',a',DK',Kmax',Kres',MaxStrs1',MaxStrs2',ResStrs1',ResStrs2',...
   ResStrs',dadN'];
dlmwrite(FileName,d,'\t')
%==========================================================
function cpt_Callback(hObject, eventdata, handles)
dadn =  getappdata(gcbf, 'dadn');
R =     getappdata(gcbf, 'r');%load ratio
p =     getappdata(gcbf, 'p');%polynomial coeff.
Ritr =  getappdata(gcbf, 'Ritr');
maxKmax =   str2num(get(handles.maxKmax,'string'));
maxdK =     str2num(get(handles.maxDK,'string'));
minKmax =   str2num(get(handles.minKmax,'string'));
mindK =     str2num(get(handles.minDK,'string'));
cptsize =   str2num(get(handles.cptsize,'string'));
Rmin =      str2num(get(handles.Rmin,'string'));
Rmax =      str2num(get(handles.Rmax,'string'));
dK=logspace(log10(mindK),log10(maxdK),cptsize);
Kmax=logspace(log10(minKmax),log10(maxKmax),cptsize);
cpt(1:25,1:25,1)=2.54e-4;%the default value of cpt (conservative)
for i=1:cptsize
   for j=1:cptsize
      cpt(i,j,2)=dK(i);
      cpt(i,j,3)=Kmax(j);
      Ri=(Kmax(j)-dK(i))/Kmax(j);
      dKsol=zeros(1,25);%set default value
      if Ri<=Rmax | Ri>=Rmin
         for n=1:length(Ritr)
            %finding the intercepts
            if Ri<Ritr(n)
               %Kmax dominated region
               dKsol(n)=10^((p(n,2)+log10(1-Ri))/(1-p(n,1)));
            else
               %DK dominated region
               dKsol(n)=10^((p(n,4)-p(n,3)*log10(1-Ri))/(1-p(n,3)));
            end
            m=find(dKsol>0 & isnan(dKsol)==0);
            L=length(m);
            if isempty(m)==0
               if (dKsol(m(L))>dK(i) & L==1)
                  cpt(i,j,1)=2.54e-11;
                  break;%go to the next element
               end
```

```
                if (dKsol(m(L))>=dK(i) & dKsol(m(L)-1)<=dK(i))
                    B=log10(dadn(m(L))/dadn(m(L)-1))/...
                        log10(dKsol(m(L))/dKsol(m(L)-1));
                    A=dadn(m(L))/dKsol(m(L))^B;
                    cpt(i,j,1)=A*dK(i)^B;
                    break;%go to the next element
                end
              end
            end
            if max(dKsol(m))<dK(i); cpt(i,j,1)=2.54e-4; end
        end
    end
end
setappdata(gcbf, 'cpt', cpt);
plotCPT_Callback(hObject, eventdata, handles);%Plotting the CPT table
%=========================================================
function plotCPT_Callback(hObject, eventdata, handles)
%Plotting the CPT table
out=get(handles.out,'value');
if out==1
    %plot cpt as 2D color plot
    color2DOut_Callback(hObject, eventdata, handles);
elseif out==2
    %plot cpt as wireframe surface
    wireOut_Callback(hObject, eventdata, handles);
elseif out==3
    solidOut_Callback(hObject, eventdata, handles);
    %plot cpt as solid surface
elseif out==4
    tableOut_Callback(hObject, eventdata, handles);
    %plot cpt as a table
end
rotate3d on;
%=========================================================
function wireOut_Callback(hObject, eventdata, handles)
%plot wireframe surface
cpt=getappdata(gcbf,'cpt');
kmax=getappdata(gcbf,'kmax');
dk=getappdata(gcbf,'dk');
dadn=getappdata(gcbf,'dadn');
minkmax=str2num(get(handles.minKmax,'string'));
maxkmax=str2num(get(handles.maxKmax,'string'));
mindk=str2num(get(handles.minDK,'string'));
maxdk=str2num(get(handles.maxDK,'string'));
```

```
mesh(cpt(:,:,3),cpt(:,:,2),cpt(:,:,1),'edgecolor','w','facecolor','k');
set(gca,'xscale','log','yscale','log','zscale','log',...
   'color',[0.502,1,0.502],'zlim',[2.54E-11,2.54E-4],...
   'ylim',[mindk,maxdk],'xlim',[minkmax,maxkmax],'box','on');
view(-37.5,30);
grid off;
xlabel('Kmax [MPam^{0.5}]');
ylabel('dK [MPam^{0.5}]');
zlabel('da/dN [m/cycle]');
for i=1:length(dk(1,:));z(:,i)=dadn(:);end;
surf(kmax,dk,z,'edgecolor','w','facecolor','r');
%=========================================================
function color2DOut_Callback(hObject, eventdata, handles)
%plot cpt as 2D color plot
cpt=getappdata(gcbf,'cpt');
dadn=getappdata(gcbf,'dadn');
[c,h]=contourf(log10(cpt(:,:,1)),50);
set(gca,'ydir','normal','zlim',[log10(2.54E-11),log10(2.54E-4)],...
   'ylim',[1,25],'xlim',[1,25],'box','on');
xlabel('Kmax');ylabel('dK');
colormap('bone');
clabelStoyan(c,'manual','fontweight','bold','color','r');
%=========================================================
function solidOut_Callback(hObject, eventdata, handles)
%plot cpt as solid surface
cpt=getappdata(gcbf,'cpt');
minkmax=str2num(get(handles.minKmax,'string'));
maxkmax=str2num(get(handles.maxKmax,'string'));
mindk=str2num(get(handles.minDK,'string'));
maxdk=str2num(get(handles.maxDK,'string'));
surfl(cpt(:,:,3),cpt(:,:,2),cpt(:,:,1));
set(gca,'xscale','log','yscale','log','zscale','log',...
   'color',[0.502,1,0.502],'zlim',[2.54E-11,2.54E-4],...
   'ylim',[mindk,maxdk],'xlim',[minkmax,maxkmax],'box','on');
shading interp;
colormap('bone');
view(-37.5,30);
grid off;
xlabel('Kmax [MPam^{0.5}]');
ylabel('dK [MPam^{0.5}]');
zlabel('da/dN [m/cycle]');
%=========================================================
function tableOut_Callback(hObject, eventdata, handles)
%=========================================================
```

```
function X_Callback(hObject, eventdata, handles)
cla;clc;
reset(gca);
legend('hide');
set(gca,'box','on');
grid on;
if ishandle(10)==1; close(10); end;
%=========================================================
function slider_Callback(hObject, eventdata, handles)
clc;cla;
cpt=getappdata(gcbf, 'cpt');
section=get(handles.section,'value');
slider=get(handles.slider,'value');
delete(findobj('type','line'));
hold on;
if section==1%const kmax
   sectionKmax_Callback(hObject, eventdata, handles);
elseif section==2%const dk
   sectiondK_Callback(hObject, eventdata, handles);
elseif section==3%const R
   sectionR_Callback(hObject, eventdata, handles);
elseif section==4%cost dadN
   sectiondadN_Callback(hObject, eventdata, handles);
end;
%=========================================================
function sectionKmax_Callback(hObject, eventdata, handles)
cpt=getappdata(gcbf, 'cpt');
mindk=str2num(get(handles.minDK,'string'));
maxdk=str2num(get(handles.maxDK,'string'));
minkmax=str2num(get(handles.minKmax,'string'));
maxkmax=str2num(get(handles.maxKmax,'string'));
slider=round(get(handles.slider,'value'));%this is an integer between 1 and 25
sectionkmax=logspace(log10(minkmax),log10(maxkmax),25);
sectionkmax=round(sectionkmax(slider)*100)/100;
for i=1:25
   for j=1:25
      if cpt(i,j,3)>sectionkmax;
         cpt(i,j,1)=nan;
      end
   end
end
mesh(cpt(:,:,3),cpt(:,:,2),cpt(:,:,1),'edgecolor','w','facecolor','k');
set(gca,'xscale','log','yscale','log','zscale','log',...
   'color',[0.502,1,0.502],'zlim',[2.54E-11,2.54E-4],...
```

```
   'ylim',[mindk,maxdk],'xlim',[minkmax,maxkmax],'box','on');
grid off;
xlabel('Kmax [MPam^{0.5}]');
ylabel('dK [MPam^{0.5}]');
zlabel('da/dN [m/cycle]');
set(handles.sectpoint,'string',num2str(sectionkmax));
%=========================================================
function sectiondK_Callback(hObject, eventdata, handles)
cpt=getappdata(gcbf, 'cpt');
mindk=str2num(get(handles.minDK,'string'));
maxdk=str2num(get(handles.maxDK,'string'));
minkmax=str2num(get(handles.minKmax,'string'));
maxkmax=str2num(get(handles.maxKmax,'string'));
slider=round(get(handles.slider,'value'));%this is an integer between 1 and 25
sectiondk=logspace(log10(mindk),log10(maxdk),25);
sectiondk=round(sectiondk(slider)*100)/100;
for i=1:25
   for j=1:25
      if cpt(i,j,2)>sectiondk;
         cpt(i,j,1)=nan;
      end
   end
end
mesh(cpt(:,:,3),cpt(:,:,2),cpt(:,:,1),'edgecolor','w','facecolor','k');
set(gca,'xscale','log','yscale','log','zscale','log',...
   'color',[0.502,1,0.502],'zlim',[2.54E-11,2.54E-4],...
   'ylim',[mindk,maxdk],'xlim',[minkmax,maxkmax],'box','on');
grid off;
xlabel('Kmax [MPam^{0.5}]');
ylabel('dK [MPam^{0.5}]');
zlabel('da/dN [m/cycle]');
set(handles.sectpoint,'string',num2str(sectiondk));
%=========================================================
function sectionR_Callback(hObject, eventdata, handles)
cpt=getappdata(gcbf, 'cpt');
mindk=str2num(get(handles.minDK,'string'));
maxdk=str2num(get(handles.maxDK,'string'));
minkmax=str2num(get(handles.minKmax,'string'));
maxkmax=str2num(get(handles.maxKmax,'string'));
rmax=1-mindk/maxkmax;
rmin=1-maxdk/minkmax;
dr=(rmax-rmin)/25;
slider=round(get(handles.slider,'value'));%this is an integer between 1 and 25
sectionr=1-cpt(25:-2:1,1,2)./cpt(25:-2:1,1,3);
```

```
sectionr=[sectionr;(1-cpt(1,3:2:25,2)./cpt(1,3:2:25,3))'];
%this is a vector with half of all possible R (step 2)
sectionr=sectionr(slider);
for i=1:25
   for j=1:25
      r=1-cpt(i,j,2)/cpt(i,j,3);
      if r>sectionr;
         cpt(i,j,1)=nan;
      end
   end
end
mesh(cpt(:,:,3),cpt(:,:,2),cpt(:,:,1),'edgecolor','w','facecolor','k');
set(gca,'xscale','log','yscale','log','zscale','log',...
   'color',[0.502,1,0.502],'zlim',[2.54E-11,2.54E-4],...
   'ylim',[mindk,maxdk],'xlim',[minkmax,maxkmax],'box','on');
grid off;
xlabel('Kmax [MPam^{0.5}]');
ylabel('dK [MPam^{0.5}]');
zlabel('da/dN [m/cycle]');
set(handles.sectpoint,'string',num2str(sectionr));
%=========================================================
function sectiondadN_Callback(hObject, eventdata, handles)
minkmax=str2num(get(handles.minKmax,'string'));
maxkmax=str2num(get(handles.maxKmax,'string'));
mindk=str2num(get(handles.minDK,'string'));
maxdk=str2num(get(handles.maxDK,'string'));
cpt=getappdata(gcbf, 'cpt');
slider=round(get(handles.slider,'value'));%this is an integer between 1 and 25
sectiondadn=logspace(-10,-4,25);
sectiondadn=sectiondadn(slider);
n=1;
for i=1:25
   for j=1:25
      if cpt(i,j,1)>sectiondadn;
         l3(n,:)=cpt(i-1,j-1,:);
         cpt(i,j,1)=nan;
         n=n+1;
      end
   end
end
mesh(cpt(:,:,3),cpt(:,:,2),cpt(:,:,1),'edgecolor','w','facecolor','k');
set(gca,'xscale','log','yscale','log','zscale','log',...
   'color',[0.502,1,0.502],'zlim',[2.54E-11,2.54E-4],...
   'ylim',[mindk,maxdk],'xlim',[minkmax,maxkmax],'box','on');
```

```
grid off;
xlabel('Kmax [MPam^{0.5}]');
ylabel('dK [MPam^{0.5}]');
zlabel('da/dN [m/cycle]');
set(handles.sectpoint,'string',num2str(sectiondadn))
%=========================================================
function corrections_Callback(hObject, eventdata, handles)
clc;
corrChoice=get(handles.corrections,'value');
if corrChoice==1
   Rtransition_Callback(hObject, eventdata, handles);
elseif corrChoice==2
   Ktransition_Callback(hObject, eventdata, handles);
elseif corrChoice==3
   SlopeKmax_Callback(hObject, eventdata, handles);
elseif corrChoice==4
   SlopeDK_Callback(hObject, eventdata, handles);
end
%=========================================================
function SlopeKmax_correction(hObject, eventdata, handles);
% this function will correct the Kmax slope of the CPT
% (as a mean value)
p=getappdata(gcbf,'p');
p(1,:)=mean(p(1,:));
setappdata(gcbf, 'p', p);
% calculate and plot theCPT:
cpt_Callback(hObject, eventdata, handles);
% Light up the warning message:
set(handles.CPTcorrection_label,'visible','on');
%=========================================================
function CPT_tip(hObject, eventdata, handles);
% this function will calculate CPT at the crack tip, using Kres
n=str2num(get(handles.n_edit,'string'));
H=str2num(get(handles.H_edit,'string'));
Sy=str2num(get(handles.Sy_edit,'string'));
E=str2num(get(handles.E_edit,'string'));
ProcessZone=str2num(get(handles.d_edit,'string'));
kmax=getappdata(gcbf,'kmax');
dk=getappdata(gcbf,'dk');
kmin=kmax-dk;
dadn=getappdata(gcbf,'dadn');
a_init=str2num(get(handles.ainit_edit,'string'));
Width=str2num(get(handles.W_edit,'string'));
Geometry=get(handles.Geometry_menu,'value');
```

```
dX=str2num(get(handles.dX_edit,'string'));
%neutralize the negative load ratios:
% [i,j]=find(kmin<0);
% kmax(i,j)=nan; dk(i,j)=nan;
waitmess=waitbar(0,'Outer loop');
% deb=figure; hold on;
%If newman data is to be used:
Smin=zeros(25,5);
choice=2;
for i=1:length(kmax(:,1))
   for j=1:length(kmax(1,:))
      if isnan(kmax(i,j))==0 %avoid cases with insufficient data
         % calculate the minimum stress distribution
         CPZ=1/((1+n)*pi*4)*(dk(i,j)*1e6/Sy)^2; % Cyclic plastic zone size
         % Calculate the driving force parameters at the crack tip
         if kmin(i,j)<0
            %Cyclic plastic zone size under neg R(with some extra):
            CPZ=1/((1+n)*pi*3)*(kmax(i,j)*1e6/Sy)^2;
            % One approach to negative load ratios
%              [MaxStrs,ResStrs,X,CPZr]=...
%                 rice(a_init,ProcessZone,dX,kmax(i,j)*1e6,...
%                 kmax(i,j)*1e6,n,H,E,Sy,a_init+CPZ,0,0);
%              [kr]=WeightFun(ResStrs,X,Width,Geometry);
%              kres(i,j)=min(kr)/1e6;
%              % The following is only valid for Donald data (1997)
%              %-----------------------------------------------
%              dk0=9.76; %MPa
%              C=0.12; %1/mm
%              a=log(dk(i,j)/dk0)/C*1e-3+a_init; %m
%              alpha=a/Width;
%              F=(1-0.5*alpha+0.37*alpha^2-0.044*alpha^3)/sqrt(1-alpha);
%              %-----------------------------------------------------
%              Smax=kmax(i,j)/F/sqrt(pi*a); %Far field stress [MPa]
%              dS=dk(i,j)/F/sqrt(pi*a); %Pa
%              Smin(i,j)=(Smax-dS)*1e6; %Pa
            Smin(i,j)=0*Smin(i,j); %Stress concentration around the tip
            [MaxStrs,MinStrs,X,CPZr]=...
               rice(a_init,ProcessZone,dX,dk(i,j)*1e6,...
               kmax(i,j)*1e6,n,H,E,Sy,a_init+CPZ,1,Smin(i,j));

            % Calculate the internal stress intensity factor
            if choice==1% By clamping force method
               kres(i,j)=-0.3936*kmax(i,j);
               MaxStrs=MaxStrs./Sy;
```

```
            MinStrs=MinStrs./Sy;
%               %Remove Baushinger effect
%               Bs=find(MaxStrs>1); %Locations for Baushinger stres corrections
%               MinStrs(Bs)=MinStrs(Bs)-(MaxStrs(Bs)-1);
            [NegS,NegInd]=find(MinStrs<=0); %get the neg min stress profile
            X1=max(NegInd); %upper limit for the integration
            X=X./X(X1);
            a0=trapz(X(1:X1),MinStrs(1:X1)); %Area under the neg.min. strs profile
            for ii=1:100
               [MaxStrs,Mintrs,Xdummy,offset]=...
                  rice(a_init,ProcessZone,dX,dk(i,j)*1e6,kmax(i,j)*1e6/100*ii,...
                  n,H,E,Sy,a_init+CPZ,0,0);
               MaxStrs=MaxStrs./Sy;
               ar(ii)=trapz(X(1:X1),MaxStrs(1:X1))+a0;
            end
            kint(i,j)=interp1(ar,1/100:1/100:1,0)*kmax(i,j);
         elseif choice==2;%By weight function method
            kres(i,j)=-0.3919*kmax(i,j);
            [ki]=WeightFun(MinStrs,X,Width,Geometry);
            ki=real(ki);
            ii=find((MaxStrs-MinStrs)>=2*Sy);
            kint(i,j)=ki(ii(end))/1e6;
         end
         dkint(i,j)=kres(i,j)-kint(i,j);
         kmaxtip(i,j)=kmax(i,j)+kres(i,j);
         dktip(i,j)=kmax(i,j)-kres(i,j)+dkint(i,j);
%           figure(deb);
%           cla;
%           plot(X,MinStrs./Sy,'r.-',X,ki/kmax(i,j)/1e6,'r.-',...
%              [X(1),X(end)],[kint(i,j)/kmax(i,j),kint(i,j)/kmax(i,j)]);
%           drawnow;
%           dktip(i,j)=dk(i,j);
      else
         R=kmin(i,j)/kmax(i,j);
         if choice==1;% By clamping force method (no Bauschinger effect)
            p=[0.0891,0.5549,0.3936];
         elseif choice==2;%By weight function method
            p=[-1.8464,4.0244,-3.1668,1.0225,0.3554,-0.3919];
%              CPZ=1/(pi*4)*(dk(i,j)*1e6/Sy)^2; % Cyclic plastic zone size
%              [MaxStrs,MinStrs,X,CPZr]=...
%                 rice(a_init,ProcessZone,dX,dk(i,j)*1e6,...
%                 kmax(i,j)*1e6,n,H,E,Sy,a_init+CPZ,0,0);
%              % Calculate the residual stress intensity factor
%              [ki]=WeightFun(MinStrs,X,Width,Geometry);
```

```
            end
            kint(i,j)=polyval(p,R)*kmax(i,j);
            kmaxtip(i,j)=kmax(i,j)+kint(i,j);
            dktip(i,j)=dk(i,j);
            Smin(i,j)=nan;
            dkint(i,j)=nan;
            kres(i,j)=nan;
          end
        else
          kmaxtip(i,j)=nan;
          dktip(i,j)=nan;
          Smin(i,j)=nan;
          kint(i,j)=nan;
          dkint(i,j)=nan;
        end
    end
    waitbar(i/length(kmax(:,1)));
end
close(waitmess);
% close(deb);
for i=1:length(dk(1,:));z(:,i)=dadn(:);end;
hold on;
setappdata(gcbf, 'dktip',dktip); % modify dk in the CPT
setappdata(gcbf, 'kmaxtip',kmaxtip); % modify kmax in the CPT
setappdata(gcbf, 'kint',kint); % internal streess intensity factor
setappdata(gcbf, 'smin',Smin); %mnimum applied stress
setappdata(gcbf, 'dkint',dkint);
setappdata(gcbf, 'kres',kres);
%plot the applied and the tip values
for i=1:length(dk(:,1))
    loglog(kmax(i,:),dk(i,:),'ko-','markerfacecolor','w');
    loglog(kmaxtip(i,:),dktip(i,:),'ko-','markerfacecolor','k');
end
maxKmax=str2num(get(handles.maxKmax,'string'));
maxDK = str2num(get(handles.maxDK,'string'));
minKmax=str2num(get(handles.minKmax,'string'));
minDK = str2num(get(handles.minDK,'string'));
ylabel('DK [MPam^{0.5}]');
xlabel('Kmax [MPam^{0.5}]');
set(gca,'xlim',[minKmax,maxKmax]);
set(gca,'ylim',[minDK,maxDK]);
set(gca,'xscale','log','yscale','log');
% put labels for dadn
L=length(kmax(1,:));
```

```
for q=1:25
   text(kmax(q,L),dk(q,L),['\leftarrow',num2str(dadn(q))],...
      'fontsize',8);
end
% calculate the new slopes on the dk-kmax plot
for i=1:length(dktip(:,1));
   j=find(isnan(dktip(i,:))==0 & isnan(kmaxtip(i,:))==0);
   if length(j)>=2
      x=kmaxtip(i,j);
      y=dktip(i,j);
      s1(i,:)=polyfit(log10(x),log10(y),1);
   else
      s1(i,1:2)=nan;
   end
end;
s1=s1(:,1)
setappdata(gcbf,'s',s1);
%=========================================================
function Kstar_Callback(hObject, eventdata, handles);
%This callback calculates the crack driving force and plots it versus
%experimental data for different load ratios.
%Both CPT at the tip and applied have to be calculated in advance
dk=getappdata(gcf,'dk');
dktip=getappdata(gcf,'dktip');
kmax=getappdata(gcf,'kmax');
tipkmax=getappdata(gcf,'kmaxtip');
dadn=getappdata(gcf,'dadn');
s=getappdata(gcf,'s');
p=s./(s-1);
set(gca,'xscale','log','yscale','log','xlim',[1,100],'ylim',[1e-12,1e-3']);
xlabel('K* [MPam^{0.5}]');
ylabel('da/dN [m/cycle]');
hold on;
for i=1:length(dk(1,:))
   j=find(isnan(dktip(:,i))==0 & isnan(tipkmax(:,i))==0);
   Kstar(j,i)=tipkmax(j,i).^p(j).*dktip(j,i).^(1-p(j));
   plot(Kstar(j,i),dadn(j),'k.-');
end
% find the mean
for i=1:length(dk(:,1))
   j=find(Kstar(i,:)>0);
   meanKstar(i)=mean(Kstar(i,j));
end
plot(meanKstar,dadn,'r-','linewidth',3);
```

```
setappdata(gcbf,'Kstar',meanKstar);
%find the needed corrections
cla;
hold on;
xlim('auto');
r=getappdata(gcf,'r');
dkint=getappdata(gcf,'dkint');
i=find(r==0);
for j=1:i-1
   edkint(:,j)=kmax(:,i)-kmax(:,j);
   tkint(:,j)=-dktip(:,i)+dktip(:,j);
   plot(edkint(:,j),dadn,'b.-',tkint(:,j),dadn,'r.-',dkint(:,j),dadn,'g.-');
end;
%=================================================================
function [rx,ry,rz]=RegCoef(x,y,z,X,Y,Z);
% calculae the sum of squared errors both in x and y direction
% x,y - raw data
% X,Y - fitted data
rz=(lnterp2(X,Y,Z,x,y)-z)^2;
ry=(lnterp2(X,Z,Y,x,z)-z)^2;
rx=(lnterp2(Z,Y,X,z,y)-z)^2;
% these are the standard values from AFGROW
% dadn=[2.54E-11,5.08E-11,2.54E-10,5.08E-10,1.02E-09,1.52E-09,...
%       2.54E-09,5.08E-09,7.62E-09,1.02E-08,1.52E-08,2.54E-08,...
%       5.08E-08,1.02E-07,2.54E-07,5.08E-07,1.02E-06,2.54E-06,...
%       5.08E-06,1.02E-05,1.52E-05,2.03E-05,2.54E-05,0.0001016,2.54E-4];
ASTM data reduction
function []=dadN(am,N,n);
%this function calculates dadN and corresponding a for incremental polynomial
%method ONLY
 am=am(:)*1e-3;          %convert a to meters
 n=(n-1)/2;
   for i=1+n:length(am)-n;
      C1=(N(i-n)+N(i+n))/2;         %scaling to avoid numerical problems
      C2=(N(i+n)-N(i-n))/2;
      x=(N(i-n:i+n)-C1)/C2;         %this is the 'x' axes
      y=am(i-n:i+n);               %this is on the 'y' axes
      Quad=polyfit(x,y,2);          %these are the coefficients of the
                                    %parabola fit
      dadn(i)=Quad(2)/C2+2*Quad(1)*(N(i)-C1)/(C2^2);      %calculate dadn
      mid=(am(i-n)+am(i+n))/2;         %This is the middle of the interval
      a(i)=polyval(Quad,mid)*1000;     %calculate the crack length at the middle
                                       %of the interval
   end;
```

```
 a=a.'
 dadn=dadn.'
```
Methods for determination of P_{op}

ACR

```
function [Pop,Dop]=ACR(xy,Low);
clc
[Pmin,i]=min(xy(:,1));
Dmin=xy(i,2);
[Pmax,i]=max(xy(:,1));
Dmax=xy(i,2);
DP=abs(Pmax-Pmin);
% Make a liear least squares fit in [Low,High] range
% of the unloading curve
% use centering and scaling as described in the help
i=find(xy(:,1)>=Pmin+(Low/100)*DP);
Line=polyfit(xy(i,1),xy(i,2),1);
C=Line(1);
%secant compliance
Cs=(Dmax-Dmin)/(Pmax-Pmin);
%starting compliance (between 2,12 and 9,19%)
P2=Pmin+0.02*DP;
P12=Pmin+0.12*DP;
P9=Pmin+0.09*DP;
P19=Pmin+0.19*DP;
i=find(xy(:,1)>=P2 & xy(:,1)<=P12);
Line=polyfit(xy(i,1),xy(i,2),1);
C1=Line(1);
i=find(xy(:,1)>=P9 & xy(:,1)<=P19);
Line=polyfit(xy(i,1),xy(i,2),1);
C2=Line(1);
Cn=(C1+C2)/2;
U=(Cs-Cn)/(C-Cn);
Pop=Pmax-U*DP;
i=find(xy(:,1)>=Pop);
if isempty(i)==0
   i=i(1);
   Pop=xy(i,1);
   Dop=xy(i,2);
else
   Pop=0;
   Dop=0;
end
```

ASTM

```
function [Pop,Dop,CO,Pm]=ASTM(lxy,uxy,...
```

```
            Low,HalfSegment,MaxDeviation,Pmax,Pmin);
%Find the open crack compiance
%Make a liear least squares fit in [Low,High] range
%ALWAYS use the unloading curve
DP=Pmax-Pmin;
index=find(uxy(:,1)>=Pmin+(Low/100)*DP);
Line=polyfit(uxy(index,1),uxy(index,2),1);
% Calculate the slopes of the segments
% using the loading curve according to ASTM (unloading is better though)
if get(findobj('tag','lounlo'),'value')==1
   xy=lxy;
else
   xy=uxy;
end
DP=(HalfSegment/100)*DP;
for i=round(100/HalfSegment):-1:1;
   ULim=Pmin+i*DP;
   LLim=ULim-2*DP;
   index=find(xy(:,1)>=LLim & xy(:,1)<=ULim);
   Segment=polyfit(xy(index,1),xy(index,2),1);
   %Calculate the slope deviation (SD)
   SlopeDeviation(i)=(Line(1,1)-Segment(1,1))/Line(1,1);
   %Calculate the load, corresponding to this SD
   Pm(i)=(ULim+LLim)/2;
end;
%find maxdev crossing on the slopes plot
Pop=Pmin;
for i=1:length(SlopeDeviation)-1
   if SlopeDeviation(i)>MaxDeviation &...
         SlopeDeviation(i+1)<MaxDeviation
      seg=polyfit(SlopeDeviation(i:i+1),Pm(i:i+1),1);
      Pop=polyval(seg,MaxDeviation);
      break
   end;
end;

%find maxdev crossing on load-displ. plot
i=find(xy(:,1)>=Pop);
i=i(1);
Dop=xy(i,2);
Pop=xy(i,1);
%Create a structure array with the results
%Round the results to 4 digits.
CO=round(SlopeDeviation*1e8)/1e8; %slope deviation
```

```
Pm=round(Pm*1e8)/1e8;%...and the corresponding load
Pop=round(Pop*1e8)/1e8;%opening load
Dop=round(Dop*1e8)/1e8;%and the corresponding displ.
LL
function [Pop,Dop]=LL(xy);
clc;
L=length(xy(:,1));
for i=3:1:L-3
   [one,S1,mu1]=polyfit(xy(1:i,1),xy(1:i,2),1);
   [two,S2,mu2]=polyfit(xy(i:L,1),xy(i:L,2),1);
   [y,rsd1]=polyval(one,xy(1:i,1),S1,mu1);
   [y,rsd2]=polyval(two,xy(i:L,1),S2,mu2);
   rsd(i)=sum(rsd1)+sum(rsd2);
end;
[rsd,i]=min(rsd(3:L-3));
Pop=xy(i,1);
Dop=xy(i,2);
LPL
function [Pop,Dop,Pcl,Dcl]=LPL(xy);
clc;
% approx. 60 sec per file
L=length(xy(:,1)); %The number of the experimental points
if L>20
   D=1e6;
   for i=2:L-5
      for n=i+3:L-2
         Quad = polyfit(xy(i:n,1),xy(i:n,2),2);
         FirstLine(1) = polyval(polyder(Quad),xy(i,1));
         FirstLine(2) = -Quad(1)*xy(i,1)^2+Quad(3);
         SecondLine(1) = polyval(polyder(Quad),xy(n,1));
         SecondLine(2) = -Quad(1)*xy(n,1)^2+Quad(3);
         QD=sum(abs(polyval(Quad,xy(i:n,1))-xy(i:n,2)));
         FLD=sum(abs(polyval(FirstLine,xy(1:i-1,1))-xy(1:i-1,2)));
         SLD=sum(abs(polyval(SecondLine,xy(n+1:L,1))-xy(n+1:L,2)));
         if D>=QD+FLD+SLD
            D=QD+FLD+SLD;
            cl=i;
            op=n;
         end
      end;
   end;
   Pop=xy(op,1);
   Pcl=xy(cl,1);
   Dop=xy(op,2);
```

```
   Dcl=xy(cl,2);
else
   Pop=nan;
   Pcl=nan;
   Dop=nan;
   Dcl=nan;
end
LPL2
function [Pop,Dop,Pcl,Dcl]=LPL2(xy);
clc;
% approx. 60 sec per file
L=length(xy(:,1)); %The number of the experimental points
if L>20
   D=1e6;
   for i=2:L-5
      for n=i+3:L-2
         Q=polyfit(xy(i:n,1),xy(i:n,2),2);
         FL=polyfit(xy(1:i,1),xy(1:i,2),1);
         SL=polyfit(xy(n:L,1),xy(n:L,2),1);
         QD=sum(abs(polyval(Q,xy(i:n,1))-xy(i:n,2)));
         FLD=sum(abs(polyval(FL,xy(1:i-1,1))-xy(1:i-1,2)));
         SLD=sum(abs(polyval(SL,xy(n+1:L,1))-xy(n+1:L,2)));
         if D>=QD+FLD+SLD
            D=QD+FLD+SLD;
            cl=i;
            op=n;
         end
      end
   end
   Pop=xy(op,1);
   Pcl=xy(cl,1);
   Dop=xy(op,2);
   Dcl=xy(cl,2);
else
   Pop=nan;
   Pcl=nan;
   Dop=nan;
   Dcl=nan;
end
PL2
function [Pop,Dop]=PL2(xy);
clc;
L=length(xy(:,1)); %The number of the experimental points
if L>20
```

```
   for i=3:1:L-3
      [Q,S,muQ]=polyfit(xy(1:i,1),xy(1:i,2),2);
      [Ln,S,muL]=polyfit(xy(i:L,1),xy(i:L,2),1);
      QD=sum(abs(polyval(Q,xy(1:i,1),[],muQ)-xy(1:i,2)));%residuals
      LD=sum(abs(polyval(Ln,xy(i:L,1),[],muL)-xy(i:L,2)));%more residuals
      D(i)=QD+LD;%total residuals
   end
   [D,i]=min(D(3:L-3));
   Pop=xy(i,1);
   Dop=xy(i,2);
else
   Pop=nan;
   Dop=nan;
end
Q
function [Pop,Dop]=Q(xy,Low);
%!!!!!!Low is the lower bound for the open crack
% assumption. I must be in Percent DP
clc;
Pmax=max(xy(:,1));
Pmin=min(xy(:,1));
DP=Pmax-Pmin;
Low=find(xy(:,1)>=Pmin+Low*DP/100);
Low=Low(1);
L=length(xy(:,1));
% Make a liear least squares fit in [Low,High] range
% of the unloading curve
[Line]=polyfit(xy(Low:L,1),xy(Low:L,2),1);
Dmax=polyval(Line,Pmax);
Dmin=polyval(Line,Pmin);
DD=Dmax-Dmin;
area=trapz(xy(:,2),xy(:,1));
area=area-Pmin*(Dmax-xy(1,2));
%   Check for nonsense due to nonlinearity
if area>=DP*DD/2; area=DP*DD/2; end;
%   Calculate the opening load
Pop=sqrt((DP*DD-2*area)/Line(1));
Pop=Pop+Pmin;
i=find(xy(:,1)>=Pop);
if isempty(i)==1
   Pop=Pmax; % this is a nonsence, but...
   Dop=Dmax;
else
   Pop=xy(i(1),1);
```

```
   Dop=xy(i(1),2);
end
Digitizing the CP table from literature
function varargout = digitize(varargin)
% Last Modified by GUIDE v2.5 16-Apr-2004 12:58:17
% Begin initialization code - DO NOT EDIT
gui_Singleton = 1;
gui_State = struct('gui_Name',       mfilename, ...
                   'gui_Singleton',  gui_Singleton, ...
                   'gui_OpeningFcn', @digitize_OpeningFcn, ...
                   'gui_OutputFcn',  @digitize_OutputFcn, ...
                   'gui_LayoutFcn',  [] , ...
                   'gui_Callback',   []);
if nargin & isstr(varargin{1})
   gui_State.gui_Callback = str2func(varargin{1});
end
if nargout
   [varargout{1:nargout}] = gui_mainfcn(gui_State, varargin{:});
else
   gui_mainfcn(gui_State, varargin{:});
end
% End initialization code - DO NOT EDIT
%==================================================
% --- Executes just before digitize is made visible.
function digitize_OpeningFcn(hObject, eventdata, handles, varargin)
clc
handles.output = hObject;
guidata(hObject, handles);
[ImageFile,ImageDir]=uigetfile('*.*','Select the image file');
dadNImage=imread([ImageDir,'\',ImageFile]);
dadNImage=flipud(dadNImage);
colormap('bone');
axes(handles.axes1);
imagesc(dadNImage);
set(handles.axes1,'ydir','normal');
%================================
function varargout = digitize_OutputFcn(hObject, eventdata, handles)
varargout{1} = handles.output;
%====================================
%Define origin, axes and stuff
function Origin_button_Callback(hObject, eventdata, handles)
%this burtton also resets everything
Origin=ginput(1);
axes(handles.axes1);
```

```
hold on;
delete(findobj('type','line'));
plot(Origin(1),Origin(2),'kh','markerfacecolor','r','markersize',12);
axes(handles.axes2);
cla;
setappdata(handles.figure1,'Xmin',Origin(1));
setappdata(handles.figure1,'Ymin',Origin(2));
setappdata(handles.figure1,'Xmax',nan);
setappdata(handles.figure1,'Ymax',nan);
setappdata(handles.figure1,'DK',nan);
setappdata(handles.figure1,'dadN',nan);
setappdata(handles.figure1,'R',nan);
%=========================================================
function Xmax_button_Callback(hObject, eventdata, handles)
Ymin=getappdata(gcbf,'Ymin');
if isempty(Ymin)==0
   [Xmax,y]=ginput(1);
   hold on;
   delete(findobj('type','line','linestyle','--','marker','h'));
   plot(Xmax,Ymin,'kh--','markerfacecolor','r','markersize',12);
   setappdata(handles.figure1,'Xmax',Xmax);
end
%=========================================================
function Ymax_button_Callback(hObject, eventdata, handles)
Xmin=getappdata(gcbf,'Xmin');
if isempty(Xmin)==0
   [x,Ymax]=ginput(1);
   hold on;
   delete(findobj('type','line','linestyle',':','marker','h'));
   plot(Xmin,Ymax,'kh:','markerfacecolor','r','markersize',12);
   setappdata(handles.figure1,'Ymax',Ymax);
end
%=========================================================
function Digitize_button_Callback(hObject, eventdata, handles)
clc;
lspec=['ko-';'ks-';'kx-';'k>-';'k<-';'k^-';...
   'kv-';'kd-';'k*-';'k+-';'kp-';'kh-';...
   'ro-';'rs-';'rx-';'r>-';'r<-';'r^-';...
   'rv-';'rd-';'r*-';'r+-';'rp-';'rh-';'bo-'];
R=getappdata(gcbf,'R');
DK=getappdata(gcbf,'DK');
dadN=getappdata(gcbf,'dadN');
Xmin=getappdata(gcbf,'Xmin');
Xmax=getappdata(gcbf,'Xmax');
```

```
Ymax=getappdata(gcbf,'Ymax');
Ymin=getappdata(gcbf,'Ymin');
DKmax=str2num(get(handles.DKmax_edit,'string'));
DKmin=str2num(get(handles.DKmin_edit,'string'));
dadNmax=str2num(get(handles.dadNmax_edit,'string'));
dadNmin=str2num(get(handles.dadNmin_edit,'string'));
LoadRatio=str2num(get(handles.LoadRatio_edit,'string'));
Xscale=log10(DKmax/DKmin)/(Xmax-Xmin);
Xoffset=Xmin*Xscale-log10(DKmin);
Yscale=log10(dadNmax/dadNmin)/(Ymax-Ymin);
Yoffset=Ymin*Yscale-log10(dadNmin);
set(handles.axes2,'xscale','log','yscale','log',...
   'ylim',[dadNmin,dadNmax],'xlim',[DKmin,DKmax]);
if
isempty(Xmin+Xmax+Ymax+Ymin+DKmax+DKmin+dadNmax+dadNmin+LoadRa
tio)==0
   i=find(R==LoadRatio);
   if isempty(i)==1;
      if isnan(R(1))==0; i=length(R)+1; end;
      if isnan(R(1))==1; i=1; end;
   end
   R(i)=LoadRatio;
   DK(:,i)=nan;
   dadN(:,i)=nan;
   DoFlag=1;
   n=1;
   while DoFlag==1
      [X(n),Y(n)]=ginput(1);
      if ( X(n)<Xmin | X(n)>Xmax | Y(n)<Ymin | Y(n)>Ymax ) == 0
         if n>1
            if ( (X(n)<X(n-1)) | (Y(n)<Y(n-1)) ) == 1
               n=n-1;
               load gong;
               sound(y,Fs);
               errordlg('DK or da/dN cannot be decreasing');
               uiwait;
            end
         end
         %take care of the image
         axes(handles.axes1);
         hold on;
         delete(findobj('type','line','marker','o','linestyle',':'));
         plot(X,Y,'ko:','markerfacecolor','y');
         %take care of the log scale graph
```

```
            DK(n,i)=10^(X(n)*Xscale-Xoffset);
            dadN(n,i)=10^(Y(n)*Yscale-Yoffset);
            axes(handles.axes2);
            hold on;
            delete(findobj('type','line','linestyle','-'));
            for m=1:length(R)
               plot(DK(:,m),dadN(:,m),lspec(m,:));
               legend(num2str(R'),2);
            end
         else
            DoFlag=0;
         end
         n=n+1;
      end
      [i,j]=find(dadN==0);
      dadN(i,j)=nan;
      DK(i,j)=nan;
      setappdata(handles.figure1,'R',R);
      setappdata(handles.figure1,'dadN',dadN);
      setappdata(handles.figure1,'DK',DK);
   else
      load gong;
      sound(y,Fs);
      errordlg('Missing something?');
      uiwait;
   end
%==========================================================
function Standardize_button_Callback(hObject, eventdata, handles)
clc;
dadNstd=[2.54E-11,5.08E-11,2.54E-10,5.08E-10,1.02E-09,1.52E-09,...
     2.54E-09,5.08E-09,7.62E-09,1.02E-08,1.52E-08,2.54E-08,...
     5.08E-08,1.02E-07,2.54E-07,5.08E-07,1.02E-06,2.54E-06,...
     5.08E-06,1.02E-05,1.52E-05,2.03E-05,2.54E-05,0.0001016,2.54E-4];
dadN=getappdata(gcbf,'dadN');
DK=getappdata(gcbf,'DK');
R=getappdata(gcbf,'R');
StdFile=nan.*zeros(length(dadNstd),length(R)+1);
StdFile(:,1)=dadNstd(:);
axes(handles.axes2);
delete(findobj('type','line','color','r','linestyle',':'));
hold on;
for i=1:length(R)
   n=find(DK(:,i)>0);
   StdFile(:,i+1)=10.^interp1(log10(dadN(n,i)),log10(DK(n,i)),...
```

```
        log10(StdFile(:,1)));
    plot(StdFile(:,i+1),StdFile(:,1),'r+:');
end
setappdata(handles.figure1,'StdFile',StdFile);
%==========================================================
function SaveAs_button_Callback(hObject, eventdata, handles)
clc;
R=getappdata(gcbf,'R');
StdFile=getappdata(gcbf,'StdFile');
[R,PermutationIndex]=sort(R);
PermutationIndex=[1,PermutationIndex+1];
StdFile=StdFile(:,PermutationIndex);
StdFile(2:length(StdFile)+1,:)=StdFile;
StdFile(1,2:length(R)+1)=R(:)';
StdFile(1,1)=nan;
[MatFile,MatFilePath] = uiputfile('mat1.txt','Save Material Data File As');
dlmwrite([MatFilePath,'\',MatFile],StdFile,'\t');
```

Appendix D

This appendix shows the results of a numerical calculation (since there is no closed form solution) of the internal stress intensity factor using clamping force method for different load ratios. The maximum load was kept constant. Both kinematic and isotropic hardening rules were used. The real material behavior is a mixture of these two ideal cases.

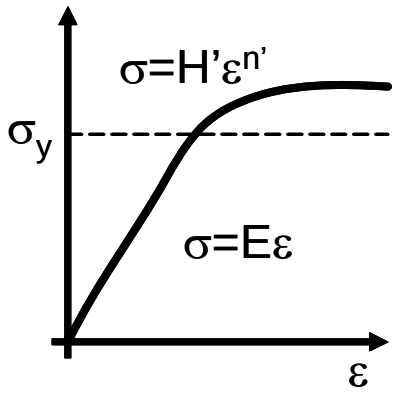

Elastic – plastic

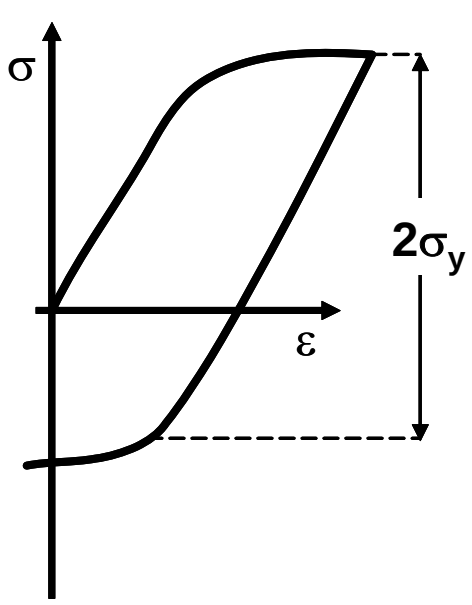

Kinematic hardening

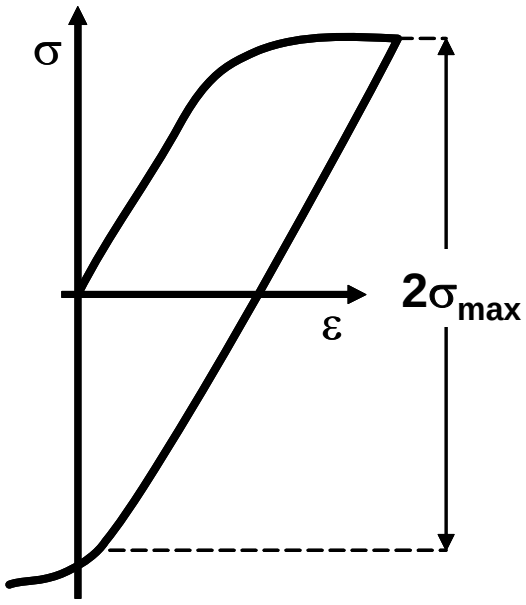

Isotropic hardening

Material – al.2324-T39
K_{max}=10 $Mpam^{0.5}$

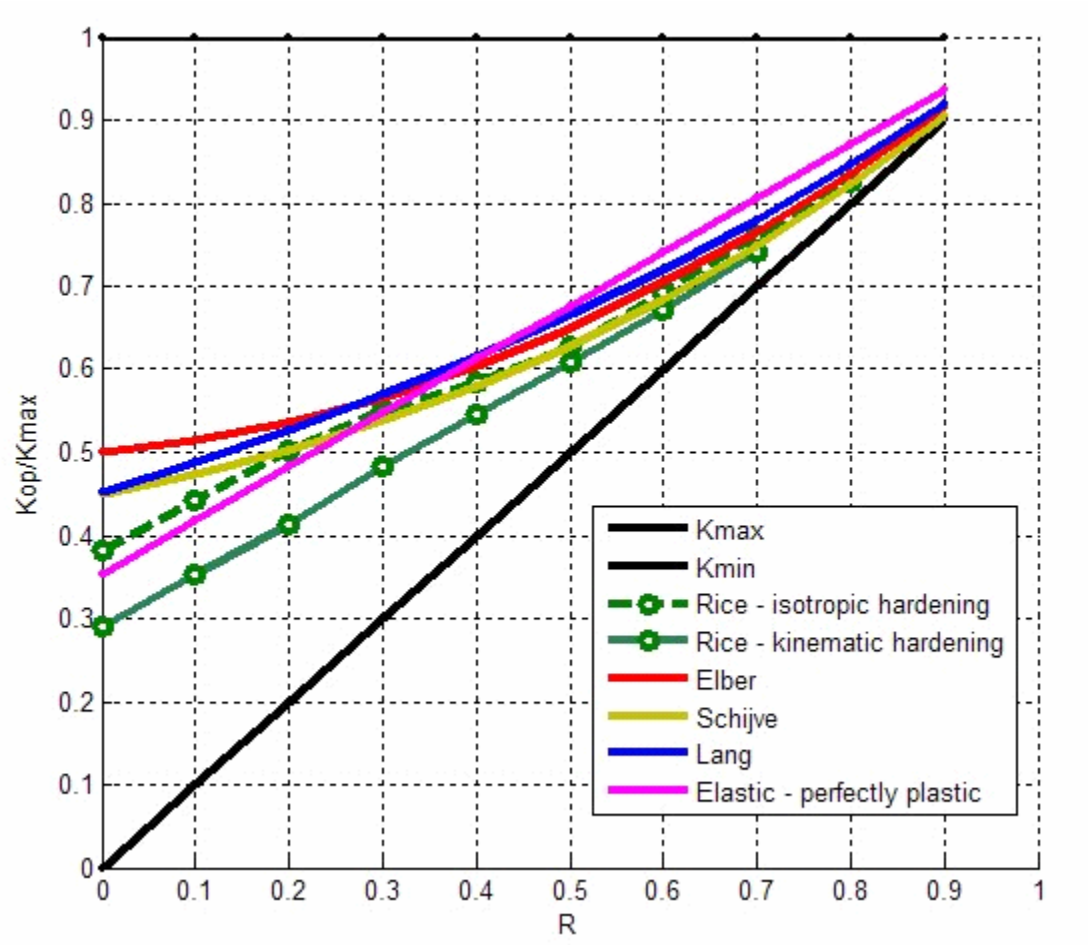

Appendix E

This appendix contains plots of crack propagation tables and the slopes of the constant da/dN curves for different materials. The data was digitized from the literature using the MatLab program listed in Appendix C.

Analysis of the data from Donald

The data is for three aluminum alloys – 23424, 7055 and 6013. It was digitized from the following source:

Bray, G. H., Donald, J. K. Separating the Influence of Kmax from Closure-Related Stress Ratio Effects Using the Adjusted Compliance Ratio Technique. Advances in Fatigue Crack Closure Measurement and Analysis: Second Volume, ASTM STP 1343, R. C. McClung, J. C. Newman, Jr., Eds., American Society for Testing and Materials, 1998

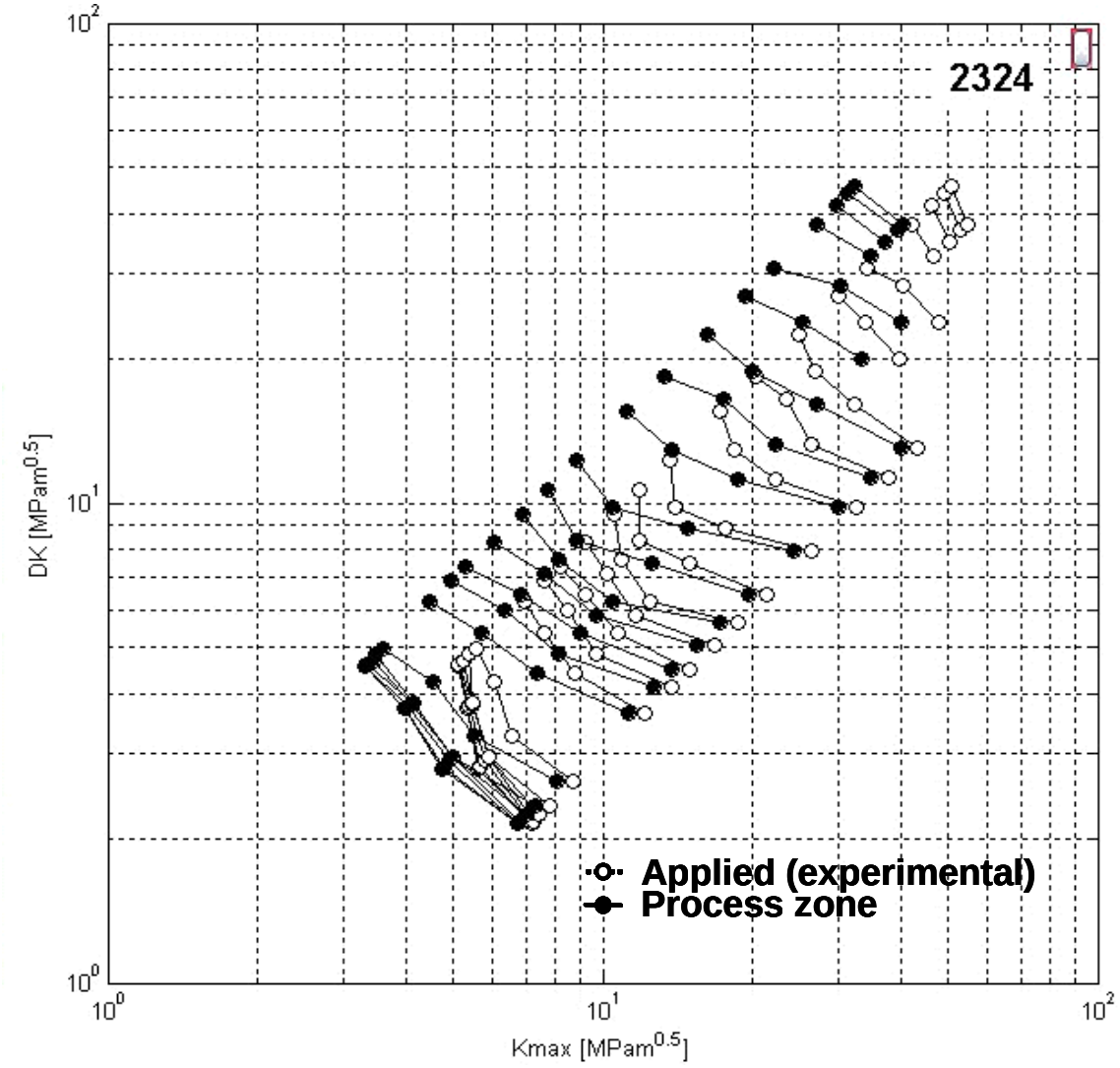

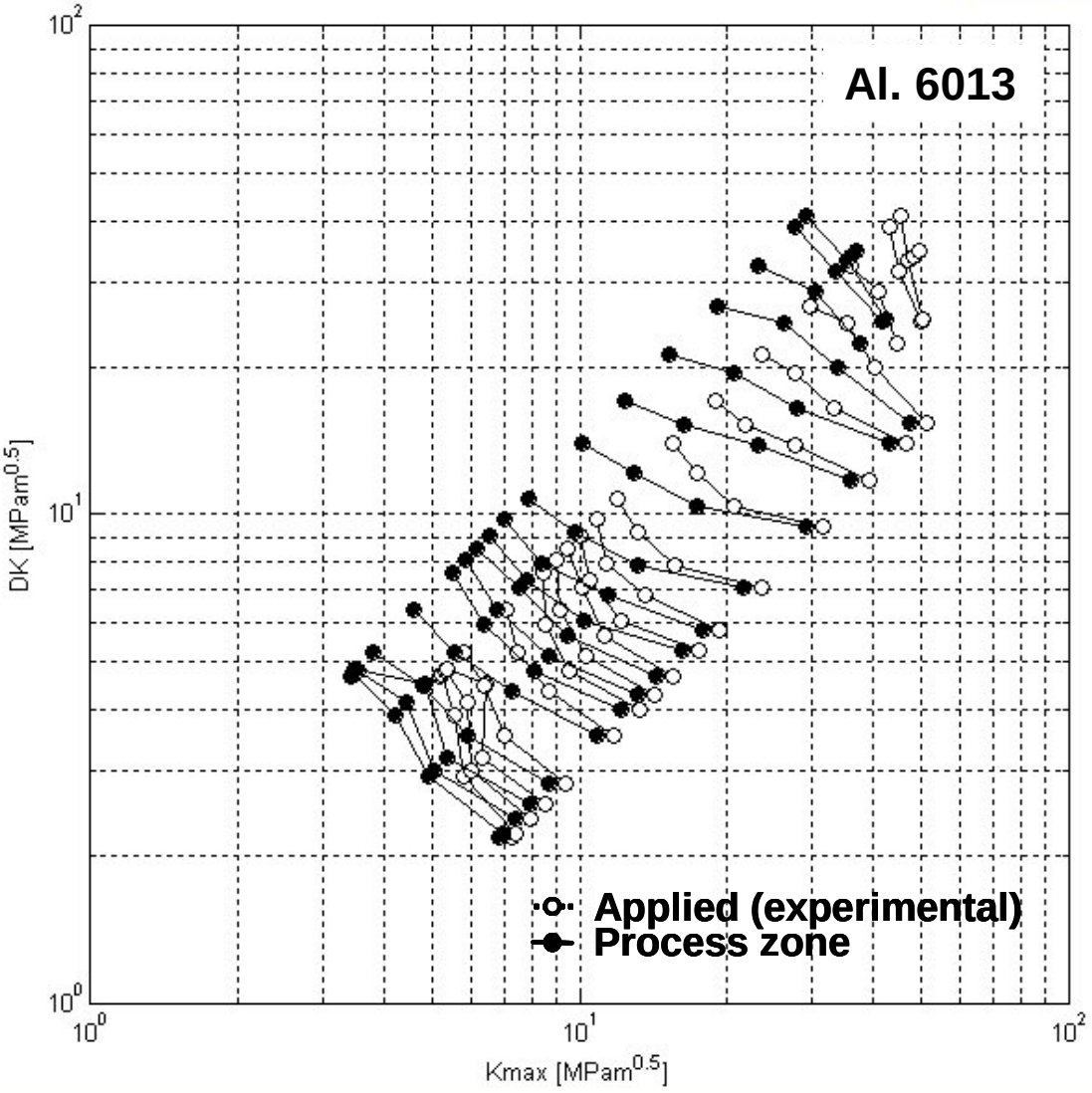
Al. 6013
Applied (experimental)
Process zone
DK [MPam^0.5]
Kmax [MPam^0.5]
10^0
10^1
10^2

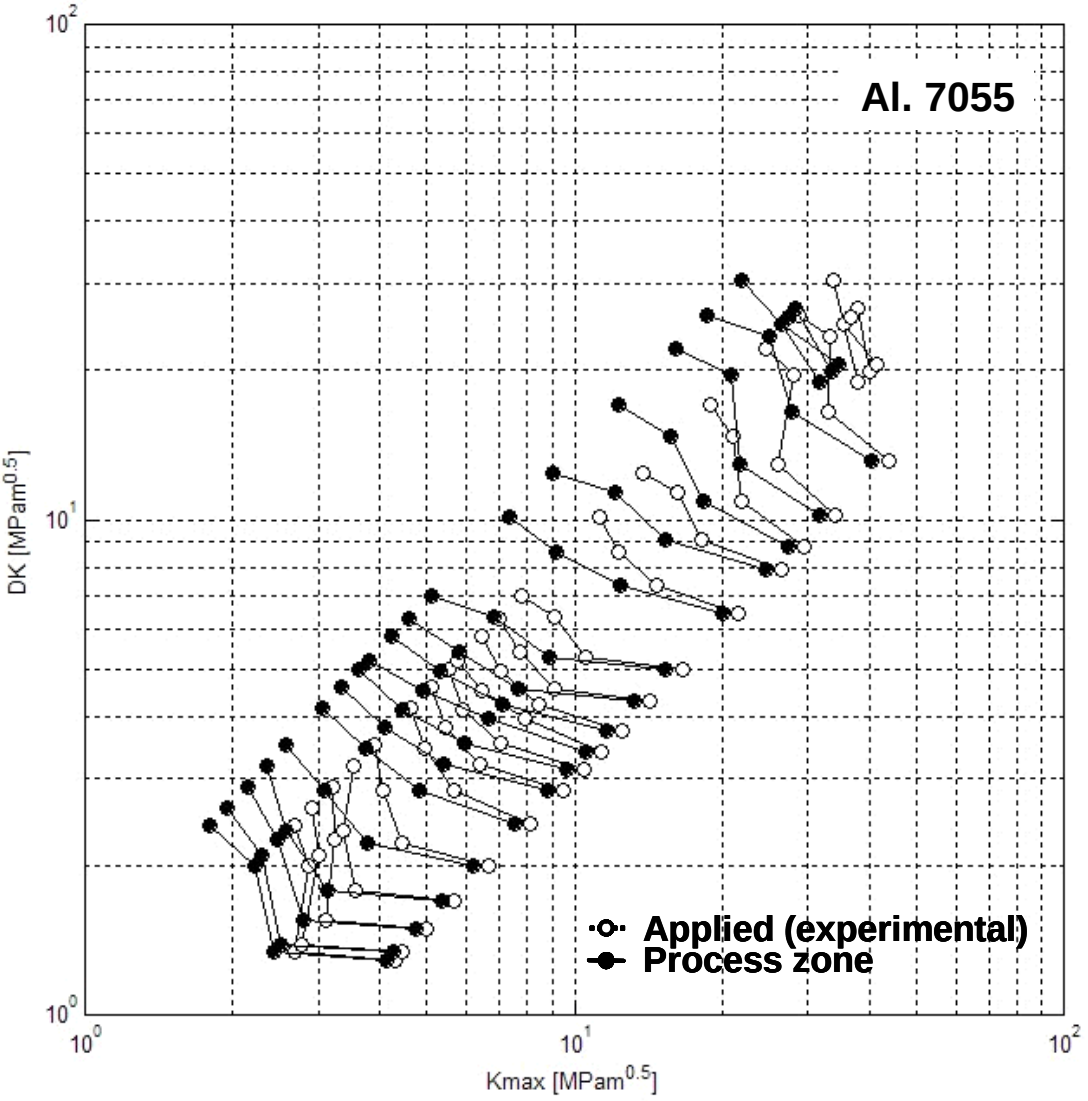
Al. 7055
Applied (experimental)
Process zone
DK [MPam^0.5]
Kmax [MPam^0.5]
10^0
10^1
10^2

Slopes of the constant da/dN curves in the ΔK-K_{max} plot

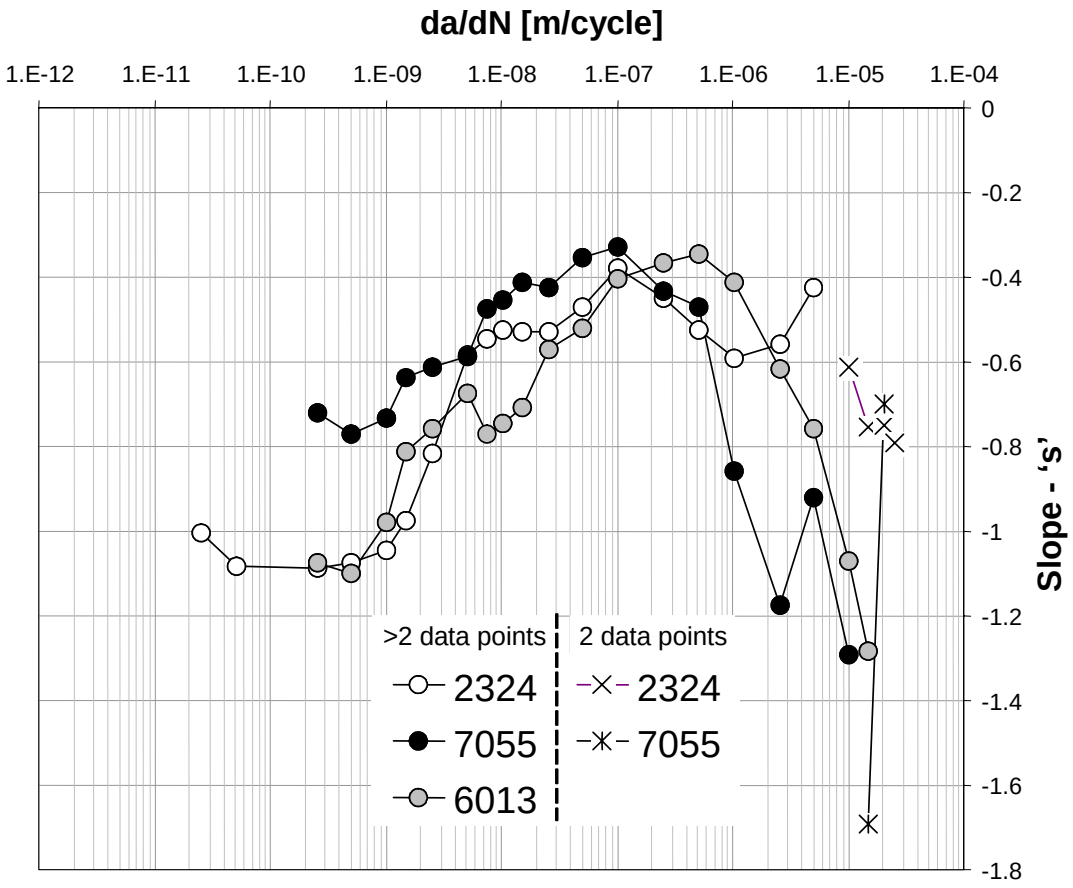

Analysis of the data from Dubenski, Hudson and Phillips

The Data, presented in this section is for al. 2024 and was digitized from the sources below:

Phillips, E. P., "The Influence of Crack Closure on Fatigue Crack Growth Thresholds in 2024-T3 Aluminum Alloy," *Mechanics of Fatigue Crack Closure, ASTM STP 982*, J. C. Newman, Jr. and W. Elber, Eds., American Society for Testing and Materials, 1988, pp. 505-515.

Hudson, C. M., "Effect of Stress Ratio on Fatigue-Crack Growth in 7075-T6 and 2024-T3 Aluminum Alloy Specimens," NASA TN D-5390, 1969.

Dubensky, R. G. 1971, "Fatigue crack propagation in 2024-T3 and 7075-T6 aluminum alloys at high stress," NASA CR-1732.

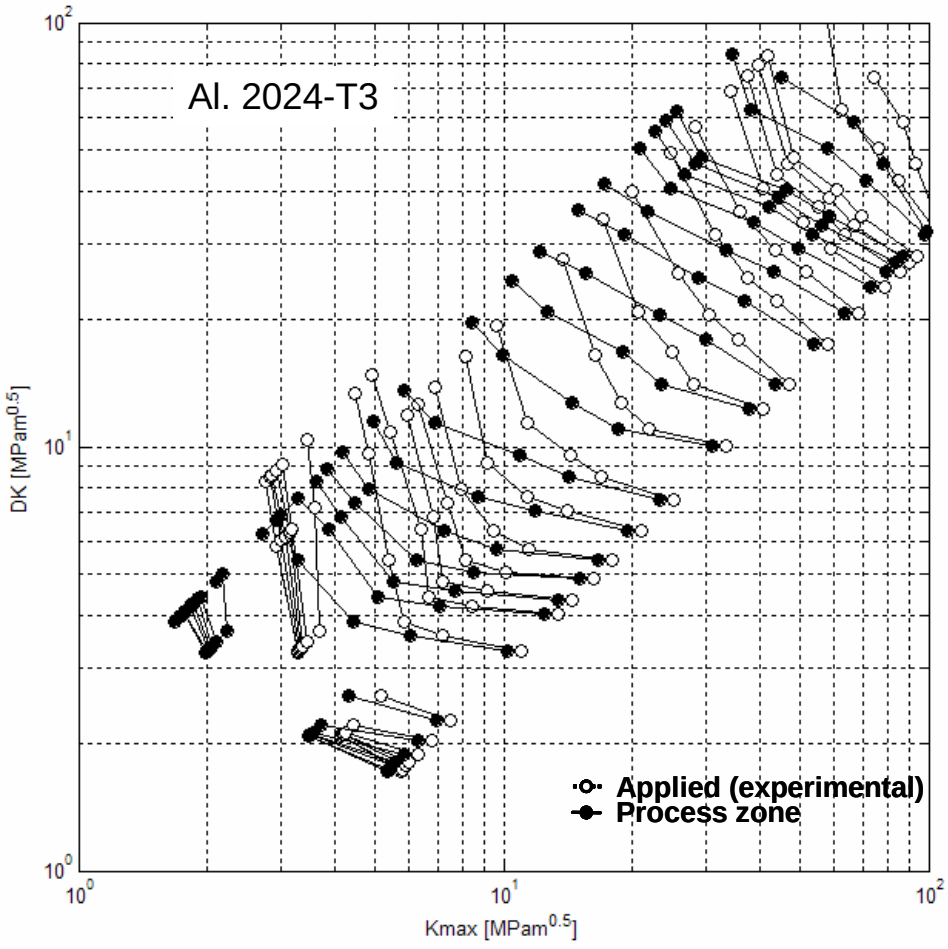

Slopes of the constant da/dN curves in the ΔK-K_{max} plot